AUGUST 2021 | HydrocarbonProcessing.com

HYDROCARBON PROCESSING®

Cover Image: A steam turbine rotor receiving new seals and blades in the Stork workshop in Essen, Germany. Photo courtesy of © Stork Technical Services.

99TH ANNIVERSARY | 1922–2021 |

HP Industry Perspectives

Correction: OASE blue technology composition in June CO_2 capture article

The June issue of *Hydrocarbon Processing* featured the article "A critical analysis of CO_2 capture technologies." The article highlighted the recent developments in commercial solvent-based technologies and compared their economics with a proprietary hydrated sorbent process for CO_2 capture developed by the authors' company.

It has come to the attention of *Hydrocarbon Processing* of an inaccuracy regarding BASF's OASE blue technology for CO_2 capture. The factual inaccuracy is in reference to the following sentence:

> "Linde and BASF Group are jointly developing a post-combustion capture technology using BASF's novel amine blended solvent comprising aqueous solutions of the tertiary amine methyl diethanolamine (MDEA) and 10 wt% of additive cyclic diamine (piperazine)."

The technology developers have informed *Hydrocarbon Processing* that the OASE blue technology solvent is not comprised of MDEA and 10 wt% of additive cyclic diamine (piperazine). The actual composition of the solvent is at the heart of the proprietary technology, and the technology developers have assured that the composition has not been revealed in public.

Correction. We want to sincerely thank the BASF OASE team, as well as the authors of the article, for their help regarding this inaccuracy. The inaccuracy has been edited in the digital version of the magazine. However, the inaccuracy is still prevalent within the printed issue of the magazine. Therefore, the editors of *Hydrocarbon Processing* are providing this correction notice to our readers who might have been inaccurately informed on the OASE blue technology composition.

Hydrocarbon Processing strives to provide the most accurate information on technologies, services and products within the hydrocarbon processing industries (HPI). This has been the goal of the publication for more than 99 yr. This objective is not possible without the collaboration with technical professionals in many disciplines that comprise the refining and petrochemical processing industries. We appreciate the guidance and assistance from our audience to provide our global readership with the most accurate and up-to-date material of HPI technologies. HP

HYDROCARBON PROCESSING®
www.HydrocarbonProcessing.com

P. O. Box 2608
Houston, Texas 77252-2608, USA
Phone: +1 (713) 529-4301
Fax: +1 (713) 520-4433
Editors@HydrocarbonProcessing.com

PUBLISHER Catherine Watkins

EDITOR-IN-CHIEF/ ASSOCIATE PUBLISHER Lee Nichols

EDITORIAL

Executive Editor	Adrienne Blume
Managing Editor	Mike Rhodes
Digital Editor	Stephanie Bartels
Technical Editor	Sumedha Sharma
Reliability/Equipment Editor	Heinz P. Bloch
Contributing Editor	Alissa Leeton
Contributing Editor	ARC Advisory Group
Contributing Editor	Anthony Sofronas

MAGAZINE PRODUCTION / +1 (713) 525-4633

Vice President, Production	Sheryl Stone
Manager, Advertising Production	Cheryl Willis
Manager, Editorial Production	Angela Bathe Dietrich
Assistant Manager, Editorial Production	Melissa DeLucca
Graphic Designer	Krista Norman

ADVERTISING SALES
See Sales Offices, page 81.

CIRCULATION / +1 (713) 520-4498 / Circulation@GulfEnergyInfo.com
Director, Circulation Suzanne McGehee

SUBSCRIPTIONS
Subscription price (includes both print and digital versions): One year $399, two years $679, three years $897. Airmail rate outside North America $175 additional a year. Single copies $35, prepaid.

Hydrocarbon Processing's Full Data Access subscription plan is priced at $1,995. This plan provides full access to all information and data *Hydrocarbon Processing* has to offer. It includes a print or digital version of the magazine, as well as full access to all posted articles (current and archived), process handbooks, the *HPI Market Data* book, Construction Boxscore Database project updates and more.

Because *Hydrocarbon Processing* is edited specifically to be of greatest value to people working in this specialized business, subscriptions are restricted to those engaged in the hydrocarbon processing industry, or service and supply company personnel connected thereto.

Hydrocarbon Processing is indexed by Applied Science & Technology Index, by Chemical Abstracts and by Engineering Index Inc. Microfilm copies available through University Microfilms, International, Ann Arbor, Mich. The full text of *Hydrocarbon Processing* is also available in electronic versions of the Business Periodicals Index.

DISTRIBUTION OF ARTICLES
Published articles are available for distribution in a PDF format or as professionally printed handouts. Contact Foster Printing at Mossberg & Co. for a price quote and details about how you can customize with company logo and contact information.

For more information, contact Jill Kaletha with Foster Printing at Mossberg & Co. at +1 (800) 428-3340 x 149 or jkaletha@mossbergco.com.

Hydrocarbon Processing (ISSN 0018-8190) is published monthly by Gulf Energy Information, 2 Greenway Plaza, Suite 1020, Houston, Texas 77046. Periodicals postage paid at Houston, Texas, and at additional mailing office. POSTMASTER: Send address changes to Hydrocarbon Processing, P.O. Box 2608, Houston, Texas 77252.

Copyright © 2021 by Gulf Energy Information. All rights reserved.

Permission is granted by the copyright owner to libraries and others registered with the Copyright Clearance Center (CCC) to photocopy any articles herein for the base fee of $3 per copy per page. Payment should be sent directly to the CCC, 21 Congress St., Salem, Mass. 01970. Copying for other than personal or internal reference use without express permission is prohibited. Requests for special permission or bulk orders should be addressed to the Editor. ISSN 0018-8190/01.

Gulf Energy Information

BPA WORLDWIDE

President/CEO	John Royall
CFO	Ed Caminos
Vice President, Upstream and Midstream	Andy McDowell
Vice President, Finance and Operations	Pamela Harvey
Vice President, Production	Sheryl Stone
Vice President, Downstream	Catherine Watkins

Publication Agreement Number 40034765 Printed in USA

Other Gulf Energy Information titles include: *Gas Processing™, Petroleum Economist®, World Oil®, Pipeline & Gas Journal* and *Underground Construction.*

LEE NICHOLS, EDITOR-IN-CHIEF/ASSOCIATE PUBLISHER
Lee.Nichols@HydrocarbonProcessing.com

Advancing ideas and best practices by learning from others

For 99 yr, *Hydrocarbon Processing* has provided hydrocarbon processing industry (HPI) professionals around the world with the latest technologies, best practices, know-how and case studies. The primary goal of this material is to keep our global audience up-to-date on the latest solutions to help optimize the plant environment for safer, more efficient and more profitable operations.

Due to the nature of refining and petrochemical plant operations, it is imperative that these new technologies and practices are explained by those engrained within the industry. Whether these come in the form of a technical article or column, whitepaper, webcast or social media post, ideas and know-how must be distributed throughout these industries to ensure frontline engineers, technologists/licensors, engineering/construction and plant personnel are effectively informed on critical issues that can affect plant operations. These values are the basis of this publication and the ideals of this industry—learning from others.

A virtual path. With many challenges affecting the global refining and petrochemical industries, a venue to discuss solutions and advance ideas is paramount. For this reason, *Hydrocarbon Processing* launched two virtual events under the name International Refining and Petrochemical Conference (IRPC). These events bring together more than 1,500 people in nearly 70 countries to discuss the latest technologies, case studies and best practices to improve facility operations, processing units, workflows, safety and supply chains.

IRPC Operations. Modeled after a successful IRPC Process Technology event, IRPC Operations will be held virtually September 21–22. This global, virtual event will feature three tracks that focus on optimizing refining and petrochemical plant operations. Nearly 70% of the event's presentations will be led by owner-operator organizations from nearly 20 countries around the world.

The event's keynote presentations will provide viewers the latest technologies and project information on key themes affecting the HPI, such as carbon capture, the increasing production of petrochemicals and using available tools (e.g., digital technologies) to increase reliability and operational excellence. These keynotes include:

- **Decarbonizing Shell Pernis: Porthos CCS and other projects:** Andy Goose, *President,* Shell Catalysts and Technologies
- **A critical analysis on CO_2 capture technologies:** Ajay Jha, *Senior Scientist, Refining R&D,* Reliance Industries Ltd.
- **Wading through the perfect storm—Delivering performance excellence in a digital era:** Walter Pesenti, *Global Operational Excellence Manager,* INEOS Aromatics
- **The future of petrochemicals: An outlook:** Dr. Thomas Kevin Smith, *Chief Economist and Managing Director,* American Chemistry Council.

The keynote presentations will be followed by tracks on the following topics: alternative fuels, biofuels and clean fuels; catalysts; digital transformation; engineering and construction; environment and safety; maintenance and reliability; process controls, instrumentation and automation; process optimization; refining-petrochemical integration; valves, pumps and turbomachinery; and water management.

IRPC Operations is a free, online event; however, you must register to attend. To register, access the agenda or view sponsorship opportunities, visit www.IRPC-Operations.com. HP

INSIDE THIS ISSUE

LEE NICHOLS, EDITOR-IN-CHIEF/ASSOCIATE PUBLISHER
Lee.Nichols@HydrocarbonProcessing.com

HP Construction

ASIA-PACIFIC

Ulsan PP Co., a JV between **PolyMirae Co. Ltd.** (a partnership between **LyondellBasell** and **DL Chemical**) and **SK Advanced,** commissioned its 400,000-tpy polypropylene (PP) facility in June. The plant, located in Ulsan, South Korea, will help satisfy increasing PP demand in Asia. The plant will use LyondellBasell's Spheripol PP process technology to produce PP.

Sarawak Petchem Sdn. Bhd. is building a 1.7-MMtpy methanol plant in Bintulu, Sarawak, Malaysia. The more than $1-B project is being built by Samsung Engineering. In June, Sarawak Petchem awarded a technology licensing contract to **Air Liquide Engineering and Construction** to provide its Lurgi MegaMethanol technology for the plant. Under the contract, Air Liquide will also build an air separation unit that will produce 2,200 tpd of oxygen. The capital-intensive methanol plant is scheduled to begin operations in 2023.

Crown LNG plans to build a 7.2-MMtpy LNG receiving terminal on India's east coast, 11 km offshore Kakinada. Crown LNG announced it will take FID on the project in late 2022. If built, the facility will begin operations in late 2025/early 2026. The terminal will help east India increase natural gas imports, which will be used for power generation and fertilizer and petrochemicals production.

Bangladesh Chemical Industries Corp. plans to commission its $1.25-B Ghorasal Polash Urea Fertilizer factory in 4Q 2023. Once completed, the 2,800-tpd granular urea production complex will be the largest factory in the country's industrial sector. The factory, being built by **Mitsubishi Heavy Industries** and **China National Chemical Engineering,** will help satisfy increasing demand for fertilizers in the country.

CANADA

Covenant Energy awarded a technology licensing contract to **Haldor Topsoe** for the company's 6,000-bpd renewable fuels facility. The project, located in Saskatchewan, will use Haldor Topsoe's HydroFlex technology to produce clean diesel from vegetable oil. The plant is scheduled to begin operations in early 2024.

EUROPE

As part of a new deep refining complex at the Moscow refinery, **JSC Gazpromneft-MNPZ,** a subsidiary of **PJSC Gazprom Neft,** awarded an engineering and procurement contract to **Técnicas Reunidas** to build a 2.4-MMtpy grassroots delayed coking unit (DCU). The installation of the DCU is part of Gazprom Neft's $4.8-B modernization and upgrade of the Moscow refinery. The project is scheduled to be commissioned in 2025.

Horisont Energi has selected **Technip Energies** to conduct a conceptual study for the design of Europe's first large-scale blue ammonia project. The Barents Blue carbon-neutral ammonia plant will be in Hammerfest, Norway. The plant, based off Haldor Topsoe's SynCOR Ammonia technology, will capture 99% of produced CO_2 and transport it and inject it deep under the Barents Sea.

UPM-Kymmene has awarded a contract to **Siemens** to supply electrification, automation and digitalization technologies for the company's biorefinery being built in Leuna, Germany. The 220,000-tpy facility will convert 100% wood into bio-based mono-ethylene glycol, mono-propylene glycol and renewable functional fillers. The biorefinery will be completed in late 2022.

Galp Energia plans to install a 100-MW electrolyzer at its Sines refinery in Portugal. The new electrolyzer will help the refiner power the Sines refinery and lessen the facility's carbon footprint. The project's cost could reach more than $230 MM. If needed, the project could be expanded up to 1,000 MW at a cost of more than $1.2 B.

LATIN AMERICA

Petrobras, Brazil's state-owned petroleum company, plans to invest $300 MM through 2025 to improve efficiencies at its domestic refineries—referred to as the RefTOP initiative. These investments will be made at several refineries not on the company's divestment portfolio; Petrobras is selling nine of its 13 refineries. The refineries involved in the upgrade and modernization program include the Refinaria de Paulína (REPLAN), the Duque de Caxias refinery (REDUC), Refinaria Henrique Lage (REVAP), Refinaria Presidente Bernardes (RPBC) and Refinaria de Capuava (RECAP).

At the time of this publication, Petrobras launched an international tender for engineering, procurement and construction (EPC) services for a new diesel hydrotreater to be installed at the REPLAN refinery in Paulína, São Paulo. The new unit will enable the refinery to produce Diesel S10—an ultra-low-sulfur-diesel—and increase jet fuel production. Similar projects are expected to take place at the REDUC refinery Baixada Fluminense in the state of Rio de Janeiro and the REVAP refinery in São José dos Campos, São Paulo.

The RefTOP program also includes the installation of new digital technologies, automation and process optimization techniques to improve refining efficiency, increase flexibility to process domestic presalt crudes, decrease environmental footprint and produce clean fuels.

MIDDLE EAST

Reliance and **Abu Dhabi National Oil Co. (ADNOC)** announced plans to build a capital-intensive chemical complex in Ruwais, United Arab Emirates (UAE). The more than $2.1-B project will be in the TA'ZIZ complex, a world-scale chemicals and industrial hub being developed in the UAE. Once completed, Reliance and ADNOC's new chemical

plant will produce 360,000 tpy of polyvinyl chloride, 940,000 tpy of chlor-alkali and 1.1 MMtpy of ethylene dichloride. The JV will take FID and begin awarding engineering contracts in 2022.

ADNOC also announced a partnership with **Fertiglobe** to develop the region's first large-scale blue ammonia project. The facility will be in TA'ZIZ next to the Ruwai Industrial Complex, which will provide hydrogen and nitrogen feedstocks to the project. The JV is conducting pre-FEED and FEED work and plans to take FID in 2022. If built, the blue ammonia facility will begin operations in 2025.

Approximately 120 km southwest of Abu Dhabi, ADNOC is investing to expand processing capacity of the Shah gas plant. The more than $500-MM Shah Gas Expansion and Gas Gathering project will increase the plant's processing capacity from 1.28 Bft^3d to 1.45 Bft^3d, as well as expand the existing gas gathering network. The project's EPC contract was awarded to **Saipem.** Completion of the plant and gathering system expansion is scheduled for 2023.

Saudi Aramco planned to develop a $10-B refinery and petrochemical integrated complex in the port city of Gwadar, Pakistan. However, due to inadequate infrastructure, the complex's location will more to Karachi. The project's new location puts it within the center of the China-Pakistan Economic Corridor, a collection of infrastructure projects to strengthen Pakistan's economy.

U.S.

In June, **PBF Energy** announced it has launched a study to possibly convert the Chalmette refinery's hydrocracker—idled since 2010—into a renewable diesel production complex. The cost of the conversion project would be approximately $500 MM.

Chevron Phillips Chemical has awarded an engineering and construction contract to **S&B Engineers and Constructors** for the engineering and construction of the company's hexene-1 plant. Construction of the 266,000-tpy plant, located in Old Ocean, Texas, will begin in 3Q of this year, with completion scheduled for 2023.

Thirumalai Chemicals Ltd.'s subsidiary, **TCL Specialties,** is developing a 40,000-tpy chemical plant in the Marcellus/Utica basins in the northeastern U.S. Phase 1 operations include the production of maleic anhydride, malic acid and fumaric acid. The project's first phase is scheduled to be completed in late 2023.

Genomatica was awarded a technology licensing contract by the **Cargill-HELM** JV. Genomatica will provide its GENO BDO technology for the JV's $300-MM renewable 1,4-butanediol plant in Iowa.

Dow Chemical is investing in an integrated methylene diphenyl diisocyanate (MDI) facility at its Freeport, Texas complex. The project consists of an integrated MDI distillation and prepolymers facility. Once completed in 2023, the integrated complex will enable Dow to increase MDI supplies by 30%. HP

LEE NICHOLS, EDITOR-IN-CHIEF/
ASSOCIATE PUBLISHER
Lee.Nichols@HydrocarbonProcessing.com

HP Global Project Data

Gulf Energy Information's Global Energy Infrastructure database is tracking nearly 1,100 projects around the world, totaling more than $1.8 T in active capital project investments. The Asia-Pacific region dominates in total announced investments at nearly $750 B. The closest contender is the U.S. at $320 B, followed by the Middle East at $280 B. Over the past year, the Asia-Pacific region has led in most new project announcements, equating to nearly 50% of total new project market share. Within the Asia-Pacific region, China and India comprised nearly 70% of new project announcements over the past year. HP

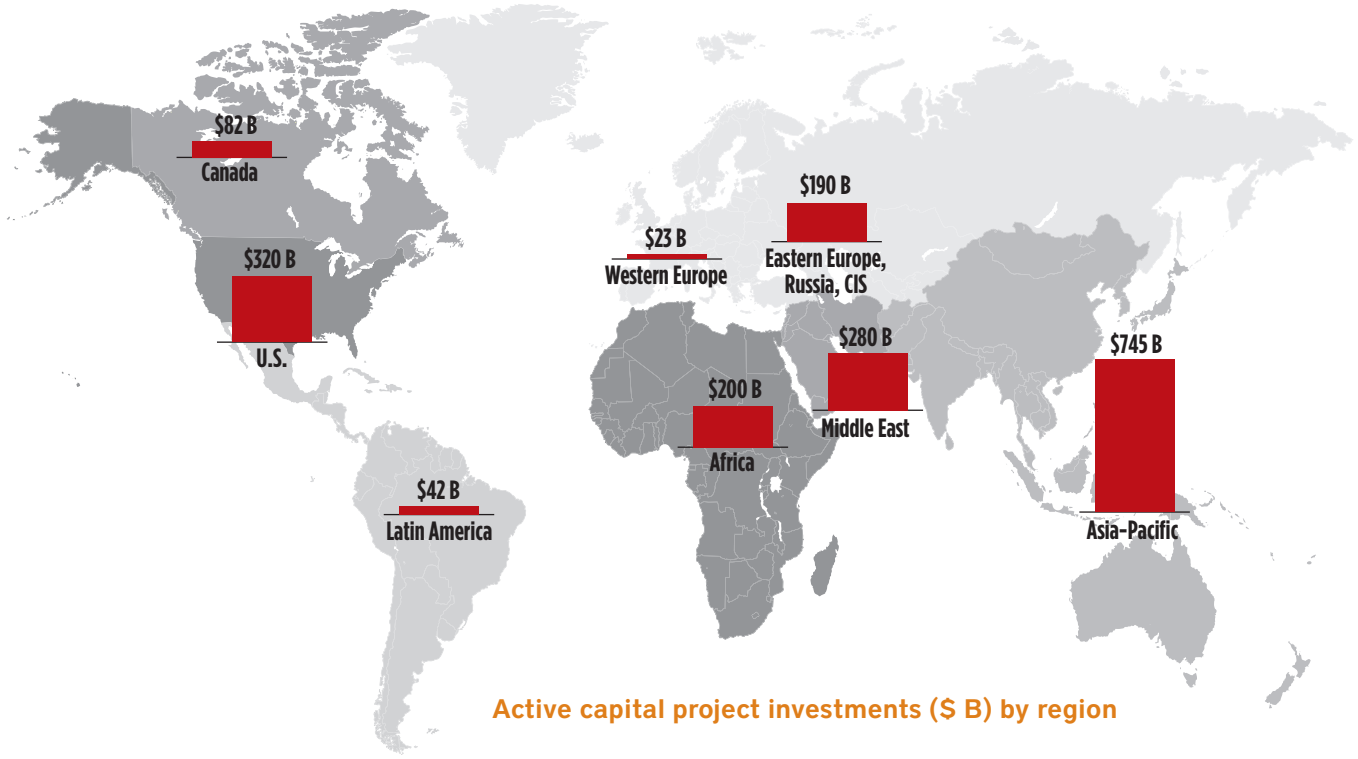

Active capital project investments ($ B) by region

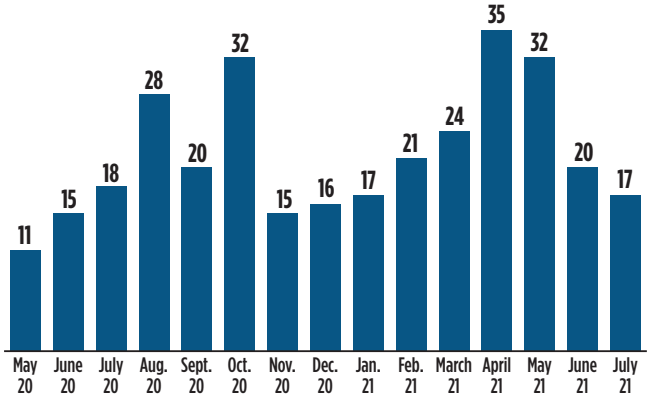

New project announcements, May 2020–July 2021

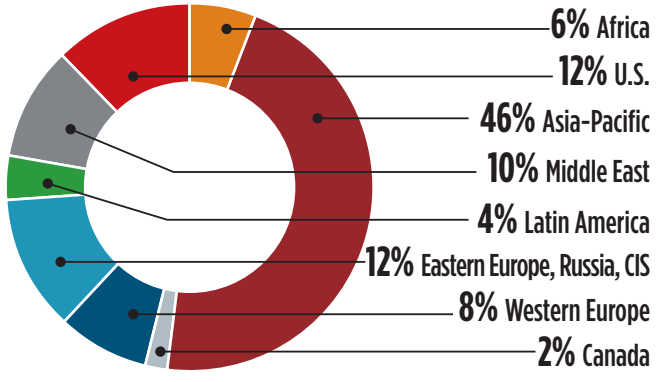

New project market share by region, 2020–2021

Global ENERGY INFRASTRUCTURE
A new market intelligence tool for the international energy industry with project data sets for hydrogen, renewables, global pipelines, LNG and downstream assets. | GlobalEnergyInfrastructure.com

HEINZ P. BLOCH, RELIABILITY/EQUIPMENT EDITOR
Heinz.Bloch@HydrocarbonProcessing.com

ARC spring dampers eliminate compressor instability

A recent book[1] describes novel approaches in applied process gas compressor technology. Among its many topics, the book[1] highlights not only where compressor rotor instabilities can originate, but also how permanent fixes can be designed in from the start and/or retrofitted after a failure event.

Prior art often includes squeeze film damper bearings (SFDs); their underlying principles resemble the well-known shock absorbers in motor vehicles. Although SFD bearings will often prove successful, reliability-related concerns may exist for the elastomeric O-rings installed in most SFDs. Static O-rings will degrade over time due to the loads imposed by the weight of a rotor assembly. It follows that most forms of degradation reduce the effectiveness of the SFD; all too often, such degradation forces an unforeseen shutdown. This brings us to the analogy of shock absorbers plus springs, as used in motor vehicles.

In large compressors, O-ring degradation effects are mitigated by designs that incorporate an ARC spring damper inside each bearing. An ARC spring damper serves to support and center the SFD, although the now lightly loaded O-rings remain in place. FIG. 1A–FIG. 1D show the sequence in which an ARC spring was installed to become part of the overall SFD bearing assembly.

In many recent applications of ARC spring technology, the novel add-on damper supports were designed and manufactured by the compressor manufacturer—in this instance, Dresser-Rand, a Siemens company located in Olean, New York. In several other compressor applications, BRG Machinery Consulting LLC assisted in advancing the ARC spring damper design by using analytical methods and participating in validation tests.

Once installed as shown in FIG. 1, ARC springs eliminated virtually all the rotor and bearing loads on the O-rings, thereby greatly improving the overall reliability of the system. Wired for instrumentation (FIG. 1C and FIG. 1D), a series of rigorous tests provided proof that all three design objectives had been reached by adding well-engineered ARC spring technology to the traditional SFD geometry:[2]

- The basic SFD oil film design should be kept the same
- The ARC spring damper should be designed soft enough to allow motion, yet strong enough to center the bearing cage shown in FIG. 1
- The ARC spring should be sufficiently robust to avoid fatigue failure.

Combining the subject ARC spring with squeeze film dampers in modern compressor bearing systems was demonstrated to be a complete success. It constitutes a permanent remedy to previously encountered instabilities that had led to severe compressor failures. HP

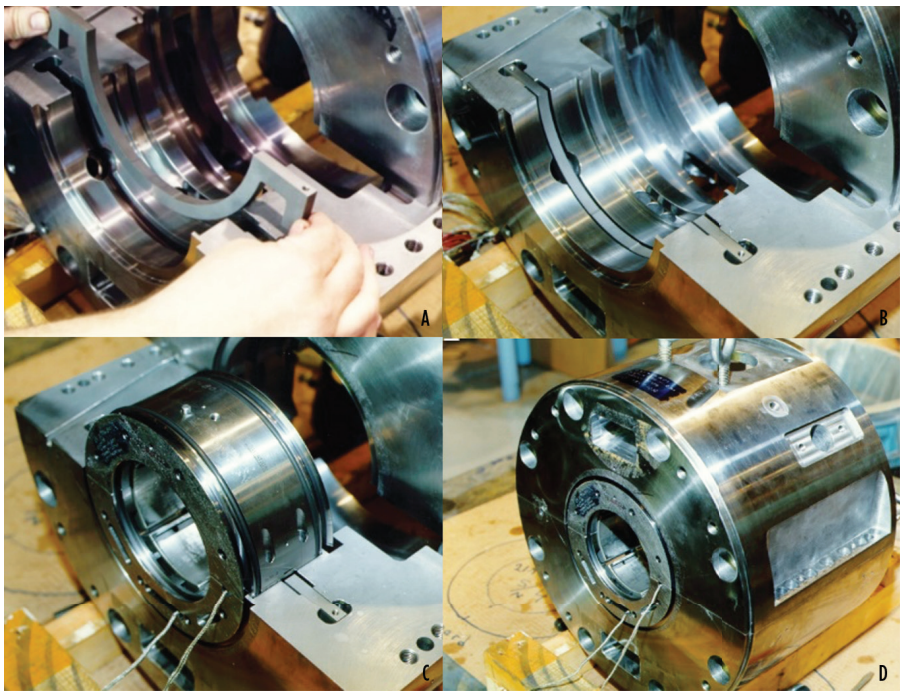

FIG. 1. Installation of an ARC spring damper.

LITERATURE CITED

[1] Elliott, H. G. and H. P. Bloch, *Compressor Technology Advances—2020 and Beyond,* DeGruyter Publishing, Berlin, Germany, 2021.

[2] Kuzdzal, M. J. and J.F. Hustak, "Squeeze film damper bearing experimental vs. analytical results for various damper configurations," Proceedings of Texas A&M University Turbomachinery Symposium, 1996.

HEINZ P. BLOCH resides in Montgomery, Texas. His professional career commenced in 1962 and included long-term assignments as Exxon Chemical's Regional Machinery Specialist for the U.S. He has authored or co-written more than 780 publications, among them 23 comprehensive books on practical machinery management, failure analysis, failure avoidance, compressors, steam turbines, pumps, oil mist lubrication and optimized lubrication for industry. Mr. Bloch holds BS and MS degrees (cum laude) in mechanical engineering from Newark College of Engineering (NCE). He is an ASME Life Fellow and was awarded lifetime registration as a Professional Engineer in New Jersey. He is one of 10 inaugural inductees into NCE's Hall of Fame, which honors its most distinguished alumni.

G. RUIBO, PetroChina Jinzhou Petrochemical Co., Jinzhou, Liaoning, China; and **P. WEI** and **L. YANSHENG,** China University of Petroleum, Beijing, China

Online treatment of a slide valve fault in an FCCU

The regeneration slide valve is a key piece of equipment that controls the ratio of catalyst to oil and reaction temperature in FCC units (FCCUs). Unplanned shutdown caused by slide valve stem fracture is a challenging problem that limits the operational period of FCCUs.

In this article, the reaction–regeneration system in a commercial, 1-MMtpy FCCU was studied to determine the influence of a regeneration slide valve fracture on the key parameters in the regenerated and spent catalyst routes. Double-valve control technology was introduced to manage the slide valve stem fracture without requiring a shutdown. Meanwhile, the axial pressure distribution in the regeneration standpipe and the variation of the reaction temperature in the riser were recorded by adjusting the sensitive aeration nozzles.

Based on the stability of the reaction temperature, the catalyst flow patterns in the vicinity of the regeneration slide valve were divided into packed-bed flow, bubbling fluidized flow and slug flow, respectively. In addition, the operating conditions corresponding to the different catalyst flow patterns were outlined to help guide the operation and adjustment of the FCCU.

Fluid catalytic cracking in China. In 2019, more than 200 FCCUs produced 70 wt% of gasoline, 30 wt% of diesel oil and 10 wt% of propylene in China.[1] The FCCU comprises two main sections: a reactor and a regenerator. The catalyst circulation between the two vessels is carried out in a vertical pipe or inclined pipe, which are collectively referred to here as a standpipe. Electro-hydraulic slide valves are typically installed at the bottom of the standpipe to control the catalyst circulation rate.

The equipment pinpointed for this study are the FCCU riser and combustor.[2,3] Since the standpipe valve system is not involved in the oil and gas cracking reaction or the catalyst regeneration process, few research reports are available on the standpipe valve system. However, this system is prone to failure in commercial FCCUs, which can cause temperature fluctuation and even unplanned shutdown.[4] The FCC slide valve comprises a stem, disc and guide rail, with the stem controlling the opening of the disc. If the stem is broken, then the opening of the slide valve and catalyst circulation rate cannot be controlled, leading to FCCU shutdown.

In November 1994, a 1-MMtpy FCCU suffered a fracture in the regeneration slide valve stem, leading to an unplanned, 5-d shutdown.[5] This article examines a proposed, online treatment technology for the slide valve stem fracture and a method of stability control for reaction temperature. Both measures can be adopted to guide the operation of the unit.

FCCU case study introduction. As shown in **FIG. 1,** the commercial setup for the 1-MMtpy FCCU comprises a reactor and a regenerator. The regenerator encompasses the combustion process and the premixing pipe technology. The riser outlet includes the direct connection technology to shorten the oil-gas reaction time and reduce the secondary cracking reaction. The feed to the FCCU includes vacuum gasoil (33 wt%), coking gasoil (17 wt%) and atmospheric residual oil (50 wt%). To improve gasoline yield, the FCCU utilizes low regeneration temperature and high reaction temperature, and the ratio of catalyst to oil is approximately 8, which is calculated according to the heat balance of the reaction–regeneration system. The key process parameters are shown in **TABLE 1.**

FIG. 2 shows a schematic diagram of the regeneration standpipe structure. An over-

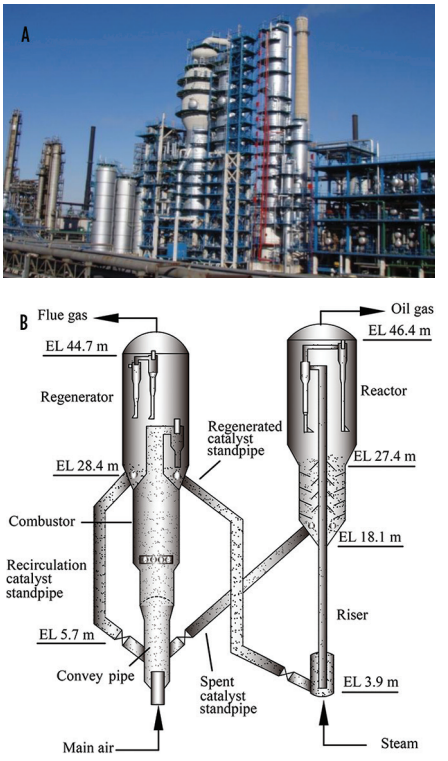

FIG. 1. Schematic diagram of the reaction–regeneration system.

TABLE 1. Operating parameters of the FCCU

Fresh feed flowrate, t × hr^{-1}	130	Temperature of the dense phase bed, °C	670
Reaction pressure, kPa	197	Combustor density, kg × m^{-3}	170
Regeneration pressure, kPa	200	Density of the dense phase bed, kg × m^{-3}	550
Reaction temperature, °C	530	Oxygen content of flue gas, vol%	3
Combustion temperature, °C	685	Ratio of catalyst to oil	8

flow hopper at the entrance of the regeneration standpipe is used to remove large bubbles carried by the descending catalyst. The standpipe consists of the top inclined pipe, the middle vertical pipe and the bottom inclined pipe. To control the stable flow of catalyst, eight aeration nozzles (labeled C1–C8) are installed along the height of the regeneration standpipe. The angle between the eight nozzles and the pipe wall is 45°. The aeration medium of the C1–C7 nozzles is 0.55-MPa plant air, and the aeration medium of the C8 nozzle is 1 MPa plant air and 270°C steam. The aeration rate of each nozzle is controlled by the flow limiting the orifice plate, which has a diameter of 2 mm–3 mm. The pressure at the standpipe entry (in kPa) is *p*i. The pressure above the regeneration slide valve (in kPa) is *p*s. The pressure at the standpipe outlet (in kPa) is *p*o.

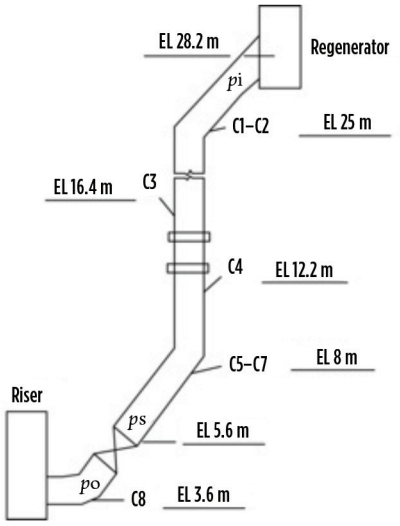

FIG. 2. Schematic diagram of regeneration standpipe.

Analysis of slide valve fault. In December 2019, the operator found that the regeneration slide valve could not be adjusted through the distributed control system (DCS), which caused the reaction temperature to fluctuate sharply. The hand wheel control was used to open the regeneration slide valve, and although the stem of the regeneration slide valve followed the shaking action of the hand wheel, the reaction temperature failed to change. Meanwhile, when the hand wheel was used to close the slide valve, the shaking action became more difficult and the opening of the regeneration slide valve would close.

Based on the described phenomena, a plant engineer determined that the stem of the slide valve had been broken. In September 2020, the FCCU was shut for maintenance. When the cover of the regeneration slide valve was opened, the stem of the regeneration slide valve was found to be broken, as shown in **FIG. 3.** It could be seen that the back side of the slide valve plate was seriously scoured, forming two obvious grooves as shown in **FIG. 3A.** The stem of the regeneration slide valve was worn and fractured as shown in **FIG. 3B,** which was caused by the scouring of the eddy flow field formed by the scavenging steam of the disc guide rail and the catalyst carried by the aeration.[4,5]

FIG. 3. Disc and stem system showing (a) the scoured valve plate and (b) the orifice of the slide valve.

Variation in regeneration catalyst route. The regeneration standpipe has two functions in the FCCU: (1) provide a steady supply of high-temperature catalyst for the riser and (2) establish a material seal above the regeneration slide valve to prevent the mixture of gas and oil. However, due to the stem fracture, the valve plate of the regeneration slide valve could only be closed rather than opened, and the control accuracy of the catalyst circulation rate worsened, which affected the standpipe pressure buildup and reaction temperature (**FIG. 4**). The axial pressure gradually increased along the height of the standpipe, as shown in **FIG. 4A,** which indicated that the catalyst was well fluidized and the standpipe had strong pressure storage.

However, the reaction temperature fluctuated sharply between 507°C and 518°C, as shown in **FIG. 4B.** The fluctuation frequency was high—more than four times per hour. When reaction temperature fluctuates greatly, it not only affects the product distribution but also reduces the gasoline yield. Moreover, it reduces the atomization effect of heavy oil. The amount of unvaporized oil in the riser increases, leading to an increase of coke.

Variation in spent catalyst route. The flow pattern of a stripper is a low-velocity bubbling fluidized bed, and the range of the apparent catalyst density is 700 kg/m^3–800 kg/m^3. When the reaction temperature fluctuates greatly, the unvaporized heavy oil droplets enter the stripper with the spent catalyst, leading to coke formation at high temperature that block the

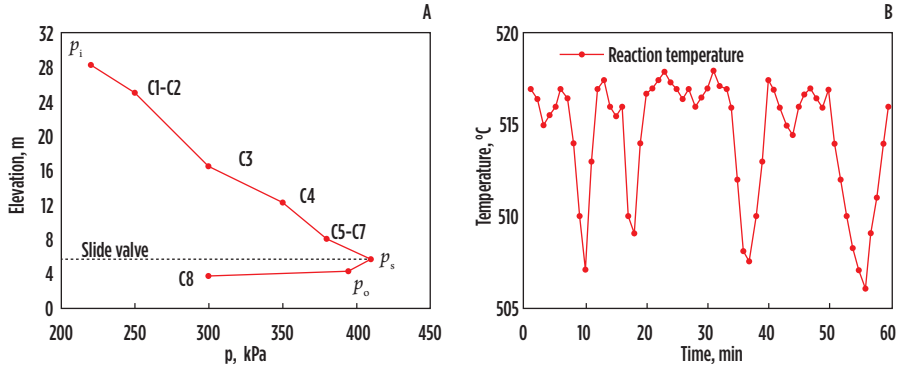

FIG. 4. Regeneration catalyst route parameter profiles: (a) pressure profile of regeneration standpipe and (b) reaction temperature curve.

grids. FIG. 5 shows the variation of key parameters in the spent catalyst route from January to September 2020. The apparent catalyst density in the stripper was 780 kg/m^3 from January to April. It began to decrease in late April, and then decreased to 100 kg/m^3 from July to September, as shown in FIG. 5A.

Meanwhile, the opening of the spent slide valve increased from 37% to 63%, and the pressure drop decreased from 77 kPa to 5 kPa, as shown in FIG. 5B, which indicated that the catalyst flowrate sharply decreased. The decrease in flowrate may have been caused by the coking in the grates, which decreased the catalyst flow area. During plant maintenance in September 2020, the soft coke that had accumulated in the bottom of the stripper grids was removed, revealing that only 20% of the catalyst flow area remained, as shown in FIG. 6.

Proposed treatment. During the stem fracture of the regeneration slide valve, the crude oil processing was negatively impacted. The FCCU needed to operate until September 2020 for shutdown maintenance. To realize stable control of catalyst circulation rate and reaction temperature, engineers carried out much experimental research. Finally, a double-valve control online treatment technology was adopted to solve the problem. In addition, the smooth control of catalyst circulation rate was realized by adjusting the flow pattern of catalyst in the vicinity of the regeneration slide valve.

Double-valve control technology. The double-valve control technology refers to the installation of stems on either side of the slide valve disc for bidirectional driving of the disc, as shown in FIG. 7A. For this device, due to the fracture of the old stem, the valve plate could be pushed only to close rather than to pull open, as shown in FIG. 7B. The technician choose to make a new hole on the regeneration slide valve and set a new stem in the direction opposite the old stem, as shown in FIG. 7C. The new stem was then used with the old stem to control the opening of the slide valve.

Reactor temperature control. The double-valve control technology guaran-

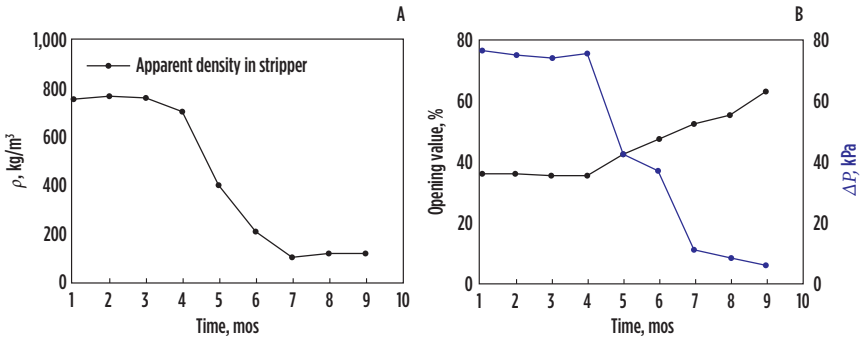

FIG. 5. Parameter profiles of spent catalyst route: (a) apparent density in stripper and (b) opening value and pressure drop of the spent slide valve.

teed the emergency switch of the regeneration slide valve, but the sensitivity to control the catalyst circulation rate was poor, and the reaction temperature still fluctuated. According to the fluidization theory,[2,3] engineers explored the influence of sensitive aeration gas on the reaction temperature. It was found that catalyst flow patterns and amplitude of reaction temperature could be adjusted by changing the aeration rate (Qa, Nm^3/hr) at the C5–C7 nozzles above the regeneration slide valve. **FIG. 8** shows the effect of Qa on the reaction temperature and the opening of the regeneration slide valve.

FIG. 6. Soft coke in grids.

Based on the stability of the reaction temperature, catalyst flow patterns in the vicinity of the slide valve were divided into packed-bed flow, bubbling fluidized flow and slug flow. In the packed-bed flow, Qa was only 30 Nm^3/hr. The opening of the regeneration slide valve was large, around 50%, but the reaction temperature was stable and the fluctuation was 510°C–515°C.

Reaction temperature increased with the increase of Qa. When Qa was 60 Nm^3/hr, packed-bed flow varied with the bubbling fluidized flow. The reaction temperature increased to 518°C–523°C, and the opening of the regeneration slide valve decreased to 40%. The catalyst was fluidized well in the vicinity of the slide valve, and the standpipe driving force was strengthened. When Qa was larger than 90 Nm^3/hr, the reaction temperature and the opening of the slide valve fluctuated significantly within the ranges of 510°C–527°C and 35%–70%, respectively. This phenomenon indicated that large bubbles appeared in front of the slide valve, referred to as the slug flow.

FIG. 9 shows the effect of Qa on the axial pressure distribution in the regeneration standpipe. The pressure distribution above the C4 cross-section was not affected by Qa, but the pressure above the slide valve increased first, and then decreased with the increase of Qa, indicating that the pressure drop of the standpipe and the catalyst circulation rate in the packed-bed flow and slug flow were lower than that in the bubbling fluidized flow. During the production process, the operating parameters and catalyst flow pattern should be adjusted in time, according to the reaction temperature fluctuation. The packed-bed flow above the slide valve is suitable for low-load condition. The bubbling fluidized flow is suitable for high-load condition, and the slug flow is the most difficult to operate. When the reaction temperature fluctuates greatly, the aeration rate above the slide valve should be reduced in time.

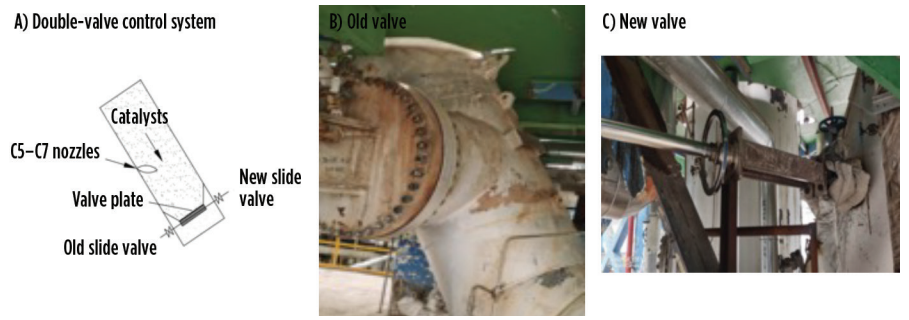

FIG. 7. Double-valve control technology.

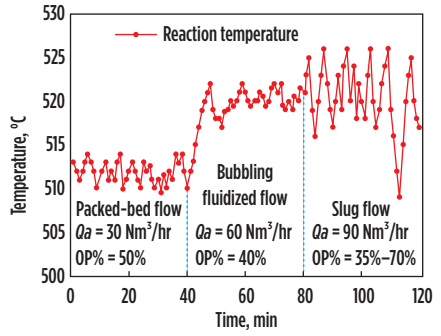

FIG. 8. Effect of aeration rate on reaction temperature.

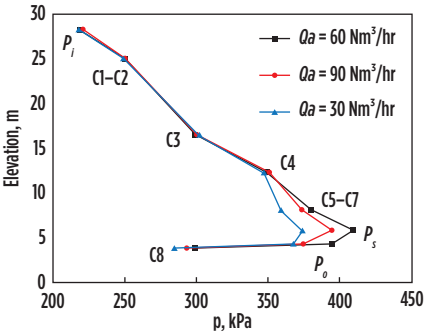

FIG. 9. Effect of aeration rate on pressure distribution.

Takeaway. This article introduced a double-valve control technology for the FCCU to realize the online treatment of a stem fracture in a slide valve, prolong the operation cycle of the FCCU and avoid an unplanned shutdown. By adjusting the aeration rate, the influence of sensitive aeration gas on the reaction temperature and the opening of the slide valve was explored, and stable control of the reaction temperature was realized. HP

ACKNOWLEDGMENTS

The authors acknowledge support by the Research Foundation of the Karamy Campus of the China University of Petroleum in Beijing (grant number RCYJ2016B-02-001). The authors also acknowledge financial support from CNPC's Technical Talents Innovation Foundation Project (2021).

LITERATURE CITED

[1] Leung, L. S. and L. A. Wilson, "Down flow of solids in standpipes," *Powder Technology*, Vol. 7, 1973.
[2] Zhao, Z. H. and X. D. Ye , "Chinese FCCU revamp improves performance," *Oil &Gas Journal*, Vol. 99, Iss. 46, 2001.
[3] Wolschlag, L. M. and K. A. Couch, "Upgrade FCC performance," *Hydrocarbon Processing*, September 2010.
[4] Knight, J. and R. Mehlberg, "Maximize propylene from your FCC unit," *Hydrocarbon Processing*, September 2011.

GAO RUIBO is a Process Engineer for catalytic cracking in the petrochemical branch of PetroChina. He has been engaged in process technology management of the FCCU for 13 yr, during which time he has carried out a number of technical renovations of the FCCU.

PENG WEI is a Process Engineer for catalytic cracking in the petrochemical branch of PetroChina. He holds a PhD in chemical engineering from China University of Petroleum.

LIU YANSHENG is a Professor of chemical engineering at China University of Petroleum in Beijing. He has worked in the chemical engineering field for more than 30 yr and is responsible for the technical revamp of several FCCUs.

M. BADUGHAISH, Saudi Aramco, Dhahran, Saudi Arabia

Case study: Reliability of low-flow, high-head pumps

Pumps are one of the key elements used in different industries, including oil and gas, petrochemicals and water treatment. Their range of applications is very wide and process requirements mandate the use of specific types and designs. Due to that wide range, it sometimes becomes challenging to select the right pump design that fits some applications.

One such application is the low-flow, high-head (LFHH) pump, which requires the use of low specific speed designs, which are commonly known by their sensitivity to operate within a wide operating range due to the narrow operating window from their best efficiency point (BEP). This makes the reliability of low specific speed pumps questionable. However, acknowledging the reliability concerns of these pumps does not relieve end users from the responsibility of carefully specifying the right process parameters prior to purchasing the pump and then operating it properly.

This article discusses an investigation into high-speed integrally geared pumps in a gas processing plant. These pumps are used to transfer hydrocarbon condensate—since commissioning, they suffered from high vibration and frequent premature mechanical seal failures. Consequently, the end user was seriously considering replacing the pumps due to their low reliability and mean time between repairs (MTBR).

Before diving into the investigation findings and recommendations, it is important to provide the reader with the design parameters of these pumps to better understand the case. The three integrally geared pumps (OH6) are designed to pump 63 gal/min of light HC condensate (0.51 relative density and 383 psia vapor pressure) and discharge with a pressure of approximately 600 psia (the pump rated differential head is 1,058 ft). The pump is rotating at 6,980 rpm. Two pumps are normally in parallel operation and the third is used as a standby. The pumps are designed with a dual unpressurized seal with API flushing Plan 11 and leak detection Plan 76.

Repair shop findings. One pump was removed to the repair shop for internal inspection. It was observed that the seal flush Plan 11 had multiple orifices (orifice pack) with a small orifice size of about 1 mm, as shown in **FIG. 1.** This is considered a small size to provide sufficient cooling for the seal. In addition, a noticeable amount of dirt upstream of the orifice was found that could have blocked the flushing line. The elasticity of all seal and pump O-rings was affected. **FIG. 2** shows that they were found to be hard and cracked, which is an indication of elastomers overheating. The O-ring of the primary seal was also found to be cut, shown in **FIG. 3.** An extrusion indicated an incorrect installation. The last observation detailed in the internal inspection was the orifice size of the seal leak detection line. It was found to be very small (< 0.5 mm). According to API 682, all orifices must have a minimum bore of 3 mm. **FIG. 4** shows the small orifice size of the seal leak detection line.

Site findings. As mentioned earlier, these pumps were designed for light flashing hydrocarbon, so the seal and seal leak detection system had been selected on that basis. The pumps were designed with dry running backup seals and API Plan 76, assuming that only gas would be seen by the seal cavity. However, it turned out that the process was not only light hydrocarbons, but contained traces of heavy products, as well.

Part of the leaked product through the primary seal to the seal cavity remained in liquid form and continued accumulating. Leak detection Plan 76 for these pumps is supposed to direct the gas to the flare header and does not account for liquid presence to be drained—the liquid level was increasing, and it was noticed that liquid was leaking from the seal leak pressure transmitter port of Plan 76. During another site observation, it was determined that individual permanent suction strainers were installed on the suction lines with 1.5-mm opening sizes. There was no differential pressure transmitter across the strainers to alert plant personnel of any blockage during operation.

Furthermore, the pumps' operating data were reviewed over an extended period of time (7 mos). The data showed that each pump was operated between 15 gal/min and 120 gal/min, which is a very wide operating range for a pump

FIG. 1. Orifice size for API flushing Plan 11.

FIG. 2. Pump and seal O-rings.

FIG. 3. Cut on primary seal O-ring.

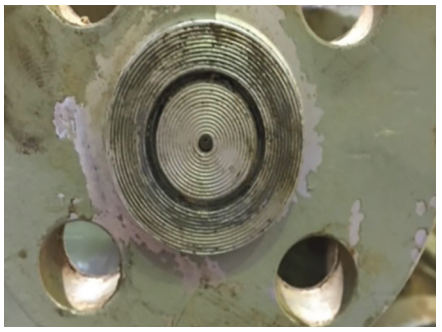

FIG. 4. Extremely small orifice bore size of the seal leak detection line.

with a rated capacity of 63 gal/min (which is also the BEP for these pumps). This far exceeded the allowable operating range, which should be 22 gal/min–75 gal/min. This indicates how severely the pumps were operated. The data also showed that this off-design operation was for an extended period of time, and that this kind of operation was for more than 10% of the extracted data duration.

It is known that operating outside the allowable operating window results in reliability issues, an increase of vibration levels and consequently frequent seal failures, which are what these pumps were experiencing. This is an indication of a poor controlling system. Therefore, the controlling system of these pumps was evaluated, and it was discovered that there was only one common flowmeter and one common recycle line. For such a parallel operation system, the individual controlling system (flow monitoring and recycling) provides more reliable operation and prevents such extreme off-design running.

Recommendations. From the above, it was clear that some modifications were required to improve how the pumps are operated and controlled considering the actual site condition. The pump vendor was consulted to increase the orifice bore size of the flush line from 1 mm to 2 mm, considering that the existing suction strainer size will prevent larger particles from blocking the orifice. This was accepted considering the differential pressure and required flow across the orifice during pump operation at higher flowrates. For the seal leak detection system, it was recommended to change Plan 76 to Plan 75 to prevent liquid from accumulating inside the seal cavity. Since changing the seal leak detection plan was a major work and would take time to implement, a short-term solution was provided. It was recommended to install a temporary drain for the seal cavity to allow plant operators to empty any liquid accumulation, as shown in **FIG. 5.**

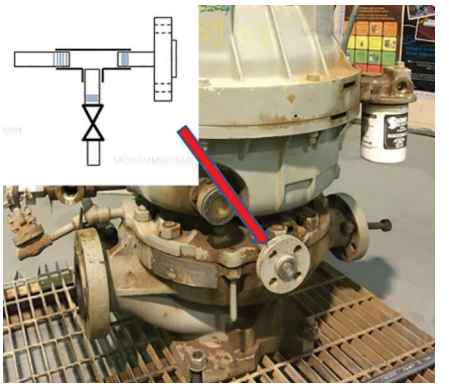

FIG. 5. Temporary port to allow seal cavity draining.

It was also recommended to install differential pressure transmitters across the pump suction strainers. Considering the strainers' opening size and the amount of particles carried out with the process, it is always recommended to monitor the strainer condition to prevent severe blockage and net positive suction head (NPSH)-related issues.

It was also important to address the controlling system deficiencies of these pumps. As mentioned above, this is a parallel operation mode controlled by a common flowmeter and a common recycle line. It was recommended to reconfigure the controllers' settings for low-/high-flow and recycle line control valve action to consider the number of pumps in operation. For example, the minimum flow setpoint should be different if one pump or two pumps are running.

Takeaway. It is true that low specific speed pump designs are relatively more sensitive than other designs and require more diligence in operation and controlling. It is important for end users to thoroughly evaluate the process needs and specifications before procuring these pumps and their auxiliary systems. Investing in a good controlling system can easily achieve a payback when considering equipment reliability and availability aspects. HP

MOHAMMED BADUGHAISH is a Mechanical Engineer with 12 yr of experience in rotating equipment within the oil and gas industry. His work experience has focused on hydraulic pumps, troubleshooting and maintenance. He works as a pump engineer in Saudi Aramco's Consulting Services Department. He obtained his BS degree from King Fahd University of Petroleum and Minerals (KFUPM) and an MS degree in mechanical engineering from the University of Central Florida.

S. HUNSICKER, Swagelok, Solon, Ohio

Keeping fugitive emissions costs down with low-E valves

Fugitive emissions have become an increasingly critical area of interest for chemical processing and refining facilities. If left unmitigated, these uncontrolled leaks can be detrimental to a facility's bottom line—and not just in the form of lost system gases that can lead to waste. Fugitive emissions can also lead to fines if the facility is found to be noncompliant with current emissions regulations.

With the U.S. Environmental Protection Agency (EPA) and other regulatory bodies reaching agreements with companies to reduce fugitive emissions, it is imperative to increase understanding of these potentially costly leaks and to understand how to mitigate them within a plant's fluid systems. Being proactive is critical, as part of the solution may require altering supply chains and upgrading systems. This article explores some essential strategies for actively addressing fugitive emissions to help reduce leaks, maintain compliance and keep costs low.

Fugitive emissions essentials. Fugitive emissions most often result from leaking process equipment, leading to the unwanted escape of volatile organic compounds (VOCs). These VOCs can include, but are not limited to gases such as benzene, methane and isopentane. When released, these substances endanger air quality and form ozone, which is why governmental regulatory bodies aim to control fugitive emissions. Plants that violate emissions regulations can have large fines levied on them, so it pays to remain in compliance (**FIG. 1**).

Often, the major sources of fugitive emissions—accounting for nearly 62% of the release of uncontrolled VOC emissions at a typical plant—are the dynamic and static seals on valves, pumps and flange connections. To combat fugitive emissions, facilities can install low-emissions (low-E) valves, which testing has proven will conform to low emissions standards. Sometimes, purchasing low-E valves is even mandated under a consent decree between the EPA and a processing plant, often as the result of a civil case.

EPA consent decrees. The role of the EPA in enforcing environmental requirements, laws and regulations (including U.S. laws like the Clean Water Act and the Clean Air Act) is clear. When voluntary compliance is impossible, the EPA can turn to the courts to make sure that plants comply with the applicable laws and/or regulations.

For chemical plants and refineries, the most common enforcement mechanism that the EPA will use is called a consent decree. A typical consent decree requires plant owners and operators to take specific actions to improve their fugitive emissions problems within a specified amount of time. If a plant does not meet these requirements, then civil penalties—including heavy fines—often follow.

Although refineries and processing plants have many available avenues to mitigate fugitive emissions, consent decrees will often require a plant to establish an enhanced leak detection and repair (LDAR) program. They can also mandate that the plant uses low-E valves in the future.

Enhanced LDAR tactics and low-E valves. Rigorous LDAR strategies are designed to mirror the leak detection and oversight methods that the EPA uses. In the case of valves, EPA audits include paper audits and field testing to quantify

FIG. 1. The presence of bubbles during a leak test can reveal fugitive emissions escaping from valves. Technicians should be trained to decide whether to tighten or replace the fitting connection.

the levels of fugitive emissions. Once the leaks are identified, the plant will usually implement one or a combination of the following methods to reduce fugitive emissions levels:

- Institute a comprehensive plan whereby leaks are identified through in-situ testing of valves and other connections using EPA Method 21
- Identify, document and repair leaks within a defined time frame
- Lower allowable leak limits for valves, connections and pumps.

Improved LDAR strategies often also include the stipulation that any new valves installed must be low-E valves. Interestingly, there is often no single specified method for determining what a low-E valve is in the EPA consent decrees—that determination is left up to the processing plant or refinery in question. In most cases, there are several options for deciding what a low-E valve is, and it frequently encompasses the plant accepting one of the two following methods for classifying valves as low-E:

1. A written guarantee that the valve will not leak above 100 parts per million (ppm) for 5 yr
2. A written guarantee, certification or equivalent documentation stating that the valve has been tested pursuant to generally accepted good engineering practices and has been found to be leaking at no greater than 100 ppm.

Valves certified as "low-E" are ideal to reduce fugitive emissions, whether they are specified for a new system or added to enhance an LDAR program. Installing low-E valves before the EPA finds high fugitive emission levels can save plants significant money by avoiding costly refits.

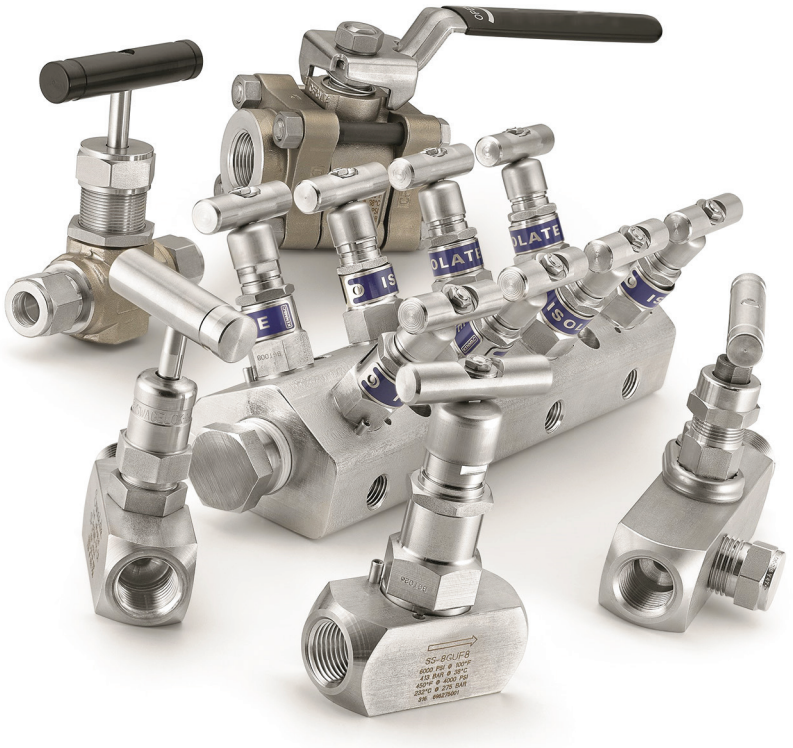

FIG. 2. Installing low-E valves before the U.S. EPA finds high fugitive emissions levels can save plants significant money in the long run by avoiding costly refits.

It can be challenging to understand the difference between those two options, so the following will examine them in greater detail, highlighting both the advantages and disadvantages of each.

Written guarantee by the manufacturer. To document the purchase of low-E valves, a plant could have the manufacturer provide a written guarantee that the valves will not leak more than 100 ppm for 5 yr. However, the problem with this idea is that the plant operator needs to think about what will happen if the valves do leak. Will any compensation be involved, or will the manufacturer simply replace the leaky valve? Can the plant operator recoup the costs associated with the valve replacement?

If the leakage incident triggers an EPA-levied fine (which can often be as high as $10,000/d per incident), what recourses would the plant operator have to cover all the costs involved? Would the manufacturer cover these costs, as well? Many uncertainties are involved with a manufacturer's guarantee, especially when tests exist that can reveal if valves are working as promised.

Low-emissions testing. Industry associations like the American Petroleum Institute (API) and the International Standards Organization (ISO) have developed actual tests to certify valves as "low-emissions" equipment. These tests include the following:

- **API 624, Type Testing of Rising Stem Valves Equipped with Graphite Packing for Fugitive Emissions:** This test covers rising stem valves, using methane as the test media. The valve must perform 310 cycles, along with three thermal cycles (where the valve is tested at ambient temperature, at an elevated temperature, and then again at ambient temperature), with a leak rate under 100 ppm methane.
- **API 641, Testing of Quarter-Turn Valves for Fugitive Emissions:** This testing involves ball valves, using methane as the test media. Each valve tested must perform 610 cycles, along with

three thermal cycles, with a leak rate of less than 100 ppm methane.

- **ISO 15848-1, Industrial Valves—Measurement, Test and Qualification Procedures for Fugitive Emissions:** This standard provides the procedures and requirements for the mechanical and thermal cycle testing of valves, with leak tests at various points. Methane or helium is used as test media.

Unlike the uncertainty involved in standard manufacturers' guarantees, the API's test results are simple to discern: They are either pass or fail, meaning that the valve is clearly delineated as low-E or not. However, those purchasing low-E valves should understand that the ISO test methodology is more complicated, with different "class" ratings that reflect how the valves perform during testing.

For example, ISO standards allow class ratings of valves as low-E that do not meet the "100 ppm or less" threshold that the EPA requires. Tightness Class CM, for example, can mean that a valve can leak more than 100 ppm methane, but less than 500 ppm methane.

In addition, the ISO 15848-1 standard states that there is no correlation intended between tightness classes when the test fluid is helium (classes AH, BH and CH) and when the test fluid is methane. In part, this is because the data collected is different depending on which fluid is used. For helium, ISO reports the results as the leak rate proportional to the stem diameter in atmospheric cubic centimeters per second (atm cm^3/sec). Since it is not reported in the more traditional "ppm" metric, this makes it difficult to determine whether the valves comply with the EPA's "100 ppm or less" standard if helium is used. Unfortunately, it is impossible to convert atm cm^3/sec to ppm because no formula exists.

Finally, third-party laboratories should conduct the tests, instead of the valve manufacturers themselves. Plant operators can feel confident that tests handled by independent third parties are not biased in any way. Therefore, manufacturers should provide valve certifications that include a seal from the third-party lab, along with the testing location and the results.

Get ahead of emissions requirements. Valves that are certified as "low-E" are ideal to reduce fugitive emissions, whether they are being specified for a new system or being added to enhance an LDAR program. Installing low-E valves before the EPA finds high fugitive emissions levels can save processing plants significant money in the long run by avoiding costly refits (**FIG. 2**). The valves also allow facilities to remain compliant with current environmental best practices. Therefore, it is helpful to ensure that plant personnel know which valves to order for low-VOC service, so that the plant can maintain operational and environmental integrity. When assistance is needed in determining what low-E solutions might work best for specific applications, it is best to consult with an experienced fluid system specialist to secure third-party-tested solutions that will keep the facility in compliance. HP

SEAN HUNSICKER is a Market Manager for Swagelok.

S. ZARDYNEZHAD, TurboTech Consulting Corp., Calgary, Alberta, Canada

Dual-mechanical seal arrangement for hot pump service

Selecting mechanical seals for hot services in an oil refinery or petrochemical plant is always a challenging task—and it is a task that needs careful attention, since the wrong seal selection can have a significant impact on pump reliability and availability. Hot pumping services include liquid temperatures above 175°C (347°F); however, this article includes lessons learned based on liquid temperatures of more than 200°C (392°F). This work is based on the author's experience in dual mechanical seal arrangement selection for large-scale hydrocarbon processing plants.

Mechanical seal categories, types and arrangements. The seal configurations covered by the API 682 standard[1] are classified into three arrangements (i.e., 1, 2 and 3). The definitions of these arrangements are detailed in **TABLE 1.** Arrangement 2 and Arrangement 3 seals are classified in three orientations: face-to-back (FB), back-to-back (BB) and face-to-face (FF); however, Figure 3 in API 682 shows only an FB configuration for Arrangement 2. **FIG. 1** shows three configurations based on Arrangement 3 as per API 682.

Arrangement 2, which is used in API Plan 52 (unpressurized), is not a suitable plan for hot pumping services due to the risk of leakage in the primary seal. In addition, this arrangement has low cooling efficiency, and, since it is connected to the plant's flare system, the back pressure from the flare system may cause an issue for the pump mechanical seal during operation. This article includes several lessons learned using Arrangement 3 (pressurized) for hot pumping services. The following will examine the differences between the three arrangements shown in **FIG. 1.**

Comparison of configurations. Comparisons of the three different configurations in **FIG. 1** are detailed in **TABLES 2, 3, 4** and **5.**

The installed population of Arrangement 3 seals arranged in series (3CW-FB) is relatively small vs. other configurations (3CW-FF and 3CW-BB) as per API 682. However, recently, by new modification, the FB design is more popular. Both BB and FF configurations (3CW-BB and 3CW-FF) potentially offer more compact designs, and can provide higher levels of performance in clean services. However, the FB series configuration is preferred because any abrasive contamination is centrifuged out and, therefore, has less effect on the inner seal. In the event of loss of barrier fluid pressure, the seal will behave like an Arrangement 2 seal.

Cost of using API Plan 32, Arrangement 3 FB configuration. The following will show how to calculate the cost of using Plan 32 in an FB configuration. Assume that light vacuum gasoil (LVGO) is selected as the seal flush—i.e., Plan 32 for a bearing pump with two sets of dual mechanical seals. If the minimum flush liquid is specified as 20 l/min for each mechanical seal in the seal drawing, then each pump needs 40 l/min. If the pump runs continuously for 300 d/yr, then the pump needs 40 l/min × 60 min × 24 hr × 300 d. This equals 17,280,000 l or approximately 109,000 bbl/yr.

Assuming that the cost of LVGO is equal to $30/bbl, then using LVGO as Plan 32 would cost $3.27 MM/yr for each pump. The same amount should be considered for the hot standby pump, because the inner seal of the standby pump

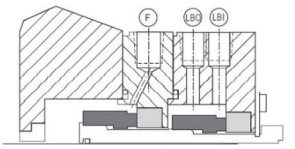

A) 3CW-FB, contacting wet seals in a face-to-back configuration

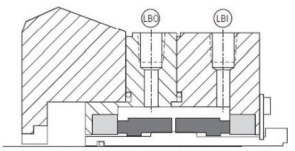

B) 3CW-BB, contacting wet seals in a back-to-back configuration

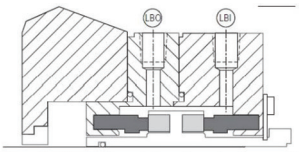

C) 3CW-FF, contacting wet seals in a face-to-face configuration

FIG. 1. Mechanical seal Arrangement 3 per API 682.[1]

TABLE 1. Mechanical seal arrangement definitions per API 682.1

Arrangement	Definition	API plan
1	Seal configurations having one seal per cartridge assembly	Different API plans can be used
2	Seal configuration having two seals per cartridge assembly, with the space between the seals at a pressure less than the seal chamber pressure	52 (unpressurized)
3	Seal configuration having two seals per cartridge assembly, utilizing an externally supplied barrier fluid at a pressure greater than the seal chamber pressure	53 and 54 (pressurized)

TABLE 2. Mechanical seal configuration definition per API 682: Arrangement 3

Configuration	Definition	Pumping liquid	Barrier liquid	External seal flush (e.g., Plan 32*)	Operating expenditure (OPEX)	Abrasive service	Remark
Face-to-back (**FIG. 1A**)	One mating ring is mounted between the two flexible elements, and one flexible element is mounted between the two mating rings	On the outer diameter (OD) of the inner seal	On the inner diameter (ID) of the inner seal and OD of the outer seal	Required	High, due to the use of Plan 32; calculate cost/yr before ordering	Highly effective	API 682 prefers FB- Clause 7.3.3.2.1. Thermal movement/ misalignment of the seal gland will impact the outer seal performance.
Back-to-back (**FIG. 1B**)	Flexible elements are mounted between stationary rings	On the ID of the inner and outer seals	On the OD of the inner and outer seals	Not required	–	Not suitable	If specified by purchaser, Clause 7.3.3.2.1. Thermal movement/ misalignment of the seal gland will impact the outer seal performance.
Face-to-face (**FIG. 1C**)	Both mating rings are mounted between the flexible elements	On the ID of the inner and outer seals	On the OD of the inner and outer seals	Not required	–	Not suitable	If specified by purchaser, Clause 7.3.3.2.1. Thermal movement/ misalignment of the seal gland will impact the outer seal performance.

* Plan 32: A clean and cool seal flush is injected into the seal chamber from an external source. Piping Plan 32 is used in services containing solids or contaminants, for which a suitable cleaner or cooler external flush will improve the seal environment. It is also used to reduce flashing or air intrusion (in vacuum services) across the seal faces by providing a flush that has a lower vapor pressure or that will raise the seal chamber pressure to an acceptable level. Refer to API 682 for more explanation.

TABLE 3. Inner seal cooling effectiveness: Arrangement 3

Configuration	Inner seal cooling effectiveness	Hot services application
Face-to-back (**FIG. 1A**)	Cooling of the inner seal is done by an external clean source (e.g., Plan 32). This significantly impacts OPEX, as the volume of seal flush is normally high.	Yes; however, the cost of Plan 32 is high
Back-to-back (**FIG. 1B**)	The barrier liquid return port is far from the inner seal faces' interfaces. Normally, the location of the barrier liquid in/out ports are near the outer seal ring. This causes the inner seal faces to not receive enough cooling where high heat generation is created with SiC-SiC hard rings at the inner seal.	No, due to poor inner seal cooling
Face-to-face (**FIG. 1C**)	The barrier liquid return port is close to the inner seal faces' interfaces. Normally, the location of the barrier liquid in/out ports are near both seal rings. This causes both the inner and outer seal faces to not receive enough cooling. Using a face-to-face arrangement, the barrier fluid does not have to flow and travel as far to reach the sealing interface of the mating rings. This will improve the efficiency of the seal face cooling, resulting in a significant reduction of heat generation.	Yes; however, it is not recommended in abrasive and dirty services

TABLE 4. Flexible element (i.e., bellows) location: Arrangement 3

Configuration	Location
Face-to-back (**FIG. 1A**)	Face-to-back configuration has rotary bellows in hot service. The rotary bellows have risk of fatigue failure due to cyclic loading when running in hot services.
Back-to-back (**FIG. 1B**)	Back-to-back configuration has rotary bellows in hot service. The rotary bellows have risk of fatigue failure due to cyclic loading when running in hot services.
Face-to-face (**FIG. 1C**)	Face-to-face configuration has stationary bellows in hot service. Using stationary bellows will help for hot service pumping where risk of thermal distortion is high. This is also the best option for absorbing misalignment, as the bellows are fixed and only need to move once to adjust to pump misalignment and not with shaft every rotation. This will help reduce cyclic loading and prevent fatigue failure of the bellows, especially in hot and dirty services.

should be kept cool during hot standby conditions, as well.

Risk of coking the outer seal. In the presence of high temperatures, hydrocarbons and barrier liquid can cause a chemical breakdown or oxidation of the hydrocarbon. Coke is a black, hard, grainy material buildup on the atmospheric side of the seal face. This buildup comprises thermally decomposed hydrocarbons that is converted to a varnish, lacquer or abrasive sludge. Heavy coke buildup can decrease the unit loading on the seal faces and cause excessive leakage. Coking will change the balance ratio of the mechanical seal and also can cause hang-ups of the mechanical seal. Coking is normally found on the atmospheric side of the seal faces.

To reduce risks of coking, the following operations are recommended:

- Reduce seal cavity temperature by using a proper plan and seal design.
- Remove the oxygen from the atmospheric side of the seal faces by adding a quench (e.g., API Plan 62) with dry steam or nitrogen. Dry steam removes the oxygen and will wash away residue; however, a nitrogen quench only removes oxygen but will not wash away residue. Do not use

TABLE 5. Advantages and disadvantages of Arrangement 3

Configuration	Advantages	Disadvantages
Face-to-back (**FIG. 1A**)	• Pumping liquid on the OD of the seal faces • Abrasive contamination is centrifuged and has less effect on the inner seal • High performance in dirty services • Low risk of solids accumulation on the faces, and low risk of hangups • Pressure reversal capability: In the event of a loss of barrier fluid pressure, the seal will behave like an Arrangement 2 seal	• Poor cooling of the inner seal by the barrier liquid • Restricted seal chamber dimensions, and the resulting cartridge hardware construction can affect the ability of the barrier fluid flush to adequately cool the inner seal • Inadequate cooling of the inner seal can result in reduced seal reliability • Use of external seal flush for inner seal cooling • Higher OPEX
Back-to-back (**FIG. 1B**)	• Greater use worldwide • Higher levels of performance because of the barrier fluid cooling due to flowing over both inner and outer seals • No need for external flush	• Process liquid is on the ID of the seal faces • Low performance in dirty services because any entrained abrasive solids will be centrifuged into the seal faces with the potential for damage • A dead zone underneath the inner seal creates susceptibility to solids accumulation • Poor pressure reversal capability
Face-to-face (**FIG. 1C**)	• Greater use worldwide • Higher levels of performance because of the barrier fluid cooling due to flowing over both inner and outer seals • No need for external flush	• Process liquid is on the ID of the seal faces • Low performance in dirty services because any entrained abrasive solids will be centrifuged into the seal faces with the potential for damage • A dead zone underneath the inner seal creates susceptibility to solids accumulation • Poor pressure reversal capability

wet steam, which can cause further seal problems.
- Select the proper type of barrier liquid, with a viscosity range and temperature as per API 682.

Recommendations. The following are recommended for mechanical seal selection in hot pumping applications:
- Ask a process engineer to clarify the condition of the pumping liquid in terms of coke, particles, corrosive elements, etc.
- Ask the vendor to design the seal based on the maximum temperature and pressure.
- Always use pressurized dual mechanical seals (i.e., API Plan 53B, 53C or 54).
- Check the seal drawing, and make sure that both the inner and outer seals are effectively cooled. It is recommended to add a flow guide to promote more turbulent flow around the inboard faces to keep the barrier fluid from burning and coking at the faces.
- Check the seal design and ensure that it promotes barrier fluid circulation for enhanced cooling. Additionally, check that the outer seal has reduced heat generation.
- Check the risk of coking formation at the outer seal and add API Plan 62 where needed.
- Check that the barrier fluid does not have to travel far to reach the sealing interface, and that the barrier liquid inlet and outlet port center and orientation are compared to the seal ring interfaces.
- Utilize stationary bellows to help the seal handle the pump's thermal distortion. An FF design with a stationary bellows assembly is also best for accommodating misalignment, as the bellows only need to move once to adjust to pump misalignment and not with every rotation. This will help reduce misalignment in cyclic loading, and will also help prevent the risk of bellows fatigue failure.

- Ask the vendor to use a bellows design featuring a high-temperature, corrosion-resistant metal, and to review the bellows material. Ensure that the seal faces remain parallel to each other, even over a wide variety of temperatures, as this helps to reduce thermal distortion.
- Calculate the cost of using Plan 32 in an FB configuration. If an FB configuration must be used, select an effective seal flush liquid with a lower cost, if possible.
- Ask the vendor to provide a seal simulation calculation to check the effect of API Plan 32 on seal cooling. Compare the seal temperature condition with and without using Plan 32.
- Always check the accuracy of the flowmeter, pressure and temperature gauges used in Plan 32. Use separate flowmeters and gauges for each cartridge.
- Make sure there is always a stable supply of seal flush. Check the risk of back pressure and fluctuation in the seal flush.
- Use stainless-steel piping material for Plan 32 as much as possible.
- Ensure that there is no misalignment between the pump casing and the seal gland and cartridge.
- Measure and confirm the thermal grout of the nozzle, piping and pump casing/pedestal.
- Consider the effects of coke formation in the mechanical seal during balance ratio sizing. Vendors design seal faces with a balance ratio to minimize heat generation between seal faces. This seal ratio also impacts seal faces' opening and closing forces.
- Remember that, per API 682, the most desirable viscosity for hydrocarbon barrier/buffer fluids is between 2 mm^2/sec (2 cSt) and 10 mm^2/sec (10 cSt) at operating temperature.
- Consider the auto-ignition temperature of the barrier liquid to prevent risks of fire in case of an outer seal failure.
- Consider that using diamond against silicon carbide instead of SiC-SiC rings could result in a reduction of friction by more than eight times. This reduction would mean significantly less heat generated at the seal faces and would help prevent coking. This would lower the heat load of the seal and would help Plan 53B, 53C or 54 perform better.
- Consider that a diamond coating will provide less heat generation and better abrasive resistance. However, it will also substantially increase barrier fluid consumption and reduce the refill period for Plan 53B, 53C and 54 systems, and two diamond coated rings will wear extremely slowly vs. SiCar-SiCar or SiCar-carbon. This means that barrier fluid consumption will remain high, and the seal will not wear in.
- Ask the vendor to design the cartridges to switch to other configurations in the future, with minimum cost.

Takeaway. Mechanical seal selection and sizing for hot pumping services must be done with experienced personnel. Many factors should be considered. The purchaser should ensure that the vendor's proposed seal is a proven design. This article explained the lessons learned in using Arrangement 3 for hot pumping services. HP

NOTE

The recommendations outlined in this article are based on personal experience and are not related to any company.

LITERATURE CITED

[1] API, API Standard 682, "Pumps—Shaft Sealing Systems for Centrifugal and Rotary Pumps," 4th edition, May 2014.

SHAHAB ZARDYNEZHAD is a registered Senior Mechanical Engineer in Alberta with more than 29 yr of experience working on many of the world's largest oil, gas and petrochemical projects. He has experience in engineering, procurement services, manufacturing, shop/field inspection, installation, commissioning, startup, reliability, and the maintenance and operation of pumps, compressors and turbines. Mr. Zardynezhad holds a BS degree in mechanical engineering from the University of Petroleum of Iran, an MS degree in industrial engineering from I.U.S.T-Iran, an MS degree in project management and an MS degree in mechanical engineering from the University of Calgary. He is a certified API inspector for rotating equipment.

H. HOJJATI and **B. HOJJATI,** WSP Canada Inc.,
Calgary, Alberta, Canada

PSV sizing: An alternative solution to the homogeneous direct-integration method

Pressure safety valves (PSVs) are designed to protect personnel and plant properties from an overpressure occurrence in equipment or piping by relieving fluid to a safe location. While other limitations exist, such as material selection and temperature-pressure rating, a proper sizing can guarantee and optimize protection. The first (and potentially most) important step in the design of a safety valve is to size it as accurately as possible.

Various approaches—theoretical and empirical— to size such a device for all fluids have been derived, developed, published and reviewed by many authors.[1–9] The theoretical equations presented are based on the homogeneous equilibrium model (HEM), assuming thermal and mechanical equilibrium for the fluid passing through the valve nozzle at any cross-section perpendicular to the flow direction (i.e., thermo-physical properties, including density, are uniform at normal direction).

For single-phase fluids, sizing equations are well established and known. They can be solved analytically or numerically and are provided in many references. These methods require thermo-physical properties of the fluid at the stagnation state (relief condition). However, the approaches for two-phase relief sizing are more complex and require the consideration of many factors.[2–9] The homogenous nonequilibrium model, for instance, may be considered for delayed flashing after the liquid reaches the saturation pressure in short nozzles. Also, due to flashing, the gas/vapor phase expands, resulting in higher gas-phase velocity compared to liquid-phase velocity. The velocity difference (known as slip effect) is incorporated into the two-phase models by defining slip ratio/ratio of the gas velocity to the liquid velocity at the throat of the nozzle. To take such effects into account, some guidelines have been provided for two-phase fluids and liquids flashing inside the nozzle.[2,3,4,9]

Among all developed methods for PSV sizing, the homogeneous direct-integration method (HDIM) is the most reliable approach in industrial applications and recommended by the American Petroleum Institute.[1] The method is general, simple and accurate enough to be applied for any fluid in the process of PSV sizing; it can be used as long as the fluid density as a function of pressure is available and can be precisely estimated by thermodynamic databases. Also, it is not subject to the many assumptions or restrictions applied to other methods.[2,3] The HDIM is also based on the homogeneous equilibrium model described above. Applying general steady-state volumetric energy balance to a homogeneous fluid flowing through an adiabatic-reversible (isentropic) process within an ideal nozzle results in a theoretical equation (Eq. 1), which relates mass flux (G) at the nozzle throat to the fluid density (ρ) and the pressure (P) variations:

$$G^2 = -2{,}000 \times \rho_t^2 \times \int_{P_r}^{P_t} \frac{dP}{\rho} \quad (1)$$

The subscripts t and r represent the properties at the nozzle throat and relief conditions, respectively. The derived equation can be used to size a PSV for any homogeneous fluid. The relationship between the fluid density and pressure through an isentropic process must be known.[1,3] The theoretical mass flux is then corrected using a dimensionless constant known as discharge coefficient (K_d), which relates the theoretical ideal nozzle mass flux to the actual mass flux and published experimentally by relief valve vendors.

Having the mass flowrate ($\dot{m}$) to be relieved, the required nozzle throat cross section area (A) can be calculated using Eq. 2:[1]

$$A = \frac{277.8 \times \dot{m}}{G \times \prod K_i} \quad (2)$$

where $\prod K_i$ is the product of all applicable correction coefficients, including discharge coefficient, backpressure (K_b), viscosity (K_v) and combination (K_c) correction factors. The throat pressure varies between relief pressure (P_r) and backpressure (P_b) in Eq 3:

$$P_r < P_t \leq P_b \quad (3)$$

Once the relief valve opens, the fluid begins flowing though the nozzle, resulting in increasing fluid velocity and decreasing fluid pressure in the flow direction. The maximum velocity will be achieved at the throat (minimal cross-section area). If the velocity approaches the sound velocity at a throat pressure less than the total backpressure, the flow becomes choked at the throat providing the maximum mass flux (e.g., for gases, two-phase fluids and vapors). Otherwise, the maximum mass flux is obtained once the throat pressure approaches the total backpressure (e.g., for liquids). The objective of the PSV sizing method is to find the maximum mass flux at the throat pressure by solving Eq. 1.

A numerical method—trapezoidal rule or Simpson's Rules—is commonly performed to solve Eq. 1 and then find the throat pressure and the maximum mass flux.

The accuracy of this approach depends strongly on the selected step size, as well as the numerical integration method. The truncation errors of the numerical integration should be minimized to achieve an acceptable solution. This can be accomplished by reducing the step size and by using a higher-order in-

tegration rule. A smaller step size decreases the truncation error, resulting in a more accurate solution; however, more calculation steps (numerous isentropic phase-equilibrium calculations) are needed, so it is a time-consuming procedure. Using the higher-order integration rule brings more complexities to the solution.

A few analytical solutions have been presented for an individual fluid to overcome the numerical issues.[1,6,8] Based on Eq. 1 and a pressure-specific volume correlation, for instance, a universal mass flux equation (similar to the Omega method for critical flow) and an equivalent critical pressure equation were applied to predict mass flux for any fluid at any condition except flashing flow of initially subcooled liquid.[6] The pressure-specific volume correlation had two parameters that can be calculated using one, two or three data points. Although the models showed a good accuracy for the mass flux and the critical pressure estimations, they were limited to the fluid state and condition.

To avoid such issues related to numerical integration and to present a universal model applicable to any fluid at any condition, an alternative solution (analytical) is proposed to solve Eq. 1. The main objectives of the presented work are to bring all PSV sizing equations under one umbrella by using Eq. 1, to reduce the number of isentropic process calculations to a few data points, to solve Eq. 1 analytically by targeting the valve throat pressure, and to calculate mass flux at the throat for sizing a PSV. This requires that the density of the fluid with respect to pressure variations can be expressed as a linear, a second-order polynomial, or an exponential function with high accuracy. Additionally, for each fluid state, a detailed example is provided to show the applicability of the approach for any fluid and to provide guidelines for PSV sizing.

Theory: An analytical approach. The approach provided is easy to follow:

1. Determine the fluid state and properties, including pressure, temperature and density at the relief condition (Point 1).
2. Determine the total backpressure and the pressure range $(P_r - P_b)$.
3. Based on the authors' experiences, 3–6 data points (including the relief condition) are enough to recognize the trend of fluid density with respect to pressure changes. Divide the pressure range into approximately n equal increments (Eq. 4):

$$(P_r - P_b)/n \tag{4}$$

   where n would be 2, 3, 4 and 5, based on the number of selected data points between 3 and 6. In this article, three data points are selected to examine the proposed model—in general, using more data points provides a better trend line for the fluid density-pressure relationship, leading to a more accurate model.
4. Decrease the relief pressure by one increment through an isentropic process and find the fluid density at the new state. In a proprietary simulator[a], for example, use an expander model palette with 100% efficiency to simulate an isentropic process and ensure that the mass entropy remains constant for both initial and final states. Repeat this step two times until the pressure approaches the total backpressure.
5. Plot the three data points (density vs. pressure) and find a proper trend for density as a function of pressure. Our experiences show that the data can be fitted to a linear, a second-order polynomial or an exponential function.
6. The regression process can be calculated by many math software tools (in Excel, for example, use a combination of *index* and *linest* functions). Fit the data points to one of the above functions and find all required constants, as well as R^2. Although other statistical rules exist, R^2 is sufficient to judge the validity of the curve fit.
7. Estimate the throat nozzle pressure from one of the following equations, calculate corresponding mass flux, and then size the PSV using Eq. 2.
8. In all cases $0 \le P_t < P_r$. If $P_b \le P_t < P_r$, then use P_t as the throat pressure. Otherwise, total backpressure should be used as the throat pressure.

A linear function. For liquids, the density as a function of pressure usually can be expressed linearly (Eq. 5):

$$\rho = aP + b \tag{5}$$

where a and b are the equation constants. Substituting Eq. 5 into Eq. 1 and taking the integral of the function results in Eq. 6:

$$G^2 = -\frac{2{,}000}{a}\left(aP_t + b\right)^2 ln\left(\left|\frac{aP_t + b}{aP_r + b}\right|\right) \tag{6}$$

To maximize the mass flux at the throat (Eq. 7):

$$\frac{d\left(G^2\right)}{dP_t} = 0 \tag{7}$$

Applying Eq. 7 to Eq. 6 results in an explicit equation, which relates the throat pressure to the relief pressure as (Eq. 8):

$$P_t = \frac{e^{-1/2}\left(aP_r + b\right) - b}{a} \tag{8}$$

Eq. 6 gives the maximum mass flux, G^2_{max}, at this pressure.

A second-order polynomial. If the fluid density-pressure trend can be fitted to a second-order polynomial, then (Eq. 9):

$$\rho = aP^2 + bP + c \tag{9}$$

Substituting Eq. 9 into Eq. 1, taking the integration results in three cases (depends on a, b and c coefficient values and signs) to calculate the mass flux, and then applying Eq. 7 to the obtained mass flux, the throat pressure can be targeted.

Case 1: $4ac - b^2 < 0$ (Eqs. 10, 11 and 12):

$$G^2 = \frac{-2{,}000\left(aP_t^2 + bP_t + c\right)^2}{\sqrt{b^2 - 4ac}}\ ln\left(\left|\frac{F_t^1}{F_r^1}\right|\right) \tag{10}$$

where

$$F_t^1 = \frac{2aP_t + b - \sqrt{b^2 - 4ac}}{2aP_t + b + \sqrt{b^2 - 4ac}} \tag{11}$$

$$F_r^1 = \frac{2aP_r + b - \sqrt{b^2 - 4ac}}{2aP_r + b + \sqrt{b^2 - 4ac}} \tag{12}$$

In this case, the throat pressure must satisfy the following implicit equation (Eq. 13):

$$2(2aP_t + b)ln\left(\frac{|F_t^1|}{|F_r^1|}\right) + \sqrt{b^2 - 4ac} = 0 \quad (13)$$

Case 2: $4ac - b^2 > 0$ (Eqs. 14, 15 and 16):

$$G^2 = \frac{-4{,}000\left(aP_t^2 + bP_t + c\right)^2}{\sqrt{4ac - b^2}}\left[tan^{-1}F_t^2 - tan^{-1}F_r^2\right] \quad (14)$$

where

$$F_t^2 = \frac{2aP_t + b}{\sqrt{4ac - b^2}} \quad (15)$$

$$F_r^2 = \frac{2aP_r + b}{\sqrt{4ac - b^2}} \quad (16)$$

The throat pressure must satisfy the following implicit equation (17):

$$2 \times (2aP_t + b)\left[tan^{-1}F_t^2 - tan^{-1}F_r^2\right] + \frac{\sqrt{4ac - b^2}}{2} = 0 \quad (17)$$

Case 3: $4ac - b^2 = 0$ (Eqs. 18 and 19):

$$G^2 = -\frac{500}{c}\frac{(bP_t + 2c)^3}{(bP_r + 2c)}(P_t - P_r) \quad (18)$$

and

$$P_t = \frac{3P_r}{4} - \sqrt{\frac{c}{a}} \quad (19)$$

where $ac > 0$ and then $\sqrt{(c/a)}$ exists.

Eqs. 13 and 17 are implicit functions of the throat pressure and should be solved by a proper algorithm. In Excel or MATLAB, one can use a "*solver*" function or "*fzero*" command to find the throat pressure, respectively. Both methods need an initial guess, which should be between the relief pressure and the total backpressure. Note that the upper and lower limits are the relief pressure and zero, respectively. Eq. 19, however, is an explicit function of the throat pressure but a less likely case, based on the authors' experience in PSV sizing.

An exponential function. When a liquid (subcooled or saturated) is flashed, its density with respect to pressure variations may be fitted with an exponential function with a higher R^2. In such a case, Eq. 20 can be used:

$$\rho = ae^{bP} \quad (20)$$

Following the same procedure, Eqs. 21 and 22 can be obtained:

$$G^2 = 2{,}000\frac{a}{b}\left[e^{bP_t} - e^{b(2P_t - P_r)}\right] \quad (21)$$

where the throat pressure for the maximum mass flux calculations can be evaluated by Eq. 22:

$$P_t = P_r - \frac{ln(2)}{b} \quad (22)$$

Constant density. Subcooled liquid density is a weak function of pressure and can be generally assumed constant within the pressure range $P_b \le P < P_r$. In such a condition, Eq. 1 can be simplified to Eq. 23:

$$G^2 = \frac{2{,}000 \times \rho_b^2}{\rho_{ave}}(P_r - P_b) \quad \text{where} \quad \rho_{ave} = \frac{\rho_r + \rho_b}{2} \quad (23)$$

Note that the flow is not choked for this condition, and the downstream total backpressure is used as the throat pressure.

Examples have been provided to support the proposed method. For all examples, three data points—at the relief pressure, a pressure in the middle of the pressure range, and the total backpressure—are selected to express a proper trend for density-pressure relationship.

RESULTS

Example A: Two-phase fluid. A balanced PSV was designed to protect a horizontal separator if the liquid outlet flow is blocked (governing case for an actual design). The drum design pressure was 1,000 kPag (PSV set pressure). The inlet fluid was a mixture of an oil (mostly heavy oil), water and hydrocarbon vapor with flowrate of 61,552 kg/hr (582.9 kg/hr vapor and

TABLE 1. Required data for Example A

K_D		Omega method		L.L Simpson's method		
P_r	1,201.1	P_r (P_{sat})	1,201.1	P_r	1,201.1	700
v_{lg}	0.1175	90% of P_{sat}	1,081	ρ_l	902.53	905.35
h_{lg}	3,319	T_r	427.6	ρ_v	8.433	4.545
C_P	4.022	P_b	332.1	Gas wt. fraction	0.0100	0.0181
v_l	0.0011	ρ_r	437.93	–	–	–
T	424.6	$\rho_{90\%}$	390.55	–	–	–
α	0.5196	–	–	–	–	–

TABLE 2. Input data and results of Example A

Input data	P	1,201.1	856.3	511.6
	ρ	437.93	283.85	98.91
Equations	Linear	$\rho = 4.9169 \times 10^{-1} P - 147.4882$, $R^2 = 0.9972$		
		$(P_t)_C$	846.5	Using Eq. 8
		$(P_t)_S$	846.5	–
		G	12,120	Using Eq. 6
		A	1,632	Using Eq. 2
	Polynomial	$\rho = -1.2990 \times 10^{-4} P^2 + 7.1416 \times 10^{-1} P - 232.452$, $R^2 = 1.0000$		Case: 1
		$(P_t)_C$	843.3	Using Eq. 13
		$(P_t)_S$	843.3	–
		G	12,467	Using Eq. 10
		A	1,587	Using Eq. 2
	Other methods	G	12,424	Using numerical integration of Eq. 1
		A	1,592	
		G	13,565	Using Omega method[8]
		A	1,462	
		G	11,878	Using method presented[9]
		A	1,665	

60,969.1 kg/hr liquid) at 427.5 *K*, which must be relieved to a storage tank (no credit was taken for the gas outlet). The entire process was simulated using a proprietary process simulator[a] and fluid properties; the hydraulics of vessels and pipes were also estimated. At relief conditions—427.5 K and 1,201.1 *kPaa* (10% overpressure and atmospheric pressure 101.1 *kPaa*)—the properties were calculated (**TABLE 1**) and the two-phase flow discharge coefficient was estimated to be $K_d = 0.873$ using the method presented by Leung.[10] Additionally, the total backpressure was calculated to be 231 *kPag* (332.1 *kPaa*) at the rated flowrate, resulting in $K_b = 1$ for the balanced PSV (Crosby backpressure curves were used). The viscosity correction factor was estimated to be $K_v = 0.990$.

Through an isentropic process, the fluid relief pressure was reduced two times (with a 345-*kPa* interval) and the density was calculated (**TABLE 2**). The data was fitted to a linear as well as a second-order polynomial using a proper regression method (**FIG. 1**). The throat pressure and the maximum mass flux were then calculated. The calculation details and results are summarized in **TABLE 2.**

The valve is sized by HDIM as well as a two-point Omega method.[8] For HDIM, the density of the fluid was calculated with a 7-*kPa* interval pressure reduction; the mass flux and the required area were then calculated from the numerical solution of Eq. 1. For the Omega method, however, the required properties at 90% of the relief (saturation) pressure (1,081 *kPaa*) were estimated through an isentropic process (**TABLE 1**) and the valve was then sized. The maximum mass fluxes and required nozzle areas calculated by both methods are found in **TABLE 2** for comparison.

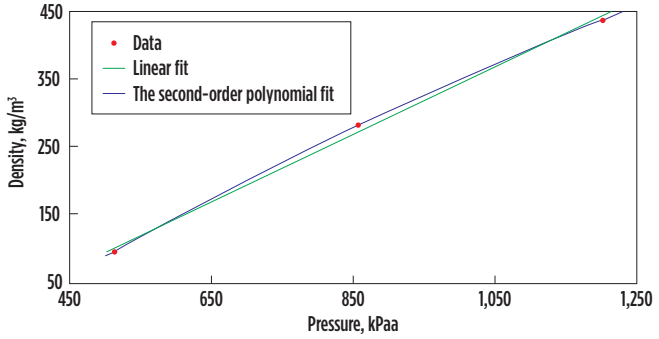

FIG. 1. A regression method with linear and second-order polynomial data.

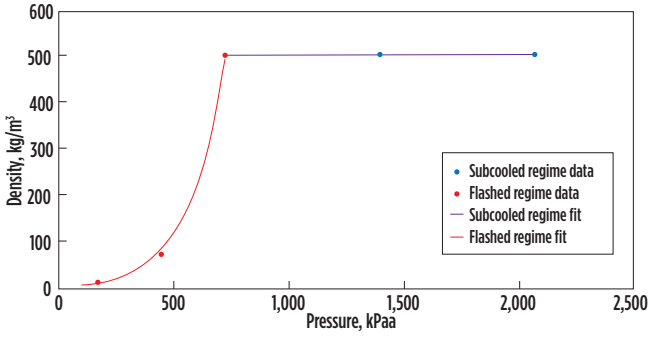

FIG. 2. Different regimes have different density trends, and variations cannot be fitted by an individual equation.

For two-phase flow PSV sizing, Simpson[9] presented a method based on a two-point interpolation scheme for properties estimation and numerical integration of Eq.1. The first point was at the relief pressure and the second one was at a pressure between 50% to 95% of the relief pressure (in this example, 700 *kPaa*). Along an isentropic path, the fluid was flashed from 1,201.1 *kPaa* to 700 *kPaa*; the input data are summarized in **TABLE 1.** Using provided two-point data, the density was estimated and then the mass flux and the required area were calculated from the numerical solution of Eq. 1 with a pressure interval of 10 *kPa*. The results are summarized in **TABLE 2** for comparison.

Although all methods led to a calculated API PSV size of "*L*", the two-point Omega method resulted in a less conservative nozzle size, which can be related to the linear interpolation data behind the model. Based on the authors' PSV sizing experiences, once the density-pressure trend deviates from a linear behavior, the two-point Omega method is not recommended for two-phase relief PSV sizing, as it may result in an undersized PSV. However, a linear trend will result in the same PSV size using all methods, including the Omega method, which is consistent with the linear-interpolation assumption applied to the two points of the Omega method (see the two-phase example in supporting examples).

For two-phase flow relief, the proposed analytical method is generally accurate enough to size PSVs; however, if slip effect or HNE model[3] is a concern, the proposed approach is still valid for PSV sizing. In such cases, the density as a function of pressure is estimated, corrected using the slip or the HNE model, and then applied for the illustrated procedure to size PSV for two-phase relief.

Example B: Subcooled or saturated liquid flashing at the throat. The most challenging part of the proposed method is when the PSV sizing process is dealing with saturated or highly subcooled liquid flashing (the liquid reaches the saturation pressure flowing through the nozzle). In this condition, two different regimes have different density trends. In the subcooled regime, the density is almost constant, whereas high-density variations can be observed after the liquid starts flashing. These variations cannot be fitted by an individual equation (**FIG. 2**). Fortunately, a solution exists for such a condition. The integral has an interval addition property allowing us to divide it into two intervals—in our case, one interval for subcooled liquid and another one for flashed liquid—that hold the same conditions. Therefore, Eq. 1 can be rearranged into (Eq. 24):

$$G^2 = G_s^2 + G_f^2 = -2{,}000 \times \rho_{sat}^2 \times \int_{P_r}^{P_{sat}} \frac{dP}{\rho} - 2{,}000 \times \rho_t^2 \times \int_{P_{sat}}^{P_t} \frac{dP}{\rho} \quad (24)$$

The maximum mass flux of the subcooled regime, G_s^2, can be estimated using Eq. 23 as well, if the density does not vary significantly over the pressure range. The flashing regime can be fitted into a second-order polynomial or an exponential function. To show the capability of the proposed solution under such a condition, consider the example C.2.3.2 of API-520-1[1], in which 378.5 L/min (11,588 kg/hr) of subcooled propane should be relieved at 2,073.2 *kPaa* and 288.7 *K*. The downstream total backpressure was 170.2 *kPaa*, leading to a backpressure correction factor unit. The discharge coefficient was 0.65 and the viscosity correction factor was assumed to be 1. The

valve was sized using a two-point Omega method, resulting in the maximum mass flux and required area of 36,890 kg/(s – m^2) and 134.5 mm^2, respectively.

To size the PSV using the proposed method, the subcooled propane at the relief condition was flashed using an isentropic path (through an expander with 100% efficiency in the simulator[a] environment). At the first stage, the pressure was decreased to find the boiling point (P_{sat} = 722.2 *kPaa*). Two sets of data (a subcooled set between P_r and P_{sat} and a flashed set between P_{sat} and P_b) were then generated and are presented in **TABLE 2.** The subcooled set was fitted to a second-order polynomial, whereas the flashed set was fitted by two functions, a seconded-order polynomial and an exponential function. At the final stage, the maximum mass fluxes were added and the required area was calculated. The results are also summarized in **TABLE 2.** Both polynomial and exponential functions show almost the same results.

Eq. 23 can be used to evaluate the subcooled mass flux using an average density of 509.28 kg/m^3 to be G_s^2 = 1,370,914,531 kg^2/(s^2 – m^4), showing the same result.

Note: If the relief pressure is at or very close to (slightly subcooled liquid) the saturation pressure, then it is recommended that the subcooled regime be ignored and the PSV be sized in one step using Eq. 1. For such a condition, the flashed data starting from the saturation point are fitted by an exponential function, but the relief pressure should be used for Eqs. 21 and 22. Simpson[9] provided an example to size a rupture disk for relieving 181,437 kg/hr of 703.3 *kPaa* condensate saturated at 689.5 *kPaa*. The discharge coefficient and the total backpressure were assumed to be 0.62 and atmospheric pressure, respectively. Using the two-point model prediction and the numerical solution of Eq. 1, the throat pressure, the maximum mass flux and the required area were calculated to be 688.8 *kPaa*, 5,136.3 kg/(s^2 – m^4) and 15,806 mm^2, respectively. Three data points at 689.5, 668.8 and 655.0 *kPaa* were selected and fitted to an exponential function, leading to Eq. 25:

$$\rho = 1.4692 \times 10^{-4} e^{0.02265P} \qquad R^2 = 0.9928 \qquad (25)$$

Using the relief pressure of 703.3 *kPaa*, the throat pressure, the maximum mass flux, and the required area can be calculated using Eqs. 22, 21 and 2, respectively, as:

P_t = 672.7 *kPaa*

G = 5,181.3 kg/(s – m^2)

A = 15,690 mm^2

Takeaway. To avoid numerous calculation steps of the numerical solution of Eq. 1 to size pressure relief valves, an analytical approach is derived to solve an integral part of the homogeneous direct-integration method by fitting three density-pressure data points to a linear, a second-order polynomial or an exponential equation (more data points, up to six, are recommended to evaluate density-pressure trend and relationship). The approach is straightforward, targeting the throat pressure, calculating the mass flux, and then sizing the PSV.

TABLE 3. Input data and results of Example B

		Subcooled regime			Flashed regime		
Input data	P	2,073.2	1,400.2	722.2	722.2	446.2	170.2
	ρ	510.24	509.28	508.32	508.32	77.882	15.845
Equations	**Polynomial**	$\rho = 1.3229 \times 10^{-8} P^2 + 1.3775 \times 10^{-3} P + 507.322$ $R^2 = 1.0000$ Case: 2			$\rho = 2.4181 \times 10^{-3} P^2 - 1.2658P + 161.230$ $R^2 = 1.0000$ Case: 1		
		$(P_t)_C$	–	–	$(P_t)_C$	608.4	Using Eq. 13
		$(P_t)_S$	722.2	–	$(P_t)_S$	608.4	–
		G_s^2	1,370,926,972	Using Eq. 14		48,872,027	Using Eq. 10
	Exponential		–		$\rho = 5.1874e^{6.2831 \times 10-3 P}$	$R^2 = 0.9978$	
		–	–	–	$(P_t)_C$	611.9	Using Eq. 22
		–	–	–	$(P_t)_S$	611.9	–
		–	–	–	G_{f2}^2	38,584,370	Using Eq. 21
Results		$G^2 = G_s^2 + G_{f1}^2$	1,419,799,000	Using Eq. 24	$G^2 = G_s^2 + G_{f2}^2$	1,409,511,342	Using Eq. 24
		G	37,680		G	37,543	
		A	131.4	Using Eq. 2	A	131.9	Using Eq. 2

For all possible fluid states to be relieved, one example was provided and compared with other sizing methods to support the approach. The results show that a second-order polynomial can represent a density-pressure relationship for all fluids through an isentropic pressure reduction process. However, the equations derived for targeting the throat pressure are implicit and must be solved by an appropriate algorithm. The linear model provides an explicit equation with less accuracy for calculating the throat pressure.

In the case of subcooled liquid flashing through the nozzle, an exponential function may offer a more accurate fitting curve to the density-pressure relationship, leading to an explicit expression for the throat pressure calculation as well. In general, the presented analytical solution is accurate enough to be applied to all fluid states for PSV sizing. It can be extended to take into account the homogenous non-equilibrium directed integration model, as well as the slip model recommended for two-phase flow relief.[2,3,9] The density at each step should be corrected accordingly before using the analytical solution. Also, for two-phase relief sizing, if the density-pressure relationship shows a high degree of non-linearity, the two-point Omega method is not recommended for PSV sizing due to the linear interpolation assumption behind the model development. HP

NOTES

[a] Aspen HYSYS

ACKNOWLEDGEMENT

The authors would like to show their gratitude and appreciation to Tony Steinicke (WSP Process Manager) and Tao Song (WSP Lead Process Engineer) for their support and feedback.

NOMENCLATURE

a, b and *c*	Coefficients of fitted equations
A	Nozzle cross-section area, mm^2
C_p	Liquid specific heat capacity, kJ/kg-K
G	Mass flux, kg/sec-m^2
h	Specific enthalpy, kJ/kg
K_b	Backpressure correction factor, dimensionless
K_c	Combination correction factor, dimensionless
K_d	Discharge coefficient, dimensionless
K_v	Viscosity correction factor, dimensionless
$\dot{m}$	Mass flowrate, kg/hr
P	Absolute pressure, *kPaa*
R^2	A statistical measure of goodness of regression, dimensionless
T	Temperature, K
v	Specific volume, m^3/kg
Greek letters	
α	Actual gas volume fraction
ρ	Density, kg/m^3
Subscripts	
b	Properties at total backpressure
C	Calculated
f	Flashed
lg	Difference between gas and liquid property
l	Liquid
max	Maximum
r	Properties at relief pressure
sat	Saturation
s	Subcooled
S	Selected
t	Properties at throat pressure
v	Vapor

LITERATURE CITED

[1] American Petroleum Institute (API), "Sizing, selection and installation of pressure-relieving devices—Part 1: Sizing and selecting," 9th Ed., 2014.
[2] Darby, R., "Evaluation of two-phase flow models for flashing flow in nozzles," *Process Safety Progress,* 2000.
[3] Darby, R., "Size safety-relief valves for any conditions," *Chemical Engineering,* 2005.
[4] Darby, R. et al., "Select the best model for two-phase relief sizing," *Chemical Engineering Progress,* 2001.
[5] Darby, R. et al., "Properly size pressure-relief valves for two-phase flow," *Chemical Engineering,* 2002.
[6] Kim, J. S. et al., "Sizing calculations for pressure-relief valves," *Chemical Engineering,* 2013.

Complete Literature Cited available online at www.HydrocarbonProcessing.com

HOSSEIN HOJJATI has more than 25 yr of industrial and academic experience. Working mostly in the oil and gas segments, Dr. Hojjati has been involved in the design of many conventional and SAGD upstream facilities, as well as natural gas plants. He graduated from Western University in Canada.

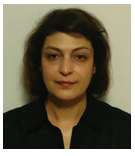

BEHNAZ HOJJATI has more than 20 yr of research, industrial (EPC companies) and academic experience. Dr. Hojjati has received numerous acknowledgements and awards, including the Ontario Graduate Scholarship in Science and Technology (OGSST) and Industrial R&D Fellowships from the Natural Science and Engineering Research Council. She graduated from Western University in Canada.

M. B. MATAR, A. A. MANE and M. RAJENDRAN,
Kuwait National Petroleum Co., Ahmadi, Kuwait

MAA refinery–Bunker fuel oil challenge: Stable and compatible VLSFO production

Studies have been conducted on strategies for bunker fuel oil (BFO) production with reduced sulfur and catalytic fines concentration limits. However, these studies conclude that refiners must face challenges in terms of BFO stability and compatibility. In addition, prices and demand for heavy fuel oil (HFO) will diminish, forcing refineries to find alternate options for its disposal. Therefore, to determine strategies for BFO production, Kuwait National Petroleum Co.'s (KNPC's) Mina Al-Ahmadi (MAA) refinery has conducted feasibility and pilot studies. These pilot studies are small-scale, preliminary studies that aim to investigate whether the blending ratio considered for the feasible components available in the MAA refinery to produce BFO as on-specification very-low-sulfur fuel oil (VLSFO) is stable for longer periods. Subsequently, the results and analysis of the trial concluded that managing blending and stream qualities is the best way to increase the level of compatibility in BFO.

This article provides a comprehensive analysis of VLSFO quality constraints and the MAA refinery's experience in VLSFO production.

Bunker fuel–An easy guide. Bunker fuel dates back to steamships that were powered by coal. These ships stored this fuel source in onboard coal bunkers. While, today, ships have fuel tanks instead of coal bunkers, these tanks are still often referred to as bunkers.

Maritime vessels use this bunker fuel to power their motors. Some water crafts use diesel (i.e., marine gasoil, which is considered a low-sulfur fuel oil) as their source of bunker fuel. However, most commercial vessels now rely on HFO to generate power to propel their ships across the ocean. HFOs can be highly polluting. They are a component of acid rain, which damages vegetation and wildlife, and these fuels can also cause respiratory diseases.

Over recent years, emission control area (ECA) limits have been gradually reduced from their initial value of 1.5% sulfur to 1% sulfur in 2010 and then to 0.1% sulfur in 2015. The global sulfur limit in marine fuels was set to 3.5% in 2012. On January 1, 2020, the International Maritime Organization's (IMO's) new sulfur regulations banned ships from using fuels with a sulfur content above 0.5% (FIG. 1).

Today, the utilization of approved alternative means of emissions reduction—which are at least as effective as using compliant fuels—is also permitted. An exhaust scrubber designed for reducing sulfur oxide (SO_x) content to the level required is considered equivalent, and fuels with higher sulfur content may still be used on vessels that are equipped with such a design. The usage of exhaust scrubbers is limited due to restrictions in the disposal of washwater, and most

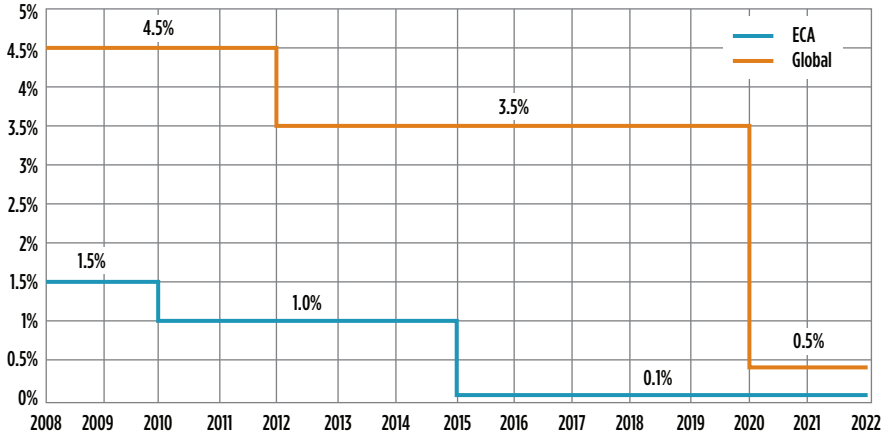

FIG. 1. The gradual reduction of BFO sulfur specifications.

TABLE 1. Fuel names after IMO sulfur regulation went into effect (January 2020)

Sulfur content	HFO (RM grades)	MDO (DMB, DFB)	MGO (DMA, DFA, DMZ, DFZ)
Sulfur ≤ 0.1%	ULSFO RM		ULSFO DM
0.1% < sulfur ≤ 0.5%	VLSFO RM		VLSFO DM
Sulfur > 0.5%	HSFO RM*		HSFO DM*

*Fuels allowed only for ships with exhaust-reduction technologies yielding SO_x reductions equivalent to using fuels with the respective sulfur limit

ports are not allowing vessels to discharge washwater near their facilities.

Refinery challenges for VLSFO bunker fuel production. Most fuels used in the market after the start of the IMO's sulfur regulation are VLSFO (fuel names are listed in TABLE 1). The switch to VLSFO has affected refinery production, since it is unlikely that HFO products can simply be desulfurized to create compliant fuels. Instead, VLSFO will consist of blends of fuels produced from different refinery streams. These blends are expected to have higher fractions of paraffinic products, which will affect the properties of VLSFO. It is important to state that VLSFO must be compliant with ISO 8217:2017[1] and must fit within the same residual marine (RM) grades as used prior to 2020. The following are some important parameters that present huge challenges while adhering to the ISO 8217:2017 specification of VLSFO.

Compatibility and/or stability. Depending on the origin and production process used, VLSFO blend streams can be aromatic or paraffinic in nature. This could lead to compatibility problems between different fuel streams.

Blending of aromatic streams with paraffinic streams results in sludge formation (after prolonged tank storage, even if initially stable), due to a change in the solubility properties of the subsequent blend.

Viscosity. The viscosity of fuel oils must be in accordance with ISO 8217:2017.1. VLSFO fuels are expected to have a broad range of viscosities, even within the same grade. Some types of VLSFO will have low viscosity levels, such as distillate marine (DM) fuel.

Cold flow properties. With VLSFO having high fractions of paraffinic components, exposure to prolonged cold conditions may lead to wax formation, which, in turn, could affect the cold flow properties of the fuel.

Calculated carbon aromaticity index (CCAI). The CCAI provides an indication of the ignition properties or ignition delay of fuels based on fuel viscosity and density. In view of the broad range of density and viscosity values of VLSFO, resulting CCAI values can also vary considerably.

Catalytic fines. The level of catalytic fines in VLSFO are unknown and might vary, depending on the refinery streams from which the fuel was produced.

The blending of VLSFO. The major challenge that refineries face is to keep the asphaltene micelles in colloidal solutions of fuel oil. The high aromaticity of fuel oil helps achieve the same. In addition, if an aromatic cutter is poured into a paraffinic base, then the initial small volume of aromatics in a paraffinic medium will disturb the low aromaticity of the paraffinic base, thereby increasing the probability of asphaltene sludging (FIG. 2).

In the opposite situation, where paraffinic blendstock is poured into an aromatic medium, the aromaticity at the interface of the two liquids will be predominantly by the aromatics and will always keep asphaltenes in the solution.

Based on typical examinations of VLSFO blendstock properties, they can be classified as a high aromaticity base (50%–60%)—i.e., vacuum bottoms and visbreaker tar bottoms—and two types of cutter stocks (aromatics and paraffinic).

Aromatic cutters are typically from fluid catalytic cracking units (FCCUs) and include light-cycle oil (LCO), heavy-cycle oil (HCO), and slurries or clarified oils (CLOs). These cutters are highly aromatic liquids (80% or higher). Paraffinic

TABLE 2. Typical properties of blending components

Description	ARD residual	VR residual	Gasoil	Trim gasoil (TGO)
Specific gravity	0.9302	0.989	0.845	0.9068
Sulfur, wt%	0.46	0.7	0.0005	0.16
Viscosity, centistokes (cSt) at 50°C	175	5,000	4	96
Asphaltenes, wt%	1.7	3.1	–	–
Vanadium, wt%	7.5	36	–	–

TABLE 3. Blend component and aromaticity

Blend component	Aromaticity
Vacuum tower bottoms	Nearly 80%
Gasoil	30%–40%

TABLE 4. Any aromatic blend will have an excess of aromaticity (more than 50%) and be stable

Blend component	Aromaticity
Visbreaker tar bottoms	47%–56%
LCO and HCO	More than 80%

TABLE 5. A hybrid blend is not guaranteed to always have an excess of aromaticity (more than 50%) and be stable

Blend component	Aromaticity
Atmospheric tower bottoms and vacuum tower bottoms	50%–60%
Gasoil	30%–40%
Cycle oil	More than 80%

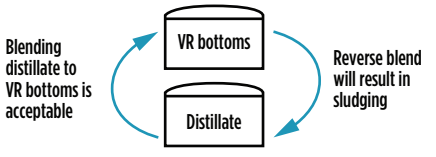

FIG. 2. Blending direction.

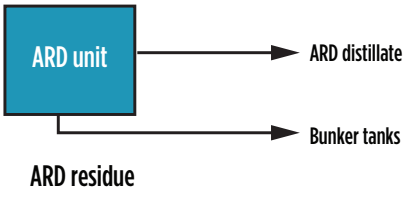

FIG. 3. KNPC's ARD unit.

cutters are typically from atmospheric and vacuum distillation units (VDUs), such as atmospheric gasoil (AGO), light and heavy AGO and vacuum gasoil (VGO). These cutters have a low aromaticity of around 30%–50%. Typical properties of blending components are detailed in TABLE 2.

Considering asphaltene content and aromaticity, VLSFO fuel oil blends can be categorized as paraffinic blends, aromatic blends and hybrid blends.

Paraffinic blends. These blends typically use vacuum tower bottoms and the cutter [e.g., light atmospheric gasoil (LAGO), heavy atmospheric gasoil (HAGO) or ultra-low-sulfur diesel (ULSD)] (TABLE 3).

Vacuum residue (VR) from the VDU can be blended with low-sulfur streams to produce the required product, keeping the resulting blend aromaticity above 40% by controlling the blend ratio and the order of blending. Trim gasoil (TGO) dropping in vacuum tower bottoms will help achieve the required aromaticity. With VR blended with distillate, the final blending aromaticity could drop below 40% and lead to sludging, depending on the blend ratio and the order of blending.

Aromatic blends. These blends typically use "cracked" blend components, such as visbreaker tar bottoms and highly aromatic cutters (i.e., LCO and HCO). Any aromatic blend will have an excess of aromaticity (more than 50%) and be stable (TABLE 4).

Hybrid blends. These blends typically use paraffinic blend components such as atmospheric tower bottoms, vacuum tower bottoms, and mixtures of both paraffinic cutters (such as AGO, LAGO and HAGO) and aromatic cutters (i.e., LCO and HCO). Depending on the blend recipe, a hybrid blend is not always guaranteed to have an excess of aromaticity (more than 50%) and to be stable (TABLE 5).

The changes in fuel production result in a different nature and quality of fuels. New fuels (such as VLSFO) that are compliant with the 0.5% sulfur limit are likely to display a wide variability of physical and chemical properties, even between fuel batches of the same ISO specification.

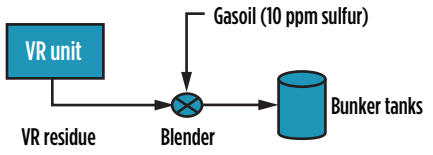

FIG. 4. KNPC's VR/ARD units.

Potential to produce VLSFO. The considerable decrease of sulfur in fuel content had a substantial effect on bunker fuel production. In response to the IMO regulation's significant reduction in sulfur requirements, refineries must make capital investments and use innovative technologies/methods to reduce the amount of sulfur and particulates in fuel oil. Apart from this, HSFO production must be minimized in anticipation of a drop in value.

VLSFO must be compliant with ISO 8217:2017 to adhere to these IMO requirements. The blending of available components in refineries plays a vital role in production. The major concern is the compatibility between different VLSFO blends. VLSFO blending is a challenge from fuel oil stability and compatibility points of view.

KNPC'S EXPERIENCE WITH VLSFO PRODUCTION

KNPC has two refineries—Mina Abdullah (MAB) and MAA. Both refineries produce clean-burning fuels, conforming to Euro 5 standards. As per design, KNPC will produce a significant amount of LSFO with viscosities of 380 cSt and 180 cSt. The components in the KNPC refinery to produce LSFO are atmospheric residue from the crude distillation units (CDUs), treated residue (ARDR) from the atmospheric residue desulfurization (ARD) units, VR from the VDUs, distillate, and LCO and HCO from the FCCU.

The option of producing the desired VLSFO product from atmospheric residue is not possible due to high sulfur content (> 4 wt%). Diverse options tried by KNPC to produce VLSFO, along with associated limitations and subsequent product qualities, are presented in detail here.

The MAA refinery's Clean Fuels Project ARD unit can produce residue with a sulfur content significantly less than 0.5%, which is further processed in the vacuum unit to keep feed sulfur at a minimum. ARD distillate can be used as a cutter to blend with VR bottoms.

Option 1: Hydrotreated ARDR. KNPC's new ARD unit's (FIG. 3) product can be directly supplied as BFO without blending with another stream with sulfur less than 0.5 wt%. ARDR sulfur will depend on the level of desulfurization, and will vary from the start of run (SOR) to the end of run (EOR). Typical properties of the ARD unit's residue are detailed in TABLE 6.

To route ARDR to the appointed VLSFO tanks, a project modification is required with controls in the unit and offsite area. The required project modification is raised, and is expected to take a long time for completion.

Impact. There will be a reduction in the conversion unit feed rate (primarily in the hydrocrackers, FCCUs and coker units), since part of KNPC's ARDR will not be processed in the vacuum re-run units, thus resulting in VGO/TGO/VR losses. Therefore, naphtha, aviation turbine kerosene (ATK) and diesel production will be reduced, as well.

TABLE 6. Typical properties of the ARD unit's residue

Parameter	Unit	ARD
Carbon residue, Conradson	% mass	3.98
Sulfur, total	% mass	0.4
Density at 15°C	kg/l	0.9259
Viscosity at 50°C	cSt	173
Sludge, hot filtration	% mass	0.036
Hydrogen sulfide (H_2S), liquid phase	ppm	0.02
Vanadium	mg/kg	5.3
Ash	% mass	0.02
Sediment	% mass	0.04
Asphaltenes	% mass	1.72
CCAI	Calculated	795

Option 2: VR residue blending with diesel. VR from the VDUs can be blended with a low-sulfur stream to produce the required product (FIG. 4). To reduce sulfur in VR bottoms, feed sulfur was kept exceptionally low. This has resulted in achieving sulfur in VR bottoms at 0.84%. Adding 10-ppm sulfur gasoil, the resulting sulfur was reduced to less than 0.5 wt% as per VLSFO requirements. The results of the final blend are detailed in TABLE 7.

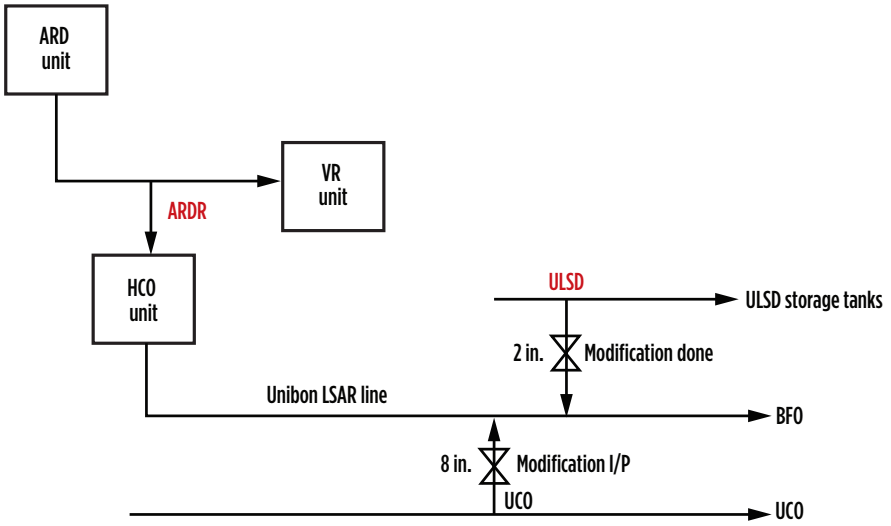

FIG. 5. MAB units' blend.

TABLE 7. Results of the final blend

Parameter	Units	Result
Ash	% mass	0.02
Density at 15°C	kg/l	0.9047
Flash point, PMCC	°C	108
H_2S	mg/kg	0.93
Pour point	°C	3
Relative density at 60°F	–	0.9052
Sulfur, total	% mass	0.48
Total sediment potential	% mass	0.04
Vanadium	mg/kg	7.2
Kinematic viscosity at 50°C	cSt	45
Aluminum and silicon	mg/kg	5.7
CCAI	–	793.1

TABLE 8. BFO results of Option 4

Parameters	MAB VLSFO	MAA tank	VLSFO import: First cargo
Sulfur, % mass	0.39	0.5	0.46
Density at 15°C, kg/l	0.894	0.896	0.937
Flash point, °C	110	> 110	104
Kinematic viscosity at 50°C, cSt	37.2	40	345
Total sediment potential, % mass	0.1	0.06	NA
H_2S (liquid phase), ppm	0.2	0.2	0.5
Ash, % mass	0.06	0.02	0.03
Aluminum and silicon, mg/kg	4	4.6	NA
Vanadium	5.7	6.7	NA
CCAI	785	785	800

The BFO viscosity quality is extremely low at 45 cSt, compared to a maximum of 380 cSt, and the CCAI is close to the maximum limit.

Impact. It requires approximately 45% of 10-ppm gasoil as cutter stock. This could lead to the possibility of final blending aromaticity dropping below 40%, which, in turn, could lead to sludging. Therefore, this option has an inherent associated risk.

Option 3: Diesel as bunker fuel. Diesel can be supplied as bunker fuel at prevailing market prices. KNPC economics will not be affected if the bunker price is the same as the export gasoil price. In this case, the bunker will be 10-ppm gasoil.

Option 4: Using low-sulfur ARDR, ULSD and UCO. The MAB refinery had successfully completed its trial run for the lab blend with ARD residue and a mix of TGO and UCO to produce LSFO. However, the blend viscosity was around 20 cSt–40 cSt. The blended batches were stable and met specifications; therefore, the MAB refinery commenced preparing VLSFO batches. The desired results were achieved after executing the modifications shown in FIG. 5. The BFO results are detailed in TABLE 8.

Option 5: VR and TGO. The MAA refinery finally achieved the most economic and feasible way of producing VSLFO, using ARD distillate, VR and TGO streams (FIG. 6). To achieve this, the ARD unit was run with ARD residue product with a maximum amount of sulfur at 0.35 wt%. The VR unit must process low-sulfur ARD residue from the ARD unit without mixing with high-sulfur ARD residue from other MAA ARD units. BFO results are detailed in TABLE 9.

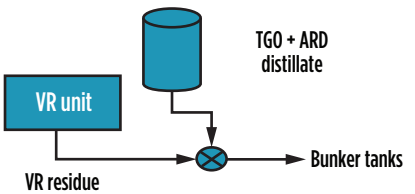

FIG. 6. VR residue with TGO blend.

By this operating condition, the VR will have sulfur at a 0.7 wt% maximum, and the viscosity will be around 4,000 cSt–5,000 cSt at 50°C. Blending low-sulfur ARD distillate and TGO from the VR unit (sulfur limit of 0.15 wt%), the required VLSFO production was achieved.

MAA refinery issues while handling imported materials. To adhere to VLSFO bunker fuel requirements, a cargo was imported with 0.46 wt% sulfur in December 2019 into the MAA refinery's bunker tanks. Prior to import, both tanks were cleaned, and the associated system was flushed thoroughly using 500-ppm gasoil. Upon completion of import, both the tanks were certified as per IMO specifications.

During this period, the MAB refinery produced a batch of VLSFO as per Option 4; therefore, a vessel was arranged to the MAA refinery. Upon loading, the ship's composite sample at the MAB refinery port met all specifications; however, prior to discharge, there were concerns on the compatibility of the remaining BFO material at the MAA refinery with the newly imported material. After quality control clearance, the imported BFO was discharged into the bunker tanks at the end of January 2020. Upon receipt, the fuel met the BFO IMO specifications but tank sulfur result samples were marginally at the specification limit (0.5 wt%). However, the batch did not have the sufficient sulfur limit margin to be supplied to vessels and with no facility for correcting the product, it was decided to dispose of (export) the product. Upon arranging a vessel to load the product, the tank samples (TABLE 10) showed that the sulfur content was 0.44 wt% and 0.46 wt%, respectively. However, samples taken over the next several weeks showed inconsistencies in mixtures. In addition, the total sediment results after mixing had presented inconsistencies. This solidified the conclusion that asphaltene (having the highest sulfur proportion to the mixture) miscible in the mixture may had precipitated due to compatibility issues and affected the sulfur results.

From these results, it can be inferred that it is imperative that all receipts of this grade fuel oil should have a maximum of 0.47 wt% (95% confidence level) and shown to be tested for compatibility before blending/mixing. This clarifies the challenges that were met and the efforts exerted to meet IMO requirements.

TABLE 9. BFO results of Option 5

Parameter	Result
Aluminum and silicon, mg/kg	0.1
Ash, % mass	0.02
CCAI	800.1
Density at 15°C, kg/l	0.9353
Flash point (PMCC), °C	114
H_2S, mg/kg	0.3
Phosphorus, mg/kg	0
Pour point, °C	-3
Relative density at 60°F	0.9358
Sulfur (total), % mass	0.45
Total sediment potential, % mass	0.1
Vanadium, mg/kg	10
Viscosity, kinematic at 50°C, cSt	276

TABLE 10. MAA refinery bunker tank results

Parameter	VLSFO 1	VLSFO 2
Aluminum and silicon, mg/kg	24.88	43.8
Ash, % mass	0.03	0.03
Density at 15°C, kg/l	0.937	0.9354
Flash point (PMCC), °C	104	100
H_2S, mg/kg	0.5	0.5
Relative density at 60°F	0.9376	0.936
Total sulfur, % mass	0.44	0.46
Total sediment potential, % mass	0.04	0.04
Vanadium, mg/kg	3.8	3.7
Kinematic viscosity at 50°C, cSt	345	348
CCAI	800	798

Takeaway. With the new IMO 2020 low-sulfur regulation, bunker production must use low-sulfur blend components to be compliant. Sludge issues can be avoided by calculating the fuel's compatibility and stability. The asphaltene content and aromaticity of fuel oil are critical to its fitness for use.

KNPC achieved the most economically feasible way of producing VLSFO by using distillate, VR and TGO streams originating from its latest clean fuels project units. This VLSFO met the IMO 0.5 BFO specifications with a minimum viscosity of 250 cSt, and was a stable product due to the low asphaltene content of the VR.

These accomplishments enable KNPC to be in position to adhere to the IMO mandatory requirements of VLSFO IMO BFO, with financial benefits. In addition, these accomplishments will help the MAA refinery to modify its production slots based on the economics and market demands. HP

ACKNOWLEDGMENTS

The authors would like to thank Rathina Sabapathi Kanagasabai, Kishor Datta Purkayastha and Mayank Garg for their help in preparing this article.

MOHAMMAD B. MATAR is a Chemical Engineer and the Team Leader for Operational Planning at KNPC, with experience in refinery operations, planning and process engineering.

ALI AL MANE is a Chemical Engineer with more than 15 yr of experience. He works in operational planning and has played a significant part in the MAA CFP commissioning.

MUTHUSAMY RAJENDRAN is a Chemical Engineer with 30 yr of experience in planning at KNPC and has worked in various fields of planning/operations and commissioning.

J. SAHA and S. CHAUDHURI, Bechtel India, Gurugram, India

Aromatic complex: A case study for relief load estimation of a heat integrated refinery unit

Refineries are moving from fuels to chemical production as the demand for fuel derived from crude oil declines in the near future. Conventional fuel-producing refineries are being targeted to reconfigure to produce more chemicals. Integration with an aromatic complex is one way to produce the chemicals for an oil-to-chemicals complex and will likely see wide industrial application in the coming years.

In an aromatic complex, aromatic compound producing units are closely integrated with one another to increase the energy efficiency of the entire complex. In the case of a common utility failure like power or cooling water, when the relief load is generated from the entire refinery, the calculation of the relief load from an aromatic complex must be performed carefully to avoid double counting of the relief load to optimize the flare header sizing. This article discusses the various approaches of calculating relief loads from an integrated aromatic complex and outlines a way to calculate an optimized relief load.

System overview. The principal products from an aromatic complex are mainly benzene, para-xylene and ortho-xylene—sometimes, a fraction of toluene and C_{10} aromatics are also produced. A simple block flow diagram of a modern integrated aromatic complex (excluding a reformer) is shown in FIG. 1. Reformed naphtha from the reformer unit is split in the reformate splitter (part of Unit B in FIG. 1) as light and heavy reformate product. Aromatic-rich components like benzene and toluene in light reformate are separated in the solvent extraction block (Unit D in FIG. 1) by extractive distillation; they are then further separated as pure benzene and toluene in the benzene toluene fractionation block (Unit C of FIG. 1). Heavy aromatic components (C_9) and sometimes toluene are sent to the trans-alkylation block (Unit E in FIG. 1) to recover more benzene and xylenes. The heavy reformate from the reformate splitter is sent to the xylene fractionation section of Unit B (FIG. 1)—from here, the mixed xylene stream containing meta and para isomers is sent to the paraxylene separation block (Unit A in FIG. 1) to separate p-xylene as product. The meta isomer is isomerized in Unit F (FIG. 1) to recover more para isomers from it.

Relief system design: Steady-state approach. In an aromatic complex, the major contributors of relief loads are the columns from various process units. Generally, the unbalanced heat load (UBH) method is used to estimate the relief loads from individual columns. Here, the UBH method has been progressively applied in evaluating relief loads from individual columns of various units, then on each process unit, and finally on the entire aromatic complex. Unbalanced mass and energy or enthalpy are calculated for a specified relief envelope, and the relief load is evaluated from that using the latent heat of vaporization. Generally, the top tray liquid composition of the column is used to estimate the latent heat of vaporization. Since multiple columns are involved in the present case study, latent heat of vaporization from the largest contributing column to relief is used to derive the relief load from unbalanced heat for the entire complex.

Case definition and methodology. In an energy integrated aromatic complex, a number of heat integration networks (HENs) exist among the units. This case study discusses the relief generated from the columns associated with the HEN among Units A–E, shown in FIG. 1. The detailed network diagram and the associated relief devices are shown in FIG. 2. Each unit inside the complex has multiple fractionating towers involved; however, for simplicity, a representative column from each unit is shown in the diagram.

In this network, mainly two streams from Unit A (paraxylene separation block), the column overhead vapor (dark solid blue line in FIG. 2) and side draw stream (ochre line in FIG. 2), are used as the reboiler heating medium of other columns in other

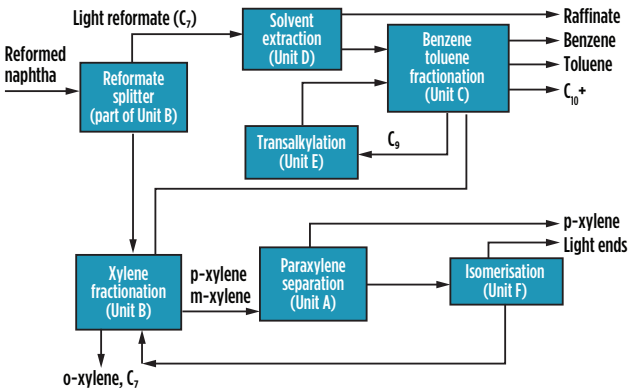

FIG. 1. Block flow diagram of a typical aromatic complex.

blocks inside the aromatic complex. The column overhead vapor is used to re-boil the column bottoms of Unit B (xylene fractionation), Unit C (benzene-toluene fractionation block) and Unit D (solvent extraction), whereas the side stream is used as heating medium in other columns inside Unit A (paraxylene separation block) and Unit E (transalkylation block).

Unit B has an internal heat integration network shown as a sub-block of Unit B in FIG. 2 and detailed in FIG. 3. The same concept of using the column overhead vapor inside the unit is used to re-boil the bottoms of the other columns of Unit B.

For a common mode of failure (general power failure is considered for the case study), the contribution of the relief load from each unit (Units A–E in FIG. 2) to the overall relief load of the complex is discussed in the sections below—from this, a realistic overall relief load is evaluated for the entire complex. The UBH method is applied for evaluating relief loads.

TABLE 1. Relief load from individual units during GEPF

Unit name	Relief valve tag	GEPF load
Unit A (paraxylene separation block)	PSV 1	700 t/hr
	PSV 2	100 t/hr
Unit B (xylene fractionation unit)	PSV 3	200 t/hr
Unit C (benzene toluene fractionation block)	PSV 4	120 t/hr
Unit D (solvent extraction block)	PSV 5	60 t/hr
Unit E (transalkylation block)	PSV 6	20 t/hr
Total GEPF relief load		1,200 t/hr

CASE STUDY

By modifiying the enthalpy balance envelope, a more optimized common mode failure load can be calculated, even with a simplified steady-state calculation for a heat integrated system.

Approach 1: Individual unit enthalpy balancing method.

During a global electrical power failure (GEPF), individual units (Units A–E) of the complex (mainly the columns) began relieving. The unbalanced heat and enthalpy across each column of the units were responsible for the resulting relief loads.

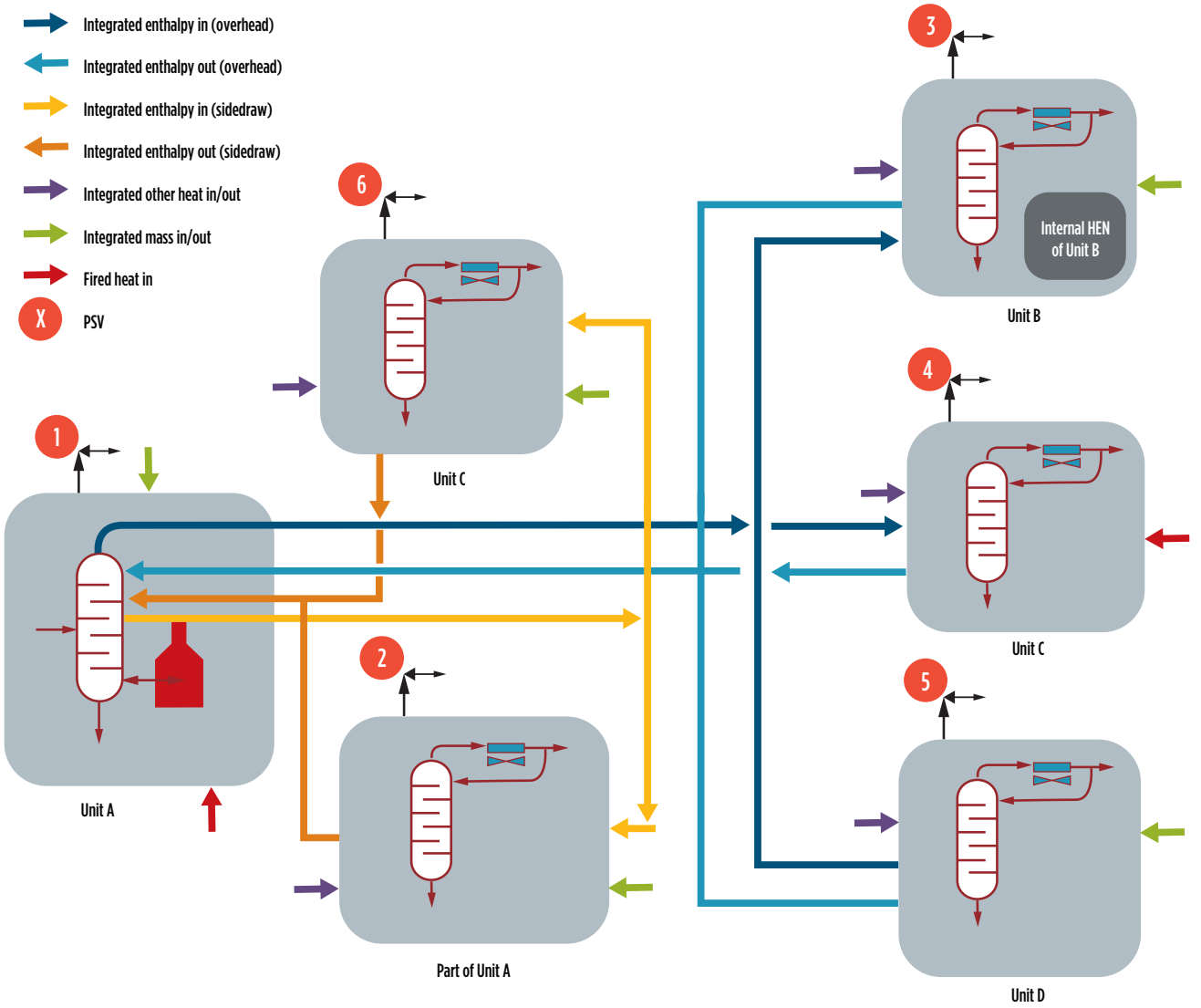

FIG. 2. Heat integration network inside the complex.

The relief load calculated by the steady-state UBH method from major sources of the units during global power failure are represented in TABLE 1. Six relief valves were considered for the case study (Units A–E), contributing to GEPF load (FIG. 2). The total calculated relief load for GEPF was 1,200 t/hr.

Approach 2: Energy balancing considering the heat integration network. For this case study, two heat integration networks of the complex were considered: one associated with the overhead circuit of the column of Unit A (dark solid blue line in FIG. 2) and another associated with the side draw circuit of the same column (ochre line in FIG. 2). Another HEN exists inside Unit B, shown in FIG. 3. A steady-state unbalanced energy calculation was performed for each HEN, and the resulting relief loads are presented in TABLE 2.

This resulted in a ~25% reduction of GEPF relief load from the complex with respect to the relief load evaluated by Approach 1.

In the next approach, it is shown that rather than analyzing the complex heat integration networks, the relief load can be evaluated and optimized by a simplified overall mass and energy balance approach for the entire complex (FIG. 3), as described in Approach 3.

Approach 3: Overall complex enthalpy balancing method. In this approach, the steady-state unbalanced mass and enthalpy balance method was applied for the overall complex (FIG. 4) during a global power failure.The unbalanced heat for the entire complex and resulting relief load is presented in TABLE 3. The latent heat of vaporization of the column associated with PSV1 was used to evaluate the relief load.

This results in a much lower GEPF relief load from the complex with respect to the relief load evaluated by Approach 2.

Results and takeaway.

1. **Expected % reduction**—Aproach 3 is quite logical, but optimistic, as the calculated GEPF load is less than the largest individual unit GEPF load. However, Approach 2 is a very plausible scenario where the contribution of the integrated HEN networks are ignored to avoid double counting, and only the contributions from independent enthalpy sources (e.g., fired heaters) are considered. Approach 2 offers signifcant savings without any additional investment in a high-integrity pressure protection system (HIPS) or additional layer of instrumented protection.

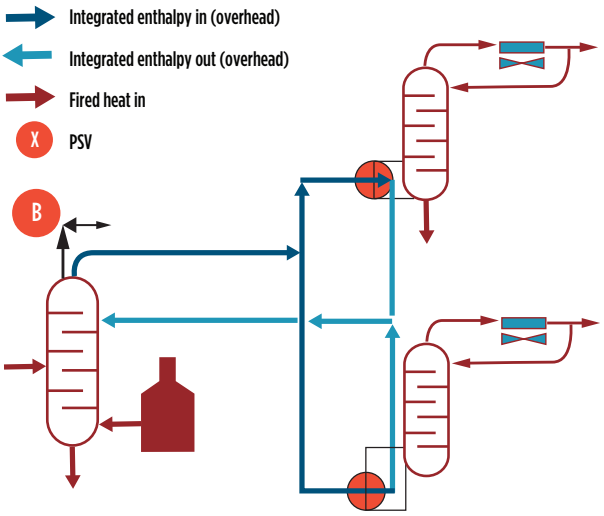

FIG. 3. Heat integration network inside Unit B.

TABLE 2. Relief load from individual HEN during GEPF

Unit name	Relief valve tag	Normalized GEPF load for publication
Unit A (paraxylene separation block)	PSV 1	700 t/hr
	PSV 2	0 t/hr
Unit B (xylene fractionation unit)	PSV 3	200 t/hr*
Unit C (benzene toluene fractionation block)	PSV 4	0 t/hr
Unit D (solvent extraction block)	PSV 5	0 t/hr
Unit E (Trans-alkylation block)	PSV 6	0 t/hr
Total GEPF relief load		900 t/hr

*This relief load is generated from the internal HEN of unit B and PSVB in FIG. 3.

TABLE 3. Relief load from overall complex enthalpy balance during GEPF

Unit name	Relief valve tag	Unbalanced heat	GEPF load
Overall complex	PSV^{O}	25 MW	500 t/hr
Total GEPF relief load			500 t/hr

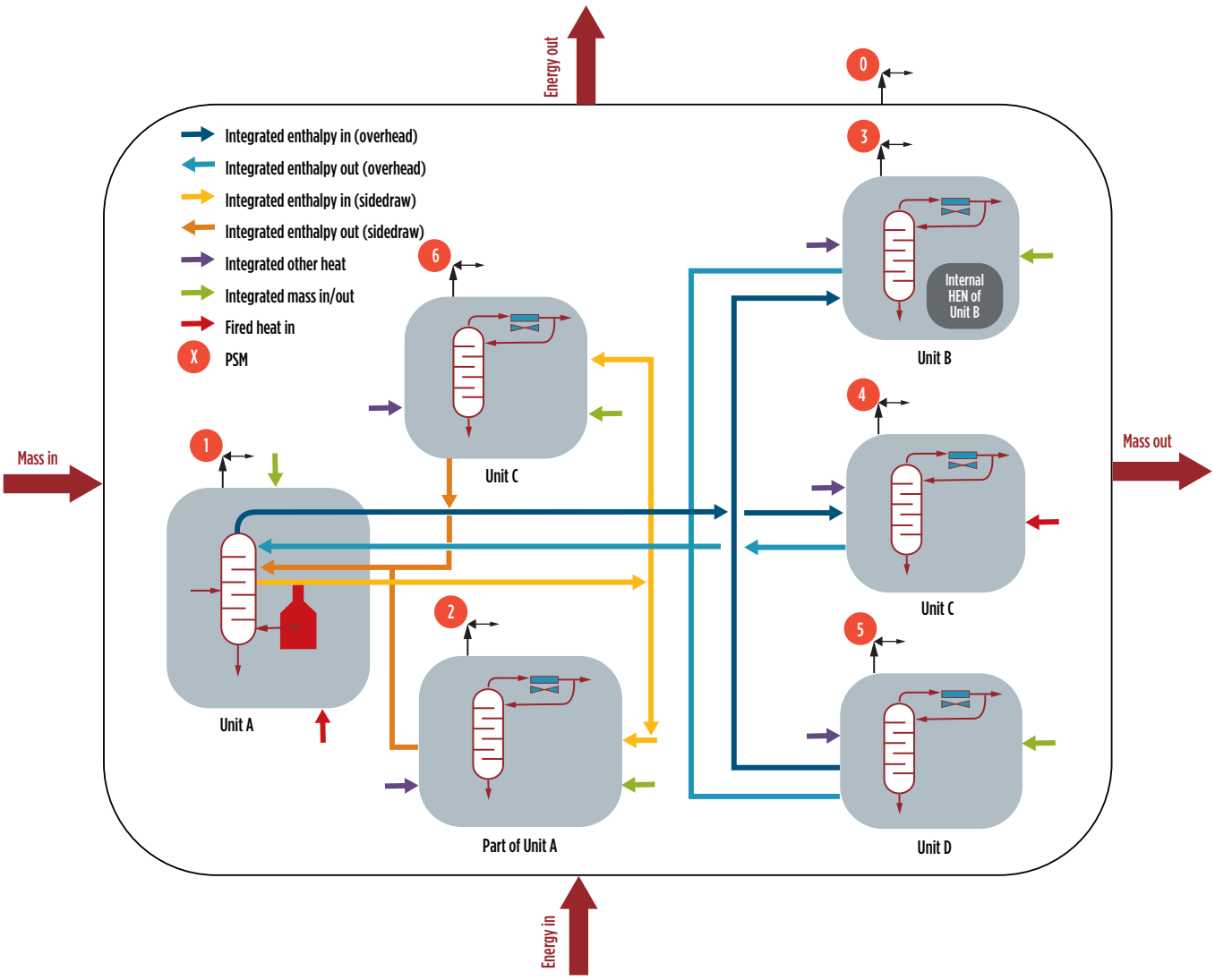

FIG. 4. Overall enthalpy balance of the complex.

2. **Impact on PSV sizing**—The authors do not recommend undersizing the individual relief valves associated with each network, but rather focus on establishing that the impact of simlutaneous release to the flare network would be much lower in a real-time scenario. They recommend a systematic approach for arriving at the reduced GEPF load.
3. **Impact on flare system sizing**—Savings are evident by simple steady-state calculation. However, the % of savings can vary depending on the type of plant and extent of heat integration networks. The approach, however, is universal and can be applied beyond an aromatic complex. This approach can be particularly handy in a revamp scenario where the real-time reductions in GEPF load of the existing system can be used to accommodate new units.
4. **Verification by dynamic simulation**—The suggested path forward to establish the findings are a dynamic simulation model that can consider the time linked response in a GEPF relief scenario with realistic system volumes, as well as favorable and non-favorable responses from the process control instruments associated with the envelope. This dynamic model, if developed and tested within the real-time simulation model of the existing plants of the operating companies, can build confidence in the approach and act as a proof of concept for generalization across the industry.

Note: The data and analysis presented should be treated as the authors' conceptual views and not directly attributed to the authors' organization. HP

JHUMA SAHA is a Process Engineer with Bechtel India. She has 16 yr of process engineering experience in petroleum refining and petrochemicals front-end engineering and detailed design. Prior to joining Bechtel India, she worked with Fluor, Foster Wheeler and Linde. She holds an MS degree in chemical engineering from Jadavpur University in India.

SUSHREE CHAUDHURI is a Process Engineer with Bechtel India. She has 20 yr of experience in petroleum refining, petrochemicals, offshore oil and gas, and flare systems, as well as front-end and detailed design. Prior to joining Bechtel India, she worked with Fluor Gurgaon and Foster Wheeler. She holds BS degrees in chemistry and chemical engineering from the University of Calcutta.

A. A. EZZAT, Contributing Editor,
Pharos University, Alexandria, Egypt

Prospects of petrochemical disruptive technology applications in Egypt Energy Hub Project

One of the most important challenges facing the Egyptian economy is the growing demand for petrochemicals in different sectors, particularly plastic materials and composites. The local market consumes approximately 2.3 MMtpy of plastic materials, which represents around 28% of market share.

The recent lean natural gas discoveries and reserves—more than 90 Tft^3—provide good feedstock for the petrochemicals industry. One of the challenges in the field of heterogeneous catalysis is the conversion of methane (CH_4) to valuable petrochemical materials, providing opportunities to improve the local petrochemical industries in Egypt.

The development of oxidative coupling of methane (OCM) is one of many disruptive technology applications having a significant impact on chemical industries.

Compared with steam cracking processes, the OCM process delivers a significant reduction in carbon emissions over traditional ethylene production processes.

OCM technology developments of methane feedstocks are a promising route for the production of light olefins as a petrochemical feedstock.

Methane-OCM process principles. OCM is defined as a process for converting methane into higher-value olefin products, improving carbon efficiency and resulting in the production of valuable fundamental petrochemicals. In this reaction, CH_4 is first oxidatively converted into ethane (C_2H_6), and then into ethylene (C_2H_4).

The fundamental chemical reaction mechanisms involve both a heterogeneous catalytic reaction, which includes the activation of CH_4 on a metal oxide surface, and a homogeneous gas-phase component, which includes free-radical chemistry.

The reactions are following Rideal-Redox type rection mechanisms. Ethane is produced mainly by the coupling of the surface-generated methyl group radicals in the gas phase.

The yield of C_2H_4 and C_2H_6 is limited by secondary reactions of $CH_3^{\cdot}$ radicals with the surface and by the further oxidation of C_2H_4, both on the catalyst surface and in the gas phase.

Generally, OCM technology is considered as a net-negative carbon dioxide (CO_2) producer per ton of olefins produced compared with traditional steam cracking processes.

This is a significant improvement in carbon emissions reduction, while concurrently capturing greater value from the molecules. In fact, the heat generation for the OCM exotherm and methane production (partly) from CO_2 is considered an offset to CO_2 emissions.

Historical background. OCM technology has attracted significant attention for producing olefins from methane. In the original process, the methane-per-pass-conversion was relatively low due to the thermodynamic limitations of the OCM adiabatic-reaction design.

The reaction exotherm improvements have been exploited by injecting ethane into a second reaction chamber, where the light alkane is thermally cracked to light olefins. Additionally, to enhance the overall carbon efficiency of the process, a catalytic methanation step is included to convert all generated carbon monoxide (CO) and a portion of the CO_2 oxidative coupling reaction co-product back to methane.

Researchers have developed the original process to improve per-pass conversion of methane, first by utilizing manganese oxide catalyst on silica. However, one drawback of this approach was its high operating temperatures, which has led to methyl radicals forming higher-carbon number products, and undesirable products (CO, CO_2 and coke).

The discovery of more selective catalysts that operate in the 400°C–600°C (752°F–1,112°F) range has provided promising yields and selectivity. However, long-term catalyst stability issues, largely due to the required high-reactor inlet temperatures, have significantly hampered them.

The introduction of advanced catalysts—based on zeolite-zinc (Zn)/chromium (Cr) metals—have been tested successfully, providing approximately 20% carbon conversion, with 80% combined C_2 selectivity in a single pass in the OCR reactor, limiting the secondary radical reactions and achieving a safe methane/oxygen ratio.

Modern OCM process. The modern OCM process technology, shown in **FIG. 1,** is based on the integration potential of the OCM process with the ethane dehydrogenation process to increase olefin production.

The modified technology is characterized by the low-temperature catalytic reaction application, where newly developed catalysts have been applied, based on zeolite-mixed-metal oxide-nanowire catalysts. This modified catalyst

produces a favorable yield, relatively high space velocity and a standard lifetime.

One of the challenges in the field of heterogeneous catalysis is the conversion of methane to valuable petrochemical materials, providing opportunities to improve the local petrochemical industries in Egypt. OCM technology developments are having a significant impact on chemical industries.

The process is based on a two-stage adiabatic reactor approach. It operates adiabatically with fewer stages at several hundred °C lower inlet temperatures, and at higher pressures, compared with the original processes.

Reactor heat recovery is a significant feature, where the exothermic heat from OCM is used to thermally crack the byproduct and fresh ethane balance to ethylene production.

To enhance the overall carbon efficiency of the process, a catalytic methanation step is included in the process. This reaction converts all generated CO and a portion of the CO_2 back to methane by using the hydrogen generated in both the OCM and ethane cracking-reaction sections of the post-OCM section of the reactor.

The reactor outlet stream is directed to the olefins cracking separation, recovery and fractionation steps.

Reaction mechanisms are summarized as follows:

(1) $2CH_4 + 0.5O_2 \rightarrow C_2H_6 + H_2O$

(2) $C_2H_6 + 0.5O_2 \rightarrow C_2H_4 + H_2O$

(3) $CH_4 + 2O_2 \rightarrow CO_2 + 2H_2O$

(4) $C_2H_4 + 3O_2 \rightarrow 2CO_2 + 2H_2O$

Reaction stoichiometry is used as information to engineer catalyst and tailor process conditions to favor reaction equilibrium, such as improving selectivity and shifting reaction toward better ethylene and ethane yields. Adding oxygen to methane, the thermodynamic barrier can be overcome and methane practical conversion limits can be achieved—i.e., the conversion of methane can be feasible at lower temperatures than the original process constraint limitations.

However, the methane/oxygen ratio should be below 2 for safe operations of the OCM reaction system. Note that ethylene deep oxidation to CO_2 is intensified during longer contact periods and endothermic gas phase EDH reaction is intensified in higher temperatures.

Thermodynamic considerations and economics. Difficulties in methane conversion exist due to its high molecular stability relative to any product to which it might be converted. Also, there are limitations to attain high ethylene yield in a methane OCM process where ethylene and ethane are more susceptible to oxidation than methane.

From the process performance side, it has been verified that OCM reactor performance of 50% ethylene selectivity and 18% ethylene yield—generating C_2 (ethylene and ethane) from methane in an OCM reactor and then converting ethane into ethylene via an EDH reactor—is economically attractive.

The feasibility of OCM depends on catalyst performance: a methane conversion in the range of 38% and C_2 selectivity of 85% (equivalent to 32% yield) can render this process economically competitive. In general, economics are highly sensitive to the price of feedstocks.

PROCESS OPERATING PARAMETERS

Feed specifications. The specification of the feed stream entering the OCM reactor has a direct impact on the ethylene selectivity and yield and on the reaction-thermal stable operation of the OCM reactor.

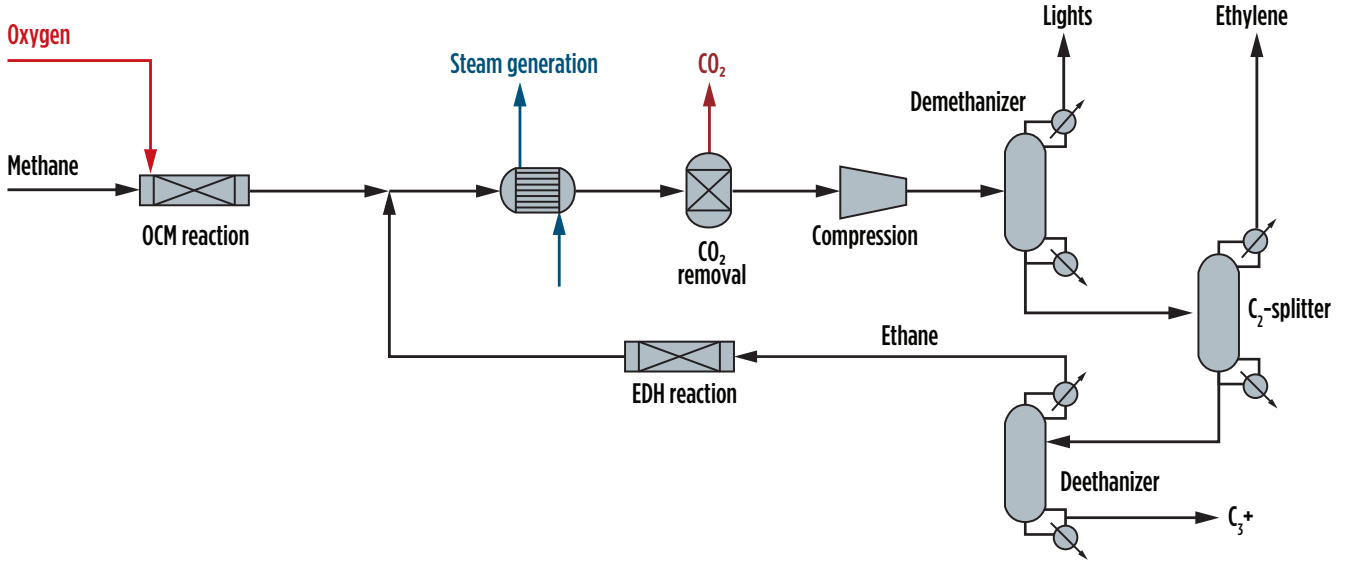

FIG. 1. A process flow diagram of the OCM process structures.

It affects the performance of the downstream units and the whole economy of the OCM process, considering that the quality of the methane, oxygen and the accompanying inert components are crucial factors in determining the operation and the economy of the OCM process.

The following parameters are the bases for analyzing the impact of the feed specifications on the performance process.

Methane-to-oxygen ratio—It has been proved that, in terms of methane conversion and ethylene selectivity and yield, using lower methane-to-oxygen ratios is preferred to target the highest ethylene yield with safe operations, i.e., securing a safe operation of OCM reactors while reducing the methane-to-oxygen ratio below 2 is essential. Under such conditions of low methane-to-oxygen ratio, the potential thermal integration with the dehydrogenation step of ethane is manifested.

Methane feed conditioning—Injecting an inert component, such as nitrogen or steam, for diluting purposes is usually recommended to provide flexibility in controlling the thermal performance of the OCM, which is considered a strongly exothermic reaction. This will result in a better distribution of oxygen along the catalytic bed, a relatively higher selectivity and an improved ethylene yield.

Ethane byproduct and reactant—Considering the shared products and complementary exothermic/endothermic thermal nature of the OCM process with ethane cracking systems, sharing the downstream units with an ethane cracking unit is well justified. Therefore, the heat integrated reactor, combining the exothermic OCM and endothermic ethane cracking reaction systems, and shared unit operations are utilized. In this integrated process, the increase of the C_2 yield and ethylene-to-ethane ratio by heat management of the OCM reactor have been realized by establishing a proper temperature profile along the bed and intensifying the gas phase dehydrogenation reaction for maximizing ethylene yield.

Formation of ethane and CO_x products. Produced methyl radicals are coupled in the gas phase of the ethane production step, undergoing homogeneous reactions. Ethane can be converted into ethylene by oxidative dehydrogenation of C_2H_6 and ethyl radical (C_2H_5) * by their interaction with surface oxygen or in the gas phase.

The formation of CO_x can occur by any of the following pathways:

C_2H_6 -------- C_2H_4 ------- CO, CO_2

$CH_3^* + O_2$– ------- CH_3O– ------- CO, CO_2

$CH_3^* + O_2$ --------- $CH_3O_2^*$ ---------- CO, CO_2

The formation of total oxidation products CO and CO_2 proceed mainly through the oxidation of CH_3 radicals. This occurs parallel to the formation of C_2H_6.

CO_2 removal section. CO_2 is generated as an undesired byproduct of the OCM reaction and should be separated right after the reactor. Due to their corrosive nature, CO_2 and water are the first components to be separated in the OCM downstream section. Suitable amine solutions are selected to attain the highest removal performances of CO_2 in terms of lowest regeneration energy consumption, and ethylene losses in the absorber.

Ethylene purification section. Ethylene purification is an energy intensive process. The separation occurs in three columns: the demethanizer, C_2-splitter and C_3+ recovery. The optimum design of this section has a significant impact on the economy of the whole process.

Demethanizer. The methane conversion in the OCM process is unavoidably low (i.e., < 50%). Consequently, a significant amount of the remaining unreacted methane should be separated from the rest of the gaseous species. Conventionally, this is performed via energy-intensive cryogenic distillation, which stands as a major source of energy deficiency in the OCM process.

Given the high concentration of methane and other light gases (H_2, CO, etc.) in the feed stream to be separated in the demethanizer, a high pressure is required to efficiently fulfill the condensation task. Normally, liquid methane has been used as a cryogenic refrigeration utility, which is required for partial condensation upstream (CH_4, H_2, N_2, CO) in the condenser.

The first cascade in the refrigeration cycle is methane; two other cascades operating with ethylene and propylene are used for efficiently closing the refrigeration cycle and internally cooling the media. This enables establishing a condenser temperature of about –112°C under 33.5 bar operating pressure in an 8.5-m diameter distillation column. The separation performance of this system is designed in a way to secure traces of methane in the C_2-rich stream and minimize the ethylene loss to < 0.3%.

Ethylene/ethane splitter. A similar approach was applied in the C_2 splitter for separating ethane from ethylene under 20 bar pressure, utilizing propylene refrigerant for establishing a condenser temperature of about –29°C using a distillate-to-feed ratio of 0.65 to secure ethylene product purity of 99.5%.

Heat integration. The optimum utilization of the heat sources and sinks in the OCM process are key factors to improve the economy and energy performance of the process, utilizing the significant generated OCM reaction heat in the EDH reactor section.

Takeaway. This technology is envisaged to meet challenges with tangible economic advantages, driven by feedstock availability and the extreme pricing dynamics of the energy industry.

Based on cost forecasts for natural gas, the gap between the ethylene price obtained with conventional technologies and the one obtained with OCM technology is expected to progressively become smaller, forecasting OCM to be competitive with traditional technologies in the near future. HP

ABBAS EZZAT works as a Petrochemical Professor at Pharos University and a Distinguished Scientist at the Materials Science Department within the Institute of Graduate Studies and Research at Alexandria University. He is also a local consultant for the Egyptian petroleum and petrochemical sectors and a Senior Associate Consultant for Channoil Consulting Ltd. in London. Prior to joining academia, he occupied several top management positions in the Egyptian petroleum and petrochemical industries. Dr. Ezzat holds an MSc degree in chemical engineering from Washington University and a PhD in petrochemical applications from Alexandria University. He completed his postgraduate studies in petroleum processing technologies from the School of Chemical Engineering at Oklahoma State University.

F. BAARS, Fluor, Amsterdam, Netherlands; and
S. ORUGANTI and **P. KALIA,** Fluor, New Delhi, India

Oil refinery/petrochemical integration in a CO_2-constrained world—Part 2

Petrochemical demand will increase with gross domestic product, while the demand for motor fuels will only show modest growth and may even decline in certain regions, given environmental/legislative pressures and the introduction of battery-powered electric vehicles. Any new oil refinery will likely include petrochemical facilities, as well.

In Part 1, published in the July issue of *Hydrocarbon Processing*, the authors reviewed several possible refinery/petrochemical complex configurations around an RFCCU (FIG. 1 from Part 1) or HCU (FIG. 4 from Part 1). It was shown that investments, and gross and net margins, vary considerably between the various configurations. This article will evaluate the impact of a CO_2 tax and crude source/pricing on IRR.

CO_2 emissions. The CO_2 emissions associated with the various configurations are reported in TABLE 6. CO_2 emissions are the total emissions of the complex due to the combustion of natural gas, refinery fuel gas and FCC coke, and exclude the CO_2 associated with generating the required electrical power or any other CO_2 emissions associated with outside battery limit facilities (such as tank heating, process water demineralization, boiler feed water preparation, flare purging and tracing). As such, the emissions reported in this article are the larger part of the Scope 1 emissions.

For the FCCU cases (A0–A2), the CO_2 emissions increase with increased complexity—e.g., increasing from 367 t/hr to 402 t/hr when going from the Base Case A0 to Case A2, primarily due to the contribution of the aromatics complex (FIGS. 5 and 6). The RFCCU is the biggest contributor to emissions, representing 45% and 41% in Base Case A0 and Case A2, respectively.

For the HCU alternatives, the CO_2 emissions gradually increase with increased complexity. In the SC cases (B2A and B2B), CO_2 emissions have increased 3x–4x relative to the base case.

In Base Case B0 (FIG. 7), the HPU and CDU/VDU are the biggest contributors, accounting for 30% and 24% of total CO_2 emissions, respectively. With the addition of the steam cracker and the aromatics complex, and converting the hydrocracker to a naphtha-oriented hydrocracker, CO_2 emissions increased from 223 t/hr to 472 t/hr (Case B3), as shown in FIG. 8.

In Case B3 (FIG. 8), the SC and aromatics units have become the biggest CO_2 emissions contributors, representing 32% and 15%, respectively. The CO_2 emissions for cases B4 and B5 are

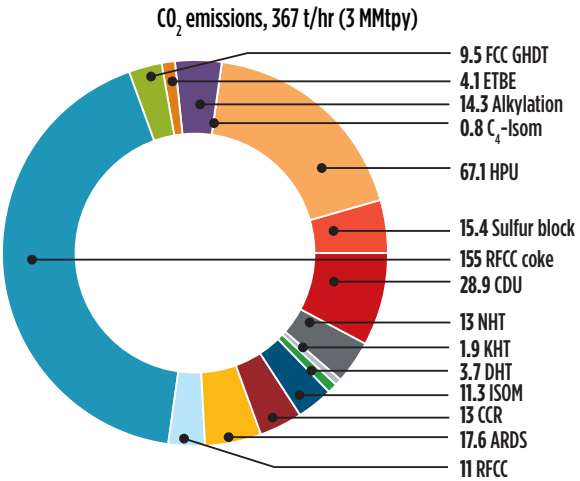

FIG. 5. CO_2 emissions for Case A0: ARDS + RFCCU.

TABLE 6. Specific CO_2 emissions for the various configurations

Case	Description	CO_2 emissions, CO_2/t crude
A0	RFCC	0.31
A1	RFCC + PP	0.32
A2	RFCC + PP + aromatics complex	0.34
B0	DCU + HCU	0.19
B1	DCU + HCU + SC	0.38
B2A	DCU + NHCU[a] + SC	0.56
B2B	DCU + NHCU[b] + SC	0.79
B3	DCU + NHCU + SC + aromatics complex	0.40
B4	DCU + NHCU + aromatics complex	0.25
B5	RHC + NHCU + aromatics complex	0.27

[a] NHCU: Hydrocracking aimed for maximum naphtha production
[b] Gasoils to the NHCU

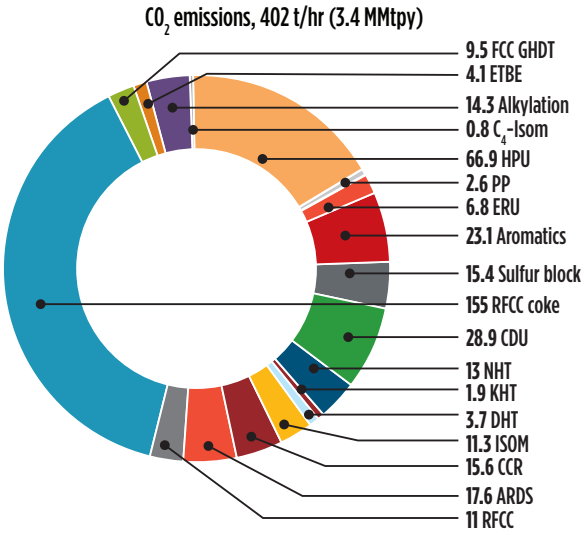

FIG. 6. CO_2 emissions for Case A2: ARDS + RFCCU + PP + aromatics complex.

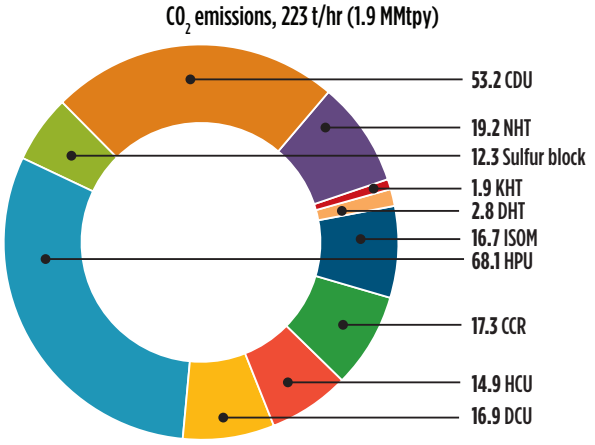

FIG. 7. CO_2 emissions for Base Case B0: DCU + HCU. **Note:** CDU and VDU emissions are combined.

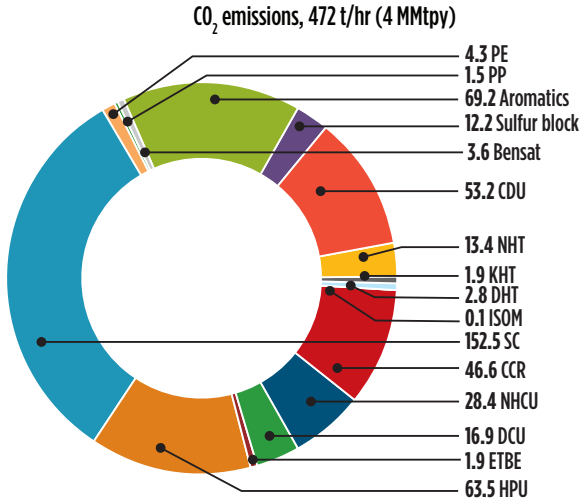

FIG. 8. CO_2 emissions for Case B3: DCU + NHCU + SC + aromatics complex. **Note:** CDU and VDU emissions are combined.

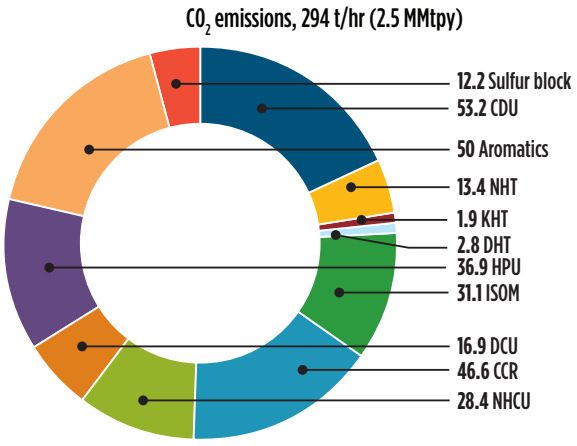

FIG. 9. CO_2 emissions, Case B4: DCU + NHCU + aromatics complex. **Note:** CDU and VDU emissions are combined.

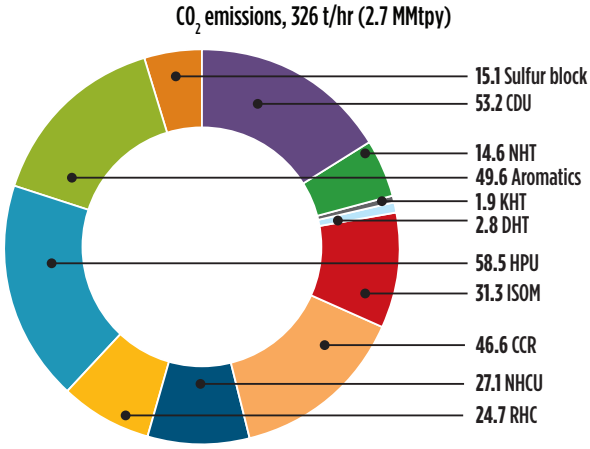

FIG. 10. CO_2 emissions, Case B5: RHC + NHCU + aromatics complex. **Note:** CDU and VDU emissions are combined.

shown in FIGS. 9 and 10. In Case B4, the aromatics complex is second to the CDU/VDU in terms of total CO_2 emissions. In Case B5, the top CO_2 emitters are the HPU (18%), the CDU/VDU (16%) and the aromatics complex (15%).

CO_2 emissions increase with increasing petrochemical production (FIG. 11). The steam cracker HCU cases (B1, B2A and B2B) have the highest emissions. The aromatics HCU cases (B3, B4 and B5) have the lower emissions at a given petrochemicals output. The FCC cases (A0–A2) are intermediate.

Effect of a CO_2 tax. The effect of a CO_2 tax on IRR are shown in FIG. 12. IRR deteriorates with an increasing CO_2 tax, but even more so for the high-CO_2 cases—e.g., Case B2B: DCU + NHCU2 + SC, with emissions of 0.79 t CO_2/t crude (TABLE 7). For Case B2B, IRR even becomes negative when the CO_2 tax reaches $125/t. For lower-$CO_2$-intensive configurations (e.g., Case B5: RHC + NHCU + aromatics complex, with CO_2 emissions of 0.27 t/t crude, or Case A2: RFCC + PP + aromatics complex, with CO_2 emissions of 0.34 t/t crude), the IRR drops only 5% when the CO_2 tax increases from zero to $125/t CO_2.

The impact of a CO_2 tax can be mitigated by reducing CO_2 emissions at the source or by opting for carbon capture where

TABLE 7. Impact of a CO_2 tax on IRR, with and without CO_2 capture options—breakeven points are shown for pre-combustion capture (blue) and post-combustion capture (green)

		CO_2 emissions, t/t crude	IRR, %				
CO_2 tax, $/t			0	50	75	100	125
Case A2: RFCC + PP + aromatics complex	No capture	0.34	18	16	14.9	13.8	12.6
	Pre-combustion capture	0.3	17.6	15.8	14.9	13.9	12.8
	Post-combustion capture	0.11	14.4	13.7	13.4	13	12.7
Case B2B: DCU + NHCU + SC	No capture	0.79	8.3	4.9	2.9	0.7	-2.1
	Pre-combustion capture	0.68	7.8	4.8	3.1	1.2	-1
	Post-combustion capture	0.25	3.7	2.4	1.8	1.1	0.3
Case B5: RHC + NHCU + aromatics complex	No capture	0.27	17.7	15.8	14.8	13.7	12.6
	Pre-combustion capture	0.24	17.3	15.6	14.7	13.8	12.8
	Post-combustion capture	0.09	14.2	13.5	13.2	12.9	12.6

TABLE 8. Impact of crude type on IRR (prices of other feeds/products and utilities are unchanged)—the configurations with the highest IRR are in green, followed by the second-highest in blue and the lowest in orange

	Case		Urals	Arab Light	CPC
RFCC	A0	RFCC	12.4	8.9	3.9
	A1	RFCC + PP	16.5	13.5	8.4
	A2	RFCC + PP + aromatics complex	18	15.8	15.8
DCU	B0	DCU + HCU	11	5.3	5.8
	B1	DCU + HCU + SC	12.4	9.6	11.5
	B2A	DCU + NHCU + SC	11.2	9	10.9
	B2B	DCU + NHCU + SC, GO to NHCU	8.3	6.5	7.8
	B3	DCU + NHCU + SC + aromatics complex	14.1	12	14.2
	B4	DCU + NHCU + aromatics complex	15.4	12.4	16.3
	B5	RHC + NHCU + aromatics complex	17.7	15.3	17.3

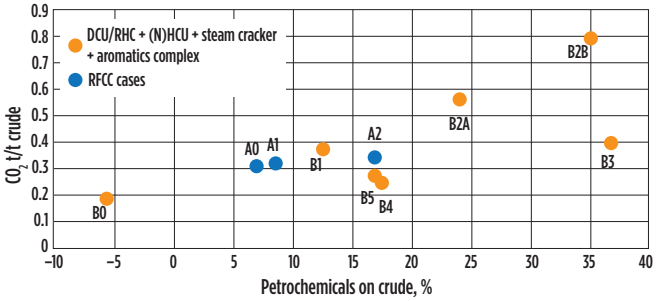

FIG. 11. CO_2 emissions vs. petrochemical output.

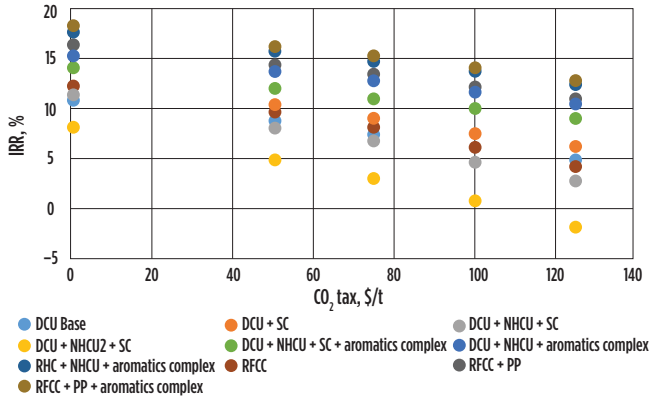

FIG. 12. Impact of a CO_2 tax on IRR.

CO_2 can be reused (e.g., enhanced oil recovery) or stored as part of a CO_2 sequestration project. Intrinsic CO_2 emissions can be reduced by implementing energy conservation methods, incorporating system electrification (such as replacing steam drivers with electric drivers and using electric heaters instead of gas-fired heaters), and replacing natural gas for bio-based materials or co-processing bio-based materials in the process units.

Two cases of carbon capture are considered: 1) pre-combustion CO_2 capture from the process gas in a hydrogen plant (also known as blue hydrogen, which will reduce hydrogen plant CO_2 emissions by 50%), and 2) post-combustion CO_2 capture from the combined complex flue gases, which reduces total CO_2 emissions by approximately 70% in this example (theoretically, higher removal rates are possible). In all cases, CO_2 is made available at the complex battery limit at a pressure of 35 barg for further transportation.

Adding CO_2 capture comes with increased investment and operational costs, both of which negatively impact economics. Relative to the reference case, IRR drops between 0.4% (in Case A2, IRR decreases 18% to 17.6%, and, in Case B5, IRR decreases from 17.7% to 17.3%) and 0.5% (in Case B2B, IRR decreases from 8.3% to 7.8%), with pre-combustion capture and no CO_2 tax enforced (TABLE 7). Post-combustion CO_2 capture reduces IRR between 3.5% (in Case B5, IRR decreases from 17.7% to 14.2%) and 4.6% (in Case B2B, IRR decreases from 8.3% to 3.7%).

IRR decreases as the CO_2 tax increases, but less so when CO_2 capture is part of the complex. At some point, the IRR with CO_2 capture exceeds the IRR without CO_2 capture, despite the higher investment and operational costs. For pre-combustion CO_2 capture, this happens when the CO_2 tax exceeds $75/t. For post-combustion CO_2 capture, this occurs when the CO_2

tax approaches $100/t for a high-$CO_2$ case (e.g., Case B2B). For lower-CO_2 cases (e.g., cases A2 and B5), the CO_2 tax would need to be more than $125/t.

Crude effects. The design crude also influences economics. Both Arab Light and Caspian Pipeline Consortium (CPC) crudes have a higher price in this study. This hurts the simple configurations (e.g., cases A0 and B0), with IRR decreasing 5%–8% (**TABLE 8**), but much less than in more complex configurations where IRR decreases only 1%–3%, as they have a higher intrinsic gross margin.

With CPC crude, the RFCC Case A0 looks poor as the gasoline pool becomes unbalanced. The smaller FCCU (and ETBE and alkylation units), relative to the Urals or Arab Light case, now requires the purchase of a significant amount of ETBE as a gasoline pool blending component. The base HCU (Case B0) also needs a high ETBE import. This disadvantage disappears when the reformate is sent to an aromatics complex (Case A2) or when a steam cracker and/or aromatics complex is included (cases B1–B5). The aromatic cases (A2, B3, B4 and B5) look particularly good when using CPC crude.

As shown, the ranking of technologies changes with crude. In the CPC case, an advanced DCU/RHCU scheme (Case B4 or B5) is more attractive than an RFCC-based scheme (Case A2).

Takeaway. Any future new refinery complex will likely integrate petrochemicals manufacturing. Existing refineries will need to look at options to expand into petrochemical units or to integrate with neighboring petrochemical plants. In general, the more integrated schemes—with a high petrochemical output—are more robust to changes in feed/product and utility pricing, as well as to the selection of crude and CO_2 tax.

CO_2 emissions will increase as petrochemical output increases—the addition of a steam cracker has a large effect on CO_2 emissions. A CO_2 tax will negatively affect the economics of any refinery/petrochemical complex.

In this article, the authors have illustrated how it paid to invest in pre-combustion CO_2 capture at the hydrogen plant when CO_2 taxes increased to $75/t. Post-combustion carbon capture did not look attractive until the CO_2 tax reached $125/t.

These projects can be implemented stagewise, with petrochemical units being built in a second phase commensurate with an anticipated reduction in motor fuel demand. Processing bio-based materials and/or streams from plastic recycle plants presents another opportunity to improve economics and sustainability.

The conclusions drawn in this analysis are based on a particular crude diet, feed and product pricing, as well as on operational and investment costs, and may change depending on local circumstances. Feedstock flexibility and a robustness for feed/product pricing changes, coupled with a proper assessment of risks and opportunities associated with each investment, should be part of a proper evaluation. HP

R. V. SCHNEIDER, Chiyoda Corp., Houston, Texas; and **D. KUROSAKI** and **M. OKI,** Chiyoda Corp., Yokohama, Japan

Advances in chemical carriers for hydrogen

Is hydrogen the fuel of the future? This most-abundant element in the universe has, for many years, played a key role in the international space program and in more down-to-earth applications for refinery upgrading and chemicals production, such as methanol and ammonia. However, production of renewable H_2 at a competitive cost, and the transport thereof, present key issues that are being studied and progressed by almost every developed country in the world.

The benefits are obvious: H_2 can be made from many and varied processes and burns completely and cleanly, with only water vapor as a byproduct of combustion. Japan has progressed its H_2 economy by developing detailed plans to replace nuclear energy and fossil fuel combustion with clean-burning H_2, both at the industrial and residential scale. Europe has, for several years, harnessed wind energy for power production; this technology also can be used for H_2 production where desired. A project is already underway in Germany to provide H_2 to an existing refinery for fuels upgrading, using wind energy to power the electrolyzer that will produce the renewable H_2.

In the U.S., California leads the way with initiatives that are not only policy-based but are also state law. Almost 9,000 fuel cell personal vehicles traverse the California freeways today, with fuel available for a 5-min fill-up from 42 stations. By 2025, it is anticipated that there will be many more fuel cell electric vehicles (FCEVs) and many more refueling stations in use, along with H_2 use in city buses and heavy transport vehicles, supported by state laws driving these developments.

Northeastern states in the U.S. will likely follow California's lead, and provincial energy ministries in Canada's eastern and western regions are already progressing initiatives that are modeled, to a degree, after those in California. While the mid-section of the U.S. would not be a likely place for H_2 to take root, a U.S. Department of Energy (DOE)-sponsored study is already underway in oil- and gas-rich Texas to consider and demonstrate H_2 as a fuel for data center backup power and mobility uses. Additionally, the Texas study will consider how the Port of Houston may benefit from material transport using H_2, similar to what is already being done in Long Beach, California.

In this article, the authors introduce liquid organic H_2 carrier (LOHC) technology and how it has been applied to the world's first global H_2 supply chain demonstration project.

Demand drivers. Demand for H_2 in the U.S. alone is more than 11 metric MMtpy. At present, the two largest uses for H_2 are hydroprocessing in refineries (57%) and chemicals production (38%, ammonia and methanol production combined). Future additional demand will be driven by a number of applications:

- Personal mobility
- Heavy transport of commercial goods
- Mass transport fuels
- Warehouse forklifts and port heavy goods movement
- Electric power backup
- Clean power generation
- Residential and industrial applications.

Estimates project that U.S. H_2 demand will grow to about 17 metric MMtpy by 2030 and to 63 metric MMtpy or more by 2050. Considering mobility applications alone, several automakers are producing personal FCEV cars—Toyota (Mirai) (FIG. 1), Honda (Clarity) and Hyundai (Nexo). While less than 10,000 FCEVs are on U.S. roads at present, projections call for up to 150,000 FCEV sales by 2025 and more than 1 MM sales by 2030.

A personal FCEV requires a fill-up of approximately 5 kg of H_2. Considering the current proven range of these vehicles and average annual use, the 2030 FCEV H_2 demand in California alone can be calculated in the range of 250,000 metric t for passenger cars only. When heavy-duty vehicles for material transport are factored into the mix, demand will be considerably higher.

By 2030, fuel cell-powered forklifts used by large-warehouse companies, such as Walmart and Amazon, could number more than 300,000. Total added H_2 demand by 2030 could be approximately 3 metric MMt, although this number is expected to increase by around 45 metric MMt by 2050—a significant volume.

Investment in the H_2 economy is forecast in the range of $8B–$10B by 2030, and hundreds of thousands of new jobs could be created. While these numbers are not concrete, they impart a sense of scale for the potential of H_2 in the U.S. and other forward-thinking countries.

Expected benefits from the integration of H_2 into the U.S. energy picture include not only decarbonization, but also a bolstering of the overall economy, preservation and strengthening of the U.S. energy

FIG. 1. Toyota's Mirai FCEV passenger car, produced starting in 2014.

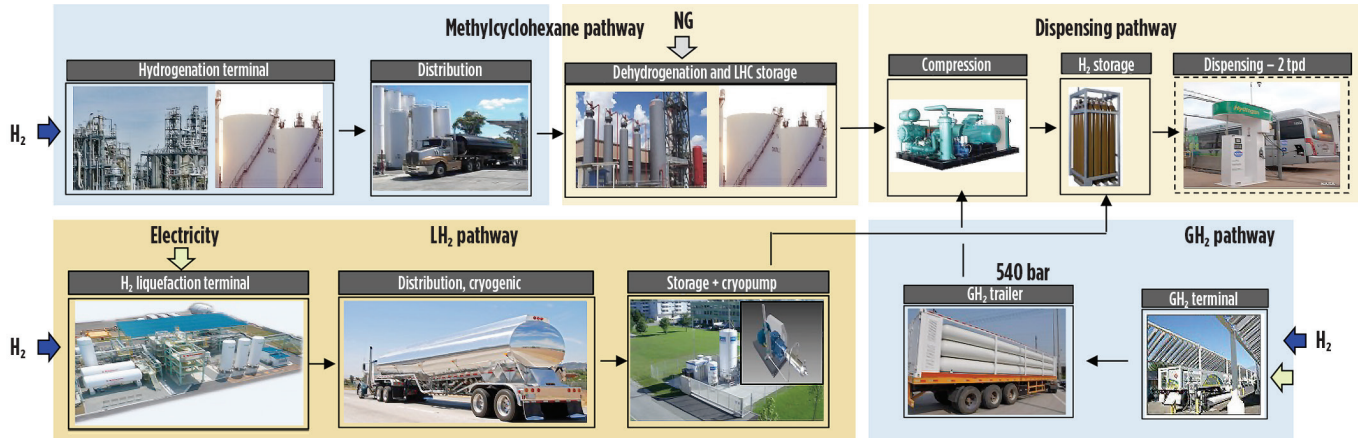

FIG. 2. Process flow showing how H_2 is liquefied for transport as a cryogenic liquid, is transported as a compressed gas or is transported within an organic carrier (LOHC).

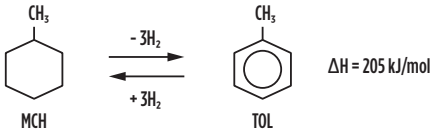

FIG. 3. Chemical reaction formula used for the hydrogen[a] process.

position and obvious improvements to health, the environment and quality of life. Benefits on a more global basis would be commensurately similar.

Options for hydrogen deployment. While the future for H_2 looks bright, production, transportation, distribution and a host of associated infrastructural issues need to be considered. Assuming H_2 availability, how to get it from where it is made to where it is most needed (and at a reasonable cost) is of paramount interest.

Historically, H_2 has been transported either as a compressed gas in tube trailers or as a cryogenic liquid. Both methods have pros and cons, but transportation selection and cost are ultimately determined by how much H_2 must be transported and over what distance.

Prior studies undertaken for localized distribution have considered and compared these conventional methodologies with newer, more promising options of transporting H_2 bound by a chemical carrier, known generically as a liquid organic H_2 carrier (LOHC).

FIG. 2 shows how H_2 is liquefied to 20K (–253°C/–423°F) for transport as a cryogenic liquid. This is an energy-intensive operation that uses around 30% of the contained H_2 energy to complete the liquefaction process. The cryogenic H_2 is then transported from the liquefaction point to the point of use by truck. As per U.S. Department of Transportation (DOT) limitations on truck transport of liquefied H_2, approximately 4,000 kg of H_2 can be transported per truckload. At the delivery site, the liquid can be cryo-pumped to the dispensing point for subsequent vaporization. At present, transportation of liquid H_2 is available only by truck; therefore, the scale of transportation is limited, and further technology development is required for large-scale liquid transportation by ship.

Alternatively, H_2 at approximately 540 bar (7,830 psi) can be transported by tube trailer from a terminal to a dispensing point where final compression (to around 700 bar/10,000 psi) is accomplished prior to ultimate utilization. U.S. DOT regulations also limit the amount of H_2 that can be transported per tube-trailer truckload to approximately 1,050 kg of H_2 per truck.

Lastly, the LOHC option may be considered as a viable alternative. LOHC is a suitable technology for large-scale, long-distance H_2 transportation, or for large-scale or daily to seasonal H_2 storage, as will be discussed in more detail in this article. In all of these cases, the distance of transport, the volume of material being transported and the distribution particulars will drive the best choice for the particular H_2 application at hand.

Advances in hydrogen storage/transport technology. A trademarked hydrogen[a] process is an H_2 storage and transportation technology for large-scale and long-distance transportation. H_2 is chemically fixed to toluene and converted to methylcyclohexane, according to the reaction shown in **FIG. 3.** Methylcyclohexane is a convenient carrier for H_2, as it is easy to store and transport under ambient temperature and atmospheric pressure. In the process, H_2 is stored and transported in large-scale quantities at a competitive cost, since cryogenic liquefaction or compression to very high pressures is not required.

The process is based on a simple process configuration. Methylcyclohexane and toluene react in fixed-bed, tubular-type reactors in the vapor phase. **FIG. 4** shows simplified process flow diagrams of the hydrogenation and dehydrogenation processes for the overall process. In the **hydrogenation process,** toluene feed is vaporized in the vaporizer (1) and mixed with H_2, including recycle gas. The mixed feed is superheated to the reaction temperature (2) and then enters the top of the reactor (3), which is a fixed-bed, tubular reactor charged with a semi-conventional hydrogenation catalyst. In the reactor tubes, toluene reacts with H_2 to produce methylcyclohexane.

Hydrogenation of toluene is an exothermic reaction. The generated heat is removed by cooling water to control the reaction temperature, and the heat is subsequently recovered as medium-pressure steam, which can be further utilized as needed. The generated steam is clean energy without carbon emissions. The effluent gas from the tubular reactor is cooled, the condensed methylcyclohexane is separated (6) from the recycle gas, and the liquid product (methylcyclohexane) is sent to storage tanks. Recycle gas is then returned to the reactor after being mixed with fresh H_2 feed. Very high product yield is achieved

in this step, which contributes to the efficiency of the hydrogen process. Toluene losses within the process are minimal.

Produced methylcyclohexane is then transported to the site of H_2 use. H_2 is recovered from the methylcyclohexane via catalytic dehydrogenation. The **dehydrogenation process** can be described as follows: The methylcyclohexane feed is vaporized in the vaporizer (11) and superheated in the charge heater (12) before entering the catalyst-packed tubes of the dehydrogenation reactor (13). This reactor is a tubular, quasi-isothermal reactor design similar to that employed in the hydrogenation process. The dehydrogenation catalyst was specially developed in-house for this process. Since dehydrogenation is an endothermic reaction, an external heating source is required. Typically, a hot oil system is applied (14) to supply the necessary reaction heat.

The dehydrogenation plant is ideally colocated within an existing complex where available waste heat at a suitable temperature level can be utilized. Reactor effluent gas is cooled to separate H_2 and condensed toluene (16). In the reactor, methylcyclohexane is reconverted to toluene and H_2. The recovered H_2 is separated from the toluene and is subsequently compressed and purified, if necessary, to meet relevant product H_2 specifications (18). Toluene is then transported back to the site of the hydrogenation plant for re-hydrogenation.

Catalyst development. Key to the success of the trademarked hydrogen process[a] was the development of a dehydrogenation catalyst that was not only robust, but also exhibited superior selectivity and stability. As depicted in FIG. 5, methylcyclohexane conversion of greater than 95% was eventually achieved at a selectivity of 99.9%, which provides for a very low level of reaction byproducts.

Accelerated, long-term testing showed remarkable stability even after 10,000 hr onstream. Commercially, a catalyst life of 2 yr could be reasonably expected. Once a suitable candidate catalyst was developed, the next steps to eventual commercialization included scale-up for manufacturing and pilot-level demo of both the catalyst and the equipment.

From April 2013–November 2014, 10,000 hr of pilot plant operation were successfully completed, and the expected performance and life of the catalysts were confirmed. In the pilot-scale test facility, methylcyclohexane and toluene were continuously dehydrogenated and rehydrogenated at a consistent rate of 50 Nm^3/hr of H_2 (FIG. 6).

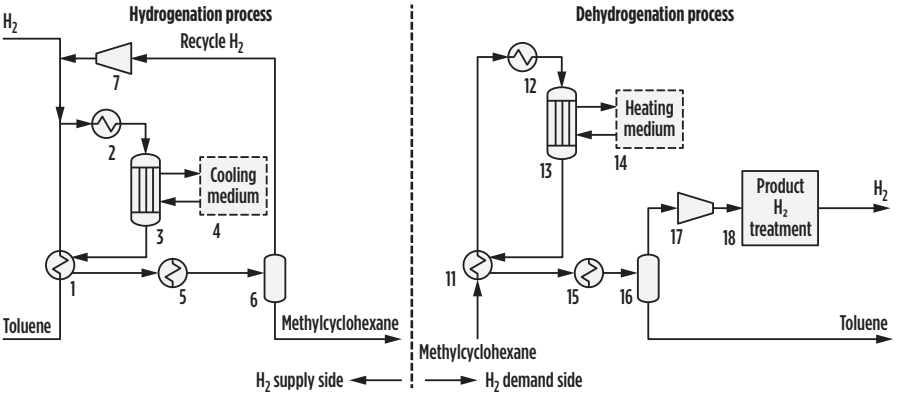

FIG. 4. Hydrogenation and dehydrogenation processes for the trademarked hydrogen process.[a]

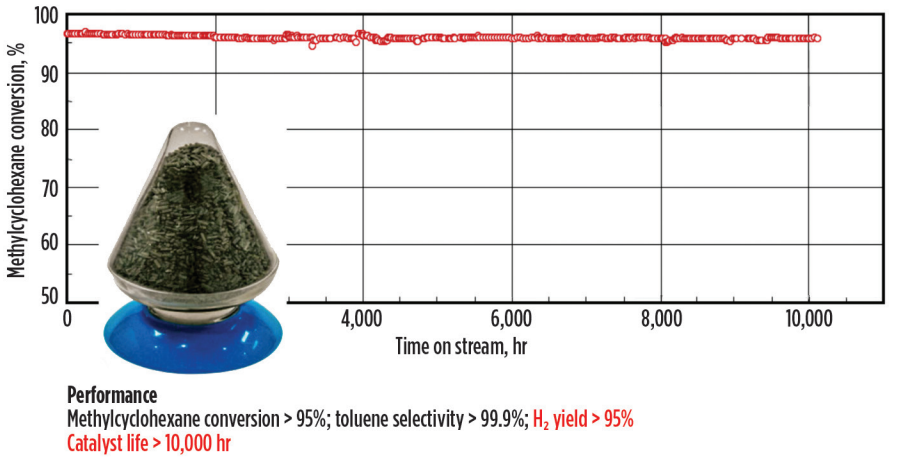

FIG. 5. Dehydrogenation catalyst development and performance.

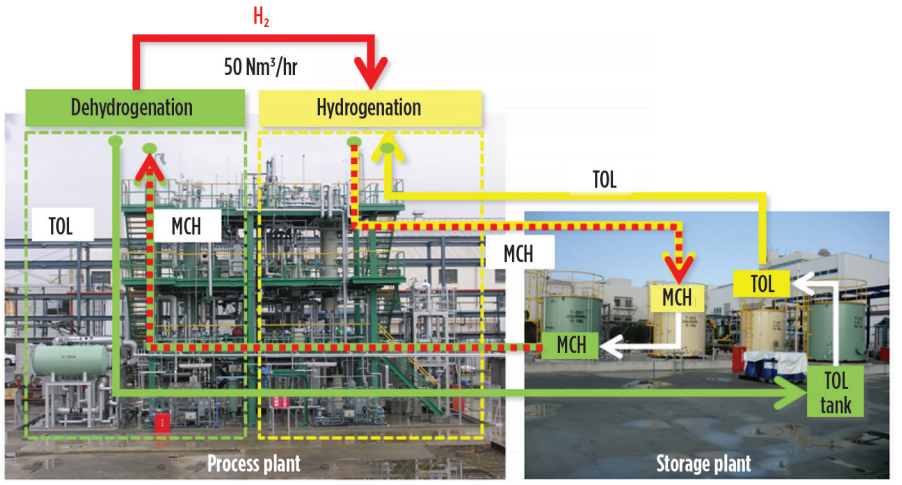

FIG. 6. Demonstration plant in Yokohama, Japan showing dehydrogenation/hydrogenation for the trademarked hydrogen process.[a]

Demonstration projects. The authors' company, along with its partners Mitsubishi, Mitsui and Nippon Yusen, established the Advanced Hydrogen Energy Chain Association for Technology Develop-

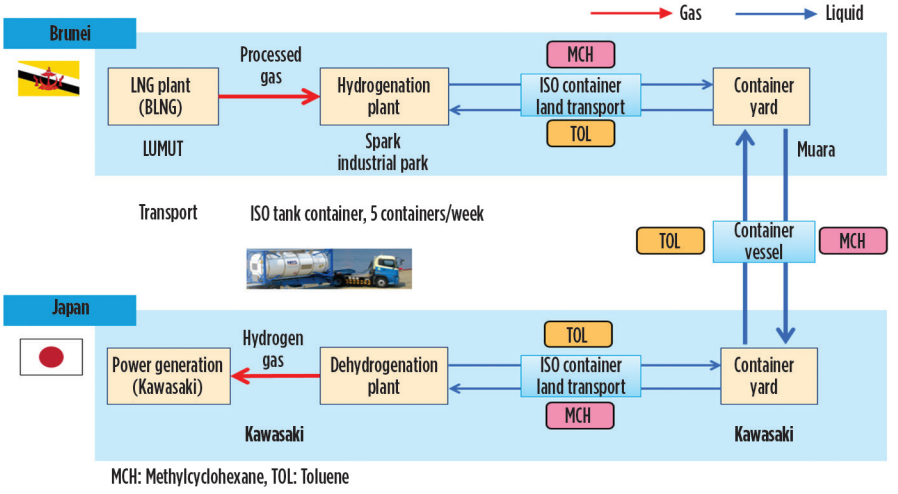

FIG. 7. Logistics flow for the AHEAD H_2 supply chain demonstration project.

FIG. 8. Demonstration hydrogenation plant in Brunei.

FIG. 9. Demonstration dehydrogenation plant in Kawasaki, Japan.

ment (AHEAD), and subsequently initiated the world's first global H_2 supply chain demo project, for which construction was completed in 2020.

Global supply chain. AHEAD's key project is aimed at demonstrating the transport of H_2 via a chemical carrier over a distance of 5,000 km, from the production site in Brunei to Tokyo Harbor. The demo project is funded by the Japanese New Energy and Industrial Technology Development Organization (NEDO).

The production and shipment of methylcyclohexane in ISO containers were started in early 2020. FIG. 7 shows the flow of material from Brunei to Tokyo Harbor and the return of toluene to Brunei. H_2 was produced at a preexisting process plant site in Brunei through conventional steam reforming of natural gas; however, the trademarked hydrogen process can be applied to H_2 from any production means.

The planned capacity of the demo system is 210 metric tpy (210,000 kgy), which is approximately the amount required for a single fueling of around 40,000 FCEVs. In the case of the demo project, the H_2 is burned in a power-generating gas turbine located within an existing site in Kawasaki, Japan. The two production sites—the hydrogenation site in Brunei (FIG. 8) and the dehydrogenation site in Kawasaki (FIG. 9)—have operated continuously throughout 2020, basically fulfilling all of the original goals of the demo program.

Power-to-gas demo. In parallel to demonstrating the trademarked hydrogen process as part of a global supply chain, additional programs were undertaken to further demonstrate the robustness of the technology. A small-scale power-to-gas demo project outline is depicted in FIG. 10. This project was carried out in Yokohama, Japan and also funded by NEDO.

Energy from a simulated wind farm was used to power an alkaline electrolyzer for H_2 production. The recovered alkaline H_2 was then purified and sent to the existing demo plant, as shown in FIG. 10. These steps demonstrate the ability to harness wind energy, which is then stored as H_2 and can be transported to any site desired. In the demo project, the recovered H_2 was purified and then utilized in a lab-scale solid oxide fuel cell (SOFC) for power production. In a real-world utilization scenario, for example, offshore wind energy could be harnessed and converted to

transportable H_2 that could then be transported by LOHC for use in clean power generation at another desired location. In this case, it is further demonstrated that having dehydrogenation adjacent to the SOFC makes possible efficient heat integration between the fuel cell, which generates waste heat, and the endothermic dehydrogenation plant.

Hydrogen fueling stations. An additional demo project funded by NEDO targeted the use of LOHC to transport H_2 for use in distributed fueling stations. These stations could service passenger FCEVs or even larger fuel cells used in heavy-duty trucks or other large transport vehicles. For this study, a small-scale, packaged dehydrogenation facility was developed for testing (FIG. 11). In the process flow, methylcyclohexane from storage is dehydrogenated in the compact recovery plant, and then recovered H_2 is purified to meet fuel cell specifications before being compressed to approximately 700 bar prior to use.

Pathway to commercialization. The hydrogen process[a] technology, having been proven at both the pilot and demo scale, was deemed ready for commercial roll-out. In the Kawasaki demonstration, H_2 produced remotely was transported via LOHC over 5,000 km and ultimately consumed in a gas turbine used for generating electric power. The demo plant's capacity of 210 metric tpy was simply a capacity of convenience—i.e., large enough to prove the capabilities of the supply chain while limiting the initial investment. Much larger and more ambitious transport programs have already been evaluated; these vary in size according to the specifics of the various applications.

The next step, envisioned for the 2025–2026 time frame, provides for utilization in mobility and industrial applications, along with gas turbine consumption of clean-burning H_2 of up to 30% in the fuel. Plans for this second chain provide for up to 1 BNm^3/yr of H_2 (90,000 metric t).

By 2030, up to 3.3 BNm^3/yr of H_2 utilization is planned. This volume is equivalent to 300,000 metric tpy, according to Japan's Hydrogen Strategy outlined in 2017. In addition, Japan announced a target to introduce 3 metric MMtpy of H_2 use by 2030, as per the Ministry of Economy, Trade and Industry's "Green growth strategy towards 2050 carbon neutrality," released in December 2020. Significant H_2 acceleration and volume increase is expected to meet this target (FIG. 12).

Future applications consider greatly expanded mobility uses both in the form of private and public transport, accelerated use in materials and goods movement both at ports and in long-haul overland

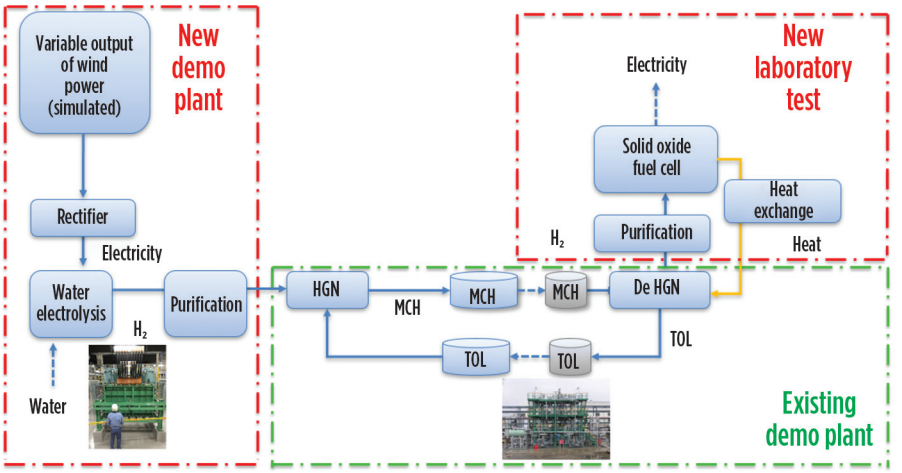

FIG. 10. Small-scale power-to-gas demonstration project in Yokohama, Japan.

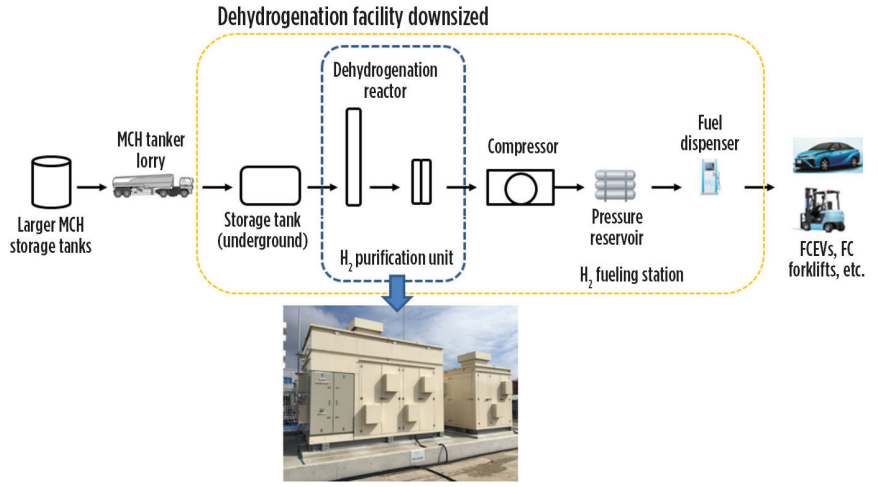

FIG. 11. Small-scale dehydrogenation facility developed for H_2 fueling demonstration project.

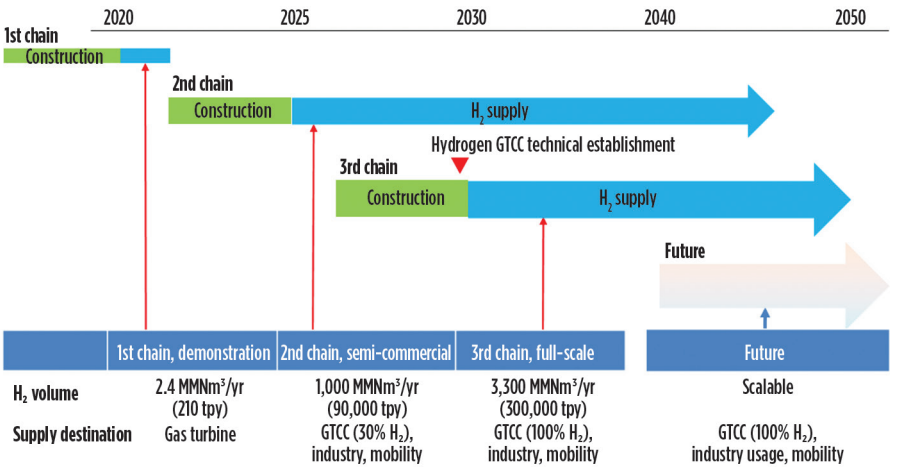

FIG. 12. Pathway to commercialization for the trademarked hydrogen technology.[a]

transport, clean industrial consumption, and gas turbine fuel with up to 100% H_2.

Transportation studies in North America. Production of H_2 via conventional methodologies, recovery of byproduct or through greener approaches, such as water electrolysis, have a marked effect on both the cost and availability of H_2. When considering H_2 as an alternative fuel, it is normal that the first question asked is usually, "What is the delivered cost of H_2?" How to best produce H_2 for the future is a broad topic not covered by this article. The authors' focus is to explore how to best deliver produced H_2 reliably and at a competitive cost.

Concurrent to the demonstration of LOHC technology, a number of wide-ranging studies have been undertaken to explore competitive options for transportation. Both locally focused and long-haul transport have been considered and reviewed. Truck transport, rail, inland waterway barges, pipelines and ocean-going tankers have been compared in a number of studies (FIG. 13).

In 2019, a detailed study was concluded with the government of British Columbia in Canada that considered the efficient transport of H_2 produced from low-cost hydropower. The trademarked hydrogen technology served as the basis, and transport of H_2 from a coastal location was considered for delivery to Japan, to the city of Vancouver, Canada and to the port of Los Angeles in California, U.S.

Another study was completed in 2019 with a U.S.-based industrial partner to produce H_2 from excess nuclear power in the Midwestern U.S. The LOHC was then transported to an industrial port located on the U.S. Gulf Coast for eventual dehydrogenation and subsequent distribution for both industrial use and/or clean power production. In this case, rail and barge transport options were investigated.

Lastly, a research laboratory of the U.S. DOE was engaged to complete another detailed transportation study. In this study, the recovery of H_2 from existing U.S. Gulf Coast sources (cracker byproduct and chlor-alkali offgas) was compared with green production of H_2 using both solar and wind energy, for transport to California for use as mobility fuel and power. Various transport options were considered, including rail and ocean-going, long-range chemical carriers.

With reference to the DOE study, several findings were noted:

- Transmission of methylcyclohexane and toluene by large product tankers (115,000 deadweight tonnage, or DWT) is 50% less expensive than transmission by rail at $0.7/kg vs. $1.53/kg. It is also important to note that greenhouse gas emissions are reduced by half when utilizing ships for transmission, compared with rail transport.
- Use of byproduct H_2 incurs the lowest cost among all of the pathways analyzed. Using ships as the transmission mode, the cost (reflected by natural gas substitution only) could be a delivered total cost of below $2/kg, including transmission cost.

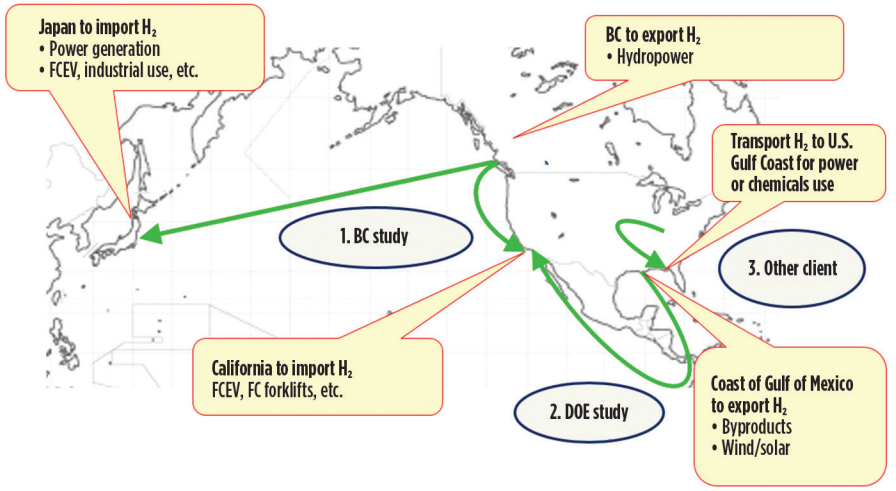

FIG. 13. Studies undertaken to explore competitive options for H_2 transportation.

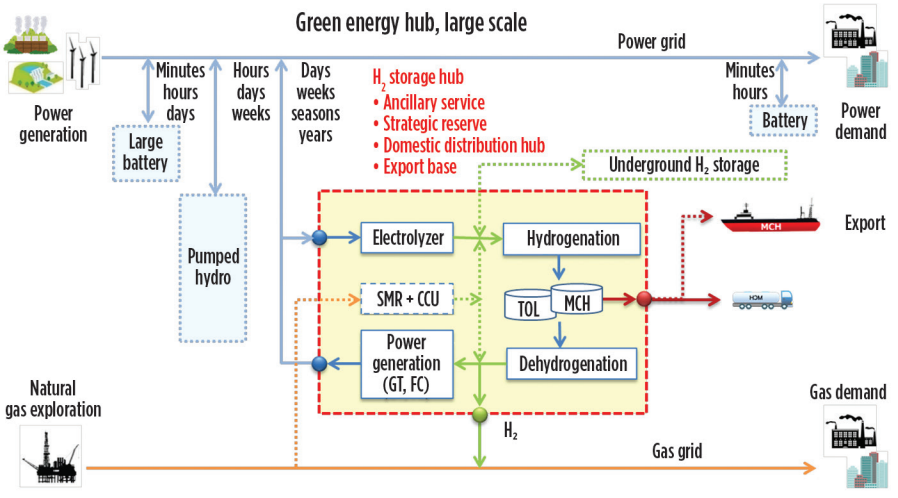

FIG. 14. The hydrogen process[a] technology as applied to a green energy hub.

Future applications. The hydrogen technology[a] has strength in large-scale transportation by ocean-going, long-range chemical carriers, as well as the potential to provide for H_2 in many applications beyond the obvious uses in mobility, material movement and clean power generation (FIG. 14). H_2 production by green or traditional methods can be utilized in remote locations for convenience and competitiveness, with shipment to any other location for centralized or decentralized recovery of H_2, depending on the desirable end use at hand.

Large-scale H_2 storage is one method to consider for storage of fluctuating renewable power, such as seasonal fluctuation, at the point when renewable power is widely introduced in the power grid network. The H_2 also can be used in the gas grid network.

Takeaway. The future for H_2, both in the U.S. and internationally, is more a matter of "when" than "if." Production and transportation costs for H_2 will come down as usage ramps up based on increasing demand. The authors believe that it is better to familiarize users with H_2 sooner rather than later, in anticipation of the transition from blue to green or renewable H_2, as consumption rises. For now, the focus must be on adaptation.

The U.S. DOE study results show the possibility of meeting the prescribed DOE target of $3.10/kg of H_2 (which dates back to 2015) in a large-scale H_2 supply chain by utilizing recovered offgas H_2 and transport from point of production to point of use. Blue H_2 can be made from conventional steam reforming of natural gas for under $0.50/kg (variable production cost), assuming gas at $2.50/MMBtu.

H_2 consumption in fuel cells for residential power, commercial applications, materials movement, personal mobility, mass transit and power generation will increase rapidly over the course of the next 10 yr. Challenges notwithstanding, these will be exciting times for both early adopters and infrastructure providers as we accelerate into a clean new world. HP

NOTE

[a] The SPERA Hydrogen™ system is a trademark of Chiyoda Corp. SPERA is Latin for "hope."

ROBERT V. SCHNEIDER, III is Senior Advisor to Chiyoda International Corp. in Houston, Texas. He was previously Senior Vice President and Director of Engineering and Licensing for Scientific Design Co. Inc. He has more than 40 yr of chemical process industry experience and a background in various process technologies including methanol, ammonia and ethylene oxide, industrial catalysis, sales and marketing, technology licensing and senior company management. Mr. Schneider previously held positions with Kvaerner Process (DAVY), the M.W Kellogg Co., United Catalysts/Sud-Chemie (now Clariant) and DuPont. He holds a BS degree in chemical engineering from the University of Louisville, Kentucky and an MBA degree from the University of South Florida. Mr. Schneider is a registered Professional Engineer in Texas, Florida and Kentucky.

DAISUKE KUROSAKI is the Group Leader for Hydrogen Supply Chain Development for Chiyoda Corp. in Yokohama, Japan. He has worked in a business development role in the H_2 supply chain business since 2014; his assignment has included promotion of Chiyoda H_2 transport technology business (SPERA), as well as responsibilities for the world's first global H_2 supply chain demonstration project between Brunei and Japan. Prior to joining the H_2 business team, he led energy conservation studies for petrochemical complexes in Southeast Asia and the Middle East. He was involved in fuel cell cogeneration system development and wind farm project development before joining Chiyoda, and has 20 yr of experience in both technical and business development roles in H_2 and related energy fields. Mr. Kurosaki holds BS and MS degrees in civil engineering from the University of Tokyo in Japan. As a part of his graduate studies, Mr. Kurosaki also studied at the University of California at Berkeley.

MASAAKI OKI is the Chief Coordinator for Hydrogen Supply Chain Development at Chiyoda Corp. in Yokohama, Japan. He has been in a business development role in the H_2 supply chain business since 2019. His assignment has included promotion of Chiyoda H_2 transport technology business (SPERA), as well as responsibilities for the world's first global H_2 supply chain demonstration project between Brunei and Japan. He was also the Lead Project Engineer for the Brunei hydrogenation plant. Prior to joining the H_2 business team, Mr. Oki was Lead Process Engineer for an LNG receiving terminal project. Previous to that assignment, Mr. Oki supported Japan Methane Hydrate Operating Co. Ltd. in the development of methane hydrate technology. Mr. Oki holds BS and MS degrees in chemical engineering from the University of Kansai in Japan.

F. D'ANTONIO, Raffineria di Milazzo, Milazzo, Italy

Continuous monitoring of creep in equipment

In this article, the development of a customized program—designed by the author and used at Raffineria di Milazzo—for the continuous monitoring of creep in vessels and piping is explained. The program extracts temperature data for each piece of equipment from the distributed control system (DCS) and calculates the equivalent creep hours according to equations derived from creep parameters introduced by researchers, such as the Larson-Miller parameter (LMP), the Manson-Haferd parameter (MHP) and the Orr-Sherby-Dorn parameter (OSDP).

What is creep? All refineries face material creep, a phenomenon that is seen when the operating temperature exceeds limits—which is typical for steel and alloy. As shown in **FIG. 1,** each metal/alloy has a temperature at which creep starts (Tcreep). When the temperature is above Tcreep, stress causes deformation. The speed of the deformation usually decreases for the first period, remains constant for the second period, and then increases in the last period.

Deformation is dangerous because it can lead to ruptures (**FIG. 1**). These failures have been experienced in several different plants all over the world, causing prolonged shutdowns and jeopardizing the safety of plant personnel.

The primary aim of this program is to provide an instrument that helps in the calculation of the equivalent creep hours per each piece of equipment in the facility. Typically, this can easily be accomplished for all vessels and piping, except for steam reformer tubes, which are not controlled by skin temperature.

Creep control. The number of hours in which equipment units are in creep is usually controlled, since this number of hours is equal to the number of plant running hours. Potential creep damages are typically controlled by using non-destructive techniques (NDTs) during turnarounds.

This kind of control, even though it is commonly used, is not ideal. During operations, the temperature can be lower than Tcreep. Conversely, temperatures above the design temperature (Tdes), which can be very dangerous, are not considered. Moreover, turnarounds are usually conducted every two years or more, so controlling creep via NDTs during a turnaround would not happen very often. Therefore, a more accurate system to control creep can be of great advantage.

In the design of sections subjected to creep, a Tdes at which the material is expected to fail is provided. If the Tdes value is unknown, then it is possible to calculate it by following these steps:

1. Calculate the stress at the design conditions of the vessel/tube.
2. Using the master creep curve that can be found for the given alloy, obtain the LMP (depending on the material, MHP or OSDP can be used).
3. From the LMP and the design number of hours, calculate the Tdes in Kelvin degrees.

Once Tdes is known (e.g., 100,000 hr), then the lifetime (t) at the temperature (T) is obtained by using an equation derived from the LMP formula (Eq. 1):

$$t = 10\text{^}((Tdes / T)(log(Tdes) + C) - C) \quad (1)$$

where *tdes* is 100,000 hr in this example, temperatures are in Kelvin degrees and C is a constant, depending on the material. Equivalent equations can be derived for the MHP or OSDP.

To calculate the equivalent creep time for each vessel/tube, the Raffineria di Milazzo information technology (IT) department created a custom application that extracts the online temperature values from the DCS for each piece of equipment, converts it to Kelvin degrees and introduces the X parameter (**TABLE 1**). If the temperature is below Tcreep, then there is no creep for the equipment and the lifetime is not affected—i.e., X is zero. The assign-

TABLE 1. Calculating the *X* parameter

Temperature (T)	*X* parameter
0 < T < Tcreep	0
Tcreep < T < Tdes	1
T > Tdes	Td/10^((Tdes/T)(log(Tdes) + C) – C)

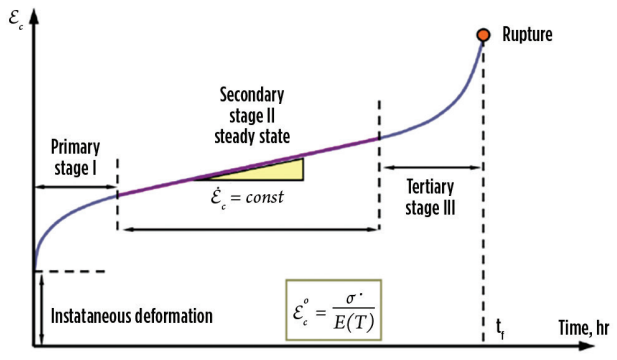

FIG. 1. Each metal/alloy has a temperature at which creep starts (Tcreep). Creep leads to deformation, which can lead to rupture.

ment of the value of 1 to *X* for Tcreep < T < Tdes is for increased safety, since creep is occurring in this range, but the lifetime is affected by a factor of less than 1. This can also be used to count the number of hours in creep regime, and it is compliant to the normal control routines made by Italian creep control bodies.

The value of the *X* parameter for T > Tdes is equal to the ratio of the design time and the remaining life at the temperature (T). In the example, if the remaining lifetime is 10,000 hr and the design is 100,000 hr, then the *X* parameter is 10. This means that 1 hr at T is equivalent to 10 hr at Tdes. An example of how the program works is shown in **FIG. 2.**

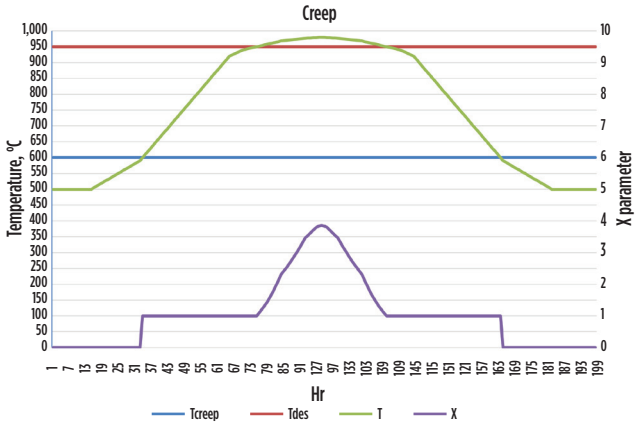

FIG. 2. An example of how the creep calculation program works.

By integrating the *X* parameter, you get the total equivalent creep time spent. In this example, overtemperature lasting 2 d, with a peak temperature of nearly 20°C above the design limit, reduces the life of equipment by a factor of 2.5. The 48 hr of overtemperature have reduced the equipment lifetime by 48 × 2.5 = 120 hr.

Due to this exponential behavior, it is easily seen that, even with relatively low overtemperatures, the lifetime reduction is important. This provides extra value to the importance of properly monitoring metal temperatures.

Takeaway. The Raffineria di Milazzo has developed this application to achieve the following advantages:

- Precisely controlling total creep hours
- Providing the ability to estimate the impact of temperature excursions.

Another advantage is that this method is easily applicable to all equipment that undergoes creep. This can greatly help to prepare effective NDT control plans, focusing on the sections that show real problems. In addition, cost reductions are possible for sections in which temperatures are far below the design limits. HP

FABRIZIO D'ANTONIO is the Asset Integrity Manager at Raffineria di Milazzo. He has been responsible for several units at the facility during his time there. He earned an MS degree in engineering and has also been a contract professor at the Università di Messina for a course on crude oil refining.

A. B. ALHAZEMI and S. B. ALHARBI,
Saudi Aramco, Madrid, Spain

Spiral heat exchanger technology

Heat exchangers are some of the most critical equipment in the oil and gas industry, as they provide the required temperature of fluid to sustain the plant's operation.

At the inlet of process plant facilities, accumulation of high sludge (high fouling) is a perennial issue that leads to inefficient performance of exchangers: shell-and-tube heat exchangers, to be precise. This also eventually leads to a drastic reduction in equipment reliability and an increase in the number of maintenance intervals, as well as high turnaround duration. Maintenance costs will be high over time, as additional inspection and maintenance are required due to the anticipated tube failures.

Even in such fouling environments, shell-and-tube heat exchangers are widely used due to their well-known designs and ease of fabrication with low manufacturing cost. Shell-and-tube heat exchanges always suffer from scaling formation created by high fouling. This results in frequent shutdowns to perform proper turnaround inspection and maintenance.

To overcome these issues, the spiral heat exchanger (SPHE) is a technology best suited for such applications with the potential for high fouling; an SPHE's self-cleaning design can remove sludge due to the turbulent flow created during the SPHE's operation.

As mentioned, the SPHE design feature creates a turbulent flow, preventing scaling within the equipment internal. Compared to the shell and tube, an SPHE is smaller, saving considerable space within the plant layout. The mechanical handling and cleaning of an SPHE is also much easier, as there are no internals like bundles within shell-and-tube exchangers. An SPHE consists of a shell and plates (which are welded to the shell) in a spiral shape that are separated by spacing studs to accommodate both hot and cold fluids in a countercurrent flow. This inherent design feature of an SPHE results in a compact design and enables cleaning of the internals by a hydro-jetting process and chemical cleaning.

Shell-and-tube heat exchangers often require a capital spare bundle to avoid long procurement lead times when in need of bundle replacement. Therefore, stocking spare bundles increases the CAPEX and requires long-term preservation and storage within the warehouse.

Based on the design features explained here and a case study, insight is provided of the advantages of the SPHE in terms of minimized plant footprint utilization, operation, mechanical handling, maintainability and ease of inspection.

DESIGN FEATURES

The SPHE's distinct design features overcome historical issues related to high fouling. The SPHE is internally shaped as a spiral—hence the name—that provides a continuous path for both fluids, with no hard corners or edges. The equipment is self-cleaning due to the turbulence created by the spacing studs between the spiral plates. SPHE design features are detailed here.

Compact design. Due to its compact design, the SPHE has a small footprint compared to shell-and-tube heat exchangers. The overall space requirements and complexities within the SPHE unit are greatly reduced. With this compact design and absence of tubes bundle, a heavy lift crane, tube bundle puller and extra space are not required during installation, operation and maintenance activities. Additionally, turnaround inspection duration and labor requirements are reduced.

Self-cleaning. Flow turbulence created by the curved pathway of the fluid acting with the spacing studs pushes any deposits as they form (FIG. 1), facilitating a self-cleaning process within the SPHE.

High overall heat transfer coefficient. With the spacing studs and the resultant fluid turbulence created within the spiral channels, the design provides a higher overall heat transfer coefficient compared to other heat transfer designs.

Spacing studs. The design and construction of an SPHE are made up of concentric channels that are separated by spacer studs. The studs, shown in FIG. 2, are welded on channels at specific locations and heights to form the channel gaps. The channel gaps and width are designed to meet requirements and working conditions unique to the end users. This versality in design allows the SPHE to be customized easily based on process conditions provided by the end users.

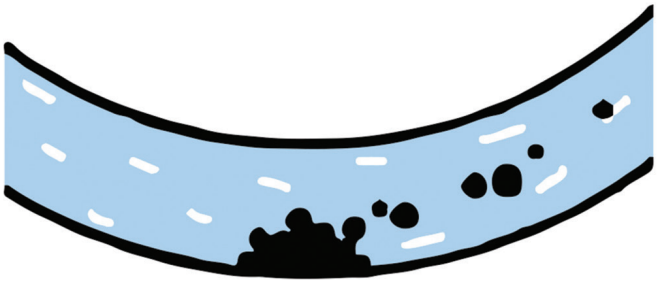

FIG. 1. Flow turbulence created by the curved pathway of the fluid acting with the spacing studs pushes any deposits as they form. Source: NEXSON.

This approach permits the design to account for flowrates, the sizes of the particles for fouling fluids, and pressure drops. Spacing studs facilitate turbulent flow in each channel, enabling a high overall heat transfer coefficient. It is worth mentioning that the number of studs and their spacing and arrangement are proprietary designs by SPHE manufacturers.

True countercurrent flow. As shown in **FIG. 3,** both hot and cold fluids flow through channels from one end to the other in opposite directions, contributing to a true countercurrent flow and resulting in high heat transfer efficiency, as well as a high overall heat transfer coefficient for SPHEs.

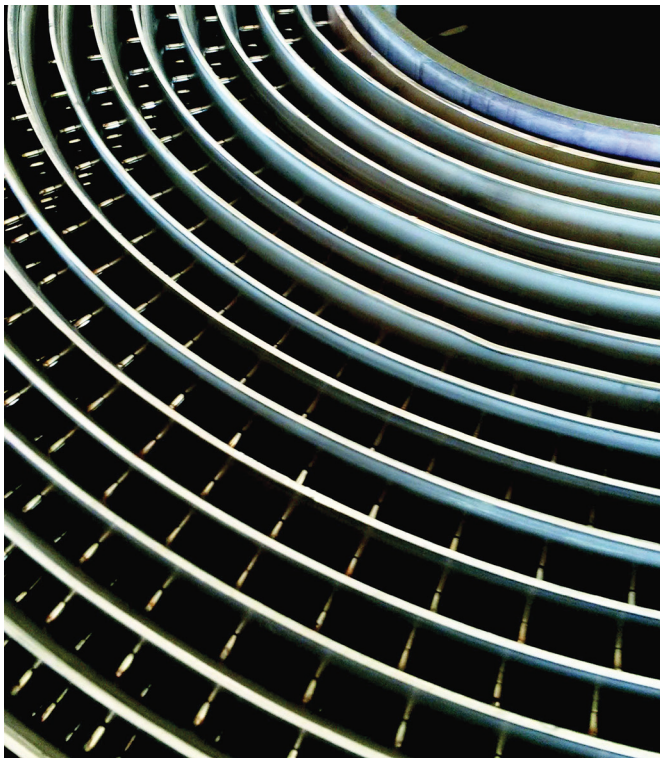

FIG. 2. Spacer studs are welded on channels at specific locations and heights to form the channel gaps.

Ease of inspection and maintenance. Due to its compact size, an SPHE can be easily accessed from both ends for required inspections and maintenance, including cleaning by hydro-jetting. Additionally, SPHEs can be chemically cleaned without removing any internals. This is in stark contrast to shell-and-tube exchangers, which require a cumbersome arrangement of a tube bundle puller device, crane, support arrangements and their associated safety risks, and logistics to transport the bundle to the maintenance shop for refurbishing.

Construction materials. Since the advent of spiral heat exchangers in the refining, petrochemicals, and oil and gas industries, manufacturers have been fabricating these heat exchangers in various metallurgies, such as carbon steels, stainless-steels, duplex, super-duplex, titanium, nickel alloys, etc., depending on the process and end-user requirements. Therefore, no limitations exist in terms of construction materials, which depends on the process fluid and conditions provided by the end users.

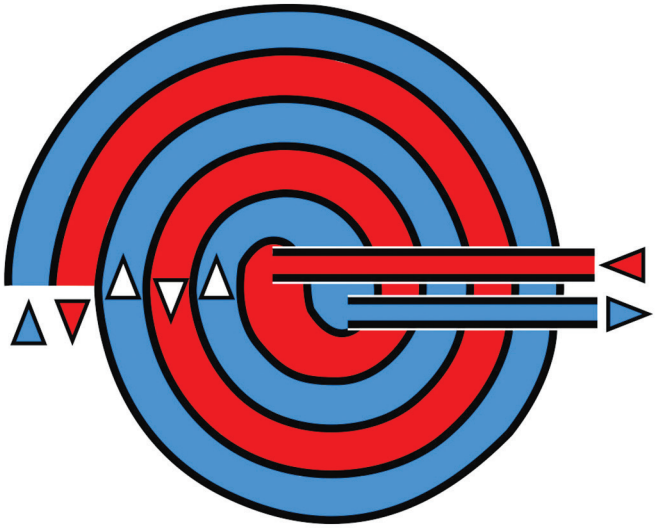

FIG. 3. Hot and cold fluids flowing in opposite directions contribute to a true countercurrent flow and result in high heat transfer efficiency. (Source: NEXSON).

TABLE 1. A comparison between spiral and shell-and-tube heat exchangers

	Spiral	Shell-and-tube
Service	• Effective fouling service • To be explored for non-fouling services	• Challenging fouling service • Ideal for non-fouling services
Design	• True countercurrent • High overall heat transfer coefficient	• Varies
Geometry	• Compact equipment (occupies small footprint)	• Larger equipment (occupies larger footprint) • Requires heavy lift • Requires bundle puller • Requires additional space
Turnaround inspection (Duration)	• Significantly shorter time • No internals to be removed • Cost is minimized	• Requires more time • Includes bundle removal and hydrotesting of shell and tubes individually and combined
Unplanned shutdown	• Very unlikely	• Yes, per historical experience
Cleaning	• Very easy for both ends • In-situ hydrojetting or chemical cleaning	• Challenging • Tube bundle removed and hydrojetted internally and externally, followed by shell and channel

Spiral vs. shell-and-tube. TABLE 1 summarizes the advantages of SHEs compared to shell-and-tube heat exchangers based on design features explained in the previous section. With fewer turnaround inspection and cleaning activities, the end user will avoid production losses and significantly decrease maintenance costs.

Technology implementation. For the Saudi Aramco Tanajib Gas plant project (part of the Saudi Aramco Marjan Increment Program), the licensor selected SPHEs for the three services here:

- Reclaimer loop heater
- Slurry cooler
- Lean/rich ethylene glycol (MEG) exchanger.

The SPHE was selected due to the high fouling phenomena that would be eliminated with this technology. Furthermore, due to the services' highly corrosive nature, the licensor specified that the material of construction must be stainless-steel alloy 6MO to sustain the reliability of the exchanger throughout its anticipated lifetime of 25 yr in service. Inspection and maintenance activities will be minimized for these services within the plant, which is a time and cost-effective proposition.

A case study performed using an HTRI run for a slurry cooler considering SPHEs and shell-and-tube heat exchangers (TABLE 2) provides a good indication of the size, weight and use of plant layout for the exchanger design with identical duties and temperature differences requirements. Slurry is a concentrated MEG solution saturated with salts and containing up to 20 wt% solid salts particles. The total salts content is 25 wt%, as per H&MB Rev.H. Salts are mainly composed of sodium chloride (NaCl), so the chloride content is high. pH is maintained between 10 and 11.5.

Based on TABLE 2, the shell-and-tube design would be eight times larger in length compared to an SPHE (compacted), confirming the advantage of having a smaller footprint in the industrial plant, excluding the need of additional space for tube bundle removal utilizing crane and truck for loading and unloading.

Another advantage is the higher velocity in the SPHE design, which in turns provides a self-cleaning effect due to the higher velocity and the turbulence created with spacing studs.

SPHE technology has been in existence since 1930; with advancements made over the years, it has proven to be the best-suited technology for such services.

This technology was implemented in the Fadhili Gas Plant in 2019 with an indication of satisfactory performance and reliability in operation with no adverse reports, including the performance of SHE implementations within applications at a petrochemical complex and another chemicals manufacturing facility.

TABLE 2. Case study results

Slurry coolers	Spiral	Shell-and-tube
Diameter	24 in.	16 in.
Length	2 ft	16 ft
Weight	3,600 lb	4,000 lb
Velocity slurry	6.56 ft/sec	0.73 ft/sec
Velocity water	3.28 fts/sec	1.21 ft/sec

Takeaway. Fouling is a chronic problem in the oil and gas industry, particularly for exchangers operating in harsh environments. The SPHE is a reliable technology that can overcome such conditions.

The SPHE's compact, true countercurrent flow design with self-cleaning effect and high heat transfer coefficients provide easy access to interior heat transfer services for field inspection, routine maintenance, or manual and chemical cleaning as required, with no involvement of heavy equipment.

The authors' company is adopting the International Standard API 664 for material selection, design, fabrication, inspection and testing. Developing a company specification, standard and special inspection requirement formed in collaboration with the company's approved spiral heat exchanger manufacturer will be the next step to govern design, fabrication and inspection for future purchase requests. HP

ABDULLAH ALHAZEMI is a Project Engineer at Saudi Aramco with a BS degree in applied mechanical engineering from King Fahd University of Petroleum and Minerals. He began his career as a Maintenance Engineer and now works at the Marjan project. Mr. Alhazemi holds PMP and SMRP certificates.

SHUJA ALHARBI works at Saudi Aramco and is a certified PMP with more than 13 yr of experience with turbomachinery and static equipment in the oil and gas industry. He earned a BSc degree in mechanical engineering.

K. BATRA and N. AGARWAL,
Engineers India Ltd., New Delhi, India

Embrace tube metal temperature factor (F_T) in fired heater design

Fired heaters are one of the most critical pieces of equipment in a refinery. They are capital intensive and occupy significant plot space, so due consideration must be given to all factors influencing a fired heater design. Estimation of peak heat fluxes and tube metal temperatures (TMTs) are some of the critical parameters that have significant impact on heater design. While providing process specifications, licensors may restrict the furnace designer on maximum allowable average radiant heat flux based on their own design considerations. Most furnace designers will strive to design the furnace at this maximum allowable average radiant heat flux value provided by the licensor, as it would minimize the heater cost, making its design competitive.

TMT plays a significant role in the final selected average radiant heat flux. A method to estimate the maximum TMT based on average radiant heat flux is specified in API 530, which underlines the various parameters and correlations to be considered for calculation.[1] The maximum TMT is estimated by calculating temperature drop using the peak heat flux and resistance offered by fluid film, fouling/coke thickness and tube thickness. Therefore, the estimation of peak heat flux is vital in the calculation for maximum TMT and final consideration of average radiant heat flux.

The adopted average radiant heat flux is multiplied by factors—such as circumferential heat flux (F_C), longitudinal heat flux (F_L) and tube metal temperature factor (F_T)—to arrive at the peak radiant heat flux, which will be used to determine the maximum TMT. Literature and guidelines[2,3,4] are available pertaining to the impact of F_C and F_L factors on heater design. F_C and F_L factors depend on tube arrangement, firing pattern and heater geometry. Moreover, these two factors (F_C and F_L) are applicable in similar ways, irrespective of service. However, the F_T factor is dependent on the service, more precisely the process fluid temperature difference at the inlet and outlet of the radiant section.

In most cases, the F_T factor has an insignificant impact and it is conservatively considered as 1. Therefore, designers may turn a blind eye to its impact in peak flux contribution. This strategy works well for heaters where the temperature difference in the radiant section is small. In some cases, however, this disregard can lead to over-sizing of fired heaters by as much as 30%, leading to substantially higher investment and limiting the heater turndown capabilities. Being conversant with the F_T factor can prevent confusion and multiple iterations by furnace designers, and can help in making the heater design more competitive.

The applicability of the F_T factor in TMT calculations and the equations governing its use are discussed here. An example of a hydrogen heater in a hydroprocessing unit is provided, where assuming an F_T factor of 1 may lead to providing an additional area more significant than required and almost no turndown. Also, an example of a product fractionator reboiler is discussed, where no significant impact exists when considering the F_T factor as 1.

Variation of peak/maximum local heat flux in a firebox.

For process fired heaters, the average radiant heat flux is calculated by dividing the absorbed duty in the radiant section by the total outside surface area of the coil in the radiant section. The average radiant heat flux is expressed in Btu/hr-ft^2 or MMKcal/hr-m^2. However, the average radiant heat flux does not represent the harshest condition in a fired heater. Within a firebox, the local heat fluxes vary significantly, as the flue gas temperature profile is not uniform. For a radiant firebox calculation, a well-stirred firebox is assumed. In reality, due to flue gas flow patterns and recirculation, the flue gas temperature may be only 537°C (1,000°F) at the heater floor, while at arch the flue temperature may reach 788°C (1,450°F). **FIG. 1** represents the heat flux distribution in a firebox.

Eq. 1 is used for estimating peak heat flux in a fired heater:

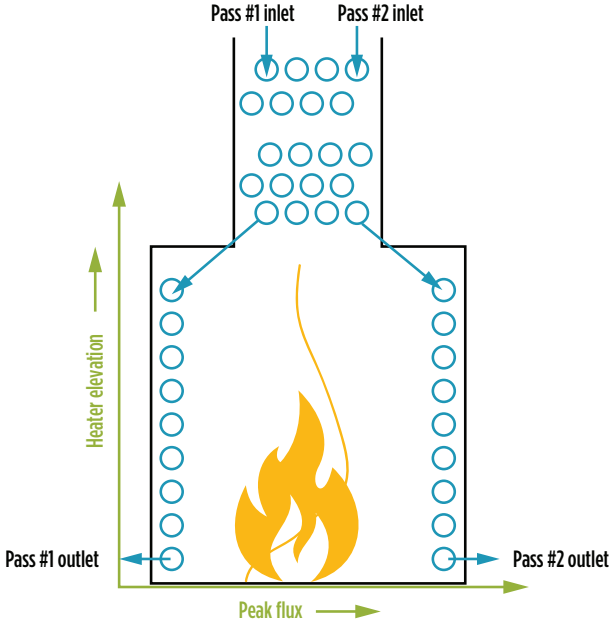

FIG. 1. Heat flux distribution in a firebox.

$$Qr, max = F_c \times F_L \times F_T \times Qr, avg \quad (1)$$

where,

F_C = Circumferential heat flux variations
F_L = Longitudinal heat flux variations
F_T = The effect of tube metal temperature on the radiant heat flux
Qr, avg = The average radiant heat flux for the outside surface
Qr, max = The maximum radiant heat flux for the outside surface.

Estimation of factors impacting peak heat flux calculation. Descriptions of factors follow below.

Circumferential heat flux factor (F_C). Circumferential heat flux is a function of coil geometry, layout and firing arrangement (single-fired vs. double-fired), shown in FIG. 2, and is estimated from Figure B.1, "Ratio of maximum local to average heat flux," provided in API 530.[1] This graph provides the value of F_C from the ratio of tube center-center spacing to tube outside diameter. **Note:** Single-fired tubes have higher F_C compared to double-fired tubes—in single firing, both sides are not exposed to the same intensity of radiations, leading to higher temperatures on one side of the tube.

Longitudinal heat flux factor (F_L). As defined in API 530,[1] F_L is used to account for variations in heat flux along the flame path, as discussed above, and depends on tube length, tube layout and flame profile. Vertical tube heaters have higher F_L compared to horizontal heaters where burners are provided along the tube length. Common values between 1 and 1.5 are used, depending on the firebox dimensions and flame aspect ratios. Computational fluid dynamics (CFD) modeling, as shown in FIG. 3, may also be used to estimate this factor for new heater configurations.

Tube metal temperature factor (F_T). API 530 provides the following correlation (Eq. 2) for estimating the tube metal temperature factor F_T for most applications:

$$F_T = (T_{g,ave}^{\ 4} - T_{tm}^{\ 4}) / (T_{g,ave}^{\ 4} - T_{tm,ave}^{\ 4}) \quad (2)$$

where,

$T_{g,ave}$ = the average flue-gas temperature, expressed in Kelvin (°R), in the radiant section
T_{tm} = the TMT, expressed in Kelvin (°R), at the point under consideration
$T_{tm,ave}$ = the average TMT, expressed in Kelvin (°R), in the radiant section.

It is important to note that:

- $F_T < 1$ near the coil outlet or areas of maximum TMT
- $F_T > 1$ near areas of lower TMT.

For most applications, F_T is estimated to be in the range of 0.9–1. However, for certain applications, dependent on the service—more precisely, the process fluid temperature difference at the inlet and outlet of the radiant section—F_T can be as low as 0.7. Therefore, ignorance of F_T can result in providing a huge heat transfer area and subsequently limiting heater turndown.

To illustrate F_T significance, the following two case studies are elaborated.

Case study 1. A hydrogen heater in a hydroprocessing unit is considered for evaluation of the F_T factor. The heater has an inlet and outlet temperature of 326°C (619°F) and 566°C (1,051°F), respectively. The heater is designed for an average radiant heat flux of 7,800 Btu/hr/ft² for double-firing arrangement. The tube size is a 5.563-in. outer diameter (OD) and tubes are placed at 2D center-center spacing. The tubes are placed vertically at the center of the cylindrical furnace in a cruciform-type arrangement. The outlet temperature is considered as the bulk fluid temperature for calculation. The weld-weld tube length is 47 ft. The peak flux for this heater is estimated as:

- F_C factor = 1.2
  - Tubes are placed in 2D spacing in a double-fired arrangement
  - Tube OD/tube spacing = 10/5.563 = 1.8
  - Refer to API 530 Figure B.1 to calculate F_C as 1.2.
- F_L factor = 1.4

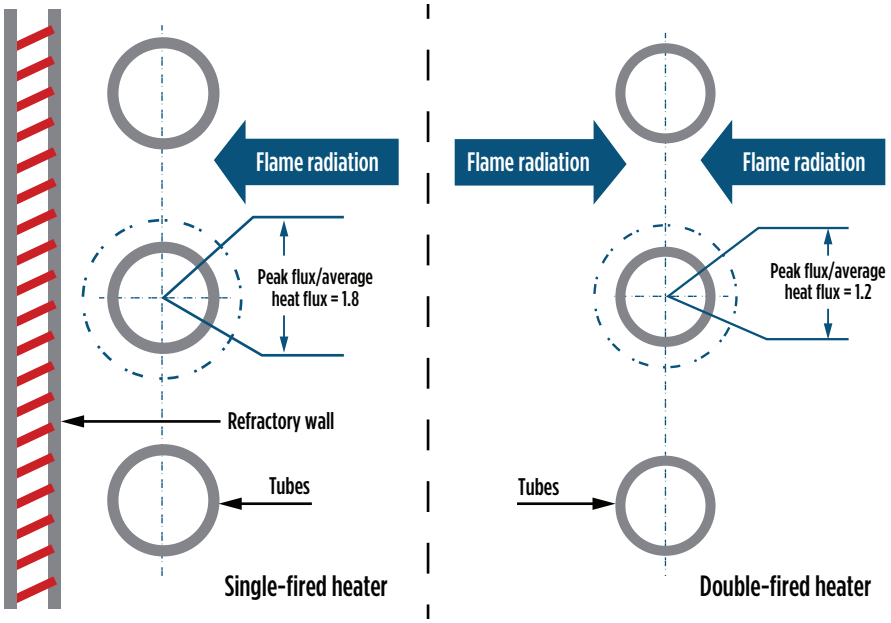

FIG. 2. Circumferential heat flux distribution in fired heaters.

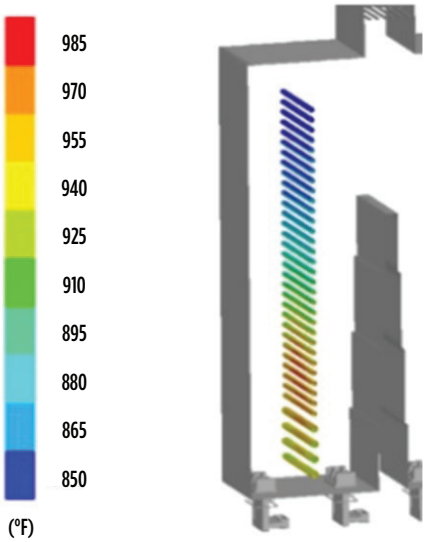

FIG. 3. Sample CFD modeling TMT contours in a horizontal box heater.

- Estimated based on firebox dimension as per internal design practices
- F_T factor = 0.744
  - Maximum tube skin temperature, °R = 1,751
  - Mean tube skin temperature, °R = 1,670
  - Average flue gas temperature, °R= 1,938
  - Use Eq. 2 specified above.

The maximum/peak local heat flux (shown in FIGS. 4 and 5) = 1.2 × 1.4 × 0.744 × 7,800 = 9,750 Btu/hr/ft^2.

However, if in the above case a conventional value of F_T factor = 1 is considered, then the calculated peak flux would increase to 1.2 × 1.4 × 1 × 7,800 = 13,100 Btu/hr/ft^2. Comparing the peak flux values for both options (TABLE 1), it is evident that the F_T factor of 0.744 lowers the peak flux by almost 25.6% when compared to an F_T factor of 1. Further, with the conventional approach (F_T factor of 1), the peak flux will lead to significantly higher TMT, resulting in high tube thickness. The furnace designer will be forced to consider a lower average radiant heat flux to maintain the peak heat flux constant to keep TMT within range for the selected tube thickness.

For this condition (F_T factor of 1), the heater is estimated to be designed for 5,800 Btu/hr/ft^2 average radiant heat flux. This would lead to almost a 34% extra heat transfer area compared to the previous option. This increase in area can result in increasing the heater cost by ~10%, limiting heater turndown, and occupying a larger plot space. Therefore, the careful selection of F_T factor is emphasized, as it is critical in optimizing the size and cost of a heater system for such services.

Case study 2. This case considers a product fractionator reboiler heater (FIGS. 6 and 7) in a hydroprocessing unit. The heater has an inlet and outlet temperature of 330°C (626°F) and 349°C (660°F), respectively. The heater is designed for an average allowable radiant heat flux of 7,800 Btu/hr/ft^2 for single-fired arrangement. The tube size is 8.625-in. OD and tubes are placed at a 2D center-center spacing. The tubes are placed vertically along the walls of a vertical cylindrical furnace. The weld-weld tube length is 60 ft. The outlet temperature is considered as the bulk fluid temperature for calculation. The peak flux for this heater is estimated as:

- F_C factor = 1.8
  - Tubes are placed in 2D spacing in a single-fired arrangement
  - Tube OD/tube spacing = 16/8.625 = 1.9
  - Refer API 530 Figure B.1 to calculate F_C as 1.8
- F_L factor = 1.6
  - Estimated based on firebox dimension as per internal design practices

TABLE 1. Comparison of radiant peak flux in a hydrogen heater

Process parameter	F_T = 0.744 (Option 1)	F_T = 1 (Option 2)
Average radiant heat flux, Btu/hr/ft^2	7,800	5,800
F_c	1.2	1.2
F_L	1.4	1.4
Peak heat flux, Btu/hr/ft^2	9,750	9,744
Max. tube metal temp. (outlet tube),°F	1,275	1,275
Extra heat transfer area compared to Option 1, %	–	34.5%

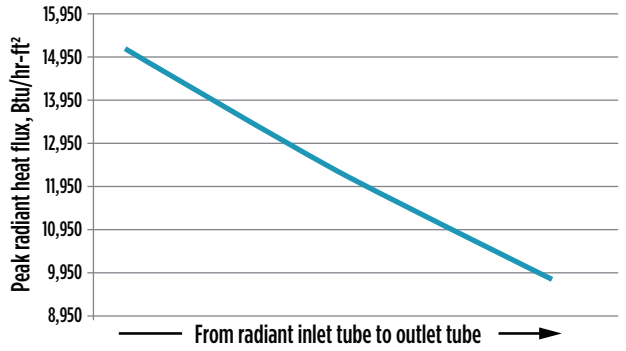

FIG. 4. Hydrogen heater: Peak radiant heat flux profile.

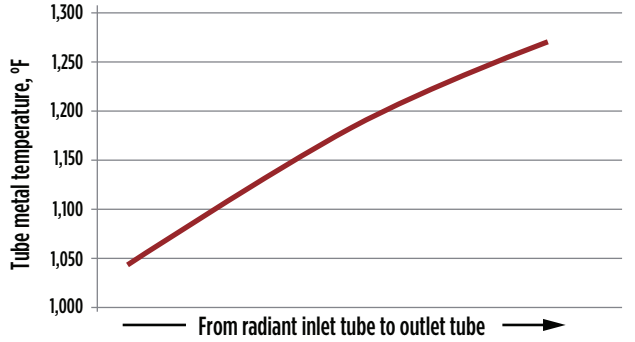

FIG. 5. Hydrogen heater: Radiant box TMT profile.

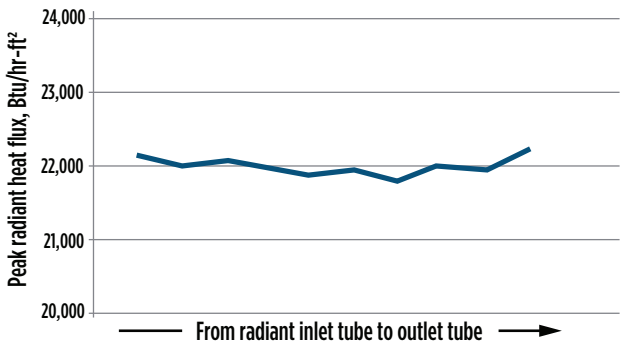

FIG. 6. PFR heater: Peak radiant heat flux profile.

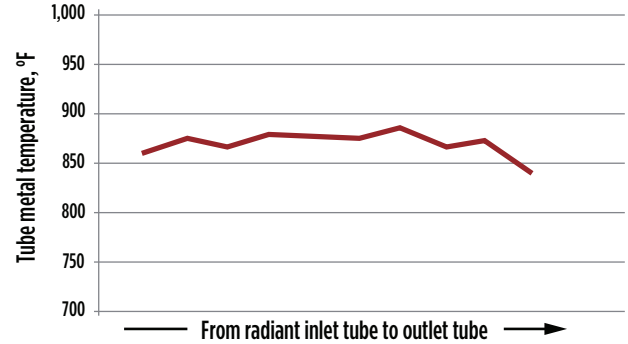

FIG. 7. PFR heater: Radiant box TMT profile.

- F_T factor = 0.99
  - Maximum tube skin temperature, °R = 1,231
  - Mean tube skin temperature, °R = 1,218
  - Average flue gas temperature, °R = 1,860
  - Use Eq. 2 specified above.

The maximum/peak local heat flux = 1.8 × 1.6 × 0.99 × 7,800 = 22,240 Btu/hr/ft² (TABLE 2).

It is evident from the above case study that there is insignificant impact on the F_T factor (0.99 vs.1) and peak heat flux (22,240 Btu/hr/ft² vs. 22,464 Btu/hr/ft²) and subsequent TMT calculation. This will be true for heaters where the process fluid temperature variation from the radiant inlet to outlet is small. In such cases, an F_T factor of 1 is a reasonable assumption.

TABLE 2. Comparison of radiant peak flux in a product fractionator reboiler

Process parameter	F_T = 0.99	F_T = 1
Avg. radiant heat flux, Btu/hr/ft²	7,800	7,800
F_C	1.8	1.8
F_L	1.6	1.6
F_T	0.99	1
Peak heat flux, Btu/hr/ft²	22,240	22,464
Max. tube metal temp. (outlet tube), °F	840	841

TABLE 3 shows a comparison of the impact of the F_T factor in the two aforementioned heaters.

Takeaway. This work has demonstrated the criticality of the F_T factor in fired heater design with case studies covering two extreme cases. It is worth noting that the overall process temperature difference in Case 1 was 240°C while it was only 19°C in Case 2. It is evident that the larger the difference in inlet and outlet temperatures across the heater, the lower the F_T factor and the higher the consequent impact on peak heat flux calculation in the radiant section. It is for this reason that a vigilant selection of the F_T factor based on the service and operating conditions will encompass a significant reduction in heat transfer area and better operational flexibility, resulting in a more competitive design. HP

LITERATURE CITED

[1] American Petroleum Institute (API) 530, "Calculation of heater-tube thickness in petroleum refineries," 7th Ed., April 2015.
[2] Barletta, T., "Why vacuum unit fired heaters coke," Process Consulting Services Inc., Houston, Texas, October 2004.
[3] Niccum, G. and S. White, "Realities of heat flux in fired heaters," Process Consulting Services, Houston, Texas, November 2020.
[4] Bernhagen, P., "Coker heater design: The heart of the coking process," Fired heater division, Foster Wheeler USA Corp., June 2019.

KAPIL BATRA works as Deputy Manager in the heat transfer department at Engineers India Ltd. in New Delhi. Mr. Batra has a progressive work experience of 8 yr in fired heaters and combustion systems. He is a chemical engineering graduate from the Laxminarayan Institute of Technology (LIT)-Nagpur.

NAVNEET AGARWAL works as Deputy General Manager in the heat transfer department at Engineers India Ltd. in New Delhi. He has more than 22 yr of experience in the fields of heat and mass transfer equipment. His work focuses primarily on fired heater design, revamp and troubleshooting for the hydrocarbon industry and manages a team of engineers working on fired heaters and combustion systems. Mr. Agarwal earned a B.Tech degree in chemical engineering from the Indian Institute of Technology, BHU.

TABLE 3. Comparison of process parameters in a hydrogen heater and product fractionator reboiler

Process parameter	Hydrogen heater	Fractionator reboiler
Radiant section inlet temperature, °C	326	330
Radiant section outlet temperature, °C	566	349
Maximum tube skin temperature, °R	1,751	1,231
Mean tube skin temperature, °R	1,670	1,218
Average flue gas temperature, °R	1,938	1,860
F_T	0.744	0.99
F_C	1.2 (double-fired)	1.8 (single-fired)
F_L, calculated based on heater dimensions	1.4	1.6
Average radiant heat flux, Btu/hr/ft²	7,800	7,800
Radiant peak heat flux, Btu/hr/ft²	9,750	22,240
Differential peak radiant heat flux with F_T impact, Btu/hr/ft²	3,355	Negligible
Decrease in peak heat flux due to F_T factor at radiant outlet, %	25.6	Negligible

S. SIMS, Emerson, Austin, Texas

Control software drives sustainable performance and production

In the face of changing dynamics around the world, hydrocarbon manufacturers are finding the need to not only change strategies, but also to continually adapt those strategies to meet new social and consumer expectations. The world has rapidly shifted its focus to sustainability, adoption of renewables and reducing the environmental impacts of process manufacturing. The organizations that will achieve speed to market and wide success with new products while embracing these goals are already building the robust foundation necessary for these changes.

Two primary ways exist to meet the future of manufacturing: build new plants with advanced technologies or automate and retrofit existing plants to increase efficiency and optimize production. These trends are playing out in industries such as gas processing and refining (FIG. 1).

Some organizations are focused on new initiatives (e.g., constructing hydrogen fuel processing facilities), while others are converting existing refineries to support carbon capture. In either case, forward-thinking organizations are employing digital transformation strategies to future-proof their investments across the equipment lifecycle.

Optimizing operations. As organizations implement sustainable manufacturing initiatives and improve speed to market, they are running into impediments common in today's manufacturing environment.

Experienced operators are leaving plants for retirement, and the workers who remain are responsible for more tasks than ever before. These personnel need tools and strategies to work more efficiently. In addition, organizations implementing initiatives (e.g., carbon capture)—often with skeleton crews—face tight margins. Carbon capture makes sense environmentally, but with the right technologies in place, it can also make sense financially.

Automation solutions provide a critical foundation of support, helping teams navigate these changes to deliver performance and production without adding excessive expenses. Plants taking advantage of advanced automation software improve efficiency and

FIG. 1. The gas processing and refining industries operate at the heart of new sustainability initiatives, such as hydrogen fuel processing and carbon capture.

reduce cost with improved process control, tighter integration among systems and better data handling—key enablers of speed to market, higher performance and more sustainable operations.

Better core process control. Performance and sustainability go together, so organizations are turning to advanced process automation technologies to simultaneously improve both.

Loop issues often occur in the plant units consuming the most energy. The author's company has found nearly two-thirds of core control loops are underperforming in typical plants—often occurring in high-energy units such as distillation columns, boilers and reactors. Many plants, particularly those focused on carbon capture practices, are moving toward fully automated monitoring. Automating monitoring makes it far less likely that busy plant personnel will overlook the asset performance issues that lead to poor loop operation and reduced performance.

In addition, organizations are using advanced process control software to optimize operations through added efficiencies, driving minute-to-minute performance improvement. Modeling and predictive control are combined with advanced control logic to identify best practices, capture them as control logic and embed them in the process through automation for consistent increases in throughput and quality.

Taking advantage of state based control (SBC) software can also optimize processes for improved performance. SBC automates control logic into production lines, helping individual process units communicate and coordinate with each other. Operators are responsible for state transitions and act as process managers, intervening only when prompted by the system. Each stage of the process is aware of variables from other process units and can automatically adjust production accordingly to eliminate risks and waste from production processes.

The emergence of simulation. Simulation software is another key lever for delivering more sustainable operations. Often, organizations must adjust production to optimize efficiency and reduce environmental impact through tighter control. However, testing a new control strategy often creates risk due to lost production while systems are in reduced capacity for testing, along with the increased likelihood of safety or environmental incidents if newly implemented controls do not operate as expected on live equipment.

Using a digital twin simulation, plants can test new process configurations on a virtual replica of the plant, seeing how changes cascade across the system and identifying any faults in execution without creating risk to safety or environmental incidents. If a change does not yield the right outcome, the team simply reverts the digital twin back to its initial state and tries a different solution until they get the results they are looking for, with no operational risk whatsoever.

FIG. 2. Secure remote monitoring provides plant personnel with timely data, enabling them to make better decisions quickly.

Moreover, the flexibility of a simulated plant environment offers a wide range of opportunities to test scenarios that may be unlikely but could still impact production or cause a plant to exceed regulations. Service interruptions, unexpected bubbles of demand, supply-chain disruptions, equipment failure and other issues can all be tested safely, and solutions can be designed to mitigate even the rarest 'what if' scenarios.

Outside of operations, digital twin simulations also provide operators a safe place to train and upskill, enabling them to gain real world experience with zero risk, even in complex scenarios that they are only likely to face a handful of times over their entire career. Advanced simulations can be used to replicate these rare situations—plant trips, process excursions, equipment failure and more—and help operators quickly gain the skills to reduce emissions and safety risks to an absolute minimum.

Better data coverage translated into actionable insights through contextualization. Timely delivery of quality data is not only critical to the operational excellence of a plant, but also essential to enable smaller groups of workers to deliver more product with improved sustainably. Fortunately, advances in automation are enabling organizations to not only access more data than ever before, but also to easily put the data in context and quickly deliver it to the right people at the right time (**FIG. 2**). This improved, on-demand access to data helps drive improvements from the plant floor up through the enterprise.

Key components for improving efficiency are reducing operator load and providing personnel with tools to help make better decisions. Alarm systems have always been critical to helping operators stay ahead of the issues reducing performance and impacting sustainability. Many staff- and resource-limited organizations are relying more heavily on alarm management, with some organizations centralizing alarm systems to reduce maintenance, while making these systems easier to update, maintain and scale consistently across multiple sites.

In combination with more powerful alarm management, the Industrial Internet of Things (IIoT) has made it possible for a plant to move away from maintenance routes. With increasing options for smaller, simple-to-install IIoT measurement points, it is now easy and affordable to add automated monitoring to the majority of a plant's assets.

Fully automated monitoring provides important benefits for organizations working with small staff numbers. Personnel can be freed from maintenance rounds to perform more critical tasks to improve operations performance and product quality. In addition, plants with assets in hard to reach, remote or hazardous areas can improve visibility without increasing the expense, time, environmental impact and safety risk of travel.

Expanding sustainability beyond the local perimeter. Better performance through improved data is also enabled by expanded access to cloud technologies. Organizations can centralize

data in the cloud, making it easy for small teams to support large fleets across the enterprise. These integrated operations centers rely on the cloud to make data accessible anytime and anywhere.

Moreover, cloud technologies pave the way for expanded use of analytics to provide detailed monitoring of reliability and performance of assets from the control system to enterprise systems. These technologies deliver solutions in real time to cloud software applications and data lakes, where they can be accessed by stakeholders across the globe. Whether they are in the plant or are thousands of miles away at a company's headquarters, staff can monitor trends in data to increase performance and efficiency, while decreasing energy use, waste and emissions to deliver more product with less environmental impact.

Driving the future of manufacturing. As organizations progress through their digital transformation journey to drive more efficient, sustainable operations, they are unlocking higher production and increased revenue. The same strategies enabling companies to achieve speed to market and improved production help build an infrastructure for a greener future—not only through carbon capture and hydrogen fuel processing, but also inherently, as performance and sustainability improve in lock step. These same organizations are also laying the foundation for remote, integrated and autonomous operations.

The trend toward reduced footprint is also a contributor to more sustainable operations. Smaller teams of plant personnel are shifting to a more supervisory role, while process management is becoming more centralized. More organizations are moving to an integrated structure, with a small group of personnel managing an entire fleet from an integrated operations center. These teams use software such as advanced analytics, remote alarm management and remote support tools to safely monitor and manage operations, while avoiding environmental incidents and simultaneously reducing the cost and environmental impact of travel. These same technologies also enable organizations to quickly standardize and deploy tools across the enterprise to control production and performance worldwide more tightly.

Many of the digital tools that will drive the future of industry are already available. Working closely with an expert automation partner, organizations looking to improve performance and sustainability can quickly identify which technologies will deliver fast, quantifiable return on investment. Those same technologies also create a scalable platform to help support advanced operations, helping companies stay competitive in the global marketplace and more easily adjust to the many changes on the horizon. HP

SEAN SIMS is the Vice President of Emerson's DeltaV platform. Previously, he served as Vice President of both the measurement solutions business for the Asia-Pacific region and for lifecycle and performance services. Mr. Sims earned a BSc degree in engineering from the University of the Witwatersrand. Prior to Emerson, he worked for Alpret Control Specialists, the local business partner for Emerson in Southern Africa, for 10 yr. During this time, he held several positions, including System Group Technical Manager, Company Engineering Director and Company Systems Director.

MIKE RHODES, MANAGING EDITOR
Mike.Rhodes@HydrocarbonProcessing.com

Software to schedule, plan and track quality assurance (QA) test activities

ESC Spectrum has released QAInsight, a subscription-based software that helps utilities and other industrial companies solve the challenges of scheduling, planning and tracking a myriad of activities related to performing QA tests required by state and federal agencies.

QAInsight serves as a company's single source for QA test data, ensuring access to information across different facilities and departments, as well as eliminating mistakes caused by missing or incorrect data resulting from spreadsheets or other error-prone collection and storage methods.

QAInsight users can see an overview of their QA activities (including QA test completion dates, operating data and recertification event deadlines among many others) color-coded to help them quickly set priorities.

While QAInsight can be configured to work with any data acquisition system (DAS), it automatically imports critical information from ESC Spectrum's StackVision™ DAS.

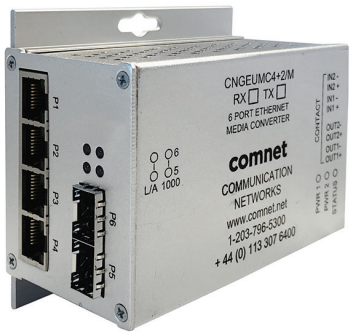

FIG. 1. The ComNet CNGEUMC4+2(TX, RX)/M.

FIG. 2. IDEC Corporation's firmware upgrade.

Link guardian unidirectional media converter

ComNet, Communication Networks, an ACRE company and a U.S.-based manufacturer of fiber optic transmission and networking equipment, is expanding its line of cybersecurity products by adding to its line of intelligent media converters. These intelligent media converters with Link Guardian create a physical layer of protection that limits network traffic to one-way communication between the source and destination networks. The ComNet CNGEUMC4+2(TX, RX)/M (FIG. 1) is designed to prevent cybersecurity attacks by limiting data flow to one direction between a secured and unsecured network. How the devices are deployed will determine which direction the data will flow.

Called a "unidirectional media converter," this physical security is more effective than software-enabled network firewalls. The company says that data connection is unhackable and invulnerable to malware.

The ComNet CNGEMUMC4+2(TX, RX)/M is a hardened, four-port, all-gigabit intelligent media converter. This product is designed to provide deterministic data transfer in only one direction (unidirectional), to segment and protect networks, devices and other digital assets (databases, historians, SCADA, PLCs, DCS, etc.) from external cyber threats.

Free firmware upgrade

IDEC Corporation has released a free firmware upgrade (FIG. 2) enabling new and existing MicroSmart FC6A Plus PLC CPUs to support the industry-standard MQTT protocol. The upgrade can be downloaded to the FC6A CPU, so it is easy for users to connect all types of field data to onsite and cloud-based brokers, and make the information readily available for users and analytical applications. Users can also send commands to the FC6A using MQTT.

Users everywhere know that Industrial Internet of Things (IIoT) data acquired from their manufacturing sites—whether from machine automation, building utilities, smart devices or any other source—is essential for supporting many other activities. Live and historized data drives visualization, alarming/notifications, control commands, predictive maintenance, deep analytics and more so sites can operate at maximum efficiency.

Traditional industrial poll/response communications protocols used with PLCs and HMIs are robust and useful, but they can be demanding for users to configure and maintain, they may inefficiently use limited bandwidth, and they often do not provide sufficient cybersecurity.

MQTT has emerged as a preferred IIoT communications protocol because it uses a lightweight and efficient publish/subscribe methodology for secure messaging between devices and centralized brokers, making information easily available for all authorized applications.

The FC6A with MQTT capability is ideal for new automation system designs, or for adding IIoT connectivity to existing systems. MQTT is supported on Ethernet port 1, so the FC6A can use existing wired, Wi-Fi or mobile data wireless networking to connect with onsite or cloud-based brokers. A typical application would publish machine data from many machines to the cloud, where it would be historized and could be transmitted to subscribing mobile applications.

No additional hardware is needed. Users can take advantage of the traditional PLC control logic and I/O functionality, or they can use the FC6A as an IIoT data concentrator for many other PLCs and in-

telligent devices. The FC6A with MQTT supports Amazon Web Services AWS IoT Core today, with future support planned for Microsoft Azure and Google Cloud.

Ammonia catalyst for sustainable CO_2 reduction

A sustainable, award-winning new ammonia synthesis catalyst has been jointly developed by Clariant and Casale: AmoMax™-Casale. Thanks to significantly higher activity than previous catalysts, AmoMax-Casale makes ammonia production more efficient and less polluting than ever before.

Producing ammonia (NH_3) creates more carbon dioxide (CO_2) emissions than any other chemical synthesis process. Clariant works to enhance its ammonia synthesis catalysts, leading to step changes like the industry proven AmoMax 10, which changed the game of ammonia synthesis from magnetite-based to wustite-based catalysts.

Born of Clariant's catalyst expertise and Casale's ammonia converter design know-how, AmoMax-Casale delivers an up to 30% higher efficiency factor thanks to a larger active surface area than previous generations of AmoMax. This performance surge significantly lowers the energy consumption of an ammonia plant, leading to a major reduction in CO_2 emissions. Higher catalyst activity means higher conversion, so the plant will consume less energy for the recirculation of the process gas in the reactor loop. Again, less CO_2 is emitted.

The combination of a higher active catalyst with the Casale design of converter internals makes the difference. A typical ammonia plant producing 1,600 tpd can potentially save $300,000/yr on energy costs and reduce CO_2 emissions by up to 85,000 t over the catalyst's average lifetime of 15 yr. Furthermore, AmoMax-Casale is capable of increasing ammonia production capacity by up to 5%.

The catalyst has already proven its performance in its first industrial reference at an ammonia plant in the Americas. The plant was upgraded to a Casale 3-bed interchanger using the AmoMax-Casale catalyst in late 2019 and is already reporting energy savings of 50,000 kcal/MT, which translates to an expected annual reduction of $700,000 in costs and 6.148 t in CO_2 emissions.

Standardized plan for a wide range of dual pressurized seal applications

John Crane has launched its new Global Standardized Plan 54 (GS 54), an API Plan 54 support system designed to fit a wide range of challenging, dual pressurized seal applications.

The new GS 54 (FIG. 3) uses best-practice design to provide clean, cooled and filtered barrier fluid, optimal seal performance and pump up-time, and supports API Plan 54 standards for leakage prevention. In tough and technically challenging processes where reliability is a prerequisite, the API Plan 54 support system provides a standard solution, removing avoidable complexity from the design and selection process. Applicable for challenging applications in the oil and gas, chemical, pharmaceutical and other high-purity industries, the support system's pre-engineered design offers high reliability and expedited customer delivery.

Designed with a focus on operational efficiency and reliability, features of the new booster include a streamlined design to minimize footprint and obstruction, a system reservoir that provides a nominal volume of 30 gal (114 l) of barrier fluid, a filter housing with 10-micron filter elements, and a shell-and-tube, water-cooled designed heat exchanger.

Purging/pressurization units

Best Purging Systems Corp. now offers UL Listed NFPA 496 Type Y&Z purging and pressurization units (FIG. 4) for enclosures up to 250 ft^3 in Class I and II, Division 2, Group A, B, C & D Hazardous Locations. These units provide all required controls indicators and alarms to meet code. Applications include large refinery control panels, special analyzers and portable laboratory equipment.

The Type Y&Z Purging and Pressurization solution meet/exceeds NEC – NFPA 70, NFPA 496, EN 50016 and IEC 60079-02 standards and is available in universal, vertical and horizontal configurations. The units can be easily mounted to any side of a protected enclosure and through a panel cutout.

Remote/mobile employee access for oil and gas and chemical industries

GE Digital has introduced Remote Operations for the oil and gas and chemical Industries, a software and appliance solution that provides remote/mobile employee access to essential equipment monitoring and control functions. GE Digital began offering Remote Operations earlier in 2020 in the power generation industry and already has many leading worldwide industrial customers using the solution.

The oil and gas industry faces challenges in providing safe and cost-effective equipment monitoring, maintenance and emergency response. At the refinery or plant, the global pandemic and economic pressures are triggering both oil and gas and chemical companies to re-think their strategies regarding contingency operations, worker location flexibility and onsite staffing. GE Digital Remote Operations solution, proven in power generation, addresses these and other challenges faced by industrials.

Remote Operations provides remote and mobile workers with secure and managed access to equipment controls regardless of type. NERC-CIP and ISA 99/62443 compliant security, multi-factor authentication and operational safeguards enable failsafe control flexibility and cooperation across all staff, onsite and offsite.

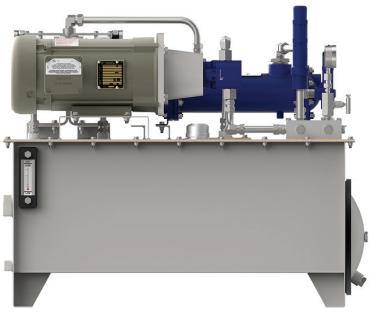

FIG. 3. John Crane's new Global Standardized Plan 54 (GS 54).

FIG. 4. Best Purging Systems Corp.'s NFPA 496 Type Y&Z purging and pressurization units.

Typical use cases for Remote Operations in the oil and gas and chemical industries include:

- Centralized monitoring of distant and dispersed equipment
- Lights-out operation of distant facilities
- Remote monitoring and controls over refinery or plant equipment
- Mobile controls and HQ collaboration for maintenance crew activities
- Anytime/anywhere access to experts to aid in equipment maintenance
- Remote/mobile monitoring and controls for in-house power generation facilities

Remote Operations is available in three upwardly compatible packages, accommodating needs from urgent continuity to fault tolerant operations centers. All include the core end-to-end security and compliance features.

- **Remote Operations Response** is a special packaged offer to rapidly enable remote monitoring and assistance. It is compatible with existing systems and requires only the addition of a pre-configured secure network appliance and firewall. Upon equipment arrival, installation can be done in a single working day with remote support from GE Digital. No operations shutdown is required.
- **Remote Operations Standard** (limited availability) delivers enhanced remote/mobile functions guarded by permitting and policy controls. Central operators can control remote/mobile worker access by time, equipment type and more. An interactive interface ensures that remote, mobile and onsite staff can work independently or together in a secure and compliant environment.
- **Remote Operations Advanced** (limited availability) provides full remote/mobile controls and additional optional operating capabilities in a high-availability configuration with failover. Remote Operations Advanced is the best choice for industrials adopting remote and distributed controls as a standard, failsafe operating model across a fleet of plants or equipment.

FIG. 5. Dover Precision Components' TruTech rings.

Magnetic target switch for position sensing

Emerson has released its TopWorx™ Magnetic Target Switch™ (MTS) to provide ready-to-install, universally-certified position sensing for explosion proof and intrinsically safe applications. The hazardous locations-approved TopWorx MTS joins the TopWorx GOTM Switch in the Emerson portfolio of position-sensing products, providing a single source for both standard and heavy-duty position sensors.

The TopWorx MTS is a magnetic, target-actuated, barrel-style switch designed to deliver trusted performance and value in applications ranging from standard industrial to extreme-duty. Featuring universal certifications, including IECEx, ATEX, UL and CSA, the TopWorx MTS can help reduce time to market by avoiding approval delays.

Available in general-purpose, intrinsically safe or explosion-proof area classifications, the 316L stainless-steel design of the MTS resists corrosion, making it suitable for use in environments including oil and gas, chemical, industrial energy, onsite utilities, mining, minerals and metals, power generation, pulp and paper, waste and wastewater.

The TopWorx MTS is built to deliver value and performance in hazardous locations requiring explosion proof and intrinsically safe applications.

Expanded high-performance materials portfolio

Dover Precision Components has expanded its TruTech™ materials brand (FIG. 5), delivering the latest advances in polymer science to enhance the performance and reliability of critical components in rotating and reciprocating machinery.

Dover Precision Components has made significant investments in its Materials Technology initiative to fully integrate materials research with engineering expertise and practical experience in machinery applications. A team of material scientists has been assembled to develop proprietary TruTech polymeric materials, optimize process parameters and ensure product quality. A dedicated materials laboratory featuring mechanical, chemical, optical and thermal analysis equipment, as well as advanced friction and wear testing, provides the necessary tools to fully evaluate materials and their signature properties. In addition, the recently constructed Dover Precision Components Innovation Lab allows testing in real-world environments to transform material properties into customer benefits.

TruTech materials are designed for optimum performance characteristics in a variety of operating conditions and have decades of proven success in the field. They are formulated from high-performance polymers, such as PTFE, PEEK, UHMWPE, PPS, polyimide and other high-temperature aromatic polymer materials, in combination with state-of-the-art fillers, carefully selected and formulated to satisfy application requirements. All formulation, manufacturing and testing is done in-house to ensure high quality standards and full traceability.

Broad research and development capabilities allow complete control of the material development process, from material composition and processing through manufacturing and product testing. Maintaining these capabilities in-house provides Dover Precision Components the flexibility to customize material solutions for specific applications and operating environments. New materials receive intensive laboratory analysis and undergo comprehensive testing before release to the field.

The Dover Precision Components Materials Technology initiative is developing material solutions to extend the useful life of Cook Compression® packing rings, wiper rings, piston rings and rider rings, as well as enhance performance in non-lubricated environments and process gases, such as hydrogen. The expanded TruTech materials portfolio also includes materials formulated to extend the service life of Waukesha Bearings® fluid film bearing products and Inpro/Seal® Bearing Isolators and Air Mizer® shaft seals. HP

Technology and Business Information for the Global Gas Processing Industry

GAS PROCESSING & LNG

GasProcessingNews.com | JULY/AUGUST 2021

SMALLER-SCALE PROCESSING

Gulf Energy Information

Special Supplement to
HYDROCARBON PROCESSING®
Pipeline & Gas Journal

EDITORIAL COMMENT

A. BLUME,
Editor-in-Chief

Worldwide, small-scale LNG liquefaction capacity is expected to expand by 30% over the next 4 yr, increasing from 33.9 MMtpy in 2021 to 43.92 MMtpy in 2025. Asia will account for 2.82 MMtpy of the new capacity, followed by North America with 2.48 MMtpy.

By country, Russia is set to lead the small-scale LNG capacity expansion by adding 2.94 MMtpy at up to 16 newbuild facilities and expansion projects by 2025. Close behind, China and Oman are expected to add 2.81 MMtpy and 2 MMtpy, respectively. While the majority (2.84 MMtpy) of Russia's capacity additions will be newbuilds and the remaining capacity will come from expansions, all of China's capacity additions will be from new plants.

In India, domestic cryogenic storage and regasification solutions provider INOXCVA is working with Japanese Mitsui & Co. to establish a virtual pipeline to service growing demand for LNG in the country. The partnership will establish small-scale LNG infrastructure, including logistics and receiving facilities at the customer end, to offer LNG access to customers not presently connected to pipelines.

Although Europe's preference for renewable energy is growing in light of its net zero carbon target, the region is still looking to LNG to supplement its energy needs. Stricter marine emissions regulations are encouraging the use of small-scale LNG as a bunker fuel. Despite sustained low oil prices and market uncertainty due to the COVID-19 pandemic, a significant increase has been seen in small-scale LNG projects in the region. **GP**

GAS PROCESSING & LNG
www.GasProcessingNews.com

P. O. Box 2608
Houston, Texas 77252-2608, USA
Phone: +1 (713) 529-4301
Fax: +1 (713) 520-4433
Editorial@GasProcessingNews.com

PUBLISHER Catherine Watkins

EDITORIAL
Editor-in-Chief — Adrienne Blume
Managing Editor — Mike Rhodes
Editor-in-Chief/Associate Publisher, *Hydrocarbon Processing* — Lee Nichols

MAGAZINE PRODUCTION
Vice President, Production — Sheryl Stone
Manager, Advertising Production — Cheryl Willis
Manager, Editorial Production — Angela Bathe Dietrich
Assistant Manager, Editorial Production — Melissa DeLucca
Graphic Designer — Krista Norman

ADVERTISING SALES
See Sales Offices, page 38.

Copyright © 2021 by Gulf Energy Information LLC. All rights reserved.

Gulf Energy

President/CEO — John Royall
CFO — Ed Caminos
Vice President, Upstream and Midstream — Andy McDowell
Vice President, Finance and Operations — Pamela Harvey
Vice President, Production — Sheryl Stone
Vice President, Downstream — Catherine Watkins

Other Gulf Energy Information titles include: *Hydrocarbon Processing*®, *World Oil*®, *Petroleum Economist*®, *Pipeline & Gas Journal* and *Underground Construction*.

CONTENTS

GasProcessingNews.com | JULY/AUGUST 2021

SPECIAL FOCUS: SMALL-SCALE LNG

ENGINEERING AND DESIGN

EQUIPMENT

COLUMNS

DEPARTMENTS

Cover Image: Zhengtai Yida LNG, located in Inner Mongolia, China, was commissioned and started up in 2018. Hangzhou Zhongtai Cryogenic Technology Corp. provided EPC for the 2,300-tpd small-scale LNG plant, which uses Enflex Group's sMR-Pro proprietary LNG process.

LNG's share of Indian gas demand to rise to 70% by 2030

The share of LNG in India's gas consumption could rise to 70% from the present 50% in 10 yr, and new import terminals are needed, according to LNG import terminal operator Petronet LNG Ltd. Prime Minister Narendra Modi has set a target to raise the share of natural gas in the country's energy mix to 15% by 2030 from 6.3% to cut its carbon footprint.

To meet that target, India's gas consumption must rise to 640 MMsm^{3}d from 155 MMsm^{3}d. Indian companies are investing billions of dollars to strengthen gas infrastructure, including laying 15,000 km of pipelines to supply cleaner fuel to households and industries. India has 17,000 km of gas pipeline network at present.

Furthermore, LNG projects with a collective capacity of 19 metric MMtpy are under construction, and plans are in the works to increase the use of LNG in trucks and buses. Replacing approximately 30% of India's crude oil imports with LNG would save $10 B at a global oil price of $74/bbl.

Excelerate Energy FSRU Returns to Bahia Blanca

Excelerate Energy LP's floating storage and regasification unit (FSRU) *Exemplar* has begun operations in Bahia Blanca, a port city located 400 mi south of the Argentine capital Buenos Aires. The *Exemplar,* with a storage capacity of 150,900 m^3, will deliver LNG for the 2021 winter season in Argentina, providing reliability and stability to the country's energy system despite operating in the challenging conditions of the South Atlantic.

The return of Excelerate's FSRU comes after the company won an international, competitive tender for seasonal regasification service in Bahia Blanca. In 2008 Excelerate developed the Bahia Blanca GasPort, South America's first LNG import terminal, and has also operated GNL Escobar, an LNG import terminal along the Paraná River, since 2011.

Panama announces $1-B gas plant

Panama intends to construct a $1-B plant for electricity generation, using natural gas, as the Central American country seeks to increase its share of cleaner energy. Consortium Consorcio Group Energy Gas Panama, made up of private companies InterEnergy Group and AES Panama, as well as the government, will be responsible for the construction, development and operation of the plant.

Called Gatun, the plant will be located at Isla Telfers near the port of Colon and have the capacity to produce 670 MW. The plant will start operations in late 2023 or early 2024.

Pembina Pipeline to buy 50% stake in Cedar LNG

Pembina Pipeline Corp. has agreed to buy a 50% stake in Canada's proposed $2.4-B, 3-MMtpy Cedar LNG project to develop the floating LNG facility in British Columbia in partnership with indigenous group the Haisla Nation. The FID is expected in 2023.

Pembina, which will acquire the equity interests in Cedar LNG from PTE Cedar LP and Delfin Midstream Inc., will operate the project going forward. Haisla will own the remaining 50% stake. Cedar LNG lies within the traditional territory of the Haisla Nation and aims to provide LNG to Asia-Pacific markets.

U.S. approves Enable's Louisiana Gulf Run pipeline

The U.S. Federal Energy Regulatory Commission (FERC) approved Enable Midstream Partners' request to build the Gulf Run natural gas pipeline in Louisiana, according to a filing. However, in what has become a recurring theme in pipeline approvals, the FERC commissioners differed on how the Commission should consider greenhouse gas emissions from proposed projects.

FERC Chairman Richard Glick and Commissioner Allison Clements said they dissented on the Gulf Run decision, in part because they said the FERC should have prepared a supplemental environmental impact statement to examine the effect that greenhouse gas emissions caused by the project will have on climate change.

Most of the gas transported on Gulf Run will go to Qatar Petroleum/ExxonMobil Corp.'s Golden Pass LNG export plant under construction in Texas. The first liquefaction train at Golden Pass is expected to enter service in 2025. The Gulf Run project includes about 134 mi (216 km) of new pipe and other facilities that will provide about 1.7 Bft^{3}d of transportation service from Enable's existing Westdale compressor in Red River Parish, Louisiana, to an interconnect with the Golden Pass Pipeline near Starks, Louisiana.

Enable previously estimated the cost of Gulf Run at $540 MM and anticipated the project could be placed into service in late 2022, subject to FERC approval. In its filing, the FERC estimated the cost of the project at $1.2 B.

LNG trade rises to record in 2020

Global LNG trade volumes rose to a record last year, led by Asia, although growth was marginal as demand was slammed by COVID-19-induced restrictions, according to a report by the International Gas Union (IGU).

Overall, LNG trade increased to 356.1 metric MMt in 2020, up by 1.4 metric MMt, or about 0.4%, from 2019, mostly driven by increased exports from the U.S. and Australia. This was smaller than the growth of 40.9 metric MMt, or 11.5%, in 2019. However, LNG was one of the few commodities that saw an increase in trade in 2020.

Extended lockdowns and the increased share of renewables in the energy mix reduced LNG net imports into Europe by 4.3 metric MMt. COVID-19 also severely impacted liquefaction development, with companies delaying FIDs on projects to 2021 and later because of the uncertain economic climate. A total of 87.3 metric MMtpy of liquefaction capacity were expected to be sanctioned in 2020, but only one project of 3.25 metric MMtpy in Mexico was approved.

New regasification projects in China and India will continue to support gas demand, while new projects under construction in Ghana, El Salvador, Cyprus and Nicaragua are expected online over the next 2 yr.

Saipem awarded gas plant project

Saipem received a letter of award from ADNOC Sour Gas, a subsidiary of Abu Dhabi National Oil Co. (ADNOC), for a new contract related to the Optimum Shah Gas Expansion (OSGE) and Gas Gathering project in the UAE. The $510-MM EPC contract covers the expansion and upgrade of the existing Shah gas plant.

The project will increase the daily gas treatment capacity of the Shah gas plant by 13%, from the current production capacity of 1.28 Bsft^{3}d to 1.45 Bsft^{3}d, representing a cumulative increase to 145% of the original design capacity of the plant.

The Shah gas plant is the largest sour gas plant in the world. Due to a higher sulfur content, the plant requires specific technologies to ensure safety and respect for the environment. The technologies utilized also will ensure continuity of production during maintenance work and minimize downtime.

Gulf Energy Information's Global Energy Infrastructure database is tracking more than 250 active gas processing/LNG projects around the world. At 40% market share, the Asia-Pacific region is the leader in total active projects globally. Many Asian nations have enacted programs to increase natural gas in their total energy mix. These initiatives provide a path to limit carbon emissions and mitigate smog in cities. However, many Asian nations rely on natural gas imports to satisfy demand. Therefore, the region is investing heavily in new LNG import and pipeline infrastructure. Asia is followed by the U.S., which holds a 17% market share in active gas processing/LNG projects. **GP**

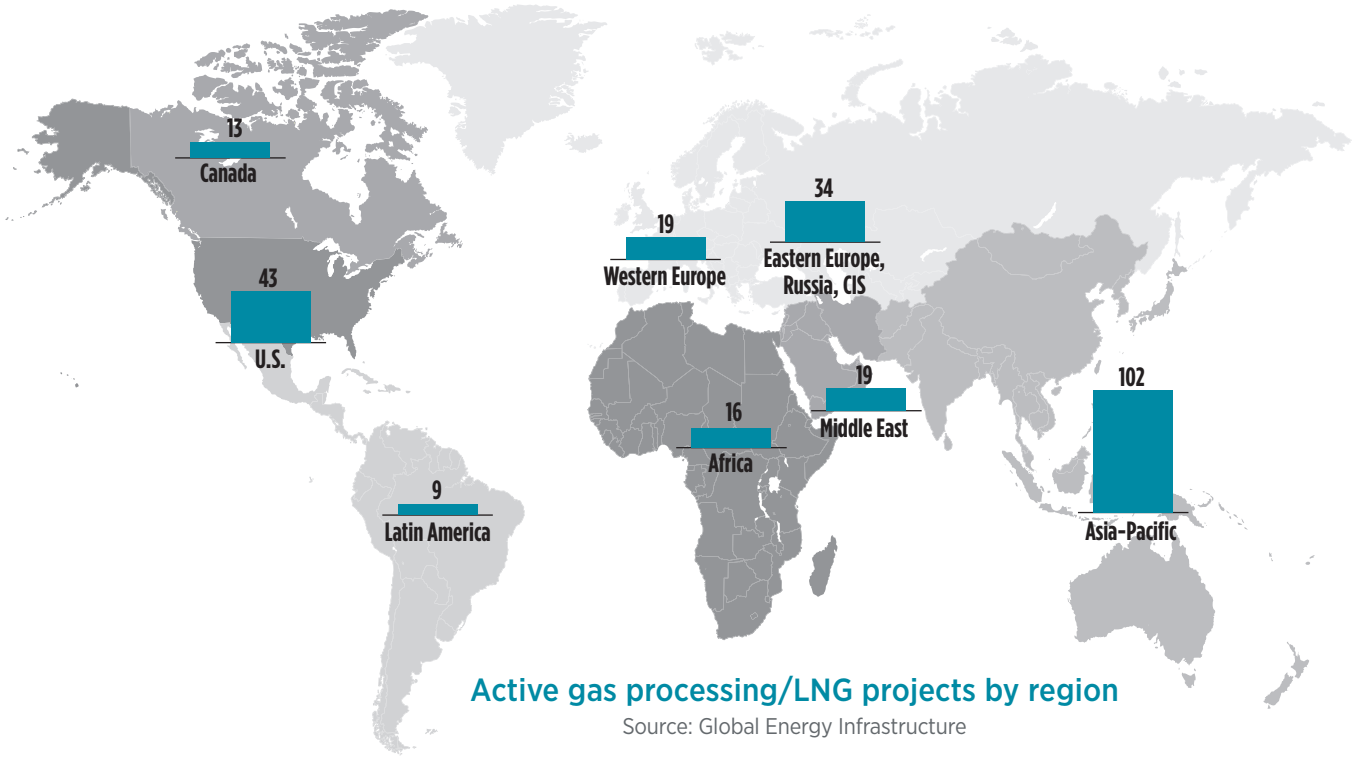

Active gas processing/LNG projects by region
Source: Global Energy Infrastructure

New gas processing/LNG project announcements, June 2020–June 2021

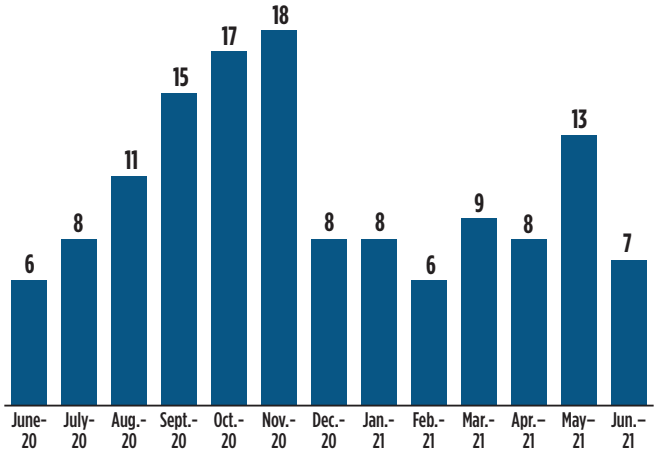

Active gas processing/LNG project market share by region

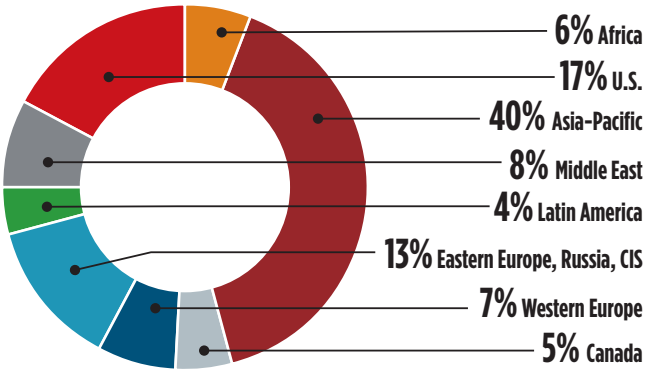

Global ENERGY INFRASTRUCTURE
A new market intelligence tool for the international energy industry with project data sets for hydrogen, renewables, global pipelines, LNG and downstream assets. | GlobalEnergyInfrastructure.com

The U.S. EIA expects domestic natural gas production to increase in 2021 as demand falls. The EIA projects that dry gas production will rise to 96.99 Bft³d in 2021 from 95.81 Bft³d in 2020 before rising to 99.63 Bft³d in 2022. That compares with 93.06 Bft³d in 2019. The EIA also expects gas consumption to fall to 82.32 Bft³d in 2021 from 83.25 Bft³d in 2020, and then rise to 82.87 Bft³d in 2022, compared with a record high of 85.15 Bft³d in 2019. In LNG news, Sabine Pass LNG has received authorization from the FERC to commission the fuel gas system for its Train 6 under construction. **GP**

U.S. natural gas spot prices at Henry Hub and NGL spot prices at Mont Belvieu, $/MMBtu

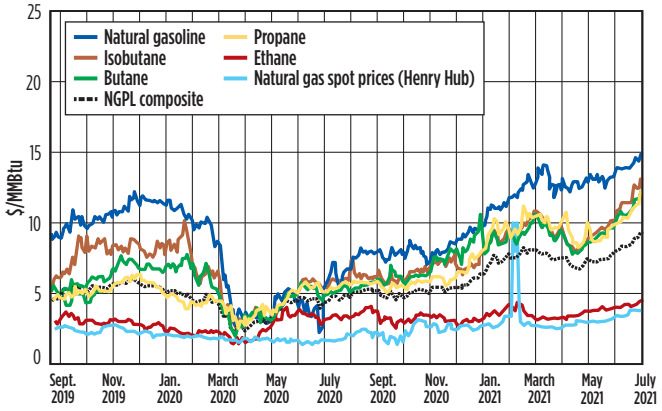

U.S. gas production (Bft³d) and prices ($/Mcf)

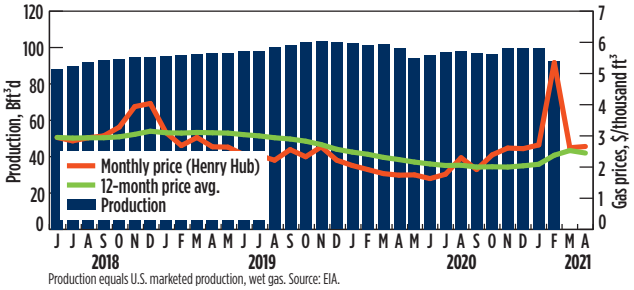

Production equals U.S. marketed production, wet gas. Source: EIA.

U.S. natural gas plant field production of NGL, LPG, ethane and propane, Mbpd

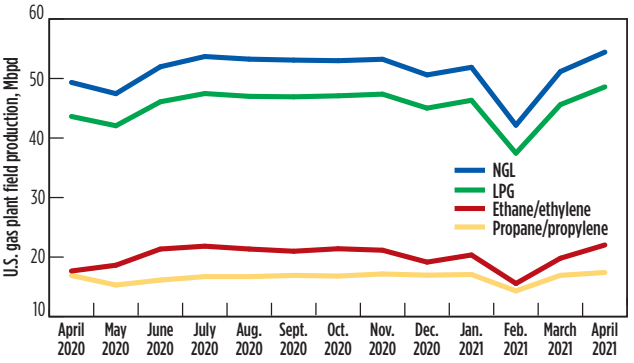

Source: U.S. EIA

LPG sector poised for sustainable fuel transformation

G. FELLER, Contributing Writer

Like virtually all industries, the liquified petroleum gas (LPG) sector was challenged by the COVID-19 pandemic throughout 2020. Healthcare workers relied on propane-fueled heaters as they performed COVID-19 tests on motorists in parking lots. Restaurants relied on propane-fueled patio heaters to keep diners fed and employees working after restrictions on indoor dining compelled them to serve meals outdoors. Millions counted on propane to keep homes comfortable and businesses running.

However, owing to its role as an essential commodity for residential cooking, a dramatic increase in outdoor living, and as a petrochemical feedstock, the LPG industry was less affected by the pandemic than many other energy commodities. As a result, global supply continued its upward trend and demand continued to grow.

Supply boosts from U.S., Mideast. Estimated global supply in 2019, the latest year of reporting, was 331 metric MMt. The U.S. accounted for nearly 85 metric MMt of LPG production, which represents more than a 10% increase over the previous year (**FIG. 1**). U.S. total production was more than twice that of its nearest rival, China. LPG production from Canada and Australia also grew in 2019; however, Saudi Arabia saw short-lived declines in output due to attacks on production facilities.

Economic and political tensions, such as the ongoing U.S.–China trade war, have provided an opportunity for upswings in production and supply in the Middle East as prime exports to Asian markets.

Demand gains in Asia-Pacific. Global demand in 2019 stood at nearly 325 metric MMt, a near-3% increase from the 2018 level. Demand is dominated by the residential sector, accounting for 44%, which is centered around the heating and cooking sectors. The petrochemical sector made up 28% of demand in 2019, followed by industrial (11%), refinery (8%), transportation (8%) and agriculture (1%). Asia-Pacific countries, and especially China and India, accounted for a significant portion of gains in demand, in both the residential and petrochemical market sectors (**FIG. 2**).

In the transportation sector, autogas demand grew by 1% globally in 2019, continuing a decade-long pattern of growth. South Korea, Turkey and Russia remain the largest markets with consumption of 3 metric MMtpy each, but eastern Europe continues to see nominal demand growth as autogas rises in popularity as an economically attractive transport fuel.

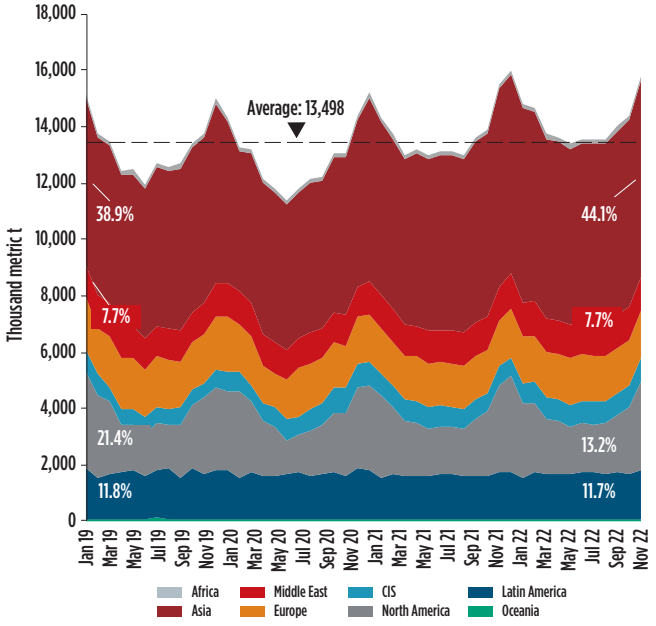

FIG. 1. Global propane demand by region, 2019–2022.

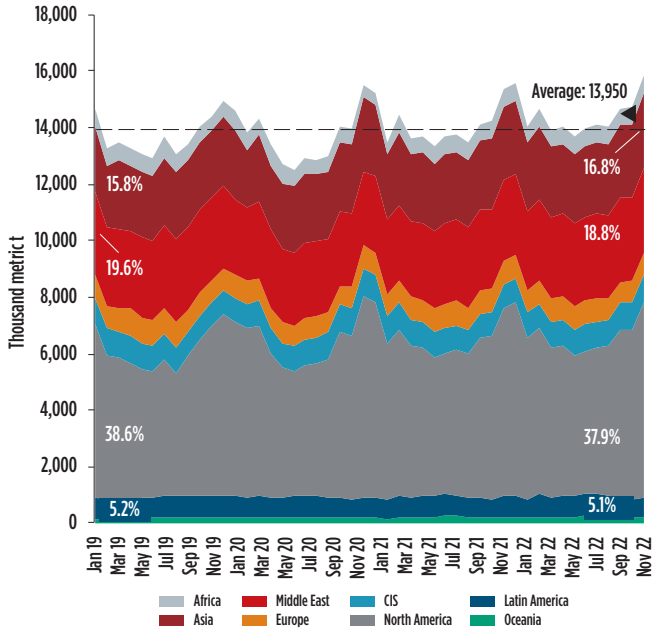

FIG. 2. Global propane supply by region, 2019–2022.

The Netherlands, Japan and Australia—some of the oldest and most reliable autogas markets—saw declines in demand averaging 10%.

LPG shipping. While 2020 figures are still being collected, 2019 saw a breakthrough in freight rates. Spot rates on the very large gas carrier (VLGC) benchmark Mideast Gulf–Japan route averaged $58/metric t compared with around $30/metric t in the last 3 yr. Time charter rates for the 12-mos period were also higher in all sectors. Amid high freight rates, favorable arbitrage conditions meant that there was some maneuvering room for those lifting from the U.S. Gulf Coast and delivering to Asia-Pacific.

The LPG fleet capacity increased further in 2019 and stood at 35 MMm^3 at the end of the year. The semi-refrigerated sector accounted for most of the rise. Around 18 VLGCs entered the fleet in the past 2 yr, following 46 in 2017 and 69 in 2016—an indication that the freight market is rebalancing—as reflected on stronger freight rates. This took the LPG fleet to 1,494 vessels.

The International Maritime Organization (IMO) regulation on bunker fuels went into effect on January 1, 2020, effectively increasing operating costs in the form of higher bunkering costs for low-sulfur fuels. Shipowners were well-prepared for this change, and the impact on freight rates was largely shrugged off.

Climate change considerations. The past 24 mos have provided an opportunity for the LPG industry to review and reposition itself in the present and future role of climate change. Industry-wide efforts to adapt, innovate and engage in mitigation practices have proven positive, both internal to the industry and externally. Innovations like bio-LPG (or renewable propane, as it is known in the U.S.), have kicked off discussions in key markets like Europe and North America.

As a byproduct of renewable diesel and jet fuel production, renewable propane chemical and physical properties are identical to propane produced from traditional sources; however, it is carbon neutral. Additionally, renewable propane producers are eligible for subsidies through California's Low Carbon Fuel Standard and the U.S.'s federal Environmental Protection Agency (EPA) Renewable Fuel Standard (RFS) program.

Beyond renewable propane, the LPG industry is investing in technology and product development toward a net zero future. This includes research and development efforts in the transportation and industrial engine market sectors, such as advanced spark-ignited engine technology, propane hybrid drive systems and advanced exhaust catalyst systems.

Similarly, LPG projects and products are beginning to play a role in providing resiliency to the electric grid through primary, backup and hybrid systems to support other renewables like solar and wind installations. Distributed power generation, grid-free and microgrid systems powered by LPG are proving highly versatile and sustainable in areas where the electric grid is overtaxed by current demand. These systems not only build in some level of resiliency to the grid, but also serve to improve energy and environmental equity.

Today, much of the developing world does not have access to clean cooking fuel. Black carbon emissions, such as those emitted from the burning of firewood, dung and charcoal, continue to be a major issue for residential air quality in many developing countries. As proposed by the World LPG Association, LPG could save millions of lives and support sustainable transformation of the household sector by becoming the go-to residential cooking fuel source.

Sector outlook. Mid-term LPG market forecasts suggest strong supply and continued growth worldwide. Global LPG production is expected to exceed 370 metric MMtpy by 2030, roughly a 14% increase from 2019 global production. Trade flows will continue to expand; however, they will likely become more complex with continued geopolitical and geoeconomics issues among the key market movers. Significant trade routes, like the Mideast Gulf to Asia-Pacific, U.S. to Asia-Pacific, and U.S. to Europe, are likely to make up a significant portion of global movements in LPG.

Continued demand in traditional residential heating and cooking segments is expected. Market projections suggest 15% growth from 2019–2030, culminating in more than 150 metric MMtpy of global demand. The cooking sector in Asia-Pacific will see the largest gain in incremental LPG demand. Alongside India, growth is forecast in several smaller markets in the region, including Bangladesh, Vietnam and the Philippines.

Continued expansion of the natural gas grid, rising energy efficiency and legislative pushes toward renewables and "carbon-free" sources will continue to impact the North American market. Similar impacts will be felt in northwest Europe and northeast Asia, based on current projections. Demand in South America, however, will continue to grow and be a consistent source for U.S. LPG exports.

Similar demand growth is expected in the global petrochemical market, primarily coming from Asia-Pacific markets, as well. Construction of new propane dehydrogenation plants will see global demand for LPG as a petrochemical feedstock.

Recently published global scenarios include the newest International Energy Agency (IEA) roadmap for the global energy sector.[1] Such studies tell much the same story: The focus of government and business leaders must be on those solutions already in hand today, rather than on technology breakthroughs that may not come in time, or that may never come.

As centralized energy systems become more brittle and system upgrades become more expensive, LPG is increasingly seen as a key distributed energy resource made attractive by its wide availability, lower relative cost and small carbon footprint. **GP**

LITERATURE CITED

[1] International Energy Agency, "Net zero by 2050: A roadmap for the global energy sector," May 2021, online: https://www.iea.org/reports/net-zero-by-2050

GORDON FELLER has been writing about energy, particularly oil and gas, since his first magazine article was published in 1978, and he has been published in more than 50 industry magazines. He has undertaken numerous research and writing projects for large institutions, including the World Economic Forum, the World Bank, and the governments of Germany, the UAE (Abu Dhabi), Japan and Canada. He has also won more than two dozen competitive fellowships. Mr. Feller graduated with a master's degree from Columbia University in New York City, New York.

Standardized, modular, small-scale LNG with low lifecycle cost

F. VAN HEERDEN, PolaireTech, Sasolburg, South Africa;
F. HANEY, DyCat Solutions, Calgary, Alberta, Canada; and **G. SKINNER,** Gasconsult, London, UK

Natural gas has developed into the fossil fuel of choice for power generation, industrial use and domestic heating. It produces 30%–40% lower carbon emissions than oil or coal, and zero sulfur emissions. The capital cost of gas-fired power plants is half that of coal-fired facilities. For this reason, LNG is regarded as a high-growth market and is expected to become a low-carbon bridging fuel, pending full deployment of renewables and green or blue hydrogen-based fuels.

At present, the bulk of LNG is produced at low cost in large baseload plants with capacities of up to 7 MMtpy per train and having significant LNG storage facilities. After shipment, LNG is typically stored in a receiving terminal, regasified and used as fuel in power plants and gas grids. In addition to bulk supplies, LNG production plants and receiving terminals can provide competitively priced LNG to smaller markets within a reasonable distance by offering break-bulk volumes.

New LNG markets, including bunker fuel and transportation fuel applications, are developing fast due to environmental pressures around carbon dioxide (CO_2), nitrous oxides (NO_x) and sulfur (SO_x) emissions. These markets are more distributed and often cannot be economically served by break-bulk volumes from existing LNG storage facilities. They are candidates for LNG sales from small-scale LNG liquefaction facilities operating on pipeline gas, flared gas, coal seam gas, biogas and small gas fields. However, these small-scale LNG plants face challenging economics given their small scale. Special emphasis must be placed on developing a competitive offering with the lowest lifecycle cost.

Achieving the lowest lifecycle cost requires:

- A process configuration that strikes a competitive balance between CAPEX and OPEX
- A project development and implementation approach that benefits from a lean, standardized, modular design; low-cost shop fabrication; and reduced project schedule.

This article describes an optimized solution to this challenge developed by the authors.

Process configuration. The selected process uses the feed natural gas in an optimized system of expanders to provide the necessary cryogenic refrigeration. As a result, no external refrigerants, such as nitrogen or mixed hydrocarbons, are required, with the following benefits:

- No requirement for refrigerant handling, storage, blending or transfer facilities, reducing the equipment count and capital cost
- No refrigerant make-up costs
- Reduced plot area
- High-efficiency process with low power demand
- Low power demand translates to low operating cost and low-cost compression equipment.

FIG. 1[a] shows the process flow scheme, which is suitable for a small-scale LNG plant with an output of up to 200,000 tpy.

The concept is based on two expander circuits: a warmer circuit shown in red and a lower-temperature circuit shown in blue. The cold outlet streams from expanders EXP1 and EXP2 are routed to the cold box, HX1, to provide cryogenic cooling and are then returned to the expanders by the recycle compressor, CP1. The expanders are configured as expander-compressors, with the compressor sections in series with the primary compressor, CP1.

A patented feature is that a partial liquefaction takes place in the low-temperature expander, EXP2. This very efficiently converts latent heat into mechanical work and reduces power demand by approximately 15%. It further reduces the size and cost of the main cryogenic exchanger, HX1.

This process arrangement has been independently assessed as having a specific power demand 10% below that of single

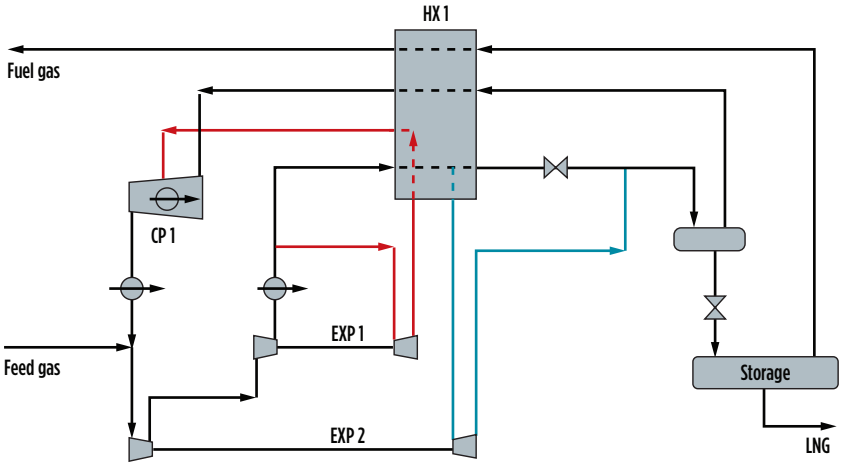

FIG. 1. Basic flow scheme of a small-scale LNG plant.

mixed-refrigerant processes and 25% below dual nitrogen expander processes.

To offer an overall optimized and integrated design, various feed gas scenarios have been developed, namely:

- Pipeline gas at pressure and containing low levels of impurities
- Low-pressure biogas or coal seam gas containing high amounts of CO_2
- Low-pressure flare gas containing low levels of heavier hydrocarbons.

Optimized integration between the feed gas preparation and the liquefaction sections of the LNG plant is important to ensure high methane recovery and the lowest lifecycle operating cost for the overall facility.

FIG. 2[b] indicates typical feed preparation arrangements for a range of feed gas scenarios and how they can be integrated with the liquefaction section. It is necessary to remove CO_2, water vapor and aromatics (benzene) to prevent freezing in the liquefier.

The CO_2 in natural gases, usually less than 5%, is conventionally removed by washing with amine. The gas is then dried with a molecular sieve. With high CO_2 feeds such as biogas and coal seam gas, an arrangement of CO_2 removal by membranes, followed by final CO_2 removal and drying with molecular sieves, may be more suitable.

Aromatics in pipeline gas, typically below 100 mol ppm, are removed with molecular sieves or other sorbents. High concentrations of aromatics in the feed gas may be condensed, together with C_5+, in the liquefaction section by an appropriate configuration of the warm expander circuit running through EXP1, with significant CAPEX savings over conventional NGL removal.

Project/product development and implementation. To develop a best-in-class, standardized and modular design,[c] innovative work processes have been applied, including:

- Structured lean design and development workshops with the entire design team, resulting in a capital-efficient design
- A proprietary, four-step project execution work process[d] was followed, comprising:
  - Step 1: Identify factors that influence modularization
  - Step 2: Determine degree of modularization and preassembly
  - Step 3: Develop optimized layout
  - Step 4: Develop modular support documentation.

Applying the aforementioned processes resulted in a design allowing 80% of the labor to be moved offsite compared to a traditional stickbuilt execution, as well as the ability to design one and build many plants.

The following sections provide more information on the concepts of lean design, standardization and modularization.

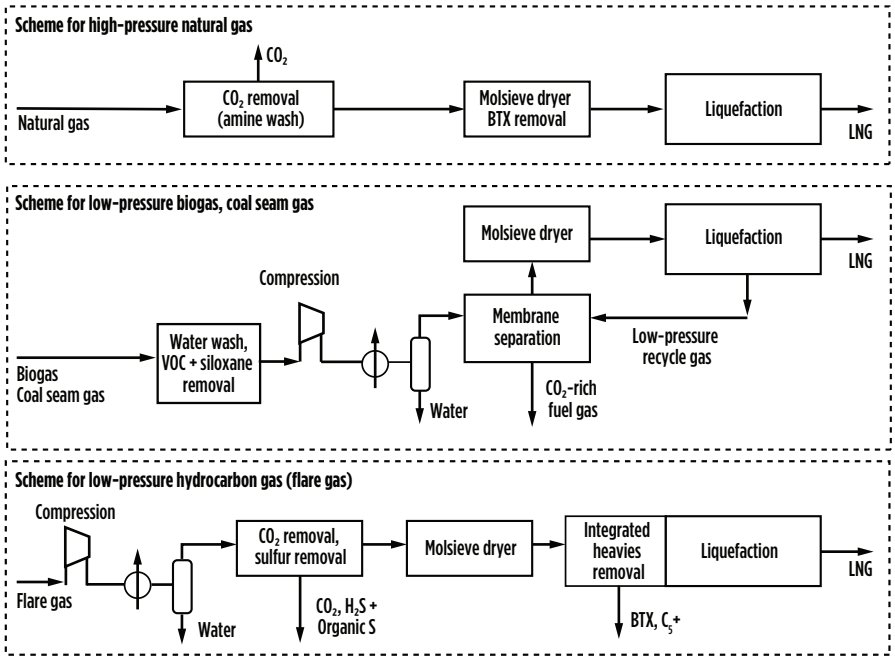

FIG. 2. Three feed gas scenarios.

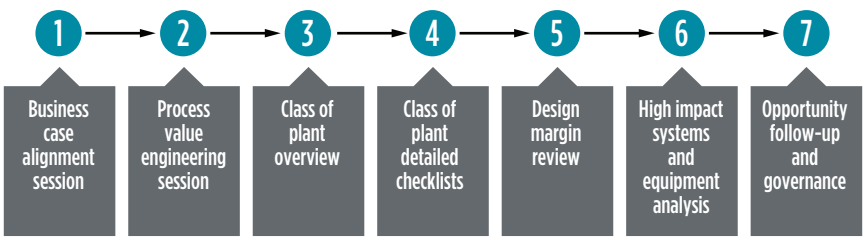

FIG. 3. Lean design process and concept.

Lean design. Lean design principles were followed to develop a design that is the lowest lifecycle cost and provides the most competitive offering. This is illustrated in FIG. 3.

Standardization. To offer a cost-competitive product, standardization was considered essential to reduce capital cost and the overall project schedule, as well as to reduce the lifecycle cost of the plants. Applying standardization supports the "design one, build many" philosophy and typically results in capital cost savings of 10%–20%, as illustrated in FIG. 4.

Modularization. The use of modules reduces onsite construction labor hours and allows for scalable, adaptable, plug-and-play units, as well as easy integration with existing systems. An added advantage is that the compact footprint optimizes the use of space. A compact modular solution also reduces capital cost due to improved labor productivity and reduced bulk material quantities.

Principles of modularization have been specified during plant development, including module definitions and basic layouts. A structured, four-step work process was applied in developing optimal modular layouts, with the aim of reducing the overall plot area and key quantities. The basic principle was to allow modularization to drive the layout, as opposed to the layout driving modularization.

For a 60,000-tpy, small-scale LNG plant, the most appropriate module transport envelope size was identified to be 14.6 ft wide × 14.6 ft high × 80 ft long. This transportation constraint fits most global inland transportation infrastructures, normally requiring only minimal permits. For smaller plant capacities, modules of 8 ft wide × 8 ft high × 40 ft long are being used, requiring no special permitting.

The modular layouts produce a percent modularization (amount of labor moved offsite compared to traditional stickbuilt designs) of approximately 75%–80%. FIG. 5 illustrates the conceptual layout for a 60,000-tpy, small-scale LNG plant and identifies the plug-and-play module definitions and numbering.

Modularization typically results in capital cost savings of 15% compared to a traditional stickbuilt execution. This number will vary in different locations depending on the craft labor cost and site productivity. An additional advantage of a modular plant is the ability to easily relocate the plant, if required.

Execution. Lean execution methods were used, including standardization and modularization, that provide program flexibility and scalability, cost and schedule certainty and overall schedule reductions. This section reviews the details on how this approach achieved a lean project execution.

Plug-and-play modules. The use of lean-designed, standardized, modular units allows for multiple plants to be built using standardized, plug-and-play process or utility modules. Each standard process module can be easily plugged in, depending on the operating requirements. For example, if local power is not available and electrical generation is required, then the appropriate electrical generator blocks can be plugged into the facility. Onsite LNG storage can be added by plugging in standard storage units. Utilities can be added by plugging in standard utility modules.

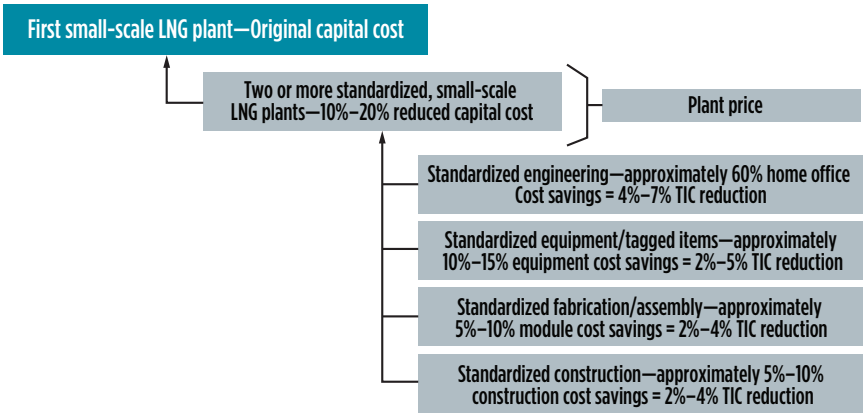

FIG. 4. Standardization ("design one, build many") concept.

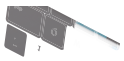

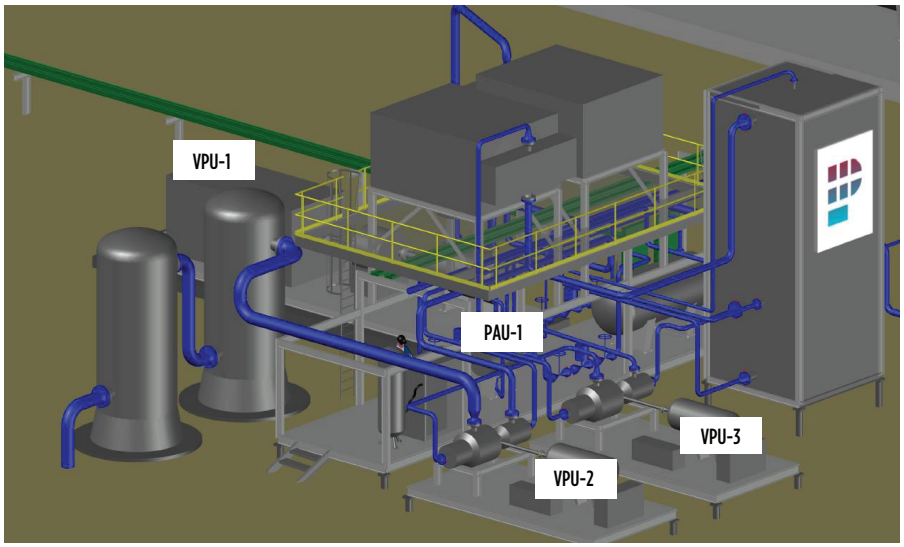

FIG. 5. Breakdown and definition of a 60,000-tpy, small-scale LNG plant module.

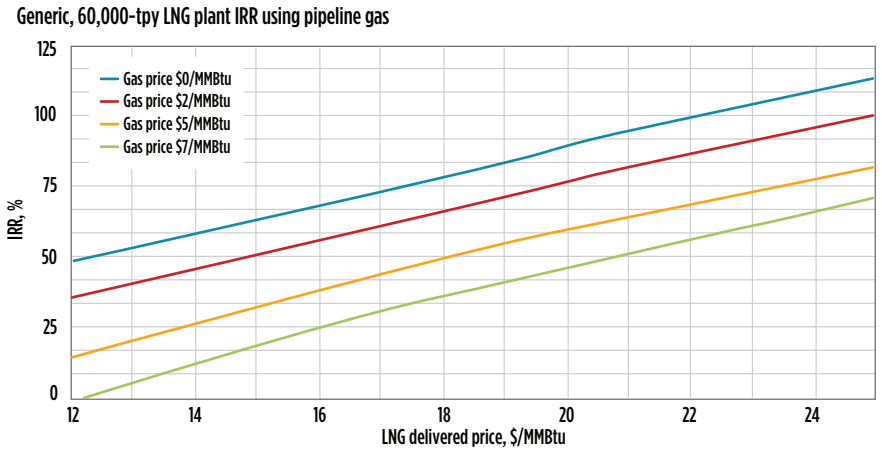

FIG. 6. Typical return on investment for a generic, 60,000-tpy, small-scale LNG plant.

A limited number of standard-capacity module templates were developed within the small-scale LNG plant range, allowing for an optimal selection to suit a customer's needs. Multiple modular trains can be installed to reach a desired overall output. An advantage of this approach is that additional trains can be added in a phased manner as the market is expanded, significantly reducing the initial capital cost and funding requirements.

Lean execution schedule. By applying a standardized design for a limited range of plant capacities, the overall execution schedule can be reduced by 40%–50% when compared to traditionally executed LNG facilities. A typical schedule would be 9 mos–12 mos from order to ready for commissioning, with modules being shipped to site ex-module yard within 6 mos–9 mos.

Commercial deployment. Commercial deployment of small-scale LNG plants is driven by four key factors:

- The need to reduce greenhouse gas emissions and decarbonize the energy industry
- The ability to supply gas competitively to users
- Alternative means of transporting gas to productive use
- Regulatory requirements.

The following section illustrates specific applications of small-scale LNG plants and highlights the economic viability of the opportunities.

Diesel fuel replacement. The use of LNG as a replacement fuel in diesel vehicles, trains, remote power stations or other industrial and heating applications presents an opportunity for small-scale LNG plants. The concept is based on extracting clean gas at pressure from gas distribution pipelines at various locations and the assumption that the LNG produced will be sold within a radius of 250 mi as a diesel replacement fuel. The opportunity is conditional on various factors, including the prevailing oil price and location of the point of use, and the location of a gas supply to feed the small-scale LNG plant. Even at relatively low oil prices, opportunities exist in land-locked countries with difficult or lengthy transportation logistics.

A case study of an optimized, 60,000-tpy, small-scale LNG plant using pipeline gas, as described in this article, is shown in FIG. 6. The figure illustrates expected returns against gas input price vs. LNG selling price. As an example, such a plant can achieve an internal rate of return of 25%, even at a $7/MMBtu gas input price, when delivering LNG to the customer at a price of $16/MMBtu.

With a diesel price of $3.16/gal ($22.80/MMBtu), this would reflect a direct fuel price reduction of around 30%. In addition, the efficiency of dual-fuel engines (LNG plus diesel) has, during field tests, been observed to be around 10% better than diesel only, resulting in additional savings for the end user. The actual cost savings and LNG plant netback price will depend on local and federal taxes and will be calculated more precisely for each specific opportunity.

Green renewable LNG from biogas. Biogas is obtained from the anaerobic digestion of domestic, industrial and agricultural waste and is typically reinjected to a gas grid or used to generate electricity. However, anaerobic digestion also presents opportunities for biogas liquefaction. In these cases, micro-scale LNG units of 5,000 tpy (or even smaller) may find application.

Harvested biogas is typically produced at atmospheric pressure and contains substantial quantities of water, N_2 and CO_2. It needs to be compressed and cleaned before being fed to the liquefaction section of an LNG plant. This results in higher capital and operating costs compared to pipeline gas but could still represent a profitable opportunity. FIG. 7 illustrates an expected return on investment for a 5,000-tpy bio-LNG plant.

It is expected that a newly constructed biogas facility would need to sell the gas to a small-scale LNG plant at a price of

around $7/MMBtu to recover its capital cost. This, in turn, requires an LNG selling price of at least $18/MMBtu—considerably higher than prevailing gas prices but potentially competitive against diesel or LPG. Furthermore, certain countries offer incentives to encourage the development of green renewable fuels, which considerably enhance the economic viability of such opportunities.

Flare gas recovery. Gas is flared from many gas fields and processing plants. The World Bank[1] estimates from satellite data that, in 2019, flared volumes exceeded 5 Tft[3] and that almost half of the total volume was generated in only four countries: Russia, Iraq, the U.S. and Iran. With the global move to net zero carbon, it would be surprising if these volumes were not targeted for recovery to beneficial use.

Flared gases are generally at atmospheric pressure and may contain quantities of heavier hydrocarbons. The gas must be compressed, and the heavier hydrocarbons recovered, before being fed to the liquefaction section of an LNG plant. The integrated heavies removal concept of the liquefaction process provides for the recovery of heavier hydrocarbons in a cost-effective way that could result in much-improved economics.

FIG. 8 illustrates the economics for a 20,000-tpy facility based on flare gas. This excludes the revenue from heavies recovery, which requires a case-by-case analysis that considers the gas composition, as well as the potential markets for the products.

Takeaway. Achieving economic viability for small-scale LNG applications is challenging, as they lack economy of scale relative to conventional LNG schemes. Applications are likely to be in the areas of liquid fuel substitution, locations where conventional fuel supplies are logistically difficult or where environmental pressures prevail.

Rigorous optimization from both a process design and detailed engineering perspective, along with the adoption of a lean, standardized, modular approach allow significant expansion of opportunities for small-scale LNG, to the benefit of gas owners and their fuel customers. **GP**

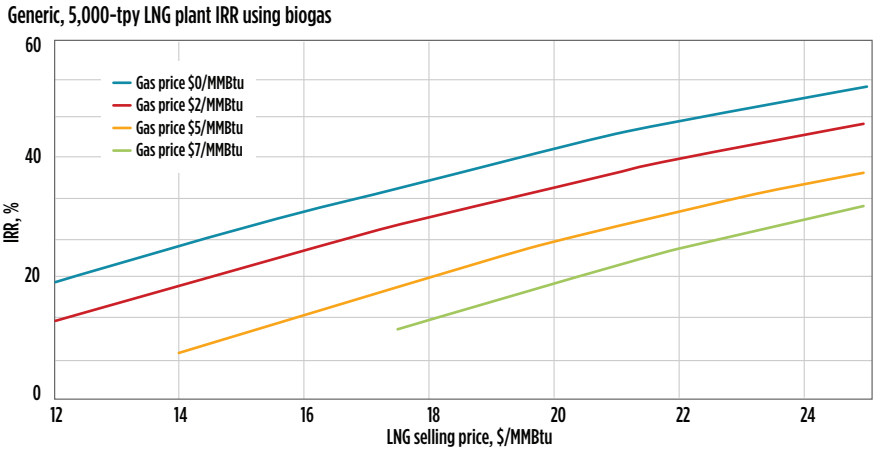

FIG. 7. Expected return on investment for a generic, 5,000-tpy biogas-based plant.

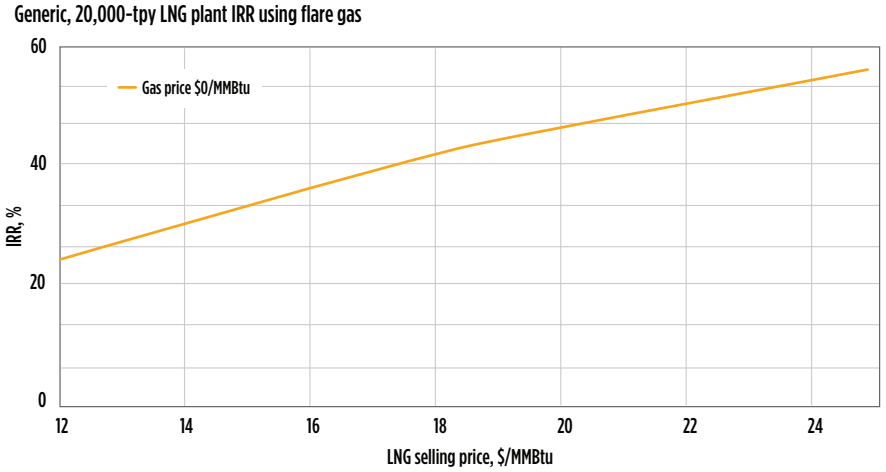

FIG. 8. Example economics for a 20,000-tpy facility based on flare gas.

NOTES

[a] The dual methane expander process described in Fig. 1 is the ZR-LNG system (Zero Refrigerant LNG), which is owned, patented and licensed by Gasconsult Ltd.

[b] The Integrated Heavies Removal process shown in Fig. 2 is owned, patented and licensed by Gasconsult Ltd.

[c] The lean, standardized, modular, small-scale LNG plants described in this article are engineered and marketed by PolaireTech.

[d] The proprietary, four-step work process used to optimize the lean, standardized, modular design is the Optimod Execution Work Process developed by DyCat Solutions Inc.

LITERATURE CITED

[1] World Bank, "Global gas flaring tracker report," Global Gas Flaring Reduction Partnership, Washington, D.C., July 2020, online: https://pubdocs.worldbank.org/en/503141595343850009/WB-GGFR-Report-July2020.pdf

FREEK VAN HEERDEN is Managing Director of PolaireTech. He graduated from Pretoria University in 1975 and joined AECI Limited in Sasolburg, South Africa as a Process Engineer. In 1998, he transferred to Sasol, an international petrochemical company, where he was involved in various coal and GTL, polymer, clean fuels and renewable energy projects globally as Engineering Manager and Technical Director. He was also a founding member of Owner Team Consultation, which assists owner organizations in the development of new projects. In 2019, PolaireTech was formed as a JV between Owner Team Consultation and Saiyl, an EPC company, to develop modular, small-scale LNG plant offerings.

FRED HANEY is President of DyCat Solutions, a company that provides innovative solutions to the heavy industrial business sector. He is a recognized leader in developing the optimum capital efficiency for owners of heavy industrial projects. He has been globally recognized as a subject matter expert for his development of modular designs, practices and execution solutions. He is also the inventor of Fluor's 3rd Gen Modular Execution.

GEOFF SKINNER is Technical Director of Gasconsult. He graduated from Oxford University and joined Foster Wheeler in the UK in 1965. From 1981 to 1986, he was Technical Director of Foster Wheeler Synfuels Corp. in Livingston, New Jersey. On his return to the UK, Mr. Skinner acted as a consultant to several multinational companies and has registered a number of patents, including LNG and hydrogen liquefaction processes.

SSLNG-to-power solutions for optimized CAPEX and OPEX

R. BRANNOCK, TGE Gas Engineering GmbH, Manchester, UK and
J. TERPITZ, TGE Gas Engineering GmbH, Bonn, Germany

LNG-to-power has become an established term in the international energy industry, whereby gas-fueled power stations are exclusively supplied from an adjacent LNG storage terminal. Typically used for remote locations with no nearby natural gas pipeline grid in the vicinity, small-scale LNG (SSLNG)-to-power is the fuel supply solution.

On demand, these terminals can be additionally equipped with LNG distribution facilities—e.g., truck or ISO container loading. The market demand development of this type of infrastructure has been observed for several years already.

SSLNG-to-power business case. Multiple key drivers exist for the development of SSLNG-to-power projects. Lower LNG costs compared to oil will always be viewed positively. Additionally, increased LNG supply is coming from the expansion of existing, large-scale production facilities and the development of new facilities, particularly in the U.S. (using shale gas feed) and Russia (using arctic-region gas). High LNG supply can be expected for the upcoming decade to ensure stability of supply. A general increase in renewable energy sources also will be seen, particularly wind and solar; however, the renewable sources may not provide sufficient electricity on demand for high energy peaks.

The worldwide target for reduction of CO_2 emissions will force the replacement of heavy-carbon fuels with lower-carbon methane fuel. Environmental and associated societal pressures will demand that governments push for greener developments, and may create further opportunity via reduced taxes, fees and funding.

Many market players understand SSLNG to mean LNG receiving installations with a yearly throughput up to 0.5 MMtpy. This is in comparison to "LNG as fuel" installations with throughputs below 0.05 MMtpy and, on the larger side, mid-scale LNG receiving terminals up to 2 MMtpy and world-scale LNG receiving terminals with throughputs greater than 2 MMtpy.

Many prospects exist in the global market whereby SSLNG-to-power installations will be viable economic and environmental solutions.

SSLNG-to-power supply chain. The typical LNG supply chain for an SSLNG plant is similar to that of other LNG supply chains. The LNG is received from an LNG liquefaction plant using an LNG carrier (LNGC) (FIG. 1); however, growth is seen in breakbulk LNG reception terminals, whereby larger deliveries are reloaded onto smaller LNGCs or barges for delivery to small-scale storage units. At the small-scale storage unit, the LNG can be stored, pumped and vaporized and then routed directly to a local power plant.

In addition to supplying fuel directly to the power station, LNG can be supplied to other customers depending on the location. This may include LNG distribution to other LNG satellite stations, to LNG fueling stations, other mini-power generation sites or for fueling marine operations (FIG. 2).

SSLNG-to-power plant outline. When establishing small-scale, standalone solutions, the first key features that must be assessed and designed are ship unloading and the requirements for additional marine infrastructure. Consideration must be given to the design of the LNG storage and regasification methods, as well as the boil-off gas management.

Additional options and synergies may be investigated. These include the "total solution" concept, whereby the power plant and LNG storage facilities are heavily integrated or have combined infrastructure. Further options may include additional truck loading for mini-scale power

FIG. 1. The typical LNG supply chain for an SSLNG plant is similar to that of other LNG supply chains, whereby the LNG is received from an LNG liquefaction plant using an LNG carrier.

TABLE 1. Case study examples for small-scale pressurized and atmospheric solutions

Case	Nominal power generation	Peak consumption	LNG required, MMtpy	Average LNG requirement, Nm^3/d	Delivery max. prefabrication, mos	Delivery stickbuilt, mos	Storage capacity	Tank concept*
1	25 MW	27.8 MW	0.034	145,160	18	20	6,000 m^3	VI bullets
2	100 MW	111.1 MW	0.135	580,640	24	26	25,000 m^3	FC S/C
3	150 MW	166.7 MW	0.203	870,960	24	26	38,000 m^3	FC S/C

*VI bullets = Vacuum-insulated bullets; FC S/C = Full containment, steel/concrete tanks

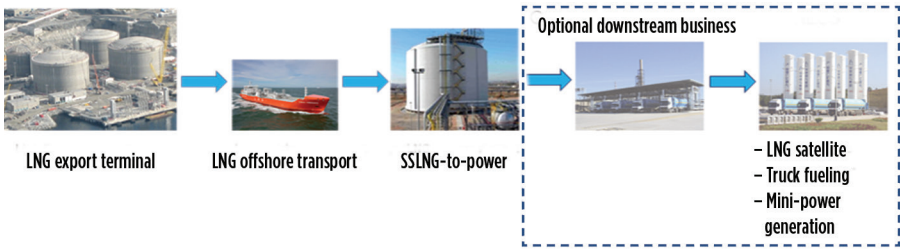

FIG. 2. In addition to supplying fuel directly to a power station, LNG can be supplied to other customers, such as other LNG satellite stations, LNG fueling stations, other mini-power generation sites or marine operations.

FIG. 3. ISO container on trailer used to store LNG at mini-scale power facilities.

distribution, local industrial consumers and vehicle refueling stations.

The high-level concept for SSLNG-to-power remains virtually the same for varying power generation levels required; however, when optimizing the concept for a particular site or project, all applicable parameters must be considered.

Case studies for SSLNG-to-power. A number of case studies have been developed for varying levels of power generation of 25 MW, 100 MW and 150 MW. Power generation is based on simple-cycle engines with a thermal efficiency of 48%, using a typical LNG heating value, with one LNG cargo delivery every 4 wk and a delivery power of 8,000 hr/yr. TABLE 1 compares examples for the small-scale pressurized and atmospheric solutions.

The delivery times of these project vary depending on several factors, including delivery times for the power units. However, when the project requires larger-size storage tanks, then the tank construction dominates the critical path.

The storage capacity is based on a 4-wk delivery term, but this will be subject to the availability of LNG in the specific market and the size of the LNG carrier available. Additional small LNGCs are coming into operation as the demand for smaller cargoes increases, which will provide a benefit to small-scale terminals. Another option may be to receive a portion of a cargo from a larger LNGC.

Modular design concept. Depending on the individual project, the construction concept can be optimized based on location and the type of equipment to be installed. Given the nature of the overall SSLNG-to-power concept, it can be assumed that the location is more than likely to be remote, with potentially low levels of infrastructure and construction labor availability.

The remote location will benefit from a minimum of in-situ construction and from equipment and plant sections being provided as modularized units. At least partial adherence to these targets will reduce construction costs by maximizing prefabrication. The modularized design approach brings clear advantages in plant expandability while fast-tracking project delivery time to enable the commencement of commercial operations and an optimized return on investment.

Mini-scale power production. At < 50 MW, these small-sized power plants usually serve the power demand of a smaller island without significant industrial power demand. The LNG can be transported via ISO containers on LNG trucks (FIG. 3) or by rail (often referred to as a "virtual pipeline"), with each holding approximately 43 m^3 of product. They can be lifted from the trailer assembly or left in-situ on the trailer for distribution in the plant.

Although the storage is modular, these ISO containers provide an option for storage solutions up to 500 m^3 and produce low levels of power generation. A significant advantage of using ISO containers is that the facility does not need to be in a marine location, but can be situated inland at more convenient sites. At the power plant, the LNG is stored in small, pressurized vessels.

Small-scale power production. As power generation requirements increase up to 50 MW, so does the size of the storage. The storage concept changes to utilize vacuum-insulated bullets, each with a typical capacity of 1,000 m^3 (FIG. 4). Economic designs up to 10,000 m^3 can be achieved, with the remainder of the plant being fully modularized, which means that the overall schedule can be reduced to approximately 16 mos–18 mos.

This concept does not incorporate a boil-off gas handling system; instead, the LNG is allowed to warm up within the storage, as the system can operate with zero sendout for up to 2 mos without any venting requirements

Star-fin ambient air vaporizers are a simple vaporization solution in this concept. They are a suitable technology for most climates; however, some additional heating may be required for colder climates.

Medium/large-scale power production. As power generation requirements increase to 50 MW–300 MW, the quantity of LNG required increases accordingly, and the storage requirement becomes greater than 10,000 m^3. The economics for the storage concept change, and the optimum solution becomes an atmospheric-type storage.

These flat-bottomed tanks must be built in-situ and are built according to the relevant EN 14620 or API 620/API 625 codes. The containment type of the tank can be defined as single, double or full. For LNG storage of this magnitude, the general concept is to have a full-containment tank with a concrete outer shell to minimize risk of leakage. However, other concepts can be adopted depending on the overall project safety requirements, which may be permissible in very remote locations.

The atmospheric LNG tanks store the liquid at its bubble point, close to atmospheric pressure. With the liquid continuously boiling, the vapor (boil-off gas) generated must be managed. The boil-off gas can be compressed directly to a sendout system or user. A recondenser system used on larger regasification terminals would not be economic in this case. With the greater sendout rate of LNG, options may exist for the vaporization concept. However, it is likely that the use of star-fin ambient air vaporizers, albeit in a larger number, will provide an economic solution due to low installation and operational costs (FIG. 5).

The total solution concept. The total solution concept combines and integrates the power plant with an SSLNG terminal. Depending on the size, the power plant could be utilizing gas engines or, as size increases, gas turbines or combined-cycle power plants.

With a total solution concept, there is a large potential for CAPEX savings within the shared facility. During the plant engineering and construction phase, common methodologies, execution strategies and teams not only produce cost savings but also should limit the amount of interfaces required between the power plant and the LNG terminal.

All plant infrastructure can be common and shared across the LNG storage and power plant. This may comprise all buildings (maintenance, control, etc.), electrical systems, monitoring systems (fire and gas, CCTV, etc.), as well as other auxiliary and safety units (fire-fighting, utilities, etc.), which will drive down the overall CAPEX. The power plant also can be designed to allow a black start capability.

Utilizing heat integration systems between the power plant and the LNG terminal, the operational expenditure (OPEX) can be reduced, but is somewhat dependent on the type of power generation used. With gas turbines, the LNG cold energy can be greater utilized with inlet air cooling. Depending on the site location, the heat or cold from the facility can be used within the terminal to reduce costs, e.g., HVAC systems. At an operational level, some reduction in staffing costs can be achieved with operational, maintenance and administration teams used across the integrated facility.

With the total concept solution, the terminal business concept can be further extended with truck loading and road/marine fueling facilities.

Competing offshore concepts. Competing offshore concepts for SSLNG-to-power exist—i.e., an FSRU with onshore power generation or a power barge.

These offshore solutions can bring advantages in project implementation schedule, depending on shipyard available capacities. The FSRUs can be constructed in a safe environment within the shipyards. Nevertheless, the mooring must be installed locally and under a high CAPEX, bringing into question the biggest advantage of an FSRU, which is flexibility of movement to another location.

The relatively high operational costs and operational risks due to storm and tsunami are another disadvantage. Difficult and extreme weather conditions may prevent an offshore installation. Requirements for dry dock inspections may also interrupt the power supply.

Takeaway. The SSLNG-to-power onshore concept is an economic and desirable solution for power generation in remote locations. The LNG storage concept is flexible and scalable, depending on the power generation required.

Technical synergies, such as heat integration between the power plant and the LNG facility, can provide an optimized power generation efficiency. This total concept solution provides CAPEX and OPEX optimization, lowers the project risk and reduces time to commercial operation. **GP**

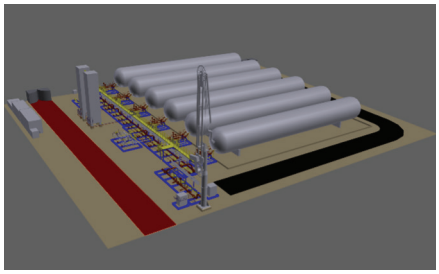

FIG. 4. As power generation requirements increase up to 50 MW, the storage concept changes to utilize vacuum-insulated bullets with a typical capacity of 1,000 m^3.

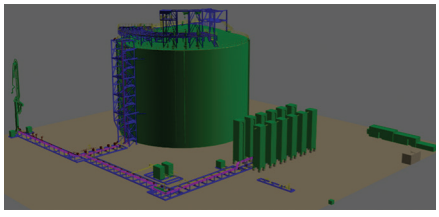

FIG. 5. For LNG storage for large-scale power production, the use of many star-fin ambient air vaporizers will provide an economic solution due to low installation and operational costs.

ROBERT BRANNOCK is the Managing Director of TGE Gas Engineering GmbH's UK branch and Technodyne International Ltd. After obtaining his MS degree in chemical engineering from UMIST in 1996, Mr. Brannock has gained more than 20 yr of oil and gas industry experience in design, engineering and commissioning of gas processing facilities and cryogenic terminals. Working with TGE Gas Engineering since 2002, he has occupied several positions and now manages its UK offices. He is also a Fellow of the IChemE.

JULIAN TERPITZ is Product Development Manager at TGE Gas Engineering GmbH. He is responsible for developing and innovating TGE Gas Engineering's offerings to the market. He received a diplom-ingenieur (master's) degree in mechanical engineering and thermodynamics from RWTH Aachen University in 1999. Since that time, he has worked for many years as Project Engineering Manager in different international projects related to liquefied gases. He also led the department of project engineering management at TGE Gas Engineering for several years. During these assignments, he gained extensive experience in the technology, management and execution of EPC projects from proposal to commissioning, as well as in leading product development projects.

Achieve three efficiencies in MR compressors for SSLNG

T. PATEL, Atlas Copco Gas and Process, Houston, Texas; **M. DREWES,** Atlas Copco Gas and Process, Köln, Germany; and **J. ZHAO,** EnFlex Group, Houston, Texas

In the equipment they use, investors in small-scale LNG (SSLNG) face a steep challenge: They must achieve cost efficiency, operational efficiency and energy efficiency—all with maximum availability. In this context, the design of single mixed-refrigerant (SMR) compressors, a critical piece of technology in SSLNG plants, takes on an important role in both the plant's efficiency and its return on investment (ROI).

As the benefits of integrally geared compressors (IGCs) have become better known across hydrocarbon processing industries, this compressor type has achieved broader acceptance. For SSLNG, this pertains particularly to compressors requiring gas or electric drives with a rated power of up to 27 MW (36,200 hp). Demand for IGCs has been especially strong for SSLNG plants with varying technical and logistical requirements compared to large-scale LNG facilities. These include quick deployment, scalability, redeployment capability and the ability to respond rapidly to market demand.

Until the early 2000s, inline (i.e., single-shaft) compressors were the dominant compressor technology in the marketplace. From then, IGCs have become more popular due to their greater efficiency and reliability, and their inclusion in the 7th edition of the API (2002, Ch. 3). Nevertheless, universally applicable statements on the differences between these two technologies must be carefully considered. This is because the specific use case and operating conditions are what ultimately drive the decision on which compression technology is used.

This article examines the deployment of integrally geared compressor technology, exploring the drivers behind the rising demand for SSLNG and the qualities that make IGCs an efficient compression solution in SSLNG plants. Characteristics discussed include the IGCs' high flexibility and lower initial investment and operating costs, which enable operators to realize agile plant deployment and improve the efficiency of a plant once it is operational. This article uses the example of a mixed-refrigerant IGC installation[a] operating at an SSLNG plant in China.[b]

Inside the Zhengtai Yida LNG plant. The Zhengtai Yida LNG plant (COVER PHOTO) is located in China's Inner Mongolia region, approximately 700 km (440 mi) from China's capital, Beijing. The plant has a 0.807-MMtpy capacity (based on 350 days of operation), and it uses an SMR cycle, the most-used cycle for liquefaction trains with a capacity of 1 MMtpy or less.

The SMR cycle uses various components, such as nitrogen, ethylene, methane, propane, butanes and/or i-pentane in place of the pure hydrocarbon refrigerants utilized in the discrete cooling steps of a cascade refrigerant cycle. Basically, SMRs operate by condensing a hydrocarbon gas mixture to a liquid and then using cooling through its vaporization to cool natural gas close to its boiling point of −162°C (−260°F). The final phase change into LNG is often accomplished with a Joule–Thomson valve.

Many proprietary SMR processes utilize a single-pressure mixed-refrigerant cycle, which compresses the refrigerant to its highest pressure. It is then sent to a series of condensers and separators before it is ultimately delivered to the heat exchanger to cool LNG. To increase efficiency, other SMR processes vaporize the mixed refrigerant in two steps: one higher-pressure and one lower-pressure stage, which can be driven either by two compressors or, ideally, a single compressor with two separate stage groupings (FIG. 1).

The relatively narrow range of compression specifications allows for the standardization of a compressor's aerodynamic design in three- and four-stage mixed-refrigerant compressors. Such standardization allows for faster compressor delivery at a lower initial investment. Given that LNG projects are naturally CAPEX-intensive (the liquefaction process can account for more than 50% of total project costs), lower compressor investment costs help improve a plant's ability to operate profitably.

Lower investment and design priorities. Unlike SSLNG plants, large-scale LNG liquefaction plants require significant investment commitments across all project phases. SSLNG plants have lower installation cost, can be built in much shorter timeframes, and use natural gas as a cost-efficient feedstock in

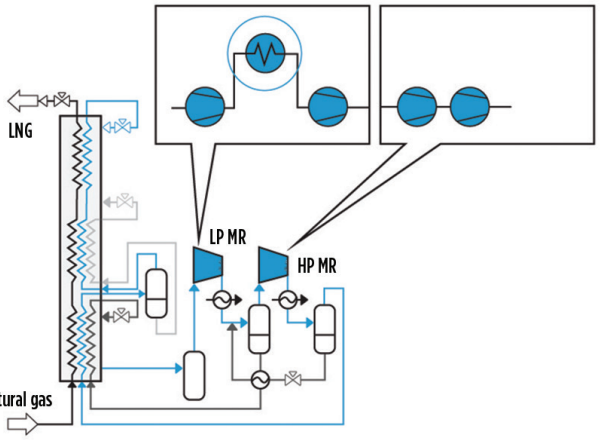

FIG. 1. The IGC unit's deployment within the SMR cycle.

numerous processes along the hydrocarbon value chain.

While SSLNG can expand the scope of LNG availability and the breadth of usage, it is important to understand that smaller-scale projects may feature different compression technology design and operating requirements compared to larger facilities. At the same time, the technologies used in larger LNG plants (including the compressors that run the refrigeration cycle) often cannot be efficiently scaled down.

As is the case across all LNG compressor applications, however, flexibility, reliability and availability are central considerations in the design of mixed-refrigerant compressor trains in SSLNG plants, such as the one installed in the Zhengtai Yida LNG plant (FIG. 2). As a result, the compressor must be designed in such a way that its aerodynamics, rotor dynamics, lube oil, seal support and control systems can precisely meet these parameters and requirements.

FIG. 2. The mixed refrigerant compressor inside the Zhengtai Yida LNG plant.

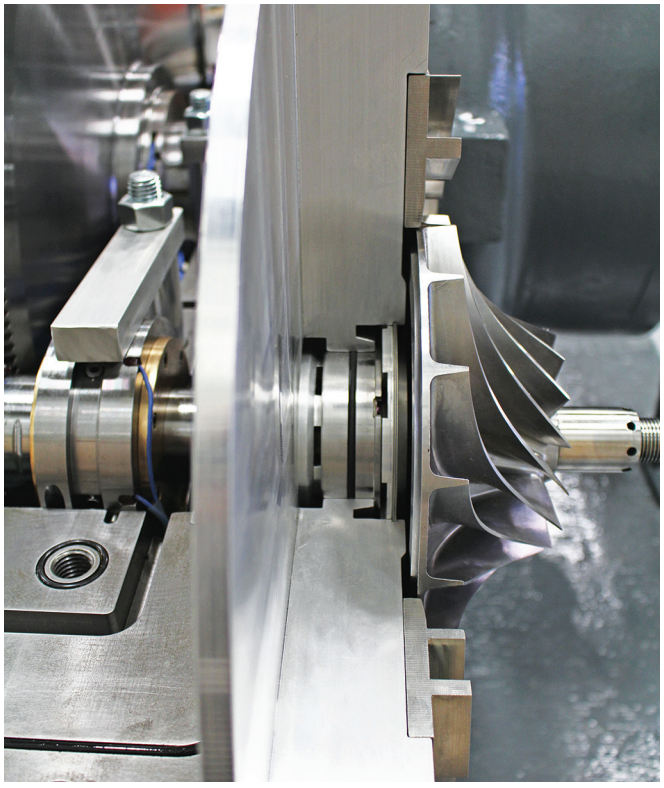

FIG. 3. An installed dry gas seal, mounted at the back of the impeller.

In terms of rotation speeds, the discrepancies in inline compressors between the optimal and actual speeds at each stage reduce efficiency for the whole machine. As a result, more power is needed to drive the compressor, resulting in greater energy usage than for an IGC. In contrast, all IGC stages are optimized to the optimum individual pinion speed by selecting the right teeth (gear ratio between the bull gear and pinion), thereby promoting overall efficiency.

Overall, therefore, compared to the more flexible IG compressors, inline compressors require more time to build, deliver and install. Once delivered, the SSLNG facility can begin operations sooner, increasing the ROI. As production facilities increasingly focus on rapid equipment deployment and flexible operation practices, the basic design (fixed speed and casing) of inline compressors makes it difficult to realize adjustments when production requirements change.

Small footprint and low maintenance. With its inherent compactness, an SMR compressor may be fitted on a comparatively small skid. In the case of the Zhengtai Yida LNG plant, for example, the IGC measures 11 m (36 ft) long by 6.4 m (21 ft) wide with the motor. Comparable inline compressors for this application and plant size can have nearly twice the footprint. In addition, IGCs weigh about 25% less than inline compressors. The IGC's compact footprint helps reduce CAPEX while increasing efficiency and offering flexible process configuration and control benefits. In addition to the compressor core and motor, the skid can accommodate instrumentation and peripherals, such as lube oil, seal support and control systems.

Additionally, the gearbox casing allows for easy access and effective "health monitoring" of gears, bearings, vibration and temperature probes. This compares favorably with the lengthier and more difficult process of removing the many bolts connecting the housing of an inline compressor, and then realigning it after reattaching the bolts.

This aspect is particularly important because SSLNG installations, including the Zhengtai Yida LNG plant, are often located in remote areas, where the logistics of aftermarket support pose a challenge. In such scenarios, onsite repair and maintenance are easier to conduct with IGCs than with inline compressors because of the onsite maintainability and smaller dimensions of the IGC compressor and its components.

Minimizing refrigerant leakage. The seal system design is critical in a mixed-refrigerant IGC and was of particular importance in the Zhengtai Yida LNG plant. Generally, standard machine design calls for a single dry gas seal to be used. However, optionally, tandem dry face seals may be used. The Zhengtai Yida LNG plant's single dry gas seal configuration provides a guaranteed seal leakage rate of 10 Nm^3/hr for the entire machine (FIG. 3).

A typical IGC for an SMR is supplied with three or four impellers and, as a result, three or four sets of seals. Field experience has shown that the vast majority of seal failures happen due to seal support system issues. A properly designed seal support system with clean, dry seal gas supply should be designed and tested prior to commissioning.

Tailored speeds and intercooling. In contrast to inline centrifugal compressor technology, IGC stages provide more flexibility regarding impeller aerodynamic design. While inline compressors are sized depending on the speed of a given driver (or a step-up gear attached to that driver), IGCs are more flexible because they are not bound by a speed requirement. As a result, an IGC's aerodynamics (such as impeller geometry) can be tailored to an application's specific requirements.

By coupling a driver to a bull gear driving several pinions, four pinions and eight compressor stages (impellers) can be mounted onto one gearbox. To accomplish this, one or two impellers (stages) are mounted at each end of the pinion shaft. Two bearings support the pinion shaft, and each impeller is provided with its own seal.

In addition to the impellers, other aero components, such as a diffuser and volutes, are optimized in accordance with process requirements. The required speed is then accomplished via the gear ratio by selecting the appropriate teeth of the bull gear and the pinion.

An inline compressor's design makes stage optimization more challenging. IGCs are seen to be "high head" compared to inline or single-shaft technology. By optimally selecting pinion speeds to correspond to geometry, higher speeds enable minimization of the size and quantity of the impellers for a given function. By enabling optimum aerodynamic performance at each stage, enhanced further by optional intercooling, the best overall efficiency can be obtained.

In an IGC, all rotors are mounted on the same gearbox, and each rotor is independently balanced. This bolsters compressor reliability, because one rotor's imbalance does not impact the others. The result at the Zhengtai Yida LNG plant IGC is an availability of 96+%.

An essential pillar for the general energy efficiency of an IGC is the possibility to install intercooling after each compressor stage. It may be installed optionally between the stages of IGCs, as with the SMR compressor at the Zhengtai Yida LNG plant. By contrast, an inline solution may pose challenges for introducing any type of intermediate cooling between the stages.

Intercooling is a necessary building block for delivering higher overall compression efficiency. Thermodynamic principles state that the temperature of a gas rises when it is subjected to pressure through compression. Doing so requires increased work and an accompanying increase in energy in the next compression stage to achieve further compression of the gas. This cooling between stages allows for compression that comes closer to reflecting an ideal isentropic process due to reduced fluid friction.

Flexibility in process control. To control mass flow and power consumption, IGCs incorporate two control types: variable inlet guide vanes (vIGV) or variable diffuser guide vanes (vDGV), depending on process characteristics and specifications. For liquefaction trains that mainly operate at 80% capacity and higher (typically the case for water-cooled condensers), vIGVs offer the most efficient solution. They help regulate spikes and troughs in inlet pressure, enabling the compressor to deliver a constant mass flow. Processes in which frequent start-ups and turndowns occur, and which require high adjustability to LNG output fluctuations, are best suited to the use of vDGVs.

To further improve process control, an SMR IGC segregates its four stages into two groupings, which allows for the independent control of each stage grouping with vIGVs and vDGVs. Inlet guide vanes in the proprietary[a] compressor design provide around 25% turndown by controlling the flow to the impellers. In addition, the vDGVs extend compressor turndown by up to 50% by controlling the discharge flow after the impeller.

By using vIGVs and vDGVs, the overall efficiency of an IGC can regularly reach the 82%–84% range. When the inherent efficiency gains resulting from integral-gearing technology are taken into account, total energy savings can reach 13%–14%. Two vIGVs are used on the Zhengtai Yida LNG plant, one at the suction of the compressor and the second after the gas returns from intercooling. They help improve overall machine efficiency and reduce power consumption.

Takeaway. Increased demand for SSLNG has brought attention to the ability of SMR IGC technology to provide a more sustainable refrigeration performance compared to other compressor technologies.

At 27 MW, the remote Zhengtai Yida LNG plant hosts the world's largest integrally geared SMR compressor for the SSLNG market. With a compact footprint, low seal leakage rates and maximum rotor stability, Zhengtai Yida LNG demonstrates the viability of IGCs as a solution, even in challenging scenarios. The deployment of IGCs is also accompanied by increased performance in terms of cost efficiency, operational efficiency and energy efficiency benefits. **GP**

NOTES

[a] Atlas Copco Gas and Process
[b] Engineered, installed and commissioned by EnFlex Group

TUSHAR PATEL has held various sales and marketing positions since joining the Atlas Copco Group in 2005, having built on more than 25 yr of global experience in various manufacturing industries. At present, he is responsible for global marketing and business development for custom-engineered centrifugal compressors and turboexpanders used in oil and gas, chemical/petrochemical, fertilizer, industrial gases and power generation (both conventional and renewable). Mr. Patel has authored conference papers for the Supercritical CO2 Symposium and the Petrobras Turbomachinery Symposium, in addition to various trade industry articles on oil and gas topics. He holds a BS degree in mechanical engineering and an MS degree in marketing management.

MICHAEL DREWES has worked as a professional engineer for more than a decade. In 2011, he joined Atlas Copco Gas and Process and was responsible for individual project proposals and framework agreements in the air separation market. Starting in 2013, he served customers with process gas compressor solutions for worldwide projects in the oil and gas market. In mid-2016, he was appointed Market Manager for fertilizer applications. Since early 2019, he has been responsible for the small-scale LNG segment. Mr. Drewes holds a MS degree in aerospace engineering from FH Aachen University of Applied Sciences and has authored multiple conference papers and trade articles in the area of hydrocarbon processing.

JAMES ZHAO joined EnFlex Group in 2017 as the Vice President of Business Development. He is responsible for technology licensing, engineering services, marketing and project supervision. He has more than 10 yr of experience in a variety of engineering, project management and marketing roles, with a special focus in the LNG, petrochemical and gas processing market segments. Mr. Zhao earned a BS degree in chemical engineering from the University of Texas at Austin and an MBA degree from Rice University. He has also authored various papers and trade articles related to the hydrocarbon processing industry.

Verification of SWS performance and capacity restoration

M. R. TARIQ and T. B. ABANG, Saudi Aramco, Dhahran, Saudi Arabia

A book by Lieberman[1] stresses that it is essential to make existing units work adequately and efficiently. Equipment that malfunctions or operates inefficiently limits production and does not permit optimal energy and equipment utilization. This, in turn, leads to higher environmental degradation, not to mention plant downtime and lost production costs. Lieberman concludes that good troubleshooting and adequate repair of malfunctioning units are central to efficiently utilizing available resources.[1]

Due to an increase in the produced water feedrate at a Saudi Aramco gas plant, there was a need to install a new sour water stripper (SWS) unit to accommodate additional produced water. Based on operational experience, the existing SWS was not performing as required, and a plan was made to install a new SWS to accommodate the total sour water feedrate. The validation of the actual capacity of the existing SWS was important to confirm the processing capacity of the new SWS unit under new project investment. An assessment was conducted through design review and process simulation. Additional verification was performed by conducting field capacity tests jointly with the gas plant and the lab team.

Based on the assessment findings, it was concluded that the existing SWS unit was capable of handling 5,000 bpd of sour water as per nameplate capacity, while maintaining H_2S specification in the treated water. Although the existing SWS unit is capable of processing the sour water feed at its original design capacity, some challenges, limitations, design deficiencies and key operational issues needed to be addressed to sustain performance in the unit. Based on the assessment study, it was recommended to utilize the existing SWS with proposed design changes and to install a new, smaller SWS to treat the additional water stream. This approach resulted in CAPEX savings for the company.

The authors present their experience and lessons learned with the SWS that initially failed to achieve its design goals due to multiple issues. The problems were correctly identified in a short, systematic and effective investigation that combined field measurements and testing with efficient hydraulic analysis. The unit was successfully repaired and optimized, which helped the company avoid a CAPEX investment.

Process description. Produced water is water trapped in underground formations that is brought to the surface along with oil or gas. It is the largest-volume byproduct or waste stream associated with oil and gas production. Management of produced water presents challenges and costs to operators. Sour water must be processed, typically in an SWS, before it can be used or disposed of in a variety of ways.

The typical inlet area facility at gas plants (FIG. 1) is designed to receive the raw feed gas with associated hydrocarbon condensate and water from multiple wells. The first equipment in the inlet area is a slug catcher, which separates the bulk of the water and hydrocarbon condensate from the gas phase. The separated hydrocarbon condensate is stabilized in the condensate stabilizers to achieve the required true vapor pressure (TVP) and then injected into the neat condensate line. The SWS is used to treat sour water flowing from the boot side of the slug catchers and three-phase separators.

The main function of the SWS is to strip out acid gases (H_2S and CO_2) from the sour water where the acid gases are being recovered in the acid flare through the flare gas recovery system (FGRS). Treated water is routed to an evaporation pond after being treated in a pre-flash drum and an SWS, as shown in FIG. 2. Water from the slug catcher is collected in a single header and flows to the pre-flash drum to facilitate hydrocarbon separation. Acid gas flashing (mainly H_2S) takes place at a pressure of 65 psig.

Water flows from the bottom of the pre-flash drum. During normal operation, water is pumped through a feed filter and then enters the top section of the SWS column. The column was equipped with random packing with a height of 10 ft. Feed entered at the top inlet nozzle. The column was designed

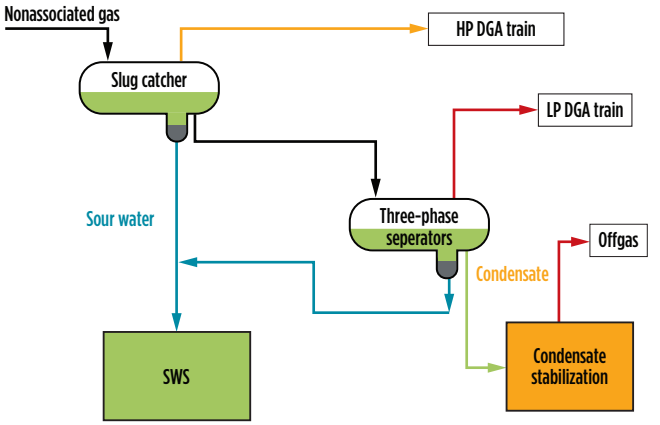

FIG. 1. Inlet area slug catchers and three-phase separators.

to operate with a pressure of 31 psig at the top and 34 psig at the bottom, corresponding to temperatures of 226°F at the top and 275°F at the bottom. These conditions were sufficient to achieve a specification of less than 10 ppmw H_2S in the bottom product.

In the stripping section of the SWS column, the sour water is contacted counter-currently with the steam to free the H_2S and CO_2. This sour water feed flows downward in the column, and steam is injected into the column to strip out the acid gases from the sour water. The steam injection rate to the SWS is controlled by monitoring the column overhead temperature. As the temperature increases, the steam flow decreases. Acid gases from the stripper column are combined with acid gases leaving from the sour water pre-flash drum to the acid flare header and recovered in the FGRS. Water, leaving the column from the bottom side, flows to the evaporation pond with H_2S < 10 ppmw, as per company standard.[2]

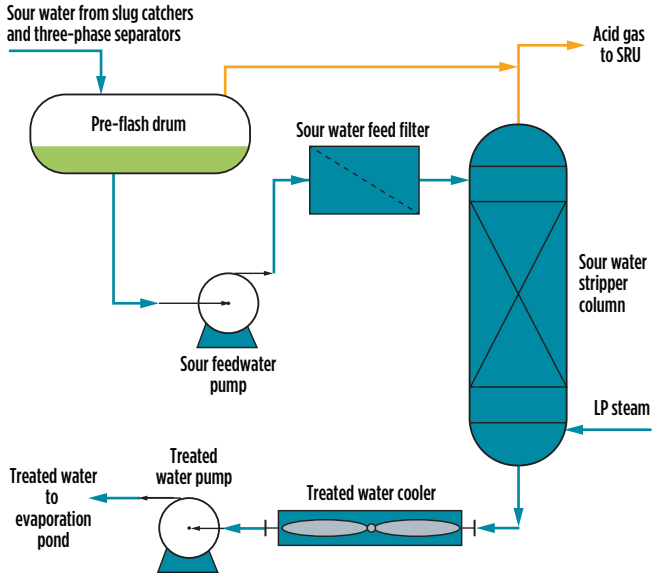

FIG. 2. Simplified PFD for the SWS.

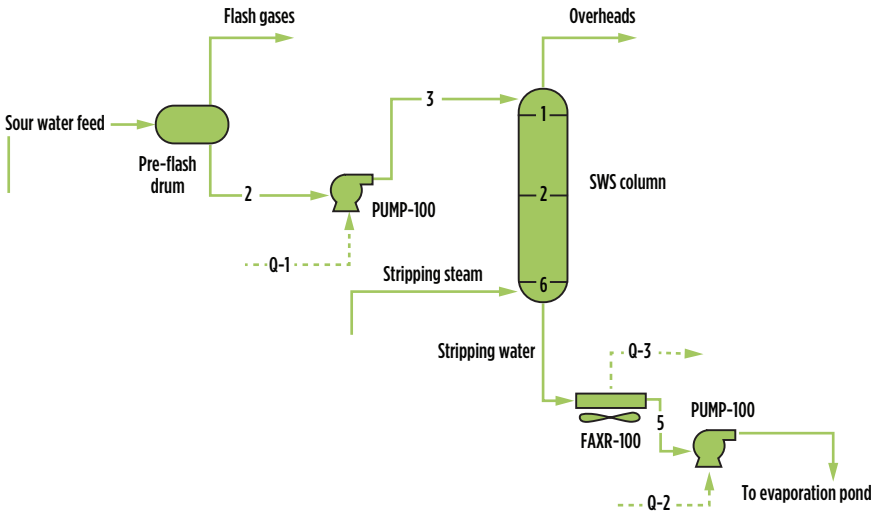

FIG. 3. Simulation model for the SWS.

Initial unit operation. A standalone SWS unit was installed at a gas plant to treat the produced water at the facility, but it was not performing as required. As per actual unit operation, the column feed flowrate was running at very low rates compared to the design rate of 5,000 bpd. At approximately 40%–50% of the design feedrate, the treated water started to go off specification, and the column pressure started to fluctuate. The top temperature fell dramatically, and the column pressures fell from their setpoints of 31 psig/34 psig. The only way of bringing the tower back under control was to reduce the column feedrate. The column was gradually brought back up to design temperature and pressure.

Several attempts were made (with small variations) to increase the feed to the design flowrate. Each attempt resulted in the same scenario, as previously described. The operating behavior and distributed control system (DCS) data were closely reviewed to establish the root cause of the problem. At feed flowrates below 1,000 bpd, the column ran without issue, with all parameters in the correct operating range. As the column feedrate increased above 1,000 bpd, an upset occurred in column pressure drop across the packing. Initially, the operators observed a rapid increase in pressure drop followed by an equally rapid fall. These peaks became more dramatic as the column feed increased, until the product went off specification.

The sudden changes in column pressure drop are a primary symptom of flood. Pressure fluctuations and a drop in the overhead temperature are also symptoms of flood. Fluctuations in the column sump level, which followed the pressure drop fluctuations, were also noticed and provided an additional symptom of flood. It was concluded that above a certain feed flowrate, the column became flooded. At this stage, the cause of the operational upset was unknown since the column was designed to operate under a much higher feed flowrate.

Study objective. The objective of the study was to assess and restore the performance of the existing SWS at the gas plant to process the sour water according to its design capacity. This study highlights the main findings and recommendations to resolve the major challenges of the SWS unit operation.

Sour water stripping is a process in which either external steam or steam generated by a reboiler—or even a hot hydrocarbon stripping vapor—is used to shift chemical reaction equilibria by heating the sour water.[3] The steam is the "gaseous solvent" used to remove and carry H_2S out of the system. In other words, the application of heat generates internal stripping steam (equivalently, live steam injection can be used) and carries ammonia, H_2S and CO_2 out of the water by:

- Heating the sour water feed to boiling point
- Reversing chemical reactions
- Diluting the partial pressure of the gases stripped by furnishing excess steam.

The process is similar to an amine regenerator; however, SWS does not

form a fully closed loop like an amine regenerator does, so maintaining a water balance is unnecessary. This means that direct steam injection can be used as a stripping agent, either alone or in conjunction with a conventional reboiler, and the surplus water added by the condensate is simply added to the plant's water inventory. Typical energy usage in the stripping process is in the range of 1 lb–1.5 lb of 50-psig-equivalent saturated steam per gallon of sour water.

Study findings and results. This assessment was completed by systematic investigation combining simulation with hydraulic analysis and actual field testing. Multiple simulation cases were performed, using a mass transfer model in a proprietary simulator to assess the maximum sour water processing capacity of the SWS system.

As per general guidelines, SWS calculations have been performed, using ideal stages in the Equilibrium Model.[4] Ideal stage calculations provide a fast and accurate means to quantify the trade-off between the number of trays and the stripping steam. In this case, the real number of trays and lengths of packed bed were used since this is an existing column; this gives the Mass Transfer Model.

In the Mass Transfer Model, the actual rates of mass and heat transfer between the phases in the column are used. The mass and heat transfer coefficients and interfacial area are based on vapor and liquid diffusivities, viscosities, densities, heat capacities and thermal conductivities. To estimate mass transfer coefficients, detailed information about the column internals is required. This information includes column diameter, surface area per unit volume and void fraction for packing. **FIG. 3** shows the model for the SWS.

A Peng–Robinson equation of state was used, as only H_2S is present in the sour feedwater. For systems that contain only a weak acid or a weak base, such as the binary systems H_2S–H_2O or NH_3–H_2O, molecular models are sufficiently descriptive to model the system behavior. Examples of molecular models are the cubic equations Peng–Robinson and Soave–Redlich–Kwong, as well as any activity coefficient models that account for only molecular species. This acid-only case is a special case, and care must be taken when modeling a sour water system. The equations are not capable of describing the behavior when both an acid and a base are present. An electrolytic model is needed to account for the ionic interactions of the dissociated species in acid-base systems, and can be used for an acid-only system, as well.

FIG. 4[4] shows the relation between the steam injection rate and H_2S in treated water. It illustrates the effect of varying the steam rate on the stripped water composition. The amount of steam used has a major effect on the composition of the stripped water. The H_2S concentration decreases rapidly as the steam rate increases. NH_3 concentration also initially decreases rapidly until it is influenced by the acid-base chemistry of NH_3 and HCN. The HCN concentration is initially insensitive to steam rate and remains constant. Once the NH_3 concentration decreases sufficiently, both NH_3 and HCN can be stripped. However, if phenol ionizes in the water, then significant removal by stripping is difficult.

The solutes to be removed are weak electrolytes that are partially dissociated into ions in solution. Therefore, the phase equilibrium of each weak electrolyte in solution plays an important role in the removal of pollutants from sour water through steam stripping. The main feed components in this system are H_2O and H_2S. Henry's law is applied to these components in the simulation because they are light gases. The reactions that occur when H_2S and CO_2 dissolve in solution are the same as in any other aqueous solution. The reactions shown in Eqs. 1–6 are of interest for this study:[3]

$$H_2O \leftrightarrow H^+ + OH^- \quad (1)$$

$$H_2S \leftrightarrow H^+ + HS^- \quad (2)$$

$$HS^- \leftrightarrow H^+ + S^= \quad (3)$$

$$CO_2 + H_2O \leftrightarrow H^+ + HCO_3^- \quad (4)$$

$$HCO_3^- \leftrightarrow H^+ + CO_3^= \quad (5)$$

$$NH_3 + CO_2 \leftrightarrow NH_2COO^- + H^+ \quad (6)$$

Effect of stripper pressure. It is sometimes said that higher stripper pressures favor sour water stripping. The experimental data presented in Reference 3 and the gas plant actual field tests show that higher pressures do not seem to favor ammonia stripping, and they certainly have a negative effect on stripped water quality in terms of H_2S.

TABLE 1 shows the effect of column head pressure on residual ammonia and H_2S levels in stripped water.[3] The simulated performance corresponds to a steam rate of 25,000 lb/hr of 50-psig steam (1.4 lb/gal), with the cross-exchanger

TABLE 1. Effect of stripper pressure on residual NH_3 and H_2S levels in stripped water[3]

Stripper head pressure, psig	Treated water	
	NH_3, ppmw	H_2S, ppmw
10	17.2	0.00002
15	21.1	0.00013
20	26	0.00058
25	31.5	0.00197

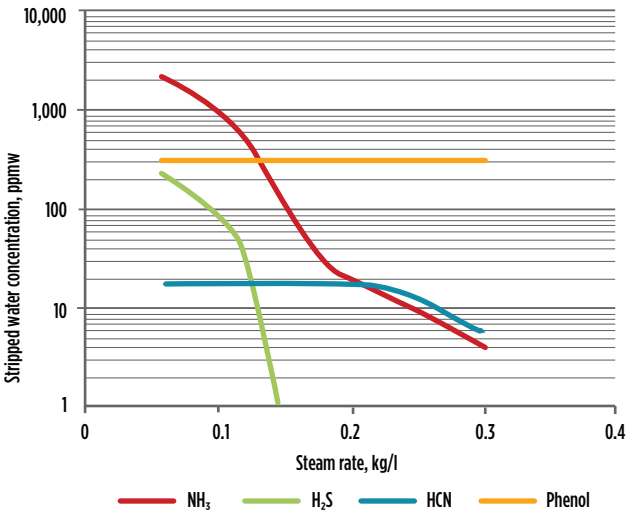

FIG. 4. Steam injection rate and H_2S in treated water.

Based on the actual performance test and a desktop study of the existing SWS train, it was recommended that a new, smaller SWS train should be provided with all tie-in points to the existing SWS. This would allow operational flexibility during normal operations, as well as during maintenance, turnaround and inspection.

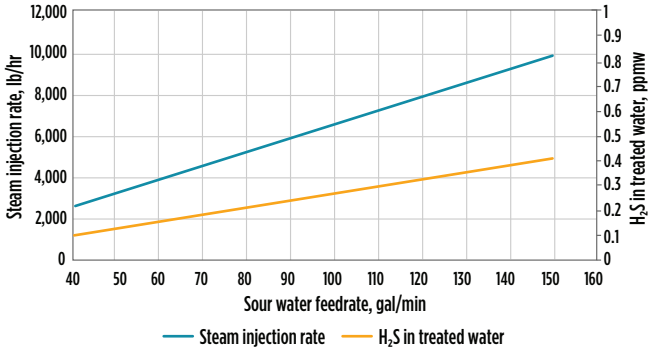

FIG. 5. H_2S in treated water vs. steam injection rate for Case 1.

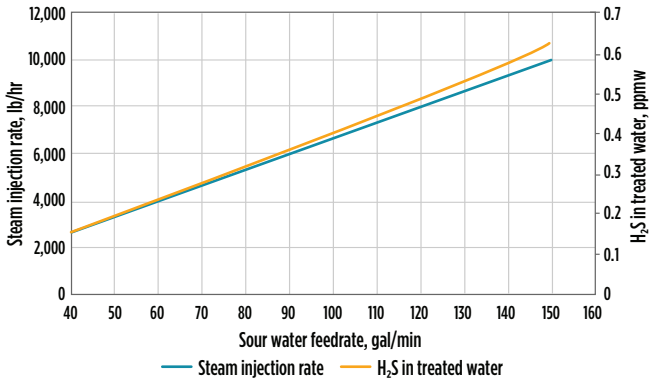

FIG. 6. H_2S in treated water vs. steam injection rate for Case 2.

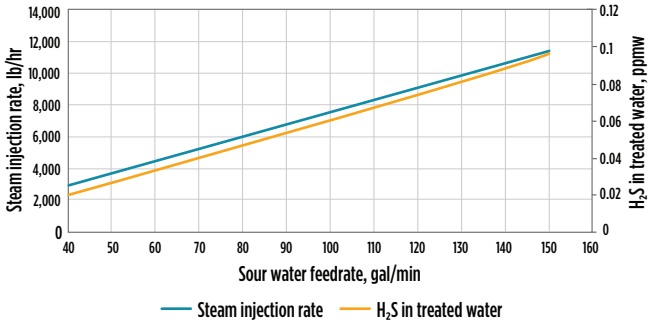

FIG. 7. H_2S in treated water vs. steam injection rate for Case 3.

set to a temperature approach of 20°F to minimize the effect of temperature differences across the stripping section. **TABLE 1** shows that a higher pressure has a negative effect on water quality with respect to ammonia, and can cause a significant increase in residual H_2S content of the stripped water under these conditions.

Simulation cases. **Case 1** examined SWS column efficiency at 100% and the steam rate as per the unit process flow diagram (PFD). **FIG. 2** showed the simplest configuration of the existing SWS at the gas plant. The unit is equipped with a stripper column containing 2-in. flexi rings (metal packing) with a 10-ft-high packing bed using six trays. Sour water was fed to the column from the top, and live steam saturated at 60 psig entered below the bottom of the packing. The column was sized for 85% of jet and downcomer flood in all cases.

Case 1 was performed under the assumption that the system efficiency was at 100% (used all column trays to match the efficiency) and that all system components (including the vessel, pumps, filters, exchanger and column internals) were working as per the original design with maximum efficiency.

Based on the simulation results, **FIG. 5** shows the trend lines for H_2S content in treated water, as well as the steam injection rate to the SWS, while maintaining the column temperature and pressure conditions as per the process flow diagram data. The simulation results for Case 1 show that the existing SWS unit is able to meet H_2S in the treated water specification at a maximum efficiency of column internals.

Case 2 examined SWS column efficiency at 85% and a steam rate as per the unit PFD. Case 2 was performed with the assumption that the SWS column internal efficiency was at 85% (with a smaller number of trays to match the 85% column efficiency) due to solids buildup and fouling issues in the system, while other unit operating conditions remained as per the unit PFD. Under these conditions, multiple simulation runs were carried out to check the unit performance, which shows that the system is still able to meet the treated water specification (**FIG. 6**). This indicates that the system was originally designed with sufficient margin.

Case 3 examined SWS column efficiency at 85% and a steam rate at 15% higher than that specified on the unit PFD. Another sensitivity simulation was conducted at a column efficiency of 85% and a steam/water ratio increase of 15% over the design ratio, while the operating pressure increased to 40 psig from 31 psig. This simulation run was conducted to match the column actual operating conditions and cover any uncertainties in the simulation model. With these conditions, the column top operating temperature was increased to 275°F compared to 229°F (the PFD value), which matched the actual field test. **Note:** This high operating temperature is still below the maximum design temperature of 400°F. Under these conditions, the system is still able to meet the treated water specification (**FIG. 7**).

Actual field test. The actual performance tests of the SWS unit were conducted multiple times to confirm the simulation findings.

Field Test 1 showed off-specification treated water due to a significantly lower steam supply to the unit of less than 12 lb/hr

steam (0.2 lb steam/gal of water) compared to the design supply of 63 lb/hr steam (1.05 lb steam/gal water). **Note:** During this test, a number of main equipment pieces were not available, including filters, the sour water feed pump and the treated water pump. Furthermore, the system was operated manually. TABLE 2 shows the results extracted from the lab report for Field Test 1. The recommendation was to repeat the test at a higher steam supply, which was implemented for Field Test 2.

Field Test 2 was conducted at a higher steam rate of approximately 48 lb/hr steam per 1 gal/min feedwater, which is 0.75 lb steam/gal water. The results showed that the H_2S in treated water was on specification. However, the system was not stable due to both the feed and treated water pumps not being in service. TABLE 3 shows the results extracted from the lab report for Field Test 2.

For **Field Test 3,** the test was repeated with a similar high steam rate (average of 45 lb/hr steam per 1 gal/min water, which is 0.75 lb steam/gal water) as in Field Test 2, while both the feed and treated water pumps were in service. The test was very successful, with all test points up to 150 gal/min (about 5,000 bpd) showing that the H_2S in treated water was within the limit and that the system was stable and under auto control. TABLE 4 shows the results extracted from the lab report for Field Test 3.

During Field Test 3, it was observed that the actual steam injection rate was lower than the recommended unit PFD value, as shown in FIG. 8. In addition, the column top temperature was higher than the unit PFD, even though the steam injection rate was lower. The simulation results shown in FIG. 7 supported the actual test results. The calculated steam injection was slightly higher than the actual steam injection, which can be attributed to the column internals or the correlation used in the simulation.

Health checks for process equipment. Based on unit simulation runs and actual field tests, the following observations were recorded for each piece of SWS equipment:

- **Pre-flash drum:** The vessel was working normally, with operating pressure as per PFD conditions. The frequency of sand jetting occured only once a week, which was not sufficient to effectively remove the sludge accumulation in the pre-flash drum and downstream equipment.
- **Sour water filter pump:** The pump was still being operated with a temporary suction strainer. In addition, only a single pump was available onsite without any standby, which limited the unit operation in case of failure on the pump.
- **Sour water mechanical filter:** Only one filter was provided with the bypass line for the sour water stripper column, which was not adequate due to high solids content in the sour water. Frequent cleaning and filter change-out are required for this filter. Furthermore, during the isolation of this filter, solids accumulated in the stripper column, which created fouling in the stripper column and reduced its performance.
- **Sour water stripper column:** Pressure control was not working properly for the stripper column while it was running on manual control. Also, the reflux pump experienced some issues due to solids in the water, which made the column operation unstable and caused difficulty in controlling the pressure and level in the column.
- **Treated water pumps:** The pumps were not running due to a mechanical issue, which was fixed for Field Test 3. Also, a temporary suction strainer was installed that caused a blockage with solids, creating cavitation.
- **Process control system:** During Field Test 1 and Field Test 2, it was observed that the system was unstable in manual mode. This instability was mainly due to the fact that the feed and treated water pumps were not in service to maintain column pressure to drain the treated water to the evaporation pond. During Field Test 3, the SWS unit ran stable on auto mode, when all feed and treated water pumps were in operation.

Integration of existing SWS with new SWS train. Based on the actual performance test and a desktop study of the ex-

TABLE 2. Lab results for Field Test 1

Number of test	Feed flow, gal/min	Sample results H_2S, ppmw
1	45	70
2	65	168
3	85	51

TABLE 3. Lab results for Field Test 2

Number of test	Feed flow, gal/min	Sample results H_2S, ppmw
1	100	< 0.4
2	120	1.7
3	150	4.1

TABLE 4. Lab results for Field Test 3

Number of test	Feed flow, gal/min	Sample results H_2S, ppmw
1	45	< 0.4
2	65	< 0.4
3	85	< 0.4
4	100	< 0.4
5	120	< 0.4
6	150	< 0.4

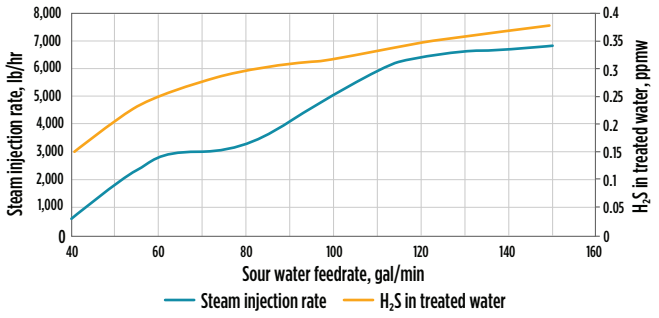

FIG. 8. H_2S in treated water vs. steam injection rate for Field Test 3.

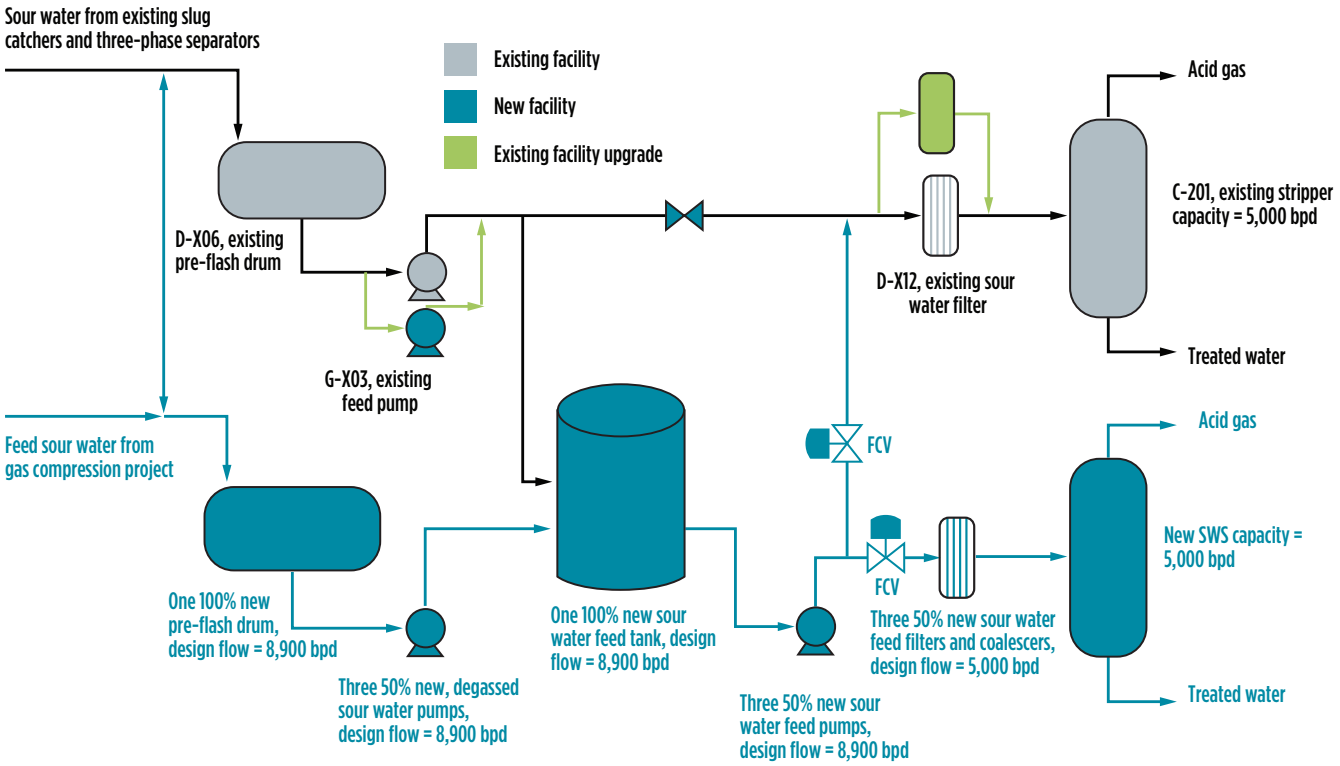

FIG. 9. Simple sketch for integration of existing SWS with new SWS train.

isting SWS train, it was recommended that a new, smaller SWS train should be provided with all tie-in points to the existing SWS. This would allow operational flexibility during normal operations, as well as during maintenance, turnaround and inspection. **FIG. 9** provides the equipment design capacity for a new SWS train and its integration with the existing SWS. The scope of work for integration under the new project is shown in dark blue color.

Lessons learned. Based on the assessment findings from the process simulations and the actual field performance tests, it was concluded that the existing SWS unit is capable of processing 5,000 bpd of sour water as per nameplate capacity, while maintaining specification for H_2S in the effluent water.

Although the existing SWS unit is capable of processing the sour gas feed at its original design capacity, the following design deficiencies and key operational issues for this unit needed to be addressed to sustain the performance:

- High solids loading in the sour water feed contaminated the system, which impacted the overall performance of the unit
- Manual operation mode was identified as one of the main challenges to maintaining stable operation of the SWS, especially at maximum design rates.

This study also produced several takeaway messages related to sour water stripping:

- Proper cleaning is required to remove the solids in process equipment that impact SWS operations
- The SWS should be operated in auto mode, with both the sour feedwater and treated water pumps in operation
- The SWS column operating temperature should be controlled as per the design data, by maintaining the ratio of steam flowrate to sour water flowrate close to the design value. **GP**

LITERATURE CITED

[1] Lieberman, N. P., *Process Engineering for a Small Planet,* Wiley, Hoboken, New Jersey, 2010.
[2] Saudi Aramco engineering standard for sour water stripper design, SAES-A-16, GPSA, Sour water stripper design.
[3] Weiland R. H. and N. A. Hatcher, "Sour water strippers exposed," Laurence Reid Gas Conditioning Conference, Norman, Oklahoma, February 28, 2012.
[4] Addington, L., C. Fitz, K. Lunsford, L. Lyddon and M. Siwek, "Sour water: Where it comes from and how to handle it," *Digital Refining,* September 2011.
[5] Ponting, J., H. Z. Kister and R. B. Nielsen, "Troubleshooting and solving a sour water stripper problem: A systematic approach identifies problems that prevented a stripper column from achieving trouble-free operation," *Chemical Engineering,* Vol. 120, Iss. 11, November 2013.

MUHAMMAD RIZWAN TARIQ is a Senior Process Engineer at the process and control systems department of Saudi Aramco in Dhahran, Saudi Arabia. He has also served as Staff/Senior Engineer at JGC Japan, Worley Oman, PDO Oman and OGDCL Pakistan. He holds a BS degree in chemical engineering from Punjab University in Lahore, Pakistan. He is also a Chartered Member of IChemE UK and a Professional Engineer with PEC Pakistan.

TAIB ABANG is an Engineering Specialist at the process and control systems department of Saudi Aramco in Dhahran, Saudi Arabia. He has also served as a Senior Engineer at Petronas LNG in Malaysia. He holds a BS degree in chemical engineering from University Malaya in Kuala Lumpur, Malaysia. He is a Chartered Engineer from the Engineering Council and a Chartered Member of IChemE UK.

Are cylinder liners necessary for high-speed reciprocating gas compressors?

S. ZARDYNEZHAD, TurboTech Consulting Corp., Calgary, Alberta, Canada

Wear is common in reciprocating gas compressors (RGCs) due to sliding and rotational motion of parts. In the design of RGCs, wear study and calculation by empirical formulas are conducted to estimate and forecast the life of the parts. However, wear during real working conditions is different from theoretical estimations and, sometimes, catastrophic failure is experienced during operation due to considerable mechanical or chemical wear.

Wear in the cylinder wall due to reciprocating motion of the piston is a good example of such circumstance and the main subject of this article. Low- and moderate-speed RGCs are normally furnished with a cylinder liner; however, high-speed RGCs may or may not be furnished with a cylinder liner. In this article, the main differences between low-, medium- and high-speed RGCs are discussed; the wear mechanism in the cylinder is explained; the importance of cylinder liners to RGCs is addressed; and the author's recommendations for decision-making when considering liners are explained.

Standards for RGC operation. The American Petroleum Institute (API) produced API Standard 618 (1964)[1] and API Standard 11P (1976).[2] These standards are frequently used for the design and manufacture of RGCs. API 618 (Edition 1) was published in 1964 based on the operating experience of 1950s compressor models. During that time, manufacturing and materials technology were not advanced and the speed was limited to 100 rpm, which is why the 1st edition of API 618 covers only low-speed compressors.

Manufacturers encouraged coupling RGCs to gas and diesel engines with speeds of 800 rpm and higher, which increased their size and cost. This led to the publication of API 11P in February 1976, approximately 12 yr after the publication of the first revision of API 618. Moderate-speed units were derived from high-speed units and added to API 618 in 1995.

TABLE 1. Comparison of rotational speed range of RGCs

Speed, rpm	Low	Medium	High
API	Not specified	Not specified	Not specified
Author's experience	100–350	350–799	800–1,800
Some manufactures	100–600	600–1,200	1,200–1,800

RGCs are classified into three types in terms of rotational speed, as shown in TABLE 1. High-speed, packaged RGCs for oil and gas service are covered under API 11P, which has been withdrawn by API and replaced by ISO 13631 (2002), "Petroleum and natural gas industries—Packaged reciprocating compressors."[3] The driver can be either an engine or an electric motor. Sometimes they are coupled via a gearbox. Their operating speed is typically 800 rpm–1,800 rpm, based on the author's experience, with engine drivers above 1,000 rpm and motor drivers of 800 rpm–1,000 rpm.

High-speed RGCs are skid-mounted and packaged. They are easy to install, easily transportable to different sites due to their modularized and compact design, and have a relatively small CAPEX. High-speed RGCs have higher maintenance costs than low- and medium-speed compressors. Low- and medium-speed compressors run at speeds of 100 rpm–799 rpm. These compressors have lower speed, higher stroke and higher efficiency over a wide range of operating conditions and require less maintenance than the high-speed units because of their lower speed. However, low- and medium-speed compressors usually must be field-erected and require heavy foundations. They have high degrees of vibration and pulsation suppression compared to low- and medium-speed compressors. Large low-speed compressors are shipped to the site as loose items (e.g., throws, frame, driver, etc.).[4]

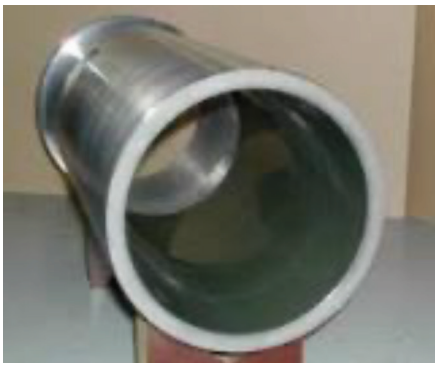

FIG. 1. API 618 compressor cylinders are frequently supplied with centrifugally cast, removable liners to reduce reconditioning costs.

API 618 compressor cylinders are frequently supplied with liners (FIG. 1) to reduce reconditioning costs. RGC cylinder liners are removable in case of accidental scoring or wear over a long period of service. In general, liners are not used in high-speed machines (API 11P/ISO 13631) where the rotating speed is higher than 800 rpm. Liners are almost always used in API 618 compressors, especially in critical services where the gas being handled is corrosive, toxic, low-temperature or high-pressure, and in special designs like free-floating piston.

However, API 618 does not define the meaning of "critical services." Liners have become a standard design for many

TABLE 2. Comparison of API 618 with API 11P/ISO 13631

Subject	API 618 (2007)	ISO 13631 (2002)/API 11P (1989)	Remarks
Application		Packaged high speed, separable	Low to moderate speed, integral
Driver speed, rpm	Low/moderate 200 rpm–799 rpm	High 800 rpm–1,200 rpm	Speed ranges are author's experience and are not addressed in API
Piston speed, lubricated, m/sec	2.8–4.5	4.6–6.1	Speed ranges are author's experience and are not addressed in API
Piston speed, non-lubricated, m/sec	2.3–3.8	Not available	Speed ranges are author's experience and are not addressed in API
Stroke	Long 229 mm (9 in.)–508 mm (20 in.)	Short 76 mm (3 in.)–203 mm (8 in.)	Stroke ranges are author's experience and are not addressed in API
Expected valve life, Theoretical	3 yr	2 yr	Author's experience, similar valve at similar services
Driver, gas engine	No	Yes	
Oil-free cylinder	Yes, and lubricated	No, only lubricated	
Critical service	Yes	No	Critical service is not defined in API 618
Service life	Minimum 20 yr		
Uninterrupted operation	Minimum 3 yr	No, gas engines need routine maintenance (sometimes at least once per year)	
Cylinder liner	Yes	Generally no	
Cylinder jacket	Yes	No	
Startup unloading	Automatic valve unloader	Bypass	
Capacity control	Automatic valve unloader	Speed and bypass	
Distance piece	Type A used for non-flammable service	Type 1 are used in many sweet gas applications	
Size	Medium to large	Small to medium	In similar applications
Cost	Higher than API 11P	Lower than API 618	In similar applications

TABLE 3. Main wear mechanisms in RGC cylinders

Wear category	Mechanism
Mechanical	Abrasive/sliding
	Particle impingement/erosion
	Adhesion/scuffing
Chemical	Corrosion

refining, gas and petrochemical industry applications, even though the gas involved may not be corrosive, toxic, low-temperature or high-pressure. Some end users insist on liners in their compressors based on maintenance lessons learned. Liners are a key subject during the RGC engineering and procurement stages, and they may increase the CAPEX of RGCs; however, liners have a significant positive impact on OPEX, especially for large or multistage cylinders and where service is critical or special, without any standby. Another benefit of a liner is to reduce the cylinder bore size to meet certain operating capacity conditions. By installing liners with different bore sizes, the same cylinder can be used to accommodate a range of capacity and pressure conditions. This is useful when renting a compressor, as opposed to buying one.[5]

API 618, API 11P and ISO 1363 do not define low-, medium- and high-speed compressors in terms of the piston and rotating speed. Normally, they are defined in the client's specifications. The main differences between API 618 (5th edition) and API 11P (ISO 1363) are summarized in TABLE 2.

Definition of wear.

Wear may be defined as material or mass removal from the surface of any part due to contact with another surface. Wear can also result due to mechanical or chemical behavior of the material. Cylinders experience wear at the point of contact with the piston rings. In horizontal arrangements, cylinder wear is greatest at the bottom because of piston weight. In compressor cylinders, different types of wear can occur, as outlined in TABLE 3.

Sliding wear. Surface-to-surface interactions happen whenever one surface slides relative to another over a distance. Friction between two parts is the main cause of this kind of wear. In RGCs, sliding wear generally happens between parts such as cylinders with piston rings. Also, hard particles may form inside cylinders, which may cause abrasive wear in the cylinder. Cylinders in RGCs are at risk of abrasive or sliding wear due to reciprocating motion and the risk of contacting the piston with the cylinder wall due to wear band ring failure (FIG. 2).

Particle impingement/erosion. This type of wear may be due to different causes:

- Solid particles enter the cylinders with gas and impinge on the cylinder from an external source (FIG. 3)
- Solid particles from broken parts, such as a broken valve due to fatigue (i.e., high vibration over a period of time), which is common.

API 618 requires valves and cylinders to be designed so that neither the valve guard nor the assembly bolting can fall into the cylinder, even if the valve assembly bolting breaks or unfastens (Clause

6.9.1.5). However, a channel design from the valve port may be needed for the inside of the cylinder, or a special valve bracing bracket may be used.

Based on the author's experience, many manufacturers deviate from this requirement due to the cost impact on casting or fabrication of the cylinders. If a broken valve is removed from the cylinder, it may drop inside the cylinder and damage the piston and cylinder wall. The author experienced a valve failure due to fatigue, which caused the broken parts of the valve to damage the piston, cylinder head and cylinder wall/liner (FIG. 3B). Note that the cost and time of replacing the cylinder head, piston and other parts are much less than the cost and time required to replace the cylinder.

Adhesion or scuffing. Adhesion or scuffing is defined as local welding between piston rings and the cylinder wall or liner. This is generally caused where lubrication is insufficient and compression temperature is high. Due to high friction and a lack of lubrication, significant heat is generated and microscopic local welding of rings and cylinders occurs. In a high-speed compressor, all cylinders must be lubricated; also, there is no jacket water in high-speed RGCs.

To remove heat from the cylinder, piston and rings due to friction (not gas compression), the vendor must inject a considerable amount of oil into the cylinders. The oil consumption of high-speed compressors may reach to 900 l/mos or higher, depending on the number of throws, the size of the cylinder, the piston speed, etc. Any lack of cylinder lubrication in high-speed compressors can cause catastrophic cylinder and piston ring wear and damage (FIG. 4).

Corrosion. A complex phenomenon, corrosion sometimes occurs in compressor cylinders due to poor material selection or preservation during shipment, construction or long storage (FIG. 5). It is less likely to happen due to improvements in material science and manufacturing technology.

Wear due to chemical behavior is not considered, assuming that material selection is carried out carefully.

Wear calculation. The wear rate is different in dry and lubricated sliding surfaces; however, general wear depends on many factors such as temperature, pressure, sliding speed, relative hardness, material microstructure, surface finish, sliding distance, etc.

FIG. 2. Cylinder sliding wear (a), piston sliding wear (b) and cylinder wear (c).

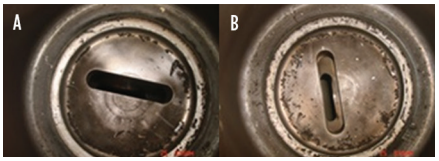

FIG. 3. Solid particles may enter the valve port and cylinders during first startup.

As a good estimation of wear on a macro scale, the Archard equation (Eq. 1) may be used:

$$W = K \times P \times V \times t \quad (1)$$

where:

W = Worn volume or wear depth
K = Coefficient of wear
P = Applied load
V = Sliding velocity of piston
t = Running time.

According to Eq. 1, the wear rate of the cylinder, piston rings, wall/liner, etc. are functions of piston speed. Therefore, it is important to clarify the maximum allowable piston speed for lubricated and non-lubricated machines at the early phase of the project. The instantaneous piston speed varies from zero at the end of the stroke [i.e., top dead center (TDC) and bottom dead center (BDC)] to a maximum near the middle of the stroke, where the crankshaft is parallel to ground level. It can be concluded that piston speed changes as a sine wave. The maximum and average piston speeds are calculated as shown in Eqs. 2 and 3:

$$V_{max} = 2\Pi rN \quad (2)$$

where:

V_{max} = Maximum piston velocity
r = Crank arm length
N = Rotational speed
Π = Pi.

$$V_m = 2S\,[N \div (60 \times 1{,}000)] \quad (3)$$

where:

FIG. 4. Wear band adhesion.

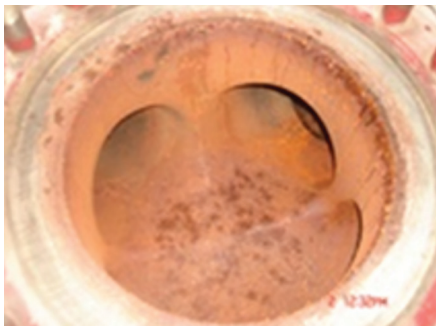

FIG. 5. Cylinder rusting due to poor preservation.

V_m = Average velocity, m/sec
S = Stroke, mm
N = Rotational speed, rpm
60 = Conversion for changing minute to second
1,000 = Conversion for changing mm to m
2 = In each rpm, the piston travel two times its stroke.

Considering Eqs. 1 and 3, a low-rotational-speed compressor (i.e., API 618,

long stroke) with average speed and pressure loading at the wear band is equal to a high-rotational-speed compressor (API 11P, short stroke) and may be expected to have similar sliding wear rates. However, the former does not normally have a cylinder liner, and the risk of other types of wear are still high.

Valves are not the subject of this paper; however, it is worth mentioning that increasing the rotational speed has a significant impact on the valve service life as one of the most critical compressor parts. Each suction or discharge valve in a compression cycle opens and closes one time. The number of openings and closings of a valve in a single stage of a single compressor with two different speeds is shown in **TABLE 4.**

In an RGC with a constant capacity, if the stroke is decreased and the rotational speed is increased, then reciprocating forces acting on the piston, cross-head, connecting rod, piston pin, etc., will increase and a higher load will be imposed on the crank shaft. In parallel, higher rotational speed causes increased acceleration of gas coming to or exiting from the cylinder via valves, which leads to greater wear of the valve components.

Under constant rotational speed, a compressor with higher stroke causes more wear on cylinder and piston rings. As an example, suppose a packaged, separable RGC (API 11P) with a double-acting, gas engine drive with speed of 1,000 rpm experiences a 1-in. increase in stroke, which causes: 1 in. × 2 × 1,000 rpm × 24 hr × 60 min × 365 d × (1/12) ft = 87,600,000 ft/yr = 26,700,480 m/yr = 26,700.5 km/yr additional movement of the reciprocating parts and the equivalent amount of additional wear. This is about three times the east-to-west distance of Russia—i.e., 10,000 km!

Increasing the cylinder diameter does not impact the velocity or acceleration of the piston. However, the volume of gas displaced by the piston increases significantly. The larger cylinder requires a larger piston, which causes higher piston weight and higher pressure in the wear band ring and cylinder. The cylinder diameter, stroke and piston velocity must be decided carefully to mitigate the risk of wear and vibration and also to minimize clearance losses.

High-speed compressor without cylinder liner. Consider a single-stage, single-acting reciprocating compressor. The theoretical capacity or the displaced volume by piston is calculated as shown in Eq. 4:

$$Q_t = \Pi \times (D^2/4) \times S \times N \times n \qquad (4)$$

where:

Q_t = Compressor theoretical capacity or the displaced volume by piston, m^3/min
D = Cylinder internal diameter, m
S = Stroke, m
N = Compressor rotational speed, rpm
n = Number of cylinders
Π = Pi.

With reference to Eq. 3, if the piston speed is assumed to be constant, then the stroke and compressor rotational speed have a reverse relation. For a constant capacity, to decrease the piston stroke, it is necessary to increase the compressor rotational speed. Decreasing the compressor stroke means decreasing the dimension of the compressor, which results in less material, less space and lower cost. In general, high-speed compressors are cheaper than low-speed API 618 compressors due to their lower stroke and lower dimension.

Adding a liner to the cylinder of a high-speed compressor has a negative impact on compressor performance and volumetric efficiency because the fixed clearance in the valve area is increased (**FIG. 6**). The valve area cannot be increased to compensate for the clearance loss due to the liner because a larger cylinder is required. A larger cylinder needs a larger piston, and a larger piston means heavier load in the wearing band, cross-head, connecting rod, bearings and crank shaft. Also, a larger piston will increase the clearance loss due to greater gas leakage from the rings.

Adding a liner in the cylinder of a high-speed compressor can reduce the volumetric efficiency and flexibility of the variable volume clearance pocket. This is largely why manufacturers of high-speed compressors do not use liners for cylinders.

The volumetric efficiency of a reciprocating compressor is the ratio of the discharged gas from the compressor to the displaced volume of the first stage, as shown in Eq. 5:

$$\eta_v = 1 - \{[Z_1 \div Z_2] \times [(P_2 \div P_1)_i]^{1/\gamma} - 1\}\, C\text{-}L \qquad (5)$$

where:

η_v = Volumetric efficiency
Z_1, Z_2 = Gas compressibility factor at suction and discharge condition
$(P_2 \div P_1)_i$ = Compression ratio at ith stage, largest compression ratio
P_2, P_1 = Absolute pressure at discharge and suction, respectively
γ = Polytrophic coefficient = 1.3–1.35
C = Clearance loss (%), to be determined by vendor (e.g., 10% < C < 15%)
L = Ring clearance for lubricated cylinder, 0.05–0.06
L = Ring clearance for non-lubricated cylinder, 0.09–0.1.

It is obvious that if C = 0, then $\eta v = 1$; however, practically, $\eta_v < 1$ (e.g., 0.97). Therefore, Eq. 5 can be rewritten as Eq. 6:

$$\eta_v = 0.97 - \{[Z_1 \div Z_2]\, [(P_2 \div P_1)_i]^{1/\gamma} - 1\}\, C\text{-}L \qquad (6)$$

For ideal and real gas at low pressure, Eq. 7 can be used:

$$\eta_v = 0.97 - \{[(P_2 \div P_1)_i]^{1/\gamma} - 1\}\, C\text{-}L \qquad (7)$$

For Eqs. 4 and 5, the actual capacity of a single-stage, single-acting reciprocat-

TABLE 4. Number of openings and closings of valves at different speeds

Category	Speed, rpm	API	Working hour	Open	Close	Total
High speed	1,000	11P	24	1,440,000	1,440,000	2,880,000
Low speed	500	618	24	720,000	720,000	1,440,000

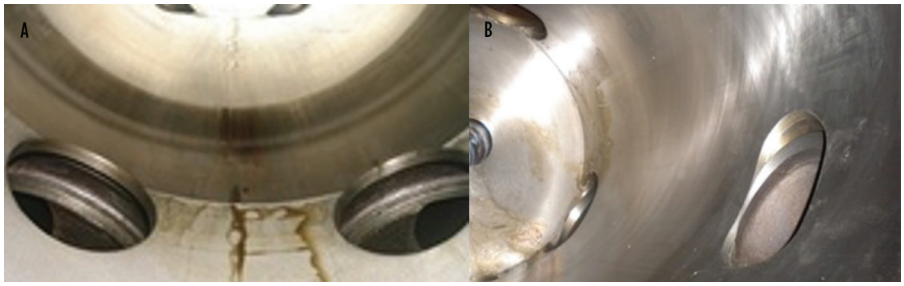

FIG. 6. Adding a cylinder liner results in a higher clearance pocket in the valve area.

ing compressor is calculated as shown in Eqs. 8 and 9:

$$Q_A = Q_t \times \eta_v \quad (8)$$

$$Q_t = V_s \times N \times n \quad (9)$$

where:

Q_t = Compressor actual capacity, m^3/min

V_s = Displaced volume by piston, $m^3 = (\Pi \div 4)(D^2 - d^2) \times S + (\Pi \div 4)(D^2) \times S = (\Pi \div 4)(2D^2 - d^2) \times S$

D = Cylinder internal diameter, m

D = Piston rod diameter, m

S = Stroke, m

N = Compressor rotational speed, rpm

n = Number of cylinders

Π = Pi.

According to Eq. 4, with constant piston speed, high-speed compressors have lower stroke and size compared to low- and medium-speed compressors. Adding a cylinder liner to a high-speed compressor increases the value of valve clearance loss and impacts volumetric efficiency and actual capacity. This is the main reason that cylinder liners are often not used on high-speed compressors.

Cost comparison. In case of damage in a cylinder bore, a liner can be replaced, or the entire cylinder can be replaced or repaired (e.g., by metal spraying). Repairing the damaged cylinder by machining, grinding or metal spraying requires time. In the author's experience, the metal sprayed on the cylinder bore will peel and flake and give less service life compared to replacing the liner. Repair may require the cylinder bore to be machined to an oversized diameter to accept a liner or larger-size piston rings.

Also, sometimes it is not possible to repair the damaged cylinder due to the cylinder thickness, jacket water location, closeness to the repair shop, etc., and it is necessary to replace the cylinder. Replacing the cylinder is more costly compared to replacing the liner, especially for large-bore cylinders and/or multi-throw configurations. Sometimes it may be difficult or very expensive to order a new cylinder after 10 yr or more because the sub-vendor that casted or forged the original cylinder may no longer be in operation, and a stock cylinder may not be available. **GP**

LITERATURE CITED

[1] American Petroleum Institute, API Standard 618, "Reciprocating compressors for petroleum, chemical, and gas industry services," 5th Ed., December 2007, Errata 2, July 2010.

[2] American Petroleum Institute, API Standard 11P, "Specification for packaged compressors for oil and gas production services," January 1989, Revised 1999.

[3] International Standards Organization, ISO Standard 13631, "Packaged reciprocating gas compressors," 1st Ed., August 2002.

[4] Bloch, H. P., *Compressors and Modern Process Applications*, John Wiley & Sons, 2006.

[5] Griffith, W. A. and E. B. Flanagan, "Online continuous monitoring of mechanical condition and performance for critical reciprocating compressors," Proceeding of the 30th Turbomachinery Symposium, Texas A&M University, Houston, Texas, 2001.

SHAHAB ZARDYNEZHAD is a registered Senior Mechanical/Pipeline Engineer in Alberta and British Columbia with more than 29 yr of experience working in the world's largest oil, gas and petrochemical projects. He has experience in engineering, procurement services, manufacturing, installation, commissioning, startup, reliability, maintenance and operation of pumps, compressors and turbines. He holds a BS degree in mechanical engineering from the University of Petroleum of Iran, an MS degree in industrial engineering from IUST Iran and MS degrees in mechanical engineering and project management from the University of Calgary in Canada. He is also a certified API inspector for rotating equipment.

Gastech 2021 moves to Dubai for in-person exhibition and conference

A. BLUME, Editor-in-Chief

Gastech 2021 highlights:

- 21–23 September 2021 at Dubai World Trade Center (live, in-person event)
- Safe and secure environment provided for attendees and delegates
- More than 4 days of networking
- Conference will host more than 300 speakers
- Exhibition will host more than 400 companies
- More than 25,000 attendees and 2,500 delegates expected to attend

www.gastechevent.com

From 21–23 September, the Gastech Exhibition & Conference will take place in Dubai, UAE as the first major energy event to be held live and in person in 2021. Gastech was originally set to take place in Singapore in mid-September; however, recent COVID-19 outbreaks across Southeast Asia have created uncertainty around accessibility and travel, prompting the decision in early June to move the conference and exhibition to Dubai.

Gastech was last held in person in Houston, Texas in September 2019 (**FIG. 1**) and was converted to an online event in 2020, due to the COVID-19 pandemic. The 2021 event, to be held at the Dubai World Trade Center, will welcome an expected 25,000-plus attendees and 2,500 delegates from more than 100 countries, as well as 400 exhibiting companies.

FIG. 1. Gastech was last held in person in Houston, Texas in September 2019. Image: Gastech/dmg events.

As the global gas and LNG industry looks toward the future, it must navigate the new energy landscape with a shared mandate to lower carbon emissions and provide affordable energy. Gastech 2021 will bring together the full energy value chain, with industry giants reconvening in a week of much-anticipated networking to share thought-provoking energy strategies, showcase unique innovations and reinforce bilateral trade relations.

In light of COVID-19 precautions, dmg events is working closely with all stakeholders and local partners to ensure that enhanced health and safety measures are in place to deliver a safe and secure environment for the event. More information on these measures is available at the event website.

Gastech Conference. The conference portion of Gastech will encompass 55 strategic and 29 technical sessions. It will host more than 300 high-level speakers including government ministers, company leaders, heads of industry organizations and other top leaders in the energy, policy, gas and LNG sectors.

The Gastech Conference will address the key issues and most promising opportunities for the gas, LNG and hydrogen sectors in the fourth industrial age. Technology innovation is occurring at an unprecedented pace and presents a significant advantage to those who embrace it. The energy industry can streamline business models and improve processes by embracing advanced digital technologies such as AI, IIoT, big data and analytics.

Conference presentations will set the tone for the future direction of the global gas and LNG industry in the post-COVID context, as the industry seeks to strike a balance between business priorities and the social license to operate. Impactful topics to be addressed include technology innovation, supply and demand dynamics, evolving partnerships, people and talent, and governance.

A number of high-level strategic conference sessions will be available this year to all attending delegates to enable conversations to take place to drive the global energy transition. Additionally, the open technical conference will address a number of topics including shipping, small-scale LNG, bunkering, hydrogen, upstream, gas processing, AI and energy end users.

New for 2021: Gastech Hydrogen. In line with the growing global energy transition, new at Gastech this year is the co-located Gastech Hydrogen event. Gastech Hydrogen is dedicated to positioning hydrogen as the clean energy solution by connecting policymakers, producers, consumers, scientists and suppliers to facilitate market development.

Key themes to be covered at the Gastech Hydrogen Conference include the harmonization of standards, key growth areas, demand creation, transmission and distribution, hydrogen use in transportation, green hydrogen, project development and building investor confidence.

For more information on the companies attending, exhibiting and speaking at the Gastech Hydrogen event, visit www.gastechevent.com/the-gastech-exhibition/gastech-hydrogen

Gastech Awards. The Gastech Awards program, to be held at an in-person VIP gala dinner at an exclusive location in Dubai, will recognize those companies and individuals who are responding in the most innovative and creative ways to address the continuous growth of global energy demand. **GP**

Wärtsilä, Vantaa Energy cooperate on a synthetic biogas project

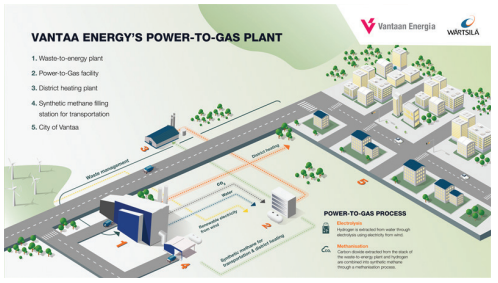

Finnish technology group Wärtsilä and Finnish energy company Vantaa Energy Ltd. have signed a cooperation agreement for pre-engineering and development of a power-to-gas (P2G) plant for Vantaa Energy. The plant, planned to be commissioned in 2025, would be the largest in Finland and also the first to produce carbon-neutral, synthetic methane on a commercial scale with a fuel capacity of 10 MW.

Synthetic methane is produced from captured CO_2 and H_2 produced with renewable energy. The companies intend to continue joint development of the project toward a commercial-scale pilot project. Synthetic biogas would replace the use of conventional natural gas in district heating, thereby reducing Vantaa Energy's CO_2 emissions. Wärtsilä will contribute its know-how in power-to-gas processes and technologies, while Vantaa Energy will bring its experience and understanding of the district heating business and project-specific requirements.

In-Field Flow Coating increases pipeline flow capacity by 20+%

Rescue Pipeline Services LLC's In-Field Flow Coating (IFC) technology for existing gas pipelines significantly increases efficiency and performance of existing (in-place) pipelines. The specially formulated, advanced "nano" composite coating utilizes small molecular structures that coat microscopic nooks and crannies in a way that is not possible with conventional coatings.

The unique nano properties, combined with expert in-situ pipeline application, result in an ultra-slick, low-friction and abrasion-resistant surface, providing lower friction loss, increased flow, lower energy consumption and reduced deposition of debris and contaminates, with minimal surface preparation. By reducing the surface roughness, the coated surface reduces the friction factor of the pipe wall, reducing pressure loss and increasing pipeline capacity.

The IFC system can make a significant difference in reducing compression costs and lowering greenhouse gas emissions. The IFC technology can be applied on long pipeline segments, of any diameter, by accessing only the ends of the pipeline.

Symbio Infrastructure plans world's first carbon-neutral LNG facility

Symbio Infrastructure and Siemens Energy have entered into an agreement whereby Siemens Energy will provide engineering services, comprehensive lifecycle equipment and technology solutions, and further carbon emissions footprint reduction solutions for Symbio subsidiary GNL Quebec's carbon-neutral Énergie Saguenay LNG project in Quebec. Siemens will also provide solutions for Symbio subsidiary Gazoduq's carbon-neutral natural gas transmission line project between Ontario and Quebec.

Énergie Saguenay's 10.5-MMtpy LNG export facility will be powered by nearby renewable hydroelectricity and is expected to set a global standard for carbon-neutral LNG production. Fed by Gazoduq's carbon-neutral natural gas transmission line, Énergie Saguenay plans to operate the lowest-carbon-intensity LNG plant in the world.

Under the agreement, Siemens Energy will provide its portfolio of greener solutions for rotating equipment, electrical and digital infrastructure. The companies will also work together to explore green H_2 development opportunities as a new potential investment initiative to be considered by Symbio. Siemens and Symbio envision the alliance aligning with the principles included in the March 2021 Energy Partnership between Germany and Canada to advance their respective net-zero aspirations.

Russia's first LNG refueling ship completes trials

The country's first ship designed to run on LNG and fuel other vessels with LNG has completed its sea trials, according to Gazprom Neft. The *Dmitry Mendeleev* is an Arc4 ice-class vessel that will be able to transport up to 5,800 m^3 of LNG. It will operate in ports on the Gulf of Finland and in the Baltic Sea, including St. Petersburg, Ust-Luga and Primorsk. The vessel is expected to enter Gazprom Neft's fleet in the second half of 2021.

Nacero develops energy transition infrastructure

Nacero has awarded Bechtel a FEED contract for the first large-scale natural gas-to-gasoline manufacturing facility in the U.S. Nacero's 115,000-bpd plant in Penwell, Texas will be the first gasoline manufacturing plant in the world to incorporate carbon capture and sequestration (CCS) and 100% renewable power.

The use of renewable natural gas and mitigated flare gas will make it possible to reduce the lifecycle footprint of Nacero's cost-competitive, zero-sulfur gasoline to zero over time. Nacero's products will be sold to retailers in Texas and the Southwest region, and through Nacero-branded outlets.

Wärtsilä to supply largest bio-LNG plant

Wärtsilä will supply a biogas liquefaction plant to Norway-based Biokraft, a subsidiary of Scandinavian Biogas Group and a major player in the global biogas market. The 25-tpd plant will extend an existing bio-LNG production plant at Skogn in Norway, also supplied by Wärtsilä, to a combined total of 50 tpd, making it the largest facility of its kind in the world.

The market for liquefied biogas continues to expand along with the increase in global efforts to restrict the use of fossil fuels. Bio-LNG is an abundant renewable energy source that is used as "green" fuel in transportation, industrial and marine applications. The Wärtsilä mixed refrigerant technology and equipment are scheduled for delivery in May 2022.

Venture Global launches CCS projects

Venture Global LNG plans to capture and sequester carbon at its Calcasieu Pass and Plaquemines LNG facilities in Louisiana. Having concluded a comprehensive engineering and geotechnical analysis, the company intends to launch a shovel-ready carbon capture and sequestration (CCS) project, compressing CO_2 at its sites and then transporting the CO_2 and injecting it deep into subsurface saline aquifers, where it will be permanently stored.

Through this undertaking, Venture Global will capture and sequester an estimated 500,000 tpy of CO_2 from its Calcasieu Pass and Plaquemines liquefaction sites. In addition, the company anticipates using similar infrastructure to capture and sequester 500,000 tpy of CO_2 from the CP2 LNG facility, once permitted. Altogether, Venture Global plans to sequester 1 MMtpy of CO_2, the equivalent of removing nearly 200,000 cars from the road each year for 20 yr. The successful deployment of CCS technology at Calcasieu Pass would be the first of its kind for an existing LNG facility in the U.S.

Uzbekistan to launch first GTL plant by late 2021

Operator Uzbekneftegaz will launch its first GTL plant in Q4 2021, helping Uzbekistan reduce its reliance on diesel and jet fuel imports. The $3.6-B plant will enable the country to use its large natural gas reserves to make diesel and other fuels. The plant will refine 3.6 Bm^3y of gas and produce about 1.5 metric MMt of fuel.

Uzbekneftegaz GTL aims to produce approximately 307,000 tpy of jet fuel, 724,000 tpy of synthetic diesel, 437,000 tpy of synthetic naphtha and 53,000 tpy of LPG.

Axpo powers LNG ferry with biomethane

Spanish ferry operator Baleària's LNG-powered ferry, *Eleanor Roosevelt,* has made a test crossing using renewable biomethane certified by Axpo Iberia. This is an important milestone for zero-emissions maritime shipping; for the first time in Europe, a high-speed ferry has made a test crossing using only fuel from 100% renewable sources.

The ferry, equipped with natural gas hybrid engines, completed the route of 133 nautical mi between Barcelona and Ciutadella (Balearic island of Menorca), using renewable biomethane. The use of biomethane as a renewable fuel on the test trip avoided more than 50 metric t of CO_2 emissions.

Eleanor Roosevelt is a pioneering fast ferry and the seventh Baleària ship to use LNG. Each year, it is estimated to reduce CO_2 emissions equivalent to eliminating more than 8,900 conventional passenger cars or planting around 27,000 trees.

Sempra Energy to advance net-zero energy systems

Sempra Energy has signed an MOU with the U.S. Department of Energy's National Renewable Energy Laboratory (NREL), providing a framework for a joint effort to advance future net-zero energy systems. The MOU, which builds on nearly 10 yr of ongoing collaboration, will continue current work in researching and developing innovative solutions to help shape a lower-carbon future through technology and applications capable of withstanding increasing energy demand and broad adoption while advancing future innovation.

Sempra Energy and NREL have been collaborating for nearly a decade on cooperative and multi-year projects exploring the development, access and integration of low-carbon fuels and microgrid technology. In 2013, Sempra Energy subsidiary San Diego Gas & Electric Co. (SDG&E) and NREL joined to establish the nation's first utility-owned community microgrid in Borrego Springs, California, connected to a local 26-MW solar field, two battery storage systems, two generators and an ultracapacitor. The microgrid, which is being upgraded so that it can operate on 100% clean energy, was designed to provide consistent power flowing to the remote desert town during emergencies and planned outages on the larger grid.

In 2017, Sempra Energy subsidiary Southern California Gas Co. (SoCalGas) and NREL partnered to create, validate and integrate the first carbon-free, power-to-gas pilot system in the U.S. The technology takes excess electricity and converts it to H_2, which can be used, stored or combined with CO_2 and fed to a bioreactor to produce renewable natural gas (RNG). This technology could provide North America with a large-scale, cost-effective solution for storing excess energy produced from renewable sources. Additionally, Sempra Energy and NREL have coordinated efforts to research the impacts of H_2 blending in natural gas networks.

Under the MOU, Sempra Energy and NREL will coordinate and share objectives focused on:

- Advancing artificial intelligence to scale solutions across the U.S. and enable cities to reach clean energy goals
- Integrating low-carbon fuel solutions, including H_2, RNG, CCUS and fuel cells
- Exploring innovative solutions towards 100% renewable energy communities, requiring and implementing smart and enhanced controls, integration and operational capabilities as a blueprint for expansion
- Enhancing electric grids with technology that upgrades the infrastructure with a focus on reliability, connectivity and security
- Promoting viable net-zero solutions that are delivered with equity and widespread community access.

GAS PROCESSING & LNG

Catherine Watkins, Publisher
+1 (713) 520-4421
Catherine.Watkins@HydrocarbonProcessing.com
www.GasProcessingNews.com

NORTH AMERICA

NORTH HOUSTON, SUGAR LAND, NORTH TEXAS, UPPER MIDWEST
Jim Watkins
+1 (713) 525-4632
Jim.Watkins@GulfEnergyInfo.com

WEST HOUSTON, CENTRAL TEXAS, ALBERTA, NEW MEXICO
Brett Stephen
+1 (713) 525-4660
Brett.Stephen@GulfEnergyInfo.com

DALLAS, MIDWEST/CENTRAL U.S.
Josh Mayer
+1 (972) 816-6745
Josh.Mayer@GulfEnergyInfo.com

WESTERN U.S., BRITISH COLOMBIA
Rick Ayer
+1 (949) 366-9089
Rick.Ayer@GulfEnergyInfo.com

SOUTHEAST HOUSTON, GULF COAST & SOUTHEAST U.S.
Austin Milburn
+1 (713) 525-4626
Austin.Milburn@GulfEnergyInfo.com

NORTHEAST U.S., EASTERN CANADA
Merrie Lynch
+1 (617) 594-4943
Merrie.Lynch@GulfEnergyInfo.com

OUTSIDE NORTH AMERICA

AFRICA
Dele Olaoye
+1 (713) 240-4447
Africa@GulfEnergyInfo.com

BRAZIL
Evan Sponagle
Phone: +55 (21) 2512-2741
Mobile: +55 (21) 99925-3398
Evan.Sponagle@GulfEnergyInfo.com

CHINA, HONG KONG
Iris Yuen
China: +86 13802701367
Hong Kong: +852 69185500
China@GulfEnergyInfo.com

WESTERN EUROPE
Hamilton Pearman
+33 608 310 575
Hamilton.Pearman@GulfEnergyInfo.com

INDIA
Manav Kanwar
+91 (22) 2837 7070
India@GulfEnergyInfo.com

ITALY, EASTERN EUROPE
Riccardo R.C. Laureri
Office: +39 02 2362500
Mobile: +39 335 6962477
Riccardo.Laureri@GulfEnergyInfo.com

JAPAN
Yoshinori Ikeda
+81 (3) 3661-6138
Japan@GulfEnergyInfo.com

KOREA
YB Jeon
+82 (2) 755-3774
Korea@GulfEnergyInfo.com

RUSSIA, FSU
Lilia Fedotova
+7 (495) 628-10-33
Lilia.Fedotova@GulfEnergyInfo.com

UK, SCANDINAVIA, IRELAND, MIDDLE EAST
Brenda Homewood
Phone: +44 (0) 1622 297123
Brenda.Homewood@GulfEnergyInfo.com

CORPORATE, FULL ACCESS SUBSCRIPTION AND CLASSIFIED SALES
J'Nette Davis-Nichols
+1 (713) 520-4426
Jnette.Davis-Nichols@GulfEnergyInfo.com

ADVERTISER INDEX

This index and procedure for securing additional information are provided as a service to advertisers and a convenience to our readers. Gulf Energy Information is not responsible for omissions or errors.